# Collapse Behaviour of Double Layer Grid Structures in Steel




By: Jonathan Adams

Supervisor: Prof. A. Zingoni

Department of Civil Engineering
University of Cape Town
P/Bag Rondebosch 7701
Cape Town

A thesis submitted in partial fulfillment for the degree of
*Master of Science in Engineering*
February 2012

# Declaration

I know the meaning of plagarism and declare that all the the work in this document, save for that which is propperly acknowledged, is my own. The work presented, or any part thereof, has not been submitted towards a degree at another university.

Jonathan Adams, 06 February 2012

# Acknowledgements

I would like to thank my supervisor, Prof. A. Zingoni, for his guidance through the research process and the patience he has shown; I thoroughly enjoyed my time at the University of Cape Town. I would also like to thank Jade Walker and my family for their encouragement, without whom, I would not have been able to see this project to fruition.

# Abstract

Flat double layer grid (DLG) structures are efficient modular, structural systems which span in two or more directions and consequently develop their resistance in three dimensions. Although such structures offer many structural, constructional and aesthetic advantages over alternative planar structures, for use in unobstructed roofing applications, they have been observed to have a propensity for sudden collapse behaviour, as witnessed in the collapse of the Hartford Coliseum roof structure in 1978.

Previous study of DLG behaviour has been undertaken through experimental and numerical analysis; these studies have confirmed the sudden collapse behaviour and sensitivity of such structures to geometric imperfections for selected cases but have not developed the full spectrum of DLG behaviour. A parameter study was therefore undertaken to identify desirable DLG pre-critical yielding behaviour and post-critical increases in grid structural resistance. The parameter study also served to identify and characterize grid plastic, failure and collapse behaviour for structures representative of those employed in practice; the Structural Eurocodes were used for this purpose.

The parameter study of DLG collapse behaviour was undertaken by nonlinear finite element analysis with the Abaqus code. Previous numerical analysis methods have relied on idealized strut representations; a new analysis method was consequently developed which could simulate the continuous response of DLG structures and account for the effect of connection stiffness and grid restraint on individual member behaviour. Analysis of DLG structures was undertaken with displacement control, such that the full load-displacement path of DLG collapse could be developed. The case of uniformly distributed loading was considered as this was believed to be the most representative load distribution for DLG roof structures. The analysis method employed was comprehensively validated through comparison with the experimental test results of Collins (1981).

DLG failure and collapse behaviour was identified and trends in such behaviour established. Pre-critical flexural yielding behaviour of DLG structures was found to represent a significant improvement in DLG failure behaviour. The degree of pre-critical plastic deformation observed for grids with low bottom:top chord area provided significant warning of structural damage prior to collapse. The less dense distribution of bottom chord members in the diagonal on square configuration is an effective and simple means of introducing pre-critical yielding behaviour in DLG structures. Significant increases in post-critical collapse were only observed in limited instance; trends in such behaviour could not be identified.

# Contents

# List of Figures

# List of Tables

# Chapter 1

# Introduction

Space grid or grid structures, comprising double- and multi-layer grids (DLGs and MLGs), are light weight structural systems which are typically used for roofing applications to span large unobstructed areas. Grid structures are more efficient structural systems than traditional truss structures as they are able to span in two or more directions and consequently offer the design engineer significant structural advantages. Although grid structures have been used extensively since the 1950's their collapse behaviour remains poorly defined.

Limited experimental and numerical analyses have led to a general understanding of the collapse behaviour of such structures, but trends in grid behaviour are hard to establish between the results of these analyses, due to: the different methods employed in experimental and numerical analyses; and the high variability of results, attributable to the sensitivity of grid structure behaviour to geometric and material imperfections. Furthermore, grid structures previously analysed have frequently represented simplified structural cases and therefore are not representative of the structures typically employed in practice. The collapse behaviour of grid structures is of particular importance as such structures are prone to sudden failure and subsequent collapse.

The undertaking of a comprehensive parametric study of the collapse behaviour of grid structures, employing a consistent means of analysis, will allow for: the characterization of initial failure and subsequent collapse mechanisms to be established; trends in grid behaviour to be observed and identified; and the identification of any desirable grid behaviour which can be exploited to allow for the safer design of such structures. Several previous studies have focused on ways of improving grid collapse behaviour, through modification of critical member behaviour, but these have not been extensively employed due to inherent complications and cost.

Attention is paid to flat grid structures, defined as prefabricated systems consisting of two parallel layers of horizontal members forming top and bottom chords which are interconnected by inclined web members (see Figure 1.1), as these are the most common implementations of double-layer grid structures. Flat grid structural behaviour is analogous with that of plate structures, while curved grid behaviour is analogous with that of shell structures.

Owing to this fundamental difference in structural behaviour, comparison between flat and curved grid structures is not pursued.

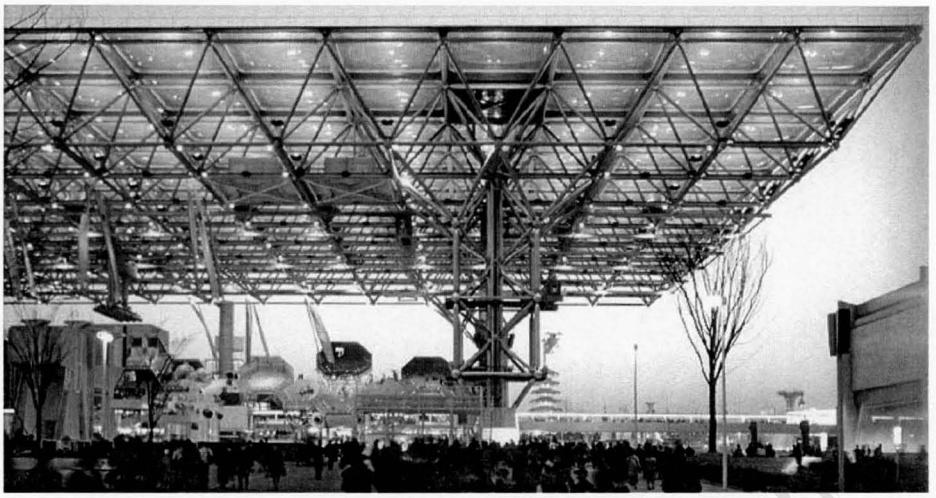

Figure 1.1: Festival Plaza DLG constructed for the World Expo 1970, Osaka, Japan (Kawaguchi, 2009).

In addition to the structural advantages offered by grid structures, grid structures also offer:

- Ease of assembly, due to their modular nature, which allows for the use of relatively unskilled labour;
- Reduced total project duration, due to repetition in member and node fabrication, ease and speed of assembly;
- Improved safety during construction, since assembly and painting is commonly undertaken at ground level. The structure is then hoisted or jacked into the final position, limiting work required at height.

Grid structures, although commonly used in many countries, have not been used extensively in South Africa. The recent introduction of Circular Hollow Sections (CHSs) in South Africa in grade S355 structural steel represents a significant opportunity to encourage the adoption of grid structures in South African structural engineering practice. Structural hollow sections, specifically CHSs, are particularly well suited to space structure applications as their resistance is not biased to particular axes and their resistance to instability in compression is high; this is consistent with the multi-directional axial load-carrying behaviour of grid structures.

The high indeterminacy of grid structures has in the past been confused with structural redundancy. Structural determinacy refers to the extent to which a structure's internal and reaction forces can be determined from equilibrium equations, while structural redundancy refers to the extent of alternate load paths within the structure. In the case of grid structures the degree of internal structural indeterminacy is high, due to the large number of members, while such structures possess a low structural redundancy, particularly in corner supported configurations.

Failure of an individual member in a grid structure through compression instability may consequently result in the sudden and progressive collapse of the structure or significant reductions in structural resistance. The collapse of the Hartford Coliseum roof, in the U.S.A. in 1978, serves as a reminder of the potentially catastrophic failure behaviour of grid structures.

## 1.1 Motivation and Research Significance

Failure and collapse behaviour of flat DLG structures, representative of member slenderness and relative section sizes used in practice, can be sudden, with little or no sign of imminent collapse. Pre-critical nonlinear and post-critical behaviour of DLG structures consequently has a significant bearing on the safety of such structures. Nonlinear pre-critical behaviour of grid structures, observed in the structure's global load-displacement response, can provide warning of imminent structural collapse, while increase in post-critical load resistance of the grid structure above the critical load may arrest the progression of structural collapse. The nature of grid post-critical behaviour can also be determined from the load-displacement response of the structure in the post-critical regime; some DLG structures fail suddenly while other DLG structure failures are observed to be gradual by comparison.

Current understanding of DLG collapse behaviour is limited to the experimental results as presented by Schmidt et al. (1976), Collins (1981), Schmidt et al. (1982) and Saka and Taniguchi (1994) which aimed to establish grid critical and post-critical behaviour, and Schmidt et al. (1980), Parke (1988), Mwakali (1990), El-Sheikh and McConnel (1993) and El-Sheikh and El-Bakry (1996) which aimed to improve grid critical and post-critical behaviour. Experimental analysis of DLG collapse behaviour has not been conducted with consistent method and consequently does not allow for significant comparison between results. Limited numerical studies have also been undertaken alongside these experimental studies but these employ simplified methods of analysis and have not been extended to account for the full spectrum of DLG collapse behaviour. A thorough set of results describing DLG pre-critical nonlinear and post-critical behaviour is therefore required. Parametric study of typical DLG structure failure and collapse will provide insight into DLG pre-critical nonlinear and post-critical behaviour.

Owing to the significant time requirements and costs associated with experimental testing of grid structures, parametric study of grid structural behaviour can only realistically be achieved through the use of numerical analysis. Grid collapse behaviour is characterized by significant geometric and material nonlinear behaviour; a reliable nonlinear analysis method is therefore required for the purpose of performing a parametric study of such behaviour. The numerical method employed should be validated against experimental results so that it can be used to reliably investigate DLG failure and collapse behaviour.

Numerical analysis of DLG structures undertaken by, Collins (1981), Smith (1984), Parke (1988), Mwakali (1990), Saka and Taniguchi (1992) and El-Sheikh and McConnel (1993) have failed to adequately capture the collapse behaviour of such structures. Differences between experimental results and previous analysis methods result from: use of the idealized

strut assumption which fails to capture the effect of global restraint on individual behaviour; neglect of geometric nonlinear effects on collapse; and neglect of the effect of connection stiffness. These studies have also failed to compare the failure and collapse behaviour of different grid configurations.

The full failure path of DLGs under uniformly distributed loading has not previously been developed. Two approaches have been employed to analyze the collapse of grid structures:

- Collapse analysis under distributed loading has been undertaken using load control, which follows the equilibrium path rather than the failure path.
- Collapse analysis of the full failure path has been undertaken with displacement control for which loading cases of one, two or four point loads, symmetrical about the point of maximum displacement, have been considered.

The differences between load and displacement controlled analyses for the case of a distributed load for identical DLGs are shown in Figure 1.2.

Comparison between load and displacement controlled analyses, for the case of a uniformly distributed load applied to identical DLGs, shows good correlation in pre-critical behaviour but this does not extend into the post-critical regime were the full failure path is not developed for the case of the load controlled analysis (see Figure 1.2).

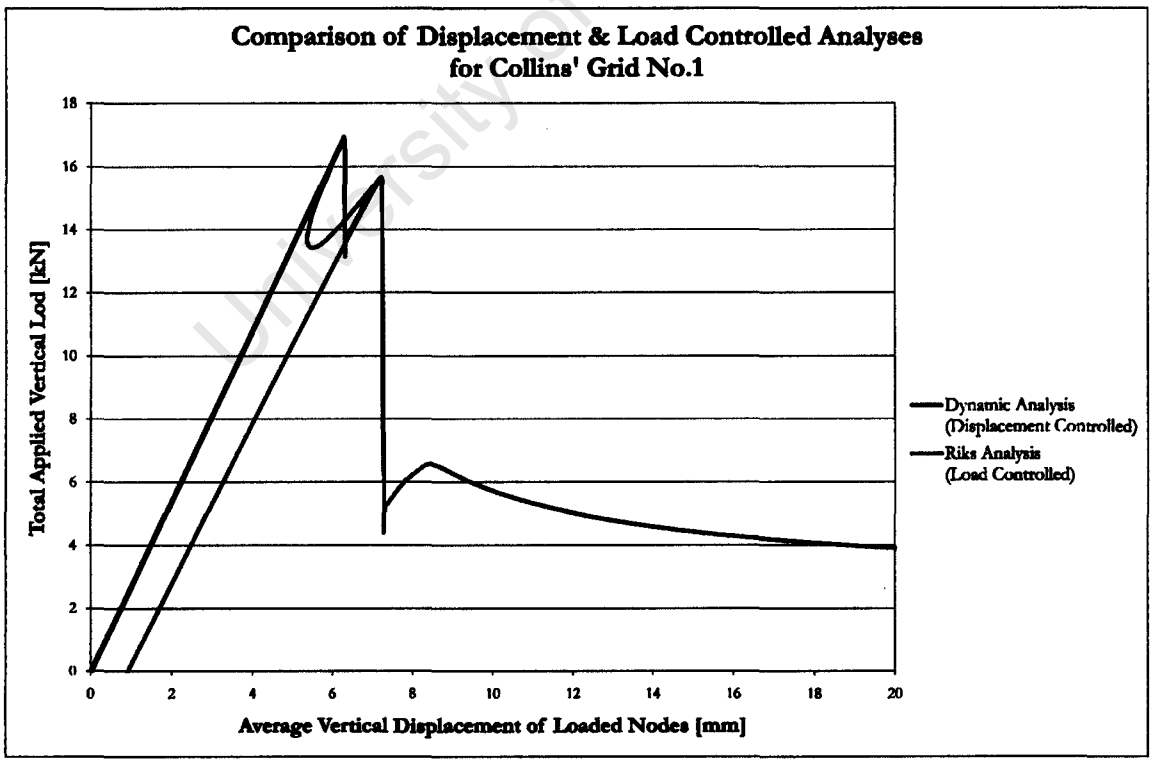


Figure 1.2: Comparison of the load-displacement behaviour of load controlled analysis (Red) and displacement controlled analysis (Blue).

The omissions of these factors, which potentially have a significant effect on grid structure collapse behaviour, present an opportunity for significant improvements in the collapse anal-

ysis of grid structures to be made. Application of the improved method of DLG structural analysis will allow for the parametric study of grid structural behaviour to be undertaken and applied to investigating improvements to DLG ductility behaviour in collapse.

## 1.2 Problem Statement

DLG structure behaviour is generally characterized by sudden failure and collapse. Authors, including Schmidt et al. (1980), Parke (1988), Mwakali (1990), El-Sheikh and McConnel (1993) and El-Sheikh and El-Bakry (1996), have proposed means of improving grid collapse behaviour but these methods have not been employed extensively due to inherent complexity and cost. The full spectrum of DLG collapse behaviour has not, in the past, been effectively investigated with a consistent approach, and therefore this is to be investigated to establish if the interaction of common structural and geometric parameters which define DLG structure behaviour result in improvements to DLG failure and collapse behaviour.



## 1.3 Research Aims

The primary aims of this research presented are to:

- Identify, categorize and compare the full spectrum of DLG collapse behaviour for square-on-square offset (SOS) and diagonal-on-square offset (DOS) grid structures, representative of the structures employed in practice, under uniformly distributed loading;
- Identify trends in grid behaviour with respect to geometric and structural parameterization of DLG structures within typical ranges of the parameter values used in industry;
- Identify grid pre-critical ductility behaviour and post-critical increases in grid resistance which can be exploited for the design of safer grid structures.

## 1.4 Research Objectives

The primary research aims are to be achieved by meeting the research objectives which are:

- Undertake a review of literature on the behaviour of DLG and MLG structures, with particular focus on collapse behaviour and numerical representations of such behaviour.
- Develop a modelling method, using commercially available finite element software, suitable for capturing the full failure path of grid structures under representative loading which is additionally suitable for application to parametric investigation.

- Verify the modelling method against published experimental results.
- Extend the validation of the numerical method to include conditions not considered in experimental testing.
- Apply the modelling method to the analysis of DLG structures of common dimensions.
- Identify all parameters which influence the collapse behaviour of DLG structures.
- Undertake a parametric study of DLG structure collapse behaviour for the identified parameters.
- Use the results of the parametric study numerical analysis to identify and categorize collapse behaviour through consideration of:
  - Global DLG structure load-displacement response;
  - Incremental deformed structural geometry;
  - Incremental distribution of stress within the structure.
- Establish trends in the results of collapse analysis through comparison of the post-processed results.
- Identify desirable structural behaviour which can be exploited for the safer design of such structures.
- Make recommendations regarding the design and analysis of DLG structures.

## 1.5 Scope of Study

The research presented will be limited to the following structures and load cases:

- **Flat DLGs of square-on-square (SOS) and diagonal-on-square (DOS) geometric configurations**; these are the most common DLG structures employed in practice.
- **DLGs with cornice edge detail and simple corner supports**; the cornice edge detail allows the supports to be inset from the grid periphery thereby reducing the tendency for local failure; corner supports allow for the DLG flexure behaviour to be observed more clearly when compared to other support configurations.
- **DLGs of aspect ratio 1:1**; DLG structures, assembled of pyramid modules, offer the greatest structural efficiency when they span in two directions. Selection of a DLG structure with square plan area allows for a DLG structure to span in two directions while maintaining equal member sizes in both directions.
- **DLGs constructed of Steel grade S355 CHS**; hot finished steel grade S355 CHSs have recently become available in South Africa and are particularly well suited to DLG structure applications for structural and aesthetic reasons.

- **DLGs consisting of uneven number of modules (9x9 for SOS grids and 7x7 for DOS grids)**; the number of modules selected was due to symmetry considerations. Employing an uneven number of top chord modules results in a single, most highly loaded compression member at the centre of each span, and allows for future study on comparable grids with varying aspect ratios.

- **DLGs under uniformly distributed loading**; such loading is the most realistic loading distribution for roof structures and is commonly specified in structural design codes for global analysis of roof structures.

- **DLGs with linear elastic rotational connection behaviour**; connection behaviour is seldom ideally pinned or fixed and can significantly affect structural behaviour. Linear elastic connection behaviour was selected as a compromise between accurately capturing grid connection behaviour and reducing model complexity and computational cost due to the large number of connections in DLG structures.

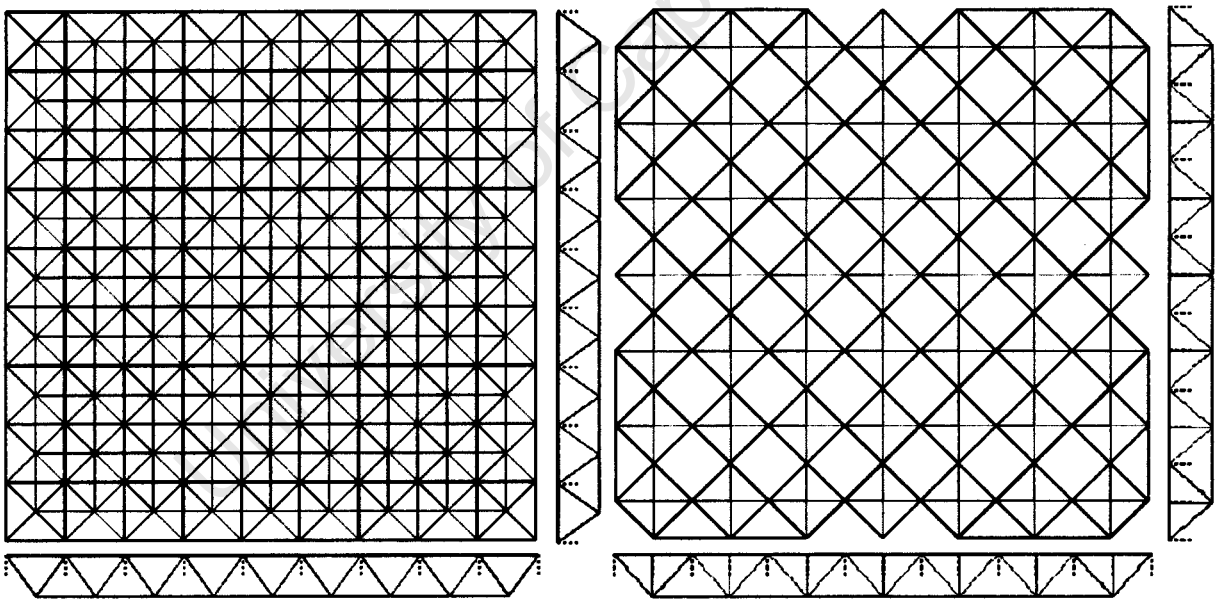

(a) 9x9 SOS (b) 7x7 DOS

Figure 1.3: DLG structures considered for parametric study.

Although DLG structure collapse behaviour is commonly influenced by the distribution of imperfections through the structure, these effects are not considered for the work presented. Imperfections are only considered at a member level to avoid problems associated with bifurcation and do not influence structural behaviour further as these imperfections are applied symmetrically about the grid centre. It is believed that greater understanding of grid structure collapse behaviour should first be established, neglecting the effects of imperfections. The distribution and magnitude of imperfections in DLG structures represent an important subject for future research.

## 1.6 Outline

A brief overview of the chapter contents is provided to guide the reader through this document.

The review of literature on grid structures is separated into two sections. General information on grid structure configuration, elastic behaviour, design and analysis is included in Chapter 2, while literature specifically related to grid structure failure and collapse is referenced in Chapter 3.

**Chapter 2, Basic Concepts and Background** DLG structure configuration and structural details specific to such structures, including connections and supports, are introduced. Aspects of grid elastic behaviour, including structural efficiency, grid design, and grid analysis found in the literature are presented and discussed.

**Chapter 3, Literature Review** Aspects of grid structure critical and post-critical behaviour are presented and discussed. Attention is paid to numerical and experimental studies on grid behaviour. Examples of grid structure failures are provided as motivation for the research undertaken.

**Chapter 4, Structural Theory** An overview of compression failure of individual structural members is undertaken. An analytical solution to the post-critical resistance of compression members is presented. An analytical method of analysing elastic grid structures is introduced which employs the analogy between DLG and flat plate behaviour.

**Chapter 5, Finite Element Analysis** Analysis methods employed for DLG structures are introduced, including elastic, stability and nonlinear methods, as well as solution strategies for the these methods.

**Chapter 6, Analysis Method** The nonlinear analysis method employed in the research undertaken is described in detail. Particular focus is placed on implementation, including solution controls and parametric scripting.

**Chapter 7, Validation** The nonlinear analysis method, introduced in Chapter 6, is validated against published experimental results. The appropriateness of the model parameterization employed is assessed; the effect of scale on grid behaviour is investigated for this purpose. The validated method is then extended to include similar cases including alternate grid configurations and loading arrangements.

**Chapter 8, Investigation Method** The method employed in the parametric study of SOS and DOS grids is introduced, and where necessary, motivation is provided for the

selection of parameters and parameter values employed.

**Chapter 9, Results and Discussion** The results of the parametric study undertaken are presented. These results are analyzed and post-processed so that trends in grid behaviour can be identified; grid behaviour is divided into pre-critical, critical and post-critical regimes for this purpose. Comparison between SOS and DOS grid behaviour is undertaken.

**Chapter 10, Conclusion and Recommendations** A summary of findings is presented. Attention is drawn to where the research presented has extended knowledge within the field of DLG structural behaviour, while areas for future study, identified as part of the research process, are highlighted. Recommendations regarding design and the analysis of SOS and DOS grid structures are summarized.

# References

Ian Martin Collins. *Collapse Analysis of Double-Layer Grids.* PhD thesis, University of Surrey, 1981.

A. I. El-Sheikh and H. El-Bakry. Experimental Study of Behaviour of New Space Truss System. *Journal of Structural Engineering*, 122(8):845–853, August 1996.

A.I. El-Sheikh and R.E. McConnel. Experimental Study of Behavior of Composite Space Trusses. *Journal of Structural Engineering*, 119:747–766, 1993.

Kawaguchi, 2009. URL `http://www.kawa-struc.com/projects/projects_0301_2.htm`. Photo only.

J. R. Mwakali. *The Collapse Behaviour of Double-Layer Space Trusses Incorporating Eccentrically Loaded Tee-Section Members.* PhD thesis, University of Surrey, 1990.

G. A. R. Parke. *The Behaviour of Space Trusses Incorporating Novel Compression Members.* PhD thesis, University of Surrey, 1988.

Toshitsugu Saka and Yoshiya Taniguchi. Effective Strength of 'Square-and-Diagonal' Double-Layer Grid. *Journal of Structural Engineering*, 118(1):52–72, January 1992.

Toshitsugu Saka and Yoshiya Taniguchi. Buckling Behavior of Square-and-Diagonal Double-Layer Grid. *Journal of Structural Engineering*, 120(4):1088–1102, April 1994.

L. C. Schmidt, P. R. Morgan, and J. A. Clarkson. Space Trusses with Brittle-Type Strut Buckling. *Journal of the Structural Division, Proceeding of the American Society of Civil Engineers*, 102:1479–1492, 1976.

L. C. Schmidt, P. R. Morgan, A. J. O'Meagher, and K. Cogan. Ultimate Load Behaviour of Full-Scale Space Truss. *Proccedings of the Institution of Civil Engineers*, 69:97–109, 1980.

L.C. Schmidt, P. R. Morgan, and A. Hanaor. Ultimate Load Testing of Space Trusses. *Journal of the Structural Division, Proceeding of the American Society of Civil Engineers*, 108:1325–1335, 1982.

Erling A. Smith. Space Truss Nonlinear Analysis. *Journal of Structural Engineering*, 110 (4):688–705, April 1984.

# Chapter 2

# Basic Concepts and Background

An introduction to DLG applications provide the context for research presented in this dissertation. DLG elastic behaviour is significantly affected by DLG geometric configurations; a review of DLG configurations including module geometry and orientation, edge detail and supports is therefore undertaken. Connector elements in DLG structure are introduced with reference to the degree of restraint they provide to individual members. Literature on DLG elastic behaviour is reviewed in the context of structural efficiency while failure mechanisms are defined.



## 2.1 Introduction

Flat DLG structures are defined as structures having two parallel layers of members in the horizontal plane forming top and bottom chords interconnected by inclined web members (Malla and Serrette, 1996) [1].

DLG structures are able to distribute applied loading in three dimensions and are consequently significantly more efficient than other two dimensional structures (Makowski, 1981). The high stiffness to weight ratio of grid structures makes them well suited to large span applications. When DLGs are used in spanning applications the principal structural resistance is developed as a force couple between compressive and tensile forces in top and bottom chord members. Although structural resistance of DLG structures is developed at a global scale, grid failure is generally governed by individual member failure. Consequently DLG resistance is governed by member cross-section capacity, member stability, ultimate joint capacity and joint stability.

DLGs typically span in two or three directions, depending on grid layout and support conditions; consequently simplified structural analogies exist between plates and grids.

[1] Grid structures may also be referred to as space frames and space trusses. The term 'space truss' implies a moment release at member joints (pin-connection) while 'space frame' implies moment continuity across joints (fixed connection).

## 2.2 Grid Structure Applications

Many examples of DLGs, designed and constructed since the 1950's, can be found in the literature. Steel space grid structures are characterized by their high stiffness to weight ratio and consequently the most typical civil applications of grid structures are for roofing, where large unobstructed spans are required, where height restrictions are imposed, or where high magnitude loading needs to be supported. The high stiffness and low weight of space frame structures has also been exploited in other structures such as tubular space frame chassis in racing vehicles and high stiffness mirror support structures for optical telescopes. Makowski (1981, chapter 1) and Ramaswamy et al. (2002) give many examples of the use of space grid structures in civil engineering practice.

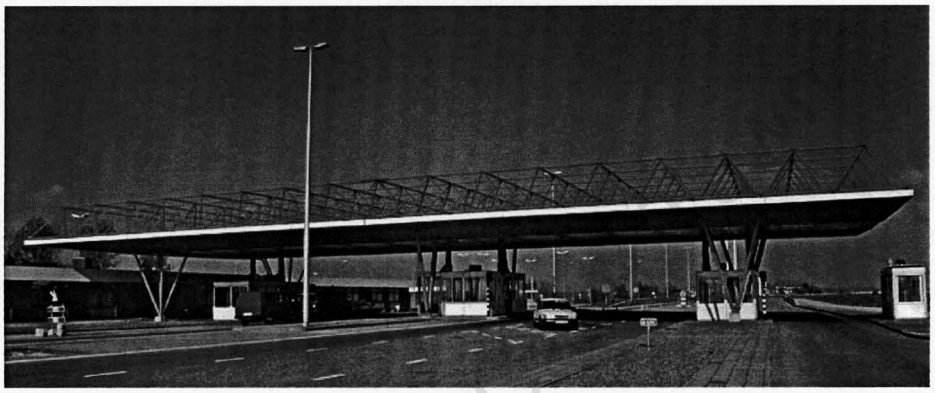

Figure 2.1: DLG structure used as a canopy for border crossing located in Nieuweschans, between the Netherlands and Belgium, constructed in 1985 (bv, 2010).

DLGs are typically used for roofing structures with clear spans of 10 to 100m (Makowski, 1981), while MLG structures are used for greater spans in applications such as aircraft hangars and sports arenas, see Figure 2.2.

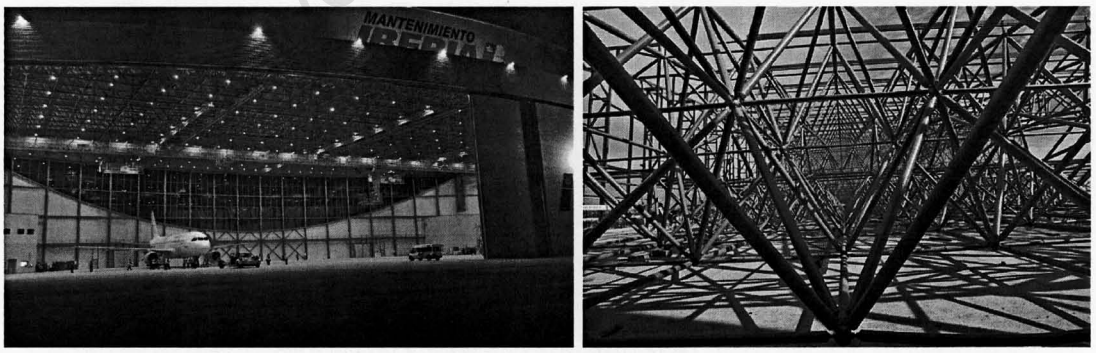


Figure 2.2: Iberia Airlines maintenance hangar, Barcelona, Spain, consists of a triple-layer grid spanning 150m. The roof is supported at the perimeter by concrete walls, steel columns, and by two steel space truss arches above the main hangar doors (flickr.com, 2010).

## 2.3 Grid Configuration

Grid structures offer the design engineer considerable freedom in the type, detail and dimensions of a specific structure. The purpose of this section is therefore to provide a generic

introduction to typical grid configurations and to identify the variables which define a particular grid structure. The various support, edge detail and geometric configurations commonly used for DLGs are presented.

The focus of the research presented is DLG structures; however for the purpose of simplicity the geometrical configurations employed for grid structures are introduced for single-layer grids (SLG) and then extended to DLG systems. SLGs are generally employed in membrane type spatial forms, or short span flat arrangements ($< 10m$), due to their high in-plane stiffness but low flexural stiffness. Flat single-layer grids consequently do not find wide application in practice and will not be considered in greater detail.

### 2.3.1 Single-layer Grids

Various SLG configurations exist, all constructed of varying combinations of square and triangular base modules. The primary difference between SLG structures is in their respective chord orientations relative to supports and the number of directions in which they span. Typical grid configurations span in two, three or four directions; Figures 2.3 to 2.5, adapted from (Makowski, 1981), illustrate these differences.



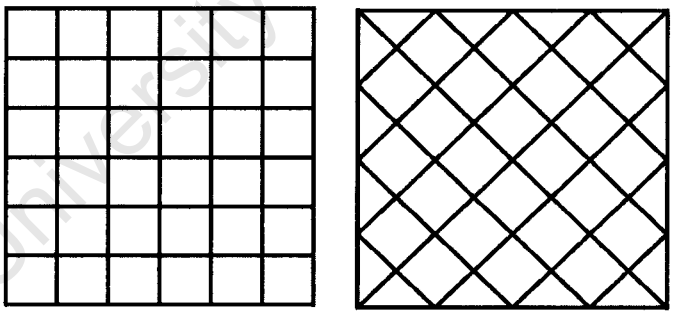

(a) Rectangular (b) Diagonal

Figure 2.3: Two way spanning single layer grids.

The most common grid configuration is the rectangular grid with chords intersecting perpendicularly to one another. Diagonal grids, with chords forming an oblique angle with supports, are frequently used for their high relative stiffness (for the case of continuous edge supports) resulting in significant reductions in vertical deflection. As flexural stiffness, $EI/L$, is dependent on member length, corner chords of diagonal grids are significantly shorter, and consequently stiffer, than central chord members. Chords spanning across corners therefore effectively provide intermediate support to longer chord members which span from corner to corner. The longer chord members consequently behave as continuous beams over yielding supports, effectively reducing midspan bending moments and deflections (Makowski, 1981).

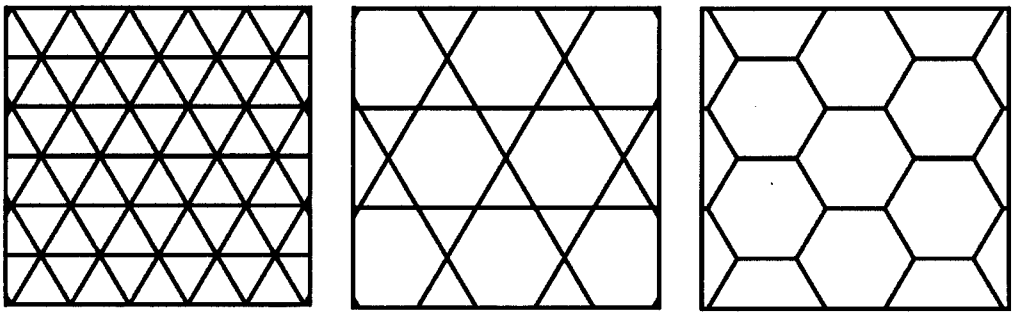

(a) Triangular (b) Triangular and Hexagonal (c) Hexagonal

Figure 2.4: Three way spanning single layer grids.

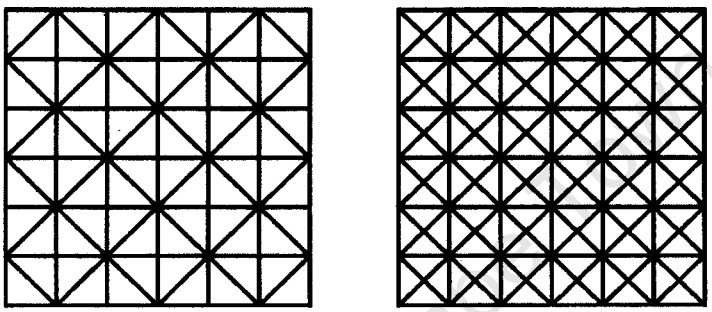

Figure 2.5: Four way spanning single layer grids.

### 2.3.2 Double-layer Grids

SLG configurations are commonly extended to DLGs where similar grid configurations are used as the upper and lower chords of such structures, Figure 2.6. DLGs are the most commonly used flat space grids, due to the typical span dimensions used in practice, and the relative simplicity of such structures when compared to multi-layered grid structures, consisting of three or more parallel layers of chord members.

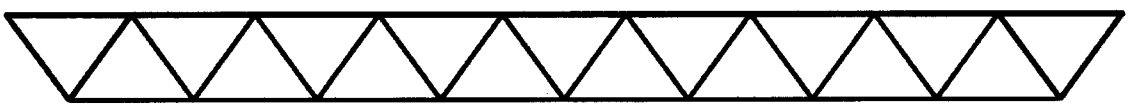

Figure 2.6: Elevation of DLG with SOS configuration.

In practice, several space grid geometries are commonly used. These vary in top and bottom chord layout, web member arrangement, spanning directions, the number of members intersecting nodes, and shape in plan. Guidance as to which grid configurations are best suited to specific cases is provided by parametric studies (of elastic behaviour), the practical experience of design engineers, and an understanding of grid structure mechanics.

A description of typical grid configurations, their advantages, disadvantages, and typical applications follows. Grid configurations commonly used employ a square or triangular base geometry. The abbreviations for grid configurations, as used in the remainder of this

document, are defined.

**Square-on-square offset (SOS)** grids consist of equally sized square chord modules offset by half a module width relative to each other, Figure 2.8a. Diagonal web members link the upper and lower chords forming a pyramid-shaped module. The pyramid apex appears to point downwards when a cornice edge detail is used and upwards when a mansard edge detail is used. Due to its rectilinear configuration, the SOS grid is easily and simply applied to roof structures for rectangular buildings. SOS grids are the most widely used arrangement for double-layer grids (Makowski, 1981), even though they do not represent the most structurally efficient configuration.

**Square-on-square set diagonally (SOSD)** grids are essentially the same as SOS grids, however, the entire grid is rotated through 45° relative to the supports, thereby reducing the effective span as discussed in Section 2.3.1.

**Square-on-diagonal and Diagonal-on-square offset (SOD and DOS respectively)** grids consist of square chord modules, one of which is rotated through 45° relative to the other, see Figure 2.7. Upper and lower chords are horizontally offset relative to each other such that the point of chord intersection of one grid is horizontally coincident with the centre of the other chord layer. SOD implies the upper chord is perpendicular to - and the lower chord is rotated relative to - the grid boundary while the inverse applies to DOS configurations.

In practice SOD and DOS grids are configured so that compression chord members are shorter than tension chord members. SOD and DOS grids therefore represent an attractive structural form as they represent efficient use of material. Additionally, fewer web members are required for SOD and DOS configurations than for comparable SOS configurations. SOD and DOS grids are easily configured to cover a rectangular plan area, edge beams are frequently used to restrain kinematic instability.

**Square-on-larger-square offset (SOLS)** grids are similar to SOS grids, however, alternate rows of lower chord members are omitted from the design in both directions, see Figure 2.8b. Chord members in the lower grid consequently extend twice the distance between nodes when compared to chord members in the upper grid. This grid configuration is particularly efficient for simply supported grids as compression chord members in the upper level are effectively restrained from buckling at regular intervals, while tension members in the lower grid, which are not susceptible to buckling, span larger distances between restraints. This configuration consequently reduces the number of chord members, web members and node connectors required in comparison with SOS grids, but provide less resistance to local applications of global shear loads.

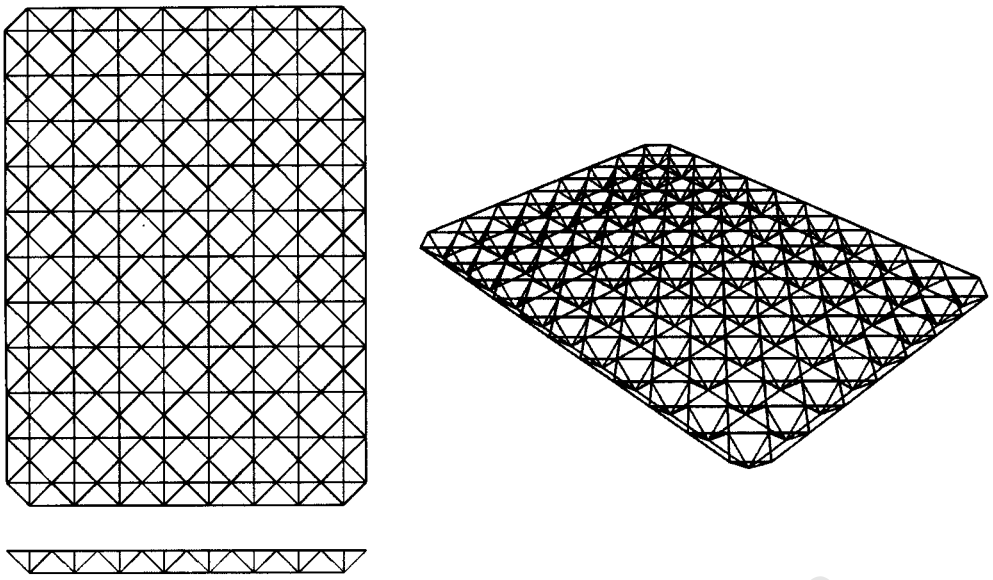

(a) Plan and Elevation (b) Isometric

Figure 2.7: DLG with DOS grid configuration (cornice edge detail shown).

**Square-on-larger-square offset set diagonally (SOLSD)** grids are essentially the same as SOLS grids, however, the entire grid is rotated through 45° relative to the supports, thereby reducing the effective span and increasing stiffness.

**Triangle-on-triangle offset (TOT)** grids consist of top and bottom layers of three-way spanning chord members. Top and bottom layers are offset from each other such that the intersection points of the top chords are positioned directly above the centroids of the triangles formed by the lower chords. Top and bottom chord members are connected by inclined web members. The three-way spanning nature of the triangular grid is attractive as it results in a structure of high stiffness. Three-way trusses are best suited to spanning plan areas assembled of triangular geometry, including diamond and hexagonal areas for example, but can be configured to cover rectangular areas. For the case where triangular grids are supported in plan by a rectilinear configuration of supports, however, the material efficiency of the structure is reduced.

**Additional grid configurations** which may also be considered in the design of such structures include grids of pentagonal, hexagonal and octagonal base geometries as introduced for single-layer grids in Section 2.3.1. These configurations, however, have not been employed extensively in practice and are not considered to offer any significant structural advantage over modules assembled of square and triangular base geometries.

### 2.3.3 Edge Detail

The edge detail selected in the design of a space grid affects the grid layout, support configuration, support location and in some cases the apparent orientation of individual modules.

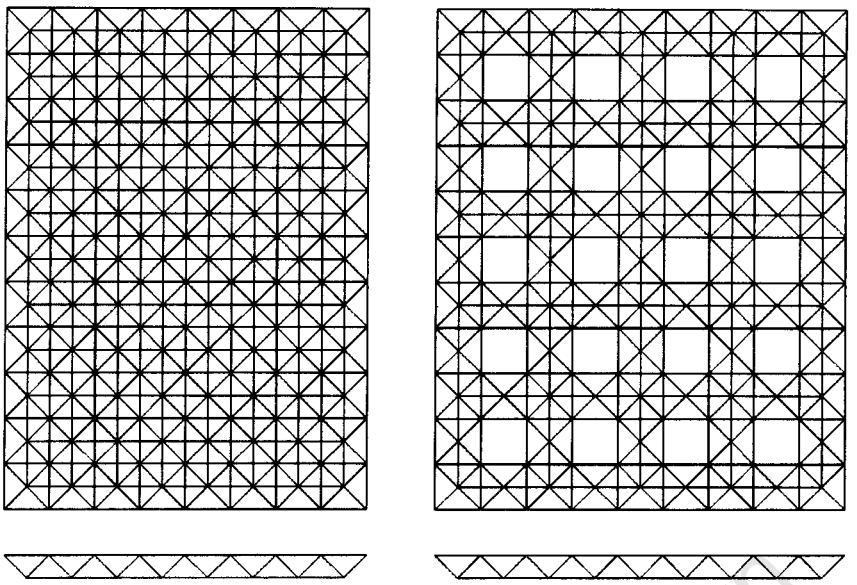

(a) SOS grid (b) SOLS grid

Figure 2.8: DLG with SOS configurations (cornice edge detail shown).

Edge detail is therefore of particular importance for aesthetic reasons and where height restrictions are imposed (supports can be configured such that the grid structure is positioned above or within the substructure). The three edge details typically employed in space grids are described below (BSC, 1973).

**Cornice Edge:** The upper chords extend half a module width beyond the lower chords in plan; the grid is typically supported at the level of the lower chords, however, support at the level of the upper chords is also possible.

**Mansard Edge:** The inverse of a cornice edge detail, the lower chords extend half a module width beyond the upper chords in plan; the grid is typically supported at the level of the lower chords, however, support at the level of the upper chords is also possible.

**Vertical Edge:** Both the lower and upper chords have the same extents in plan; this edge detail typically involves a modification to grid layout at grid edges; support is generally provided at the level of the lower chords.

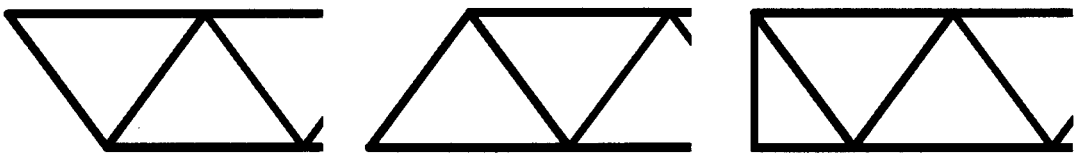

(a) Cornice Edge (b) Mansard Edge (c) Vertical Edge

Figure 2.9: DLG structure edge details.

### 2.3.4 Support Configuration

The support configuration used to restrain movement of grid structures significantly affects the behaviour of such structures. In practice, however, the support configuration is largely prescribed by aesthetics and substructure form / function. The support configuration determines effective spans and spanning directions and consequently the load distribution in the grid. Supports also provide lateral restraint to a grid and consequently appropriate releases need to be considered in design for thermal effects (expansion and contraction). Supports are provided at individual member connections or on groups of adjacent member connections, see Figure 3.18 and 1.1 respectively.

Maximum shear forces occur at supports; consequently web members adjacent to supports are typically strengthened relative to those in the rest of the grid. As with other flexural structures, continuity over supports results in more efficient use of materials. Support configurations used in the design of space grid structures can be categorized as below, and may include combinations of the following:

**Corner Support:** Support is provided to the grid at corner nodes or nodes slightly inset from the corner.

**Edge Support:** Support is provided to the grid at edge nodes along the grid perimeter.

**Continuous Corner Support:** Support is provided at corners and the grid is continuous over a number of bays

**Continuous Edge Support:** Support is provided to the grid along edges and the grid is continuous over a number of bays.

**Cantilever Support:** Support is provided at a position significantly inset from the grid boundary such that hogging moments are developed over the support.

**Yielding Support:** Support is provided, typically along the edge of a grid, by an additional structural element with its own stiffness and associated deflection. Such supports, in the form of truss girders or arches, are frequently used where large unobstructed edge spans are required such as for aircraft hangar doors.

Where possible, support of grids at extreme edges should be avoided, since such supports result in proportionally high loads in those members directly supported (Makowski, 1981). Alternate load paths in edge-supported grids are also limited. Supports inset from the grid boundary are consequently preferable. The use of cantilevers is also advantageous as it results in a considerable reduction in chord forces and grid deflection which is accompanied by only small increases in global shear forces (Makowski, 1981).

## 2.4 Node Connectors

Various commercially produced node connectors are available in a range of sizes. These node connectors are used to connect multiple bars at a single point with minimal or no eccentricities. The node connectors vary in the degree of rotational restraint which is applied to the bars connected to the node. The effective rotational stiffness of the connections affects the local member stability, global stability and the failure behaviour of the grid. Bars can, however, also be connected by conventional connection methods. Such connections include site welding and bolting. Continuous chord systems which employ conventional bolted connections have become increasingly popular in recent years due primarily to cost savings, however, several authors have also suggested that such systems demonstrate more desirable failure, than node-bar systems, due to continuity of chord members.

A selection of typical node connection systems is described. The selected node connectors demonstrate the range of connection rotational constraint conditions which extend from pinned, to partially fixed (including fixed with reduced end cross-sections), to fully fixed and continuous.



#### 2.4.0.1 Pinned Connections

The MERO connector (re-branded Novum KK), originally introduced in 1942 is a threaded spherical ball of forged steel which can accept up to 18 tubular members. The connector is the oldest and considered to be the most successful commercial system of prefabricated double-layer grids (Makowski, 1981). Connection of tubular members is achieved with effectively zero eccentricity. Bolts used to connect members to the nodes are inserted through a hole in the tubular member and pass through a cone welded to the end of the element, Figure 2.10. The MERO connector is designed to transfer axial loads only and is considered to behave as a pin for design purposes, since the significant reduction in member end cross-section reduces any moment resistance the connector may possess. The achieved joint stiffness has, however, been shown to vary considerably with bolt tightness (Davoodi, 2004).

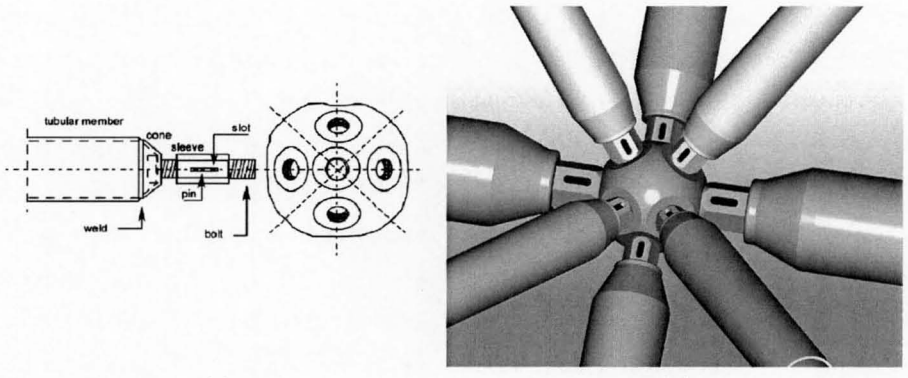


(a) (b)

Figure 2.10: Mero KK node connector (a) (Caglayan and Yuksel, 2008) (b)(KG, 2010).

#### 2.4.0.2 Reduced Cross-Section Connections

The Octatube connector, developed by Prof. Mick Eekhout in 1973, is constructed of an octagonal base plate and two semi-octagonal plates welded together at right angles. End-flattened tubes are connected to the node with high strength bolts. The connector was originally designed for industrial building applications where cost was of greater importance than aesthetics and is easily constructed in a typical steel workshop. The node connector displays rotational behaviour which falls between pinned and fixed connections.

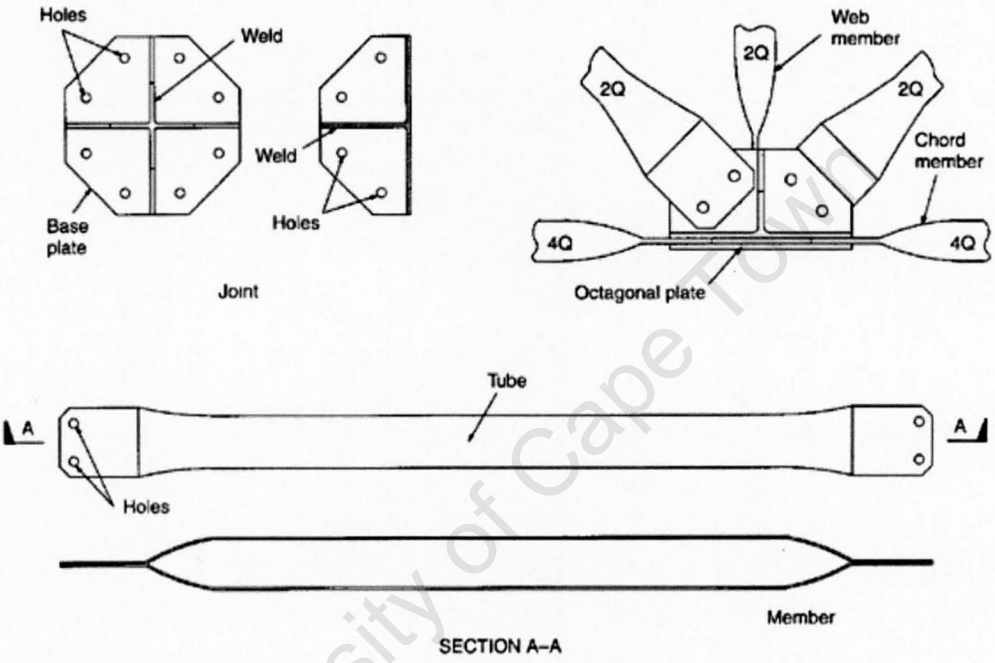


Figure 2.11: The Octatube connection system and bar with flattened ends (Ramaswamy et al., 2002).



#### 2.4.0.3 Fixed Connections

The Tuball connector, also designed by Prof. Mick Eekhout, was originally introduced in 1984. The Tuball connector is a hollow sphere connector constructed of spheroidal graphite. Tubes of full cross-section are fitted with solid props, welded together, presented to the node and then connected from within the node using high-strength bolts. The connection develops a moment-resisting rotational behaviour. Threaded rods which extend through the node are used to allow for an increased tensile capacity of the connector. Cone ends may additionally be specified for tube ends which reduce clutter at nodes for members with larger diameter. Tuball connectors are generally lighter and less expensive than alternatives constructed of forged steel (Ramaswamy et al., 2002) and have been used fairly extensively for large span applications, including hangars and sport centres, in the Middle East and India.

The Nodus system, developed by the Tubes Division of the British Steel Corporation and introduced in 1972, is a space grid system with a moment continuity type connection which

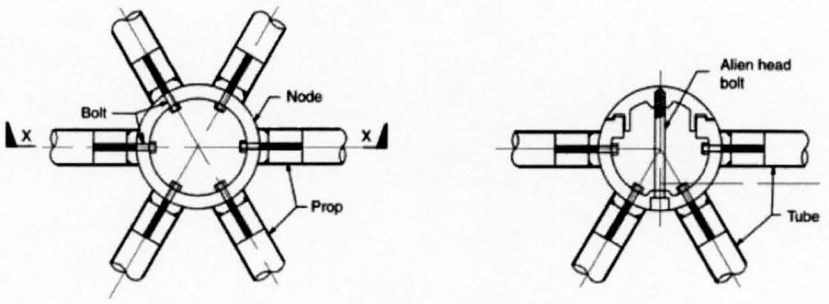


(a) Plan (b) Section X-X

Figure 2.12: The Tuball node connector (Ramaswamy et al., 2002).

allows for roof sheeting to be fixed directly to chord members (see Figure 2.13). An extensive full scale testing program was undertaken prior to commercial use which, in addition to verifying the system, was used to develop design charts for chords under combined axial force and bending moments (James, 2010). Testing of the system most notably included the static loading of a 30x30m by 1.5m deep square-on-diagonal grid to 1.5 times the superimposed load for a 24 hour period.

The Nodus system was used extensively in Britain and in other parts of the world and was designed so that all fabrication work could be conducted in a workshop; this allowed for high levels of quality control and simple site assembly. Connections were furthermore designed such that they could not be assembled incorrectly on site, introducing further inherent site quality control measures (Makowski, 1981). The Nodus system is comprised of two half-casings constructed of spheroidal graphite and end connectors which are welded to chord members. Although the system was extensively used in notable structures including the National Exhibition Centre in Birmingham (covering an area of $83300m^2$), the system has lost popularity in favour of simpler pin connected systems and has not been used in new structures since the mid 1980's.



#### 2.4.0.4 Continuous Chord Systems

A significant proportion of the cost associated with space grids may be attributed to the cost of the node connectors. The use of continuous chord systems addresses this by sacrificing structural efficiency for more widely used construction methods. Such structural systems employ continuous upper and lower chords bolted together at intersections. They are typically constructed from channel or rectangular hollow sections and bolted web sections constructed of tubular sections with stamped ends bolted to chord members, Figure 2.14. The reduction in structural efficiency of continuous chord systems is due to the introduction of eccentricities at connections and the localized reduction in web member section properties resulting from stamped bar ends. Continuous chord systems are consequently susceptible to the local instability of web members El-Sheikh (1999a).

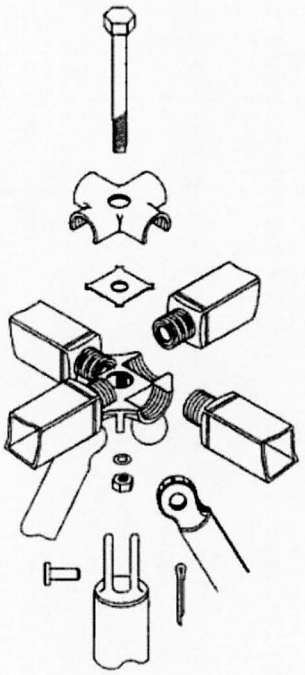

Figure 2.13: The Nodus connection system (Ramaswamy et al., 2002).

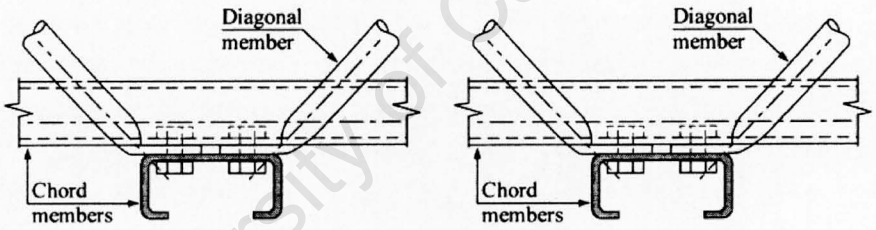


(a) Front elevation (b) Side elevation

Figure 2.14: Example of a continuous chord connection with end-flattened web members (El-Sheikh, 1999b).



## 2.5 Grid Elastic Behaviour

An introduction to the general structural behaviour of flat grid structures, in the elastic range, is given as a basis for subsequent sections on failure behaviour and analysis of such structures. Various studies are referenced which provide insight into the elastic behaviour of grid structures. Elastic behaviour has frequently been assessed from the perspective of structural efficiency which has been defined w.r.t weight, force distribution and cost. The research studies presented provide valuable insight into flat DLG structure elastic behaviour, which form the basis for failure and collapse behaviour. The studies presented, however, were undertaken with linear numerical analysis methods and do not account for imperfections; elastic behaviour described in such studies differs significantly from behaviour observed in experimental studies (see Section 3.3).

### 2.5.1 Load Distribution

El-Sheikh (1999a) defines structural efficiency as the relative distribution of load throughout a structure. An even distribution of load through a structure represents an efficient structure as applied loading is resisted by a greater portion of the structure and results in a more efficient use of materials (El-Sheikh, 1999a). In a structure where the load is unequally distributed, the structural integrity is dependent on a few highly loaded members, with the consequence that, if anything should happen to these members, the potential for load redistribution is unlikely.

El-Sheikh (1999a) investigated the standard deviation of the internal force distribution in the top, bottom and web members of space trusses in the elastic range through numerical analysis, no imperfections were considered. SOS, SOLS and SOD grid configurations were considered of dimensions 50x50x3.125m for both corner and edge supported trusses. The conclusions of this investigation by El-Sheikh (1999a) are summarized as follows:

- The distribution of forces in web members was significantly more even than in chord members;
- The internal forces in web members were low and evenly distributed, except near supports;
- The distribution of internal forces in chord members was contrastingly less even:
  - In corner-supported cases, maximum internal forces were observed for grid edge members located at midspan between the supports;
  - In edge-supported cases, maximum internal forces were observed at the truss central regions;
- The highest standard deviation of member forces was observed in top chord members in corner-supported trusses;
- SOS grids were the least efficient of the trusses investigated; SOLS and SOD trusses exhibited approximately equal efficiency.

### 2.5.2 Grid Configuration and Support Conditions

West (1967) undertook a numerical study of double-layer grid efficiency, in which a minimum weight definition was assumed. The study investigated the efficiency of five types of square grid with a clear span of 30m. Four different support conditions were additionally considered, resulting in a total of 20 numerical models which were analyzed using the stiffness method. Diagonal and three-way latticed grids, SOS, DOS and SOD configurations were considered. Support conditions included simple edge support on all four sides, simple corner support on all four corners, continuous corner support on all four corners and a final support configuration including simple edge support on two sides adjacent to a continuous corner support at the opposite corner.

The conclusions of the study on DLG efficiency are summarized as follows (Makowski, 1981):

1. The overall efficiency of DLG structures depends largely on the directional pattern of members;
2. The torsional rigidity of bars has very little effect on internal forces in DLG structures and may be neglected;
3. For DLGs square in plan, diagonal grids show advantages over three-way grids, this is as three-way grids require more material as chords parallel to supports are not fully utilized;
4. Space grids are more efficient structures than latticed grids;
5. The square-on-diagonal DLGs proved to be the most efficient grid configuration considered. Deflections were 10-15% less than in other cases and material consumption was reduced by 15-20%;
6. Grids with top chord modules smaller than the bottom chords are preferential as these configurations result in:
   (a) a reduced number of web members;
   (b) reduced compression member lengths, which increase resistance to buckling;
   (c) the increased bottom tension chord lengths, which are not susceptible to buckling;
7. Edge or stiffening beams are seldom part of the most efficient grid structures;
8. Three-way grids only offer a marginal improvement in the allowable span:depth ratio and do not result in the lightest structure;
9. A span:depth ratio of 20 is appropriate for grids simply supported around all edges or continuous over supports;
10. A span:depth ratio of 12 is appropriate for grids simply supported at the corners.

#### 2.5.2.1 Aspect Ratio

Stress distribution in DLGs is significantly affected by the grid aspect ratio (i.e. length / width). Desirable characteristics of grid structure behaviour are dependent on their ability to span in two or more directions; consequently, the most uniform stress distribution will occur in square and triangular grids for grid configurations of square and triangle base geometry respectively. In grid structures where the aspect ratio differs significantly from unity, the position of the supports needs to be considered carefully to result in a desirable stress distribution. This can be best achieved through sub-division of the grid into smaller grids with respective aspect ratios closer to one, providing this does not adversely affect building functionality.

#### 2.5.2.2 Joint Rigidity

Vaeghi Amir and Davoodi (2002) and Davoodi (2004) investigated the influence of connection stiffness and connection bolt stiffness, respectively, on the behaviour of grid structures with Mero type connections. The conclusions of Davoodi (2004) regarding bolt tightness (and consequently connections stiffness), resulting from full-size testing of SOS grids in the elastic regime can be summarized as:

- Grid structures in the elastic regime undergo largely recoverable, nonlinear behaviour due to nonlinearities in connection behaviour;
- Connection stiffness has a significant effect on grid deflections;
- The load-displacement behaviour of grid structures lies between the upper and lower limits represented by pinned and fixed connections respectively;
- Grid stiffness increases with increasing connection stiffness.

## 2.6 Grid Failure Behaviour

The factors characterizing the failure behaviour of grid structure are discussed as an introduction to the more thorough review on grid structure collapse behaviour and analysis undertaken in Chapter 3.

### 2.6.1 Failure Mechanisms

The initiation of failure in a grid structure may result from any of the following limit states as described by Marsh (2000). In most cases grid load-displacement behaviour can be assumed to be linear up until the grid critical capacity is achieved. Where the response may be characterized by nonlinear behaviour before the highest capacity is reached, the limit state is denoted with NL in parentheses. Grid structures with semi-rigid connections tend to exhibit nonlinear behaviour before collapse, due to the non-linear nature of such connections. A summary of potential grid failure mechanisms is included below.

**Tension failure**

- yielding of the gross cross-section (NL)
- rupture of the net section
- tear out at the fasteners

**Compression failure**

- buckling in torsion (singularly symmetrical sections only)

- buckling in flexure short columns
- buckling in flexure slender columns (NL)
- buckling in flexure as beam columns (NL)

**Connection failure**

- fastener failure in shear or tension
- gusset plate failure
- node piece rupture

**Nodal instability**

- rotation about the vertical or horizontal axes
- buckling of the end plates or flattened ends

The initiation of one of these failure mechanisms may result in the collapse of the structure or a load re-distribution to the surrounding members; this is largely determined by the location of the particular member where the limit state is reached. Web members are generally not critical, excluding those over supports, and several web members would need to fail for collapse to initiate. If, however, a main chord member buckles, there is little post-buckling reserve and collapse is likely (Marsh, 2000).



### 2.6.2 Local Member Buckling

In the analysis of grid structures various authors have accounted for individual member buckling in isolation. The problem associated with such an approach is that it fails to capture the restraint of adjacent members which may increase or decrease the critical load for the individual members. Owing to the nature of grid structures, effective restraint applied to individual members will differ for in and out of plan buckling; this is furthermore not captured by the idealized strut behaviour assumption.

#### 2.6.2.1 Post-Buckling Behaviour

When a compression member buckles, no additional load can be applied to the member. If the surrounding structural elements cause shortening of the buckled member, the buckled member will deflect sideways resulting in yielding spreading through the member. The formation of plastic hinges in the member will result in additional shortening. For the member to remain in equilibrium the axial force in the member will decrease (Smith, 1984). This behaviour is called 'strain softening'.

If the effective stiffness of the buckled member is greater than the stiffness of the surrounding structure on the initiation of strain softening, the member will be in unstable equilibrium. For a slight disturbance the member will further shorten until equilibrium can be re-established (Smith, 1984). This behaviour is termed the 'chordal snap through phenomena' and results in a significant reduction of axial load capacity. The initiation of chordal snap through behaviour results in load redistribution to surrounding members and may initiate progressive collapse.

### 2.6.3 Global Grid Buckling

Grid structures are most commonly used to span large areas where intermediate supports are avoided. As the global bending stiffness of grid structures is significantly greater than the bending stiffness of individual members, dominant buckling modes are observed at the member level. No research into the global buckling modes of grid structures was found.

In addition to roofing applications grid structures have also been used, on occasion, as wall supports of hangar structures, see Ishikawa et al. (2000). Such applications are rare and no research on global buckling behaviour of such structures was found. It is the author's opinion that such applications of DLG structures are more likely to exhibit global buckling modes than the conventional spanning applications of grid structures, but this cannot be substantiated.

## 2.7 Grid Structure Design

An overview of typical design considerations for space grid structures is given.

### 2.7.1 Design Codes

Although structural engineering design codes do not provide explicit rules or guidance on the design of grid structures, rules are defined relating to individual member design for combinations of axial and bending forces and provide guidance on the stability behaviour of individual members and / or groups of members (frames). General rules are specified for the static and quasi-static loading of roof structures.

#### 2.7.1.1 Loading

General loading of space grid structures can, in accordance with Eurocode 1, be divided into loading related to structure self-weight and imposed loading. Structure self-weight should include the respective contributions of fixed services, structural and non-structural elements. Imposed loads should include contributions accounting for wind load, snow or water loads, pedestrian loading (to allow access for inspections), machinery loading, and crane loading.

Wind loading of building structures is generally applied as a quasi-static load where the dynamic effects of wind are accounted for by upward factoring of the applied static wind pressure loads. Additional consideration should also be taken of seismic loading.

The application of loading to space grid roof structures is generally assumed to be uniformly distributed across the structure and applied at node points where members are connected. Additional consideration of concentrated load is also undertaken, which frequently influences local member design.

The application of load to grid structures is, however, dependent on the method employed for connecting the roofing to the frame. Systems with moment resisting connections generally allow for roof sheeting to be fixed directly to the upper chords. Systems with less rigid connections typically require roof sheeting to be connected to purlins which are in turn supported by posts at positions in line with upper chord member nodes. In the design of space grid structures, non-symmetrical arrangements of load may also need to be considered as the evenly distributed case might not be critical.



#### 2.7.1.2 Member Design

Individual members in grid structures are typically designed as axial members, since load is generally introduced at nodes and consequently bending moments are small. Joint rigidity is taken account of in the design of grid structures through the use of member effective lengths. Where loading is not introduced at nodes the more general case of beam column behaviour should be considered. For the purpose of member sizing in the research presented, design rules for axial members are used, as defined in Eurocode 3: Design of Steel Structures - Part 1-1 General Rules and Rules for Buildings. The design of axial members includes the following checks:

- Check for member cross-section yield capacity (tension and compression);
- Check for member cross-section rupture at member ends due to reduced section resulting from bolt holes or shear lag from connections;
- Check for member instability including:
  - local buckling determined by member and cross-section plate element classification;
  - flexural buckling according to European buckling curves;
  - torsional buckling (where appropriate).

#### 2.7.1.3 Member Effective Lengths

As with the design of any compression members or beams, member end constraints are accounted for by an 'effective length' factor, $k$. Rotational constraints applied at beam

ends may exhibit behaviour anywhere between pinned and fixed with $k = 1.0$ and $k = 0.5$ respectively. Effective length factors have been defined for space grid members as a function of connection type. Typical values used in the design of space grids are: for full section ends, $k = 0.7$; for reduced section ends, $k = 0.9$; and for pinched section ends, $k = 0.95$ (Malla and Serrette, 1996). However Ramaswamy et al. (2002) uses the more conservative value of $k = 0.85$ for rigidly connected members.

In the buckling of compression chord members a further distinction can be made between buckling in- or out-of-plane of the chord members. Out-of-plane buckling of chord members experience greater resistance as web members are more effective at providing restraint to out-of-plane deflection. As proposed by Madi and El-Tayem (1991), effective length values for chord members are: where both ends have a high degree of restraint $k = 0.76$ for in-plane buckling and $k = 0.67$ for out-of-plane buckling; where one end has a high degree of restraint and the other end is pinned, effective length factors of $k = 0.81$ for in-plane buckling, and $k = 0.72$ for out-of-plane buckling are specified. Murtha-Smith and Bean (1989) discuss the factors which affect the effective buckling lengths of members and give typical values for SOS grids as a function of these parameters. Parameters affecting the effective buckling lengths of individual members in space grid structures, according to Murtha-Smith and Bean (1989), can be summarized as follows:

- The relative cross-section second moments of inertia between chord and web members;
- The ratio of axial force magnitude between chord and web members;
- The angles at which members frame into joint;
- The joint flexibility.

#### 2.7.1.4 Member out of Straightness and Residual Stress

Both member out-of-straightness imperfections and residual stresses result from the fabrication process of structural steel sections. Member out-of-straightness results in decreased resistance to axial loading and is accounted for in design through the use of buckling reduction factors. Member residual stresses result in a reduction to member flexural stiffness (Balut and Gioncu, 2000). Allowable deviation from straightness of structural steel members, according to EC3 (2005), is given by the greater of L/1000 or 3mm. A value of L/1000 is used for the European buckling curves.

Balut and Gioncu (2000) describe a similar method to El-Sheikh (1997) which can be used to approximate if a specified manufacturing tolerance, $\Delta_L$, for grid member length is appropriate. The method proposed by Balut and Gioncu (2000) can be undertaken as follows:

1. The grid structure is analyzed, ignoring lack of fit resulting from member length imperfections;

2. Member lengths are adjusted by adding $\Delta_L$ to the length of compression members and by subtracting $\Delta_L$ from the length of tension members.;
3. The grid structure is re-analyzed, including member length changes;
4. Member capacity is checked according to an appropriate design code.

Balut and Gioncu (2000) further distinguish between 'adjustable' and 'non-adjustable' connection systems, where 'adjustable' implies the connection system allows for local member length modification where manufactured members deviate from the intended geometry. Adjustable systems can be used in DLG and TLG grids to reduce the effects of member length imperfection. Member length imperfections can result in significant reductions of designed grid load capacity and are consequently undesirable. Where non-adjustable connection systems are used, the effect of length imperfections need to be accounted for in design.

# References

Eurocode 3: Design of Steel Structures - Part 1.1: General Rules and Rules for Buildings BS-EN 1993-1-1:2005, 2005.

Nicolae Balut and Victor Gioncu. The Influence of Geometrical Tolerances on the Behaviour of Space Structures. *International Journal of Space Structures*, 15(3 and 4):189–194, 2000.

*Nodus, Space Frame Grids, part 1, Design.* BSC - Tubes Division, Structural Advisory Services Tubes Division British Steel Corporation Park House 118 Park Street London W1A 1EG, 1973. Year of publication not available, Year is of UCT Library reciept.

Octatube Internaltional bv, 2010. URL `http://www.octatube.nl/test/contentloader.php?grp=0&id=1`.

O. Caglayan and E. Yuksel. Experimental and finite element investigations on the collapse of a Mero space truss roof structure A case study. *Engineering Failure Analysis*, 15:458–470, 2008.

M. R. Davoodi. *Effects of Bolt Tightness on the Behaviour of Mero-type Double Layer Grids.* PhD thesis, University of Surrey, 2004.

Ahmed El-Sheikh. Effect of Member Length Imperfections on Triple-Layer Space Trusses. *Engineering Structures*, 19:540–550, 1997.

Ahmed El-Sheikh. Design of Web Members in Space Trusses. *International Journal of Space Structures*, 14(1):25–34, 1999a.

Ahmed El-Sheikh. Failure mode and strength of space truss compression chord members. *Engineering Structures*, 21:395–405, 1999b.

flickr.com. Iberia Airlines Maintenance Hangar, Barcelona, 2010. URL `http://www.flickr.com/photos/50189779@N03/`. Photo only.

Koichiro Ishikawa, Shoji Okubo, Yujiro Hiyama, and Kato Shiro. Evaluation Method for Predicting Dynamic Collapse of Double Layer Latticed Space Truss Structures due to Earthquake Motion. *International Journal of Space Structures*, 14:249–257, 2000.

Nigel James, 2010.

Mero-TSK International GmbH & Co. KG, 2010. URL `http://www.mero.de/knotensysteme.html?&L=1`.

U.R. Madi and A. A. El-Tayem. as cited by Malla and Serrette (1996). On the effective length of compression members in double-layer grids. *International Journal of Space Structures*, 6:33–39, 1991.

Z. S. Makowski, editor. *Analysis, Design and Construction of Double-Layer Grids.* Applied Science Publishers Ltd, 1981.

Ramesh B. Malla and Reynaud L. Serrette. Double-Layer Grids: Review of Static and Thermal Analyis Methods. *Journal of Structural Engineering*, 122(8):873–881, August 1996.

Cedric Marsh. Some Observations on Designing Double-Layer Grids. *International Journal of Space Structures*, 15(3 and 4):225–231, 2000.

E Murtha-Smith and J. E. Bean. as cited by Malla and Serrette. Double layer grid space frame buckling. *International Journal of Space Structures*, 4:117–127, 1989.

G. S. Ramaswamy, M. Eekhout, and G. R. Suresh. *Analysis, design and construction of steel space frames.* Thomas Telford, 2002.

Erling A. Smith. Space Truss Nonlinear Analysis. *Journal of Structural Engineering*, 110 (4):688–705, April 1984.

J. Vaeghi Amir and M. R. Davoodi. Modelling the Semi-Rigid Behaviour of the Mero Jointing System. In *Space Structures 5, Volume 1*, 2002.

F. E. S. West. as cited by Makowski (1981) . A study of the efficiency of double-layer grid structures. Master's thesis, University of Surrey, 1967.

# Chapter 3

# Literature Review

This chapter provides an overview of research conducted into the failure and collapse of DLG structures with a focus on application to numerical analysis methods and experimental testing.

An introduction to numerical analysis methods previously employed in the collapse of grid structures is provided through an overview of the idealized strut formulation of member behaviour and through review of studies which provide a general overview of collapse behaviour. More extensive and detailed studies undertaken on the collapse behaviour of grid structures through experimental analysis follows. Consideration of two significant space grid structure failures demonstrates the potentially catastrophic nature of grid structure collapse.



## 3.1 Numerical Analysis Methods

### 3.1.1 Idealized Strut Formulations

Several authors have proposed analysis methods based on idealized strut behaviour for the failure analysis of grid structures, while these methods have been validated with varying degrees of success, these numerical methods have not been extended to extensive studies on DLG post-critical behaviour.

Nonlinear behaviour of grid structures has traditionally been captured through the implementation of empirical stress-strain curves and progressive load stepping procedures utilizing truss elements. Empirical formulations of nonlinear behaviour only represent an approximate method of analysis, as they do not capture the true behaviour of a grid but rather trace the grid response to predefined member behaviour. They have, however, been used extensively due to their ease of implementation, and computational efficiency. Step-wise linearization of stress strain curves of varying degrees of complexity have been used with reasonable success (Smith, 1984).

The following assumptions have commonly been made for the implementation of linearized

stress-strain descriptions of member behaviour (Smith, 1984):

- When full tension yield occurs, the member has zero stiffness, until strain hardening initiates;
- For member compression buckling, no increase in load can be applied;
- Compression members in the post-buckling regime exhibit strain softening behaviour;
- Chordal snap through buckling may result on initiation of softening behaviour;
- Members behaving inelastically which undergo strain reversal behave elastically.

Figures 3.1a to 3.1c represent the range of stress-strain complexities previously considered. The simplest representations of stress-strain behaviour assume a constant stiffness between yield load and buckling load with zero post-yield and post-buckling stiffness (see Figure 3.1a). As the load carried by the buckled member decreases with shortening a constant post-buckled force is assumed at a value below the buckling load. Figure 3.1b demonstrates a piecewise linearization of the post-buckling softening behaviour while Figure 3.1c demonstrates a more easily implemented stepwise linearization of this behaviour, which when applied with sufficient loading steps, is comparably accurate.


Figure 3.1: Varying degrees of idealized strut response linearization (Smith, 1984).

Smith (1984) defined a linearized description of stress-strain behaviour as is shown in Figure 3.2. The key aspects of member behaviour captured by linearized stress-strain curves, with reference to Figure 3.2, are (Smith, 1984):

1. virgin linear elastic
2. pre-buckling plateau
3. pre-buckling linear elastic
4. yield or buckling plateau
5. reversing linear elastic
6. post-buckling 'step down'
7. post buckling-reversing linear elastic

These can in turn be simplified to four regimes for computational implementation as follows:

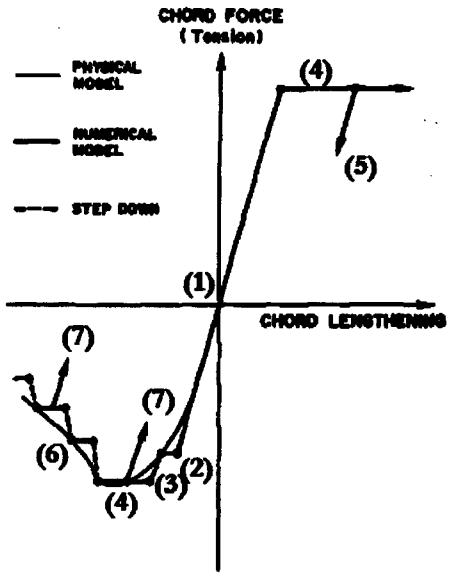


Figure 3.2: Stepwise linearization of numerical analysis procedure as developed by Smith (1984).

1. virgin linear elastic
2. constant force plateaux
3. reversing linear elastic
4. step down

The computational procedure for the implementation of these analysis methods is generally undertaken as follows (Smith, 1984): loading is introduced incrementally; for each load increment all members are checked to see if the element is to change regime, and if elements are to change regime then this is done in a zero load step; load stepping continues; when an element arrives at a constant force plateaux one of two procedures are followed:

- For updated stiffness matrix formulations the member is removed from the stiffness matrix and replaced with point loads; which are applied parallel to member orientation at each end, equal in magnitude to the bar force on reaching the plateaux;
- Or, as reformulation of the stiffness matrix for each load increment is computationally expensive, an alternative method has been used where fictitious loads are applied along the axis of each member. The magnitude of these loads is computed such that when used in conjunction with the initial stiffness matrix the result is equivalent to the stiffness of the structure minus members with zero stiffness (Smith, 1984).

Members which are removed from the stiffness matrix should continually be traced for load reversal, so that their contribution to global stiffness can be re-added to the stiffness matrix if required, although this has not always implemented.

Although Smith (1984) did not account for geometrical nonlinearities in the form of member displacement, this can be included in such analysis methods.

### 3.1.2 Effective Strength w.r.t. Buckling

The effective strength method of analyzing grids with respect to buckling is a method which can be employed in approximating the elastic buckling load of continuum representations of grid structures. This method is defined by Saka and Taniguchi (1992) as 'the strength represented in terms of stress resultants in a continuum plate and determined by periodic modes of elastic buckling deformation'. A general method of approximating effective strength of pin-jointed grids was initially developed. This method was then extended to determine the effective strength of rigidly connected lattice grids from periodic modes of elastic buckling under a uniform stress state without an overall buckling deformation (Saka and Taniguchi, 1992).

Saka and Taniguchi (1992) derived the effective strength of SOD and DOS DLGs using fundamental difference equations such that the effective bending strength could be determined by elastic buckling. Members considered consisted of uniform tubular members with rigid end parts and rotational springs connecting them, where the axes of the rotational spring coincided with that of the uniform member. The effects of member axial force were neglected in determining torsional rigidity. Member formulation allowed for the effects of rigid member ends and rotational stiffness to be investigated on the effective bending strength of the grid. The effect of web member rigidity on the effective bending strength of the grid was also considered. Saka and Taniguchi (1992) observed that the grid critical load decreased where rigid connections were employed; where pinned-connections were employed web stiffness was not observed to effect grid critical load.

Saka and Taniguchi (1992) found that the mode corresponding to higher-order deformations did not occur after a particular value of rotational spring rigidity was exceeded; furthermore, when the buckling mode corresponding to higher-order deformations occurred, the effective strength of the grid actually increased due to increased mobilization of restraint.



## 3.2 General Collapse Behaviour

A general introduction to grid collapse behaviour is undertaken through consideration of the affect of grid imperfections, point of failure initiation, chord failure, and effective strength of grid structures w.r.t. buckling, on grid collapse behaviour.

### 3.2.1 Grid Imperfections

Member damage and member geometry out of tolerance act to reduce the load-carrying capacity of grid structures in similar ways. Both factors effectively reduce the load-carrying capacity of individual members, predisposing those members to failure. Premature failure of individual members results in load redistribution to surrounding members and may initiate successive collapse.

#### 3.2.1.1 Member Damage

El-Sheikh (1999a) investigated the influence of web member damage on the behaviour of various corner- and edge-supported DLG configurations. The investigation was conducted by removing web members from a numerical structural model and conducting a non-linear failure analysis with the Abaqus finite element code. Members were removed from the model along both the centreline and a diagonal of the grid. The findings presented by El-Sheikh (1999a) can be summarized as follows:

- The most critical web members were those found at or around supports in corner-supported grids (as alternative load paths were limited);
- Edge-supported trusses were far less vulnerable to individual web failure than corner-supported trusses (there were more alternative load paths present resulting in better distribution of load);
- Failure behaviour remained unchanged except where members were removed near corner supports;
- There was no significant difference in response between different grid configurations, although SOS grids were slightly less sensitive.

#### 3.2.1.2 Geometrical Tolerances

Space grid structures are assembled from many components; consequently, the cumulative effect of member imperfections can be considerable. In this section the influence of member length imperfection, member out-of-straightness (member bowing) and member residual stresses are considered. The effects of these imperfections have been investigated through numerical analyses.

**Web member length imperfection** El-Sheikh (1999a) investigated the effect of geometric imperfections in the form of member length discrepancy on DLG configurations. A length discrepancy of 0.1%, of the perfect member length, was considered and imposed along the centreline and diagonal of corner- and edge-supported grid structures respectively. The worst case was considered by increasing the length of compression members and decreasing the length of tension members. The effect of member length discrepancy was included in a nonlinear analysis by applying an initial stress field to the members in question, using a pair of opposite but equal point loads at each end. Point loads were equal in magnitude to the elastic force required to lengthen or shorten the member by 0.1%. A 0.1% member length reduction to a tension member effectively reduced the tensile yield from $355N/mm^2$ to $155N/mm^2$ due to the initial stress state. It should be noted that the use of frame elements (an implementation of an idealized strut) in Abaqus does not allow for strain reversal.

The result of incorporating member length imperfections into the model on structural behaviour was much the same as for the web member damage investigation undertaken by the

same author. The reduction of grid strength for the case of web member length imperfection was not as severe as for the case of member damage. Grid strength reduction due to member length imperfection was 50-75% of the reduction resulting from member damage, since the member stiffness was not removed initially but rather reduced when the member failed for the case of length imperfection. A post-yield Young's modulus of E/20 and post buckling shortening behaviour with Young's modulus equal to zero was assumed.

El-Sheikh (1997) additionally investigated the effect of member length imperfections on TLG configurations, again with Abaqus, using a geometric nonlinear implementation of idealized strut assumption. Member behaviour was described as shown in Figure 3.3a. El-Sheikh (1997) accounted for member length imperfections by shifting the stress-strain curve, describing member behaviour, up or down the stress axis to account for members which were too long (Figure 3.3b) or short (Figure 3.3c) respectively.

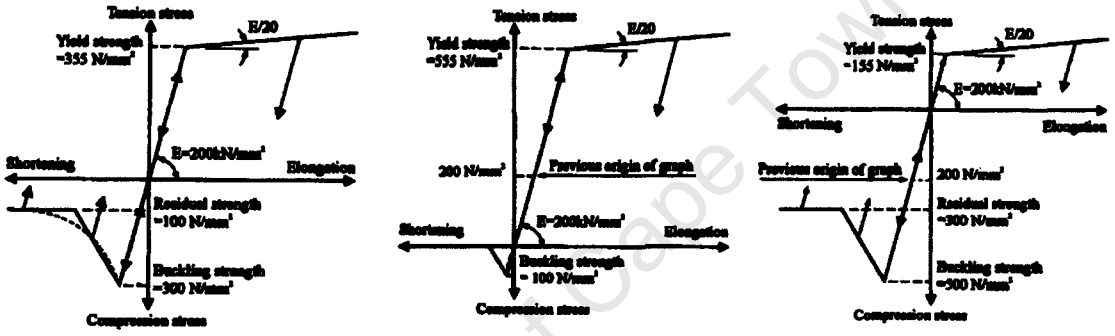


(a) Correct length (b) Member too long (c) Member too short

Figure 3.3: Member characteristics in tension and compression and effect of member length imperfection (El-Sheikh, 1997).

The results of the investigation showed that TLG structure sensitivity to member length imperfections, were most pronounced in the upper chord members, followed by lower chord members, web members and middle chord members respectively. As with DLG structures the critical location for member imperfections were located at the supports for web members, at the grid centre for chord members in edge-supported trusses, and at mid-span between supports for chord members in corner-supported trusses. Greater reductions in grid load-carrying capacity were observed, due to member length imperfections, in corner-supported grids when compared to edge-supported grids. This can be attributed to the number of alternate load paths. Failure occurred more quickly when initiated in the upper chord members when compared to failure initiation in the lower chord members.

### 3.2.2 Point of Failure Initiation

The increased sensitivity to imperfections in particular members, as detailed in Section 3.2.1, can be attributed to failure behaviour. When failure initiates through the buckling of an upper chord member, failure occurs more quickly and results in load redistribution to surrounding members pushing them towards their respective failure loads and increasing the probability of the initiation of successive collapse (El-Sheikh, 1997). Failure initiating in

bottom chord members through member yielding occurs comparatively slowly; initial failure is followed by local weakening of the truss and an outward spread of member yielding. The yielding of bottom chord members results in an increased load applied to the upper chord members directly above the yielded members and an eventual overload of an upper chord member. Overload of the upper chord member causes the chord to buckle and is generally followed by overall failure of the grid (El-Sheikh, 1997).

### 3.2.3 Chord Member Failure

El-Sheikh (1999a) reports on a parametric study which was undertaken on chord members in grid structures of the continuous chord variant. The investigation was undertaken using nonlinear numerical analysis. Channel, flanged channel and rectangular hollow sections were considered of varying slenderness and aspect ratios. Eccentricities at connections were also considered. Sensitivity of the cross-sections to connection eccentricity was evaluated. Two failure modes were observed: failure in pure bending and failure in combined bending and twisting.

The outcomes of the investigation were that rectangular hollow sections generally perform better than channel sections in continuous chord systems and that channels sections are more sensitive to load eccentricities than rectangular hollow sections.

## 3.3 Experimental Studies

A review of the experimental testing, and accompanying numerical analysis, of grid collapse behaviour is undertaken to identify the extent of previous work conducted, including achievements and shortcomings, and to identify experimental results appropriate for the validation of numerical DLG collapse analysis. Typical experimental methods and aims employed in the collapse analysis of DLG structures are introduced and used to categorize the literature presented.

### 3.3.1 Introduction

Where the experimental analysis of DLG structures has been undertaken, two general methodologies have largely been observed. The testing of DLG structures at small scales (1.5-3.75m) has been undertaken for the investigation of grid behaviour, omitting the effects of member and grid geometric imperfections, while the testing of larger grid scales has been undertaken to determine the behaviour of commercial systems, including the effects of imperfection associated with commercial tolerances.

Experimental testing of commercial systems has largely been undertaken for the purpose of validating design methods for 'real' structures. Results from the testing of commercial systems are therefore subject to the imperfections associated with structures fabricated

and assembled to conventional tolerances which include member imperfections, joint eccentricities, and locked-in initial stresses. The effects of connection behaviour are frequently simplified for design purposes and therefore experimental testing of commercial systems is also characterized by poor definitions of connection behaviour. Experimental results from the analysis of commercial DLG systems are consequently not generally appropriate for the validation of numerical models. Such experiments are characterized by many poorly defined variables which influence structure behaviour but cannot be appropriately incorporated into numerical models.

Testing at smaller scales has, consequently, been undertaken so that grid behaviour can be observed as far as possible without the effects of imperfections. Testing at smaller scales has predominantly been for the purpose of validating numerical models of DLG collapse behaviour and therefore account of connection behaviour has generally taken. Experimental analysis of grids undertaken at small scales, however, have largely been undertaken for the simplified case of a single cross-section and are consequently not representative of 'real' structures.



### 3.3.2 Experimental Aims

Experimental studies undertaken of the collapse behaviour of DLG structures were observed to fulfil two distinct experimental aims. Although not perfectly distributed chronologically, initial studies were generally undertaken with the aim of establishing grid behaviour while subsequent studies have generally tended to focus on ways of improving DLG collapse behaviour.

Regardless of the experimental scale, connection systems employed, and imperfections, experimental testing of DLG structures was found to provide valuable insight into grid behaviour. For the purposes of later comparison, the review of experimental research on DLG collapse behaviour is subdivided according to the respective experimental aims. The two categories of experimental aims considered are:

- Establishment of Grid Collapse Behaviour
- Improvement of Grid Collapse Behaviour

A discussion follows each section where a critical comparison is made between research studies.

### 3.3.3 Establishment of Grid Collapse Behaviour

Experimental testing of DLG structures to collapse has aimed to develop greater understanding of the mechanics of failure and collapse of such structures. The chronological development of such experimental work can broadly be summarized as follows:

- Collapse behaviour and the importance of geometric imperfections were established;
- Experimental results were sought for the validation of numerical methods, which were nominally free of the effects of imperfections;
- Commercial connection systems were evaluated including the effects of imperfections.

In addition to these cases further research has also been conducted into the peculiarities of grid structure behaviour such as kinematic instability.

#### 3.3.3.1 Initial Investigations

Schmidt et al. (1976) were among the first to express an interest in the failure behaviour of grid structures. They were motivated by the non-existence of experimental or theoretical work on the subject, despite their prevalence in industry.

Schmidt et al. (1976) consequently undertook the experimental analysis of three nominally identical SOS grids to failure and into the post-buckling regime. Grids were simply edge-supported at the bottom exterior nodes, had a mansard edge detail, and consisted of 6x6 modules of 0.305m long chord members. DLGs consequently had an edge-to-edge span of 1.830m; a depth of 0.216m was employed. Members were fabricated from aluminium and all had identical tubular cross-sections, of 12mm OD and 1.5mm wall thickness. Connections were achieved by end flattening the aluminium tube and using aluminium hubs of the Triodetic type. Load was applied equally to four nodes at the top level of the structure, corresponding to a 0.61m square symmetrical about the centre of the grid. The analysis was load controlled and the resulting total load measured with a precision load cell.

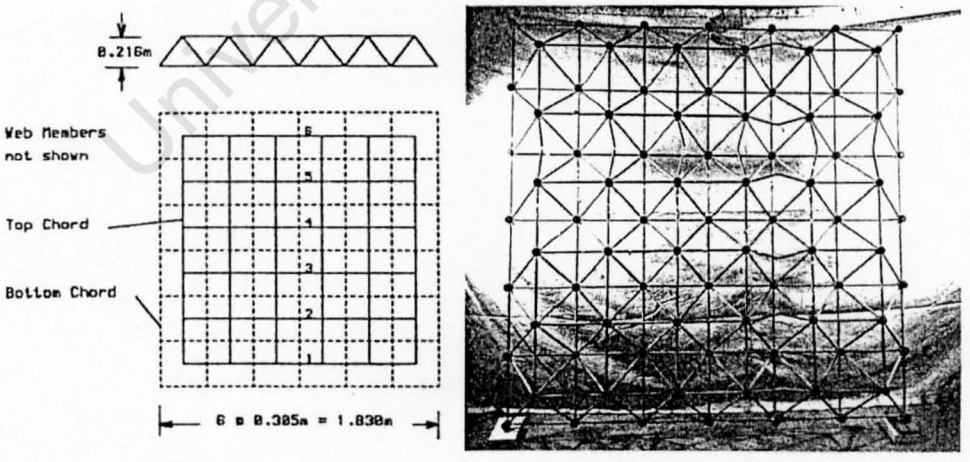


(a) Plan and elevation (b) Failure pattern

Figure 3.4: SOS DLGs as tested by Schmidt et al. (1976).

The results of the experimental test showed a stiffening of the structure in the elastic regime which is attributed to the tensioning of connections (see Figure 3.5).

Numerical modelling was concurrently undertaken using idealized strut behaviour based on individual member compression tests. Members were 'stocky'; consequently linear behaviour

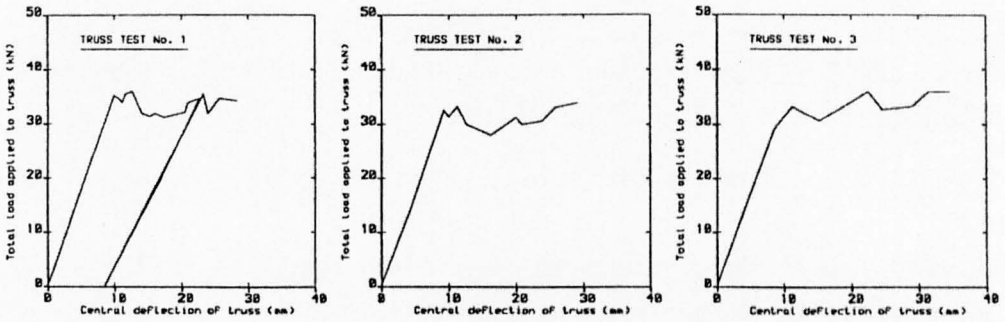


Figure 3.5: Experimental results of Schmidt et al. (1976), Test 1 was halted due to collapse of single support; elastic unloading and reloading of the structure is clearly evident after the support was reinstated. The failure behaviour was recoverable, the failure path resumed at the load observed prior to suspension of initial testing.

was assumed up to the tangent modulus. Once the tangent modulus was reached the member axial capacity was reduced to approximately 28% of the critical value. Analysis was undertaken as a series of elastic truss analyses where the applied load was scaled until a single member reached its critical load. The critical member was then replaced by a member with reduced axial capacity. Failure was guided towards a non-symmetrical pattern by initially removing one of the critical four central top compression chord members. Analysis was continued until two compression member collapse lines extended across the structure.

The comparison of experimental and theoretical results showed an over-estimation of system critical loads, this was attributed by Schmidt et al. (1976) to imperfections in the structure which resulted in non-symmetric load distribution and forced the structure towards a non-symmetrical failure pattern.

The development of collapse lines parallel to the truss edge is attributed the negligible torsional rigidity of individual members in the elastic range; Schmidt et al. (1976) notes that such a pattern would not develop in the rigid segments of a yield line pattern in a concrete slab.



#### 3.3.3.2 Validation

Collins (1981) undertook the analysis of four SOS grids with the purpose of validating a numerical method of grid failure analysis based on idealized strut behaviour. The view of Collins (1981) was that previous authors had blurred discrepancies between experimental and numerical results by attributing these to imperfections. Two resulting approaches were identified by Collins (1981) to overcome this previous shortcoming; the first was to undertake the experimental analysis of numerous grids, constructed to common tolerances, and develop a statistical description of the effect of imperfections on grid behaviour. Due to the resources required for such an approach a different approach was adopted. Collins (1981) undertook the experimental analysis by limiting imperfections as far as possible and, where previous authors had used semi-rigid connections of unknown stiffness, Collins (1981) designed a connection which would provide as close as possible to a full moment connection, so that

connection stiffness was clearly defined.

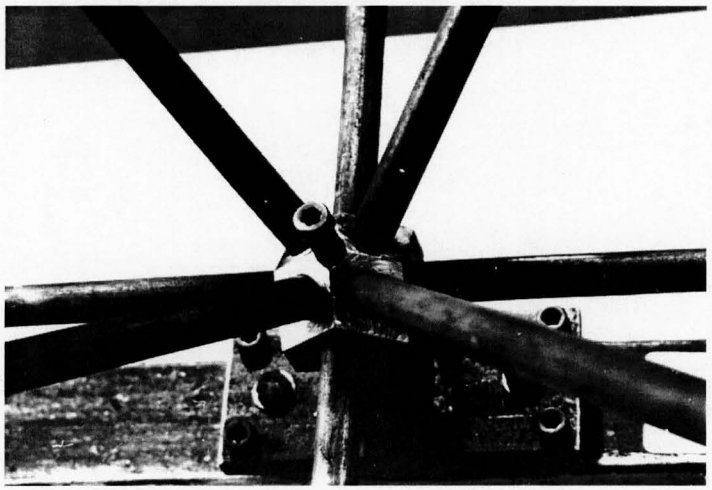

Figure 3.6: Node connection employed by Collins (1981) provided practical moment fixity. Grids were assembled on a jig to minimize 'locked in' stresses (Collins, 1981).

Four grids were tested by Collins (1981), which were nominally identical (although a different steel grade was used for Grid 4). Grids were corner-supported at the level of the bottom chords, had a mansard edge detail, depth of 0.255m and consisted of 5x5 modules with chord length 0.360m, resulting in a total span of 1.800m between adjacent supports. Grids were tested under two point loading, applied at the top chord level by actuators. Experiments were displacement controlled so that the full grid failure behaviour could be observed. Load configurations were varied for each grid; Grid 3 and 4 shared the same loading pattern.

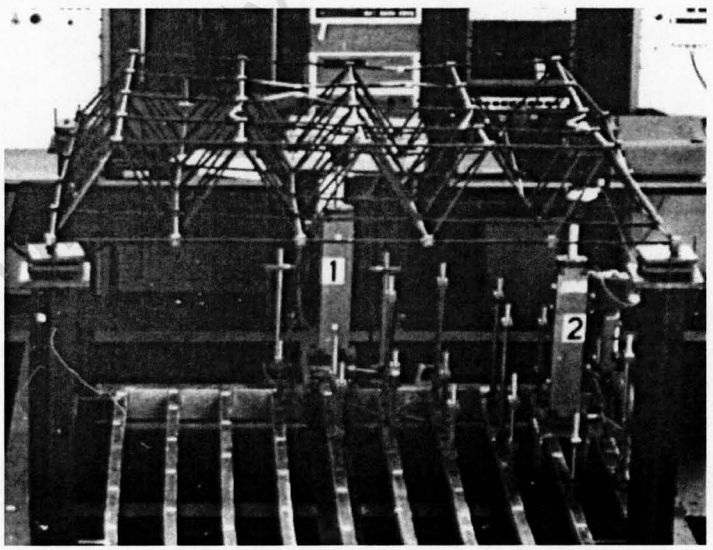


Figure 3.7: Collins' experimental set-up with grid on test frame, actuators and displacement transducers (Collins, 1981).

The results of Collins (1981) highlighted the potential for sudden failure behaviour of DLG structures, with significant and sudden drops in grid resistance observed following compression chord buckling. Symmetry of the deflection field in the elastic regime is indicative of the high degree of accuracy achieved in fabrication and assembly. Although a near symmetric failure path was observed for Grid 1, this was not the case for Grids 2-4.

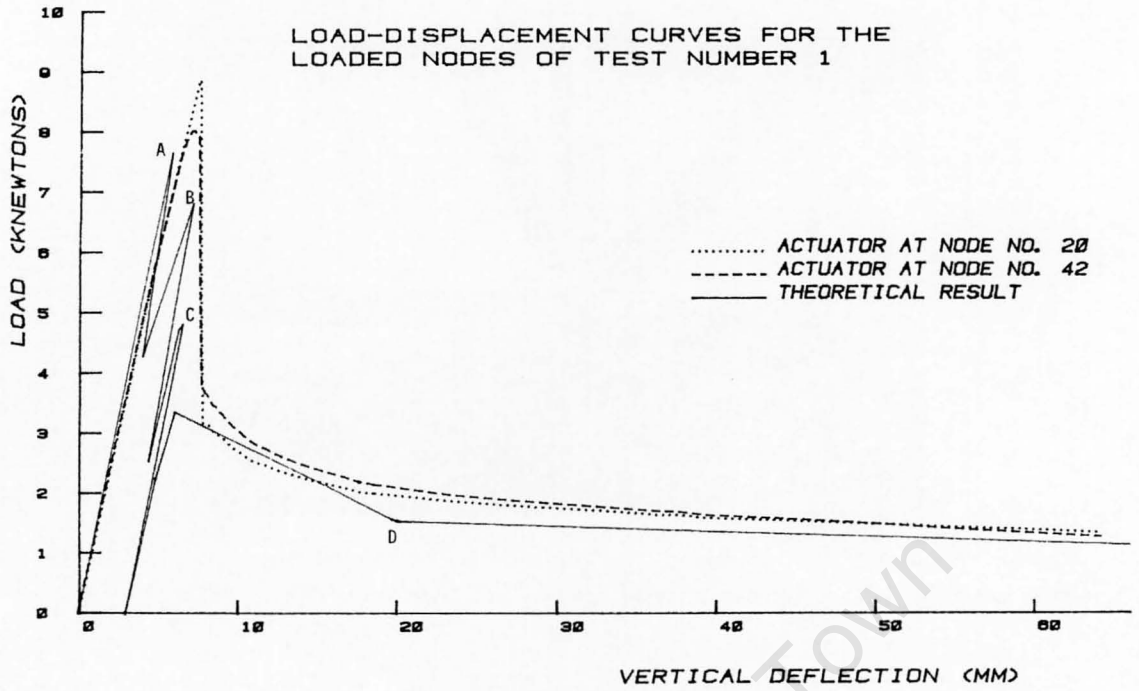


Figure 3.8: Comparison of load-displacement results for experimental and numerical analysis of Grid 1 (Collins, 1981).

Comparison of the experimental and numerical analysis results show good correlation of critical load (this is expected as strut critical loads used in numerical analysis were as measured in the experimental analysis); however, the post-buckling behaviour is less closely matched but still demonstrates good correlation between results (see Figure 3.8). Collins (1981) used a similar approach to Schmidt et al. (1976), employing a series of elastic analyses, geometric nonlinearities were not considered. Collins (1981) extended the numerical analysis method developed to the analysis of six 35x35m grids of various geometrical configurations of the Nodus type system; however, this study was restricted to grids constructed of the same cross section throughout.



#### 3.3.3.3 Commercial Systems

Schmidt et al. (1982) presents the experimental analysis to failure of 12 DLG structures, which are categorized as model tests, with spans ranging from 3 to 8ft, and large scale tests, with spans of 24 and 31ft. The grids tested included aluminium and steel structures and welded, bolted and proprietary connection systems. Particular attention was paid to joint slip and the presence of initial stresses resulting from assembly and / or welding. Due to the large variety of grid structures considered it is difficult to make any valuable deductions. The one trend that was evident, however, was that grid structures of high indeterminacy are more susceptible to imperfections. Comparison was made between experimental and theoretical analysis of the structures, in all cases the critical load was over estimated. Errors in prediction of grid critical values varied between 13% and 37%.

Fulop and Ivanyi (2004) conducted an experimental study of the elastic and failure behaviour of the proprietary space truss system, named TOP-SYSTEM, consisting of cold formed square hollow sections, welded connection plates and bolted connections. A single grid was tested three times, twice in the elastic regime (under symmetric and non-symmetric single point loads), while the third test was to failure. The grid tested consisted of a 3x3 SOS grid, with mansard edge detail, a member length of 1.20m and a grid depth of 0.849m. All members shared the same cross-section. The grid was corner supported resulting in a span of 3.6m. Experiments were said to be displacement controlled, but were stopped before the full failure behaviour could be observed. Loading was applied to the top central node for the final case considered, which was conducted till failure was observed.

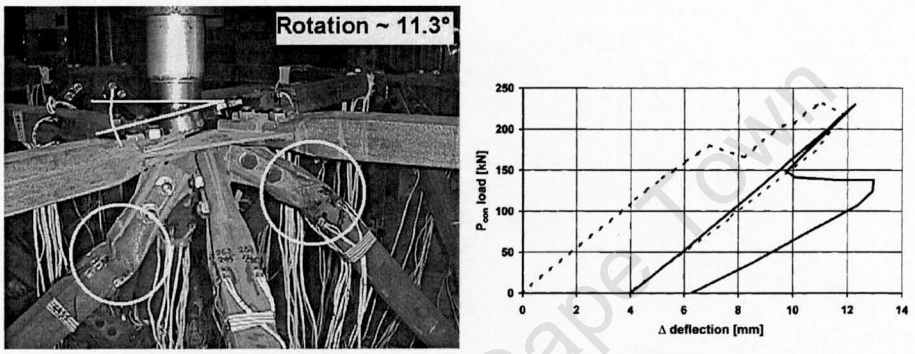


(a) Rotation of top centre node

(b) Load displacement behaviour of top centre node

Figure 3.9: Failure initiation due to rotation of TOP-SYSTEM node (Fulop and Ivanyi, 2004).



Failure of the grid was due to a sudden rotation of the top central node connection; the magnitude of this rotation was approximately 6.5° and increased to 11.3° by the time the experiment was terminated. Snap back behaviour was observed at failure, although it is not clear how this was observed under displacement control. Data recorded by strain gauges connected to individual members in the truss were decomposed into axial, torsional and bending components. The semi-rigid behaviour of the connections was evident through plots of bending moment and external load.

In addition to conventional node-bar systems, some authors have focused on DLGs with end-flattened member connections, of both continuous chord and nodal varieties. End-flattened connections systems result in grids which are typically dominated by the instability behaviour of chord and web members in close proximity to the connections; consequently the investigation of de Andrade et al. (2005) focused on methods of reinforcing these connections. Due to the dominance of local instability in grids with end-flattened joints, these studies tend not to reveal too much regarding the global behaviour of space grid structures. Studies by Malite et al. (2001), de Andrade et al. (2005), and Bezerra et al. (2009) deal extensively with matters relating to the behaviour of grids with end-flattened members including experimental and numerical work, but do not extend such work to the post-buckling regime of grid behaviour.

#### 3.3.3.4 Edge Beams

Saka and Taniguchi (1994) conducted small scale experimental testing of SOD and DOS DLG structures of module size 4x4 and 6x6. The purpose of the Saka and Taniguchi (1994) investigation was to evaluate the influence of boundary members on restraining unstable deformations. Models were constructed of brass and were tested with and without edge beams of varying stiffness; a total of 15 grids were tested. A detailed description of the experiment, element strength and node rotational stiffness are provided by Saka and Taniguchi (1994) as well as a numerical buckling load analysis. Grids were loaded at the level of the square mesh under uniformly distributed loading; experiments were load controlled. The depth of grids tested was 0.165m. Chord members in the grid layer with the square configuration were 0.330m long, resulting in grid plan dimensions of 1.320x1.320m. As compression chord member lengths were different for DOS and SOD grids, compression chord slenderness values were kept constant.

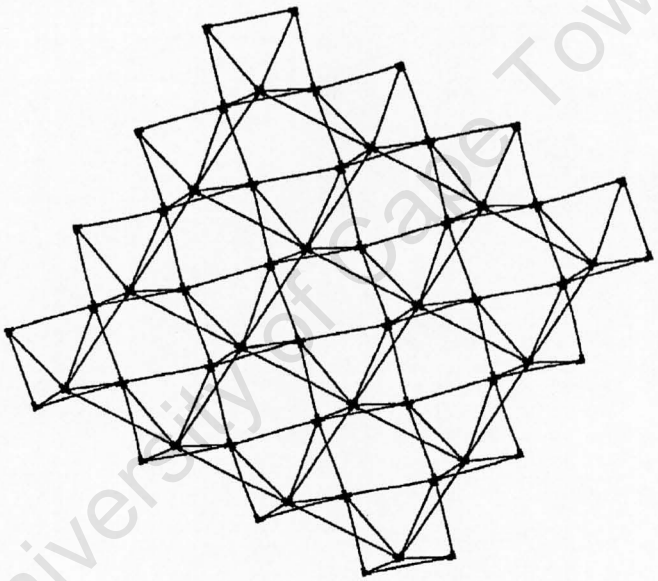



Figure 3.10: Buckled mode of DOS grid as tested by Saka:1994.

The displaced shape and load displacement behaviour of one of the 4x4 DOS grids tested by Saka and Taniguchi (1994) are shown in Figures 3.10 and 3.11 respectively. The results of the Saka and Taniguchi (1994) investigation can be summarized as follows:

- SOD grids were observed to have limited ductility after initial buckling;
- DOS grids did not exhibit any ductility after initial buckling;
- Boundary members were found to be effective in controlling the buckling of DOS grids but not SOD grids;
- Deformation capacity of SOD grids was observed to be smaller than that of SOS grids.

The concurrent numerical analysis was undertaken by Saka and Taniguchi (1994) using an Eigen-value extraction method to calculate critical values. The numerical analysis consid-

ered a uniform element with rigid end parts and rotational springs. A comparison between the experimental and numerical results obtained, demonstrated a good correlation between critical grid resistance values. The values for grid critical resistance, obtained from numerical analyses, were within the range of 94% to 122% of the experimental values. As experimental testing was undertaken with load control, however, the results could not be used for the purpose of validating nonlinear numerical analysis methods.

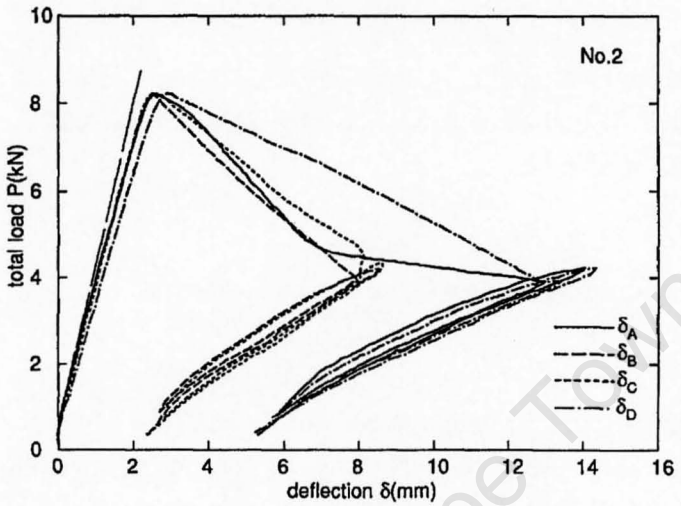


Figure 3.11: Load-displacement behaviour, for various locations, of 4x4 DOS grid tested by Saka and Taniguchi (1994) under load control.

#### 3.3.3.5 Comments

End-flattening of bars for connections, as undertaken by Schmidt et al. (1976) and Schmidt et al. (1982), introduces additional imperfections into DLG structures and adds significant complexity to behaviour. The use of end-flattened connections combined with geometric imperfections, at member and grid levels, results in non-symmetrical failure behaviour as observed in the results of Schmidt et al. (1976) and Schmidt et al. (1982). Non-symmetrical failures were also observed in the results of Fulop and Ivanyi (2004), Collins (1981) (Grids 2-4) and Saka and Taniguchi (1994); as end-flattened members were not used for these cases the divergence from symmetry of the results can only be attributed to member and grid geometric and material imperfections. Collins (1981) acknowledges the importance of symmetry in the failure behaviour of grid structures noting that the random distribution of imperfections in a grid structure will seldom result in a symmetric failure path.

The use of load-control by Schmidt et al. (1976), Schmidt et al. (1982), Saka and Taniguchi (1994), and possibly Fulop and Ivanyi (2004), results in an inaccurate representation of post-buckling behaviour as the structure's equilibrium path is traced and consequently the full collapse path of the structure is not developed.

Numerical collapse analysis, which accompanies the experimental analysis of Schmidt et al. (1976) and Collins (1981), neglects non-linear geometric effects and consequently is believed to over-estimate post-buckling grid capacity. The numerical analysis of Saka and Taniguchi

(1994) appears to be the most accurate at predicting grid critical loads; however, as this is an Eigen value extraction method, this cannot be used to investigate post-buckling behaviour.

Collins (1981) and Saka and Taniguchi (1994) both take account of connection stiffness in their numerical studies, while other authors assume pinned connections. Collins (1981) accounted for connection stiffness by employing connections which effectively provide fixed rotational restraint, while Saka and Taniguchi (1994) employ a beam element with elastic end restraints, for which appropriate values of stiffness are experimentally measured.

The experimental results of Collins (1981) demonstrate potential for use as a benchmark in the failure analysis of grid structures; however, there is confusion regarding the material yield strength of the steel used.

### 3.3.4 Improvements to Grid Critical Behaviour

Sudden collapse behaviour of DLG structures, initiated without warning, is undesirable due to safety considerations and for this reason various authors have investigated methods of introducing ductility into grid collapse behaviour. Owing to the complexity of structural collapse these structural improvements have largely been evaluated experimentally. Introducing nonlinear behaviour prior to collapse is considered a behavioural improvement, as this provides warning of imminent failure. Methods previously employed to induce such non-linear behaviour prior to collapse include: tensile yield of chord members; gradual buckling of compression chord members, by employing 'soft' members or member eccentricities; and reduction of compression chord instability through the use of composite action or continuity of chord members.



#### 3.3.4.1 Tensile Yield

Schmidt et al. (1980) undertook large scale testing of a DLG of SOD configuration. The purpose of the study was to assess the merits of allowing for considerable tension chord yielding prior to compression chord buckling.

The structure tested by Schmidt et al. (1980) was designed using numerical analysis based on idealized member behaviour which accounted for both member yielding and buckling. A proprietary connector, the Bamford Joint, was used. The grid was square in plan at the level of the top chords and consisted of 7x7, 1.372m modules; the structure was simply edge-supported at this level and spanned a distance of 9.60m edge to edge. The structure was assembled to normal construction tolerances. Load was applied at the level of the lower chords at each inner node. Schmidt et al. (1980) states that load was applied using a load distribution system that ensured the application of equal vertical loads at each point; however, no further information was provided.

Experimental results show that inelastic behaviour occurred initially through tension yielding of the bottom chord members. Tension yielding was initiated in the most highly loaded

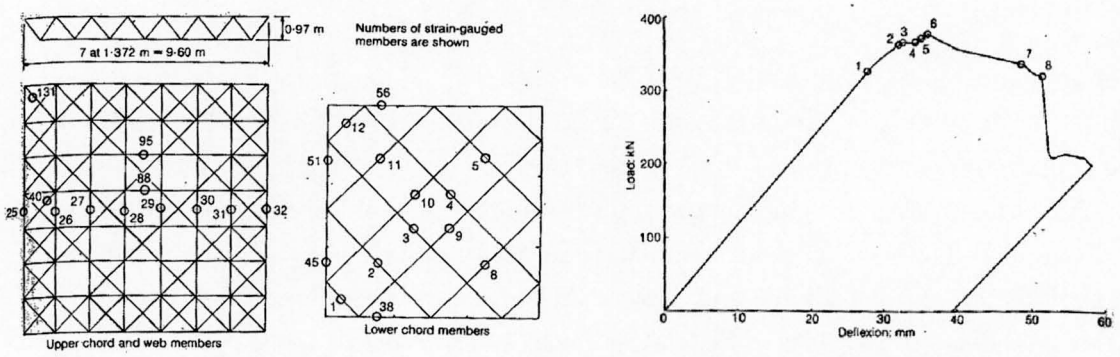


(a) Plan and elevation

(b) Load displacement behaviour

Figure 3.12: SOD DLG as tested by Schmidt et al. (1980).

bottom chord members (see Figure 3.12a for observed failure order). A decrease in grid stiffness through tension yielding was observed but hardening behaviour was maintained.

On first buckling of the compression chord members, the structure entered a softening regime. First buckling occurred for top chord members at the centre of the grid.

The experiment appeared to be load controlled due to the cut-back nature of the load displacement graph, although this is not clearly stated. The residual strength of the grid is not evident as the full failure path of the structure was not developed. As with previous work undertaken by Schmidt et al. (1976), symmetry of deformation was lost in the elastic region of the structure behaviour. This resulted in a reduction to the structure critical load as force concentrations occurred. Rotation of joint blocks is furthermore identified as a possible reason for the reduction in observed critical chord load (see Figure 3.13).

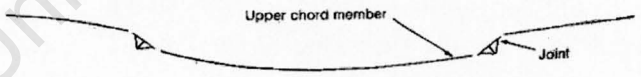


Figure 3.13: Joint block rotation is believed to have reduced member critical loads (Schmidt et al., 1980).

Testing undertaken by Schmidt et al. (1980) allowed for the full scale effect of grid structure behaviour to be accounted for. Considerable initial 'locked in' member forces were observed which were attributed to construction tolerances and construction sequencing. 'Locked in' stresses of up to 9% of the material yield stress were observed. 'Locked in' stresses were observed to become especially significant as they tended to adopt the same sign as the load in members. Ductility behaviour of the structure was observed after the critical load was reached but this is believed to have been limited by the joint stability behaviour (Schmidt et al., 1980).

Parke (1988) also investigated the potential for designing DLG structures for the tensile yielding of chord members to improve DLG failure behaviour. DLGs tested were of smaller

dimensions than those tested by Schmidt et al. (1980) and were of SOS configuration, but were constructed to more stringent tolerances (see Section 3.3.4.2 for a description of the experiment).

The results of the experimental work of Parke (1988) show significantly increased pre-critical nonlinear behaviour of Models 1 and 2 which were designed for tensile yielding; this is particularly attractive from a design perspective due to the warning provided by significant structural deflections prior to collapse. The feasibility of the design tested by Parke (1988) is questioned; however, as solid members were used for the compression chord members in these grids to prevent buckling and allow sufficient strain to develop in the tensile chords for yielding, this is not believed to be feasible for 'real' structures.

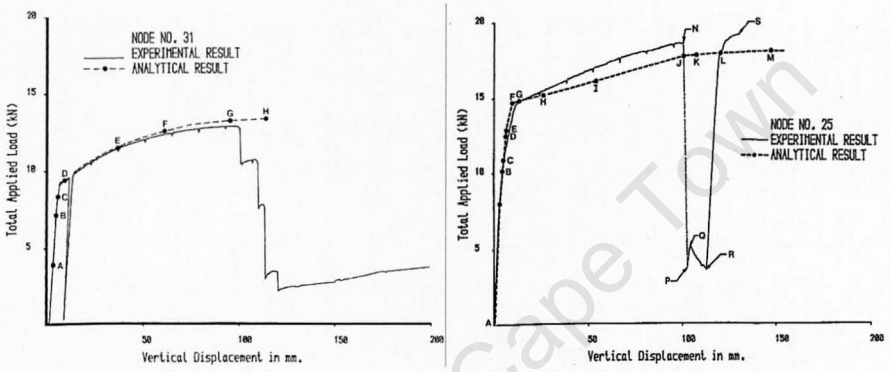


(a) Model 1 (b) Model 2

Figure 3.14: Experimental and analytical load displacement behaviour of grids designed for tensile yield (Parke, 1988).



#### 3.3.4.2 'Soft' Chord Members

Parke (1988) aimed to improve the load displacement behaviour of grid structures to failure by allowing for considerable tensile yielding of the bottom chord members (see Section 3.3.4.1) and the substitution of 'soft' members for the top chord members. 'Soft' members incorporating force limiting devices (FLDs) are designed to give individual compression members ductile failure behaviour such that a load plateau is observed after the critical compressive load of the member is reached; this is in contrast to conventional post-buckling behaviour which is characterized by a sudden decrease in load resistance. It was reasoned that the incorporation of such 'soft' members would result in a more ductile response.

The FLD designed by Parke (1988) consists of an inner and an outer tube which fit into each other, and four additional metal strips which connect the ends of these two tubes, see Figure 3.15. When the FLD member is in compression, the compressive tube loads are resisted by the metal strips which are placed into tension. The FLD is designed so that when the member critical load is reached the metal strips begin to yield in tension. The failure behaviour of the FLD in compression is, consequently, similar to a general tensile failure. For FLDs to be effective the stability of the member should be maintained; the FLD member therefore should also be designed to resist buckling.

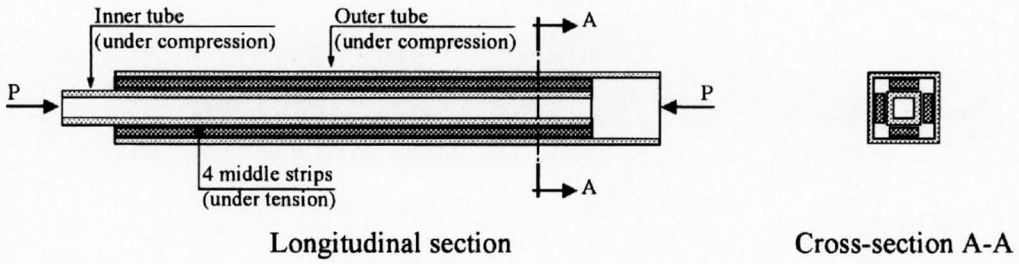


Figure 3.15: Force limiting device as proposed by Parke (1988) (El-Sheikh, 1999b)

Four grid structures were tested to failure: two to investigate the effect of tensile yielding, and two to investigate the influence of 'soft' compression members. The grids were nominally identical to those tested by Collins (1981), including, support conditions, fixed connection detail, fabrication and assembly methods. Experiments were displacement controlled. Test models 1 and 4 were loaded at the top centre node, while test models 2 and 3 were loaded at 4 top nodes, in a square pattern symmetrical about the grid centre. Member sizes and distribution are as shown in Figure 3.16

| Member type | Outside Diameter (mm) | Wall thickness (mm) | Cross-sectional area ($mm^2$) | Use |
|---|---|---|---|---|
| T1 | 4.76 | 0.91 | 11.00 | Tension members Models 1, 2 and 3. |
| T2 | 6.35 | 1.22 | 19.66 | Tension members models 4. Soft member inner tube. |
| T3 | 7.94 | 0.56 | 12.98 | Soft Member middle tube. |
| T4 | 9.52 | 0.71 | 19.65 | Soft Member outer tube. |
| T5 | 9.52 | 0.91 | 24.61 | Web members models 1, 2, 3 and 4. Top chord members models 3 and 4. |
| T6 | 10.00 | Solid | 78.54 | Top chord members models 1 and 2. |

Figure 3.16: Member sizes used in the experimental testing of Parke (1988).

The benefits of the substitution of 'soft' members for compression chord members resulted in the improved ductility of the structure represented by Grid 3 but not for the case of Grid 4; Model 4 exhibited sudden failure behaviour which was not preceded by any nonlinear response.

The numerical method of analysis employed by Parke (1988) fails to accurately track the post-buckling behaviour; this is thought largely to be due to geometric nonlinear effects which were not considered. As collapse progresses, lines of failed members extend across the grid significantly exposing the post-buckling response of the structure to geometric nonlinear effects.

Despite the introduction of significant pre-critical nonlinear behaviour into the structural responses of Grids 1-3 all cases were additionally characterized by significant drops in load resistance in the post-buckling regime. Consequently when the critical load of such structures is exceeded, collapse of the structures will follow.

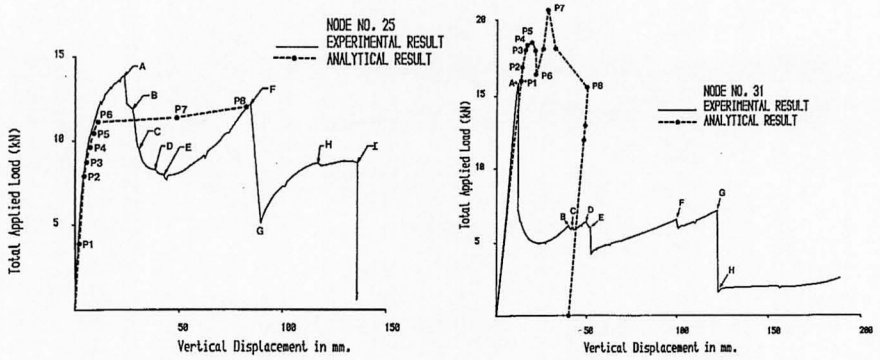


(a) Model 3 (b) Model 4

Figure 3.17: Experimental and numerical load-displacement behaviour of grids designed with soft compression members (Parke, 1988).

### 3.3.4.3 Chord Eccentricity

Mwakali (1990) investigated the collapse behaviour of DLG structures incorporating eccentrically loaded T-section members. Mwakali (1990) hypothesised that, by using the smoothed buckling behaviour of eccentrically loaded compression members, the brittle failure behaviour of grid structures could be transformed to a more ductile failure mode. Numerous tests of individual members were undertaken to determine the optimal balance between improved ductility in failure and reduction in load resistance for this purpose.

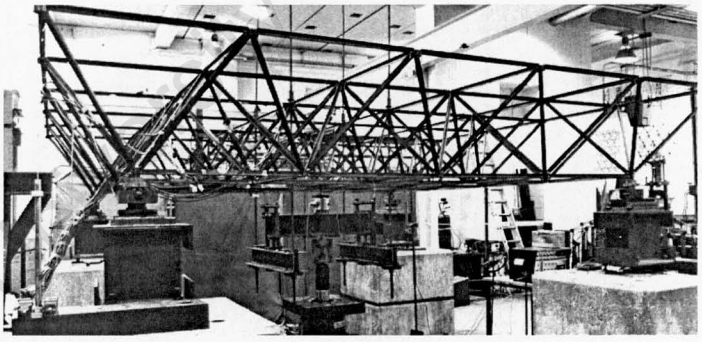

Figure 3.18: SOS, corner-supported, cornice DLG assembled of T-sections (Type-1) as tested by Mwakali (1990).

Two types of grid were tested experimentally by Mwakali (1990). The initial grid tested, Type-1, was a SOS, 5x5 module, bottom corner-supported DLG of member length 749mm, constructed with welded connections of the triodeteic type (see Figure 3.18) and a mansard edge detail. Top chord members were connected with an eccentricity of 5mm. Load was applied under displacement control at the four top nodes closest to and symmetrical about the grid centre. The results of this grid test showed no significant variation from conventional concentrically connected grids. The lack of variation from conventional grid behaviour was not known, but was attributed either to the non-existence of actual connection eccentricity in the grid assembly or the global restraint effects on member behaviour differing from member behaviour tested in isolation.

A second grid configuration, Type-2, was consequently tested by Mwakali (1990). This grid was smaller, 2x2 module, SOS grid configuration, with mansard edge detail and chord length 749mm. Compression chord members were eccentrically connected with a bolted connection; all other connections were welded. Corner web members were round bars to avoid web failure at the supports. Support and load configurations were as for Type-1. Six Type-2 grids were tested, which differed in top chord eccentricity; eccentricities of 0mm, 5mm, 10mm and 15mm were considered.

Accompanying numerical analysis of the structure, undertaken with idealized strut behaviour resulted in over-estimation of critical loads.

It was found that increasing eccentricity reduced the structure ultimate load, resulted in a more rounded attainment of ultimate load, and an increased ductility in the post-critical regime (see Figure 3.19). Numerical analysis showed that the increase in ductility behaviour of the Type-2 grid was less than for Type-1 grids due to the small scale of Type-2 grids with fewer alternate load paths after initial failure. However the difficulty associated with implementing an appropriate value of member eccentricity make the appropriateness of such a method for improving grid ductility behaviour questionable, especially when considered within the context of typical construction tolerances.



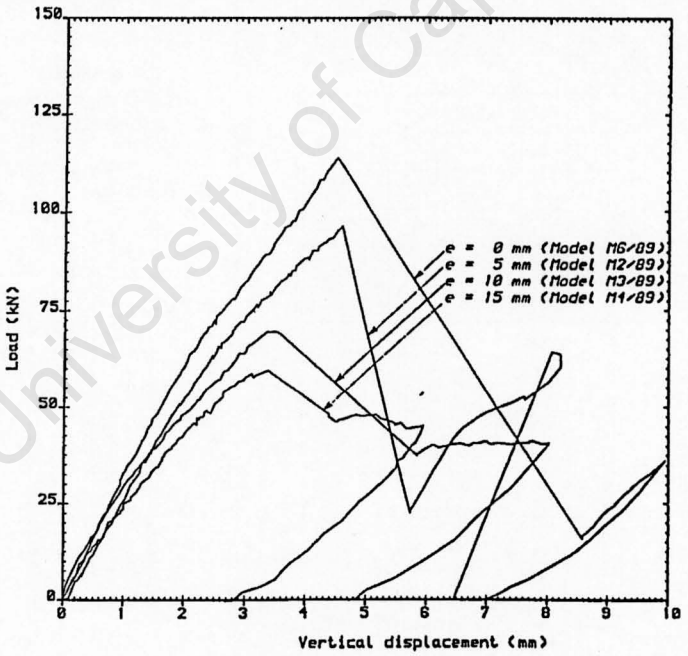


Figure 3.19: Effect of compression chord member eccentricity on Type-2 grid load-displacement responses (Mwakali, 1990).

#### 3.3.4.4 Composite Action

El-Sheikh and McConnel (1993) investigated the effect of composite action on the failure behaviour of DLG structures. Traditional composite structural systems use more than one material, so that the respective strengths of the selected materials can be exploited. For the

case of DLG structures a concrete slab was used to restrain instability of top chord members.

El-Sheikh and McConnel (1993) considered SOS, 5x5 module, cornice edge detail, corner-supported DLG structures for their investigation. Three girds, named Truss 1-3, of nominally identical geometry were tested to failure. Load control was used and load was applied in 4kN increments. Each grid consisted of 0.8m modules, with plan dimensions of 4m x 4m, spans between supports of 3.2m and a depth of 0.575m. Upper chord members were channel sections (flanges pointing upwards), webs at supports were round bar sections and all other sections were circular hollow sections; Mero node connectors were used. Load was applied at the intersection of the top chords at 16 points by an articulated load frame which allowed for a relatively uniform distribution of load to be applied.

The grids considered were designed to investigate the failure behaviour of grid structures and to validate the viability of composite behaviour on grid structures. Experimental results were additionally used to validate a numerical analysis method for composite and non-composite space grids, based on a 2-noded beam element with end springs and a 4-noded plane stress element for the concrete slab. Experimental analysis of the connection stiffness was also undertaken.

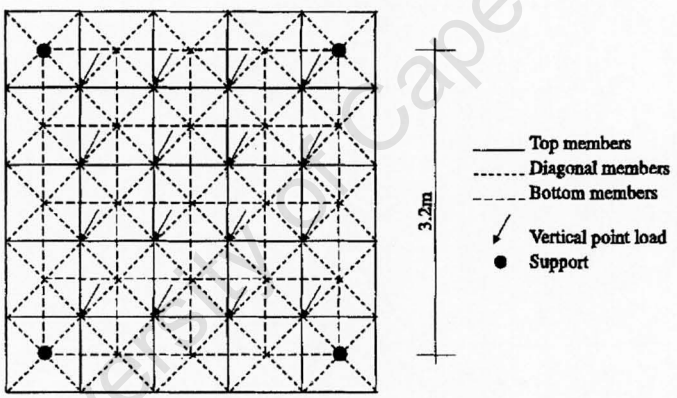


Figure 3.20: Double layer, corner supported, cornice, SOS truss as tested by El-Sheikh and McConnel (1993).



Truss 1, a non-composite grid was designed with over-strength top chord members to investigate the effectiveness of the use of over-sized members in preventing the problem of sudden decrease in load resistance following top chord buckling. Trusses 2 and 3 were designed with the purpose of investigating the effects of composite action and were designed with identical steel work. Truss 2 was a non-composite structure which was tested to assess the load-carrying capacity of the grid during the construction stage where wet concrete was to be supported by the structure before concrete strength and composite action have been developed; the case of propped construction was not considered. Truss 3 was designed as a composite truss; shear studs allowed for shear interaction between the grid and the hardened concrete slab and were designed so that failure did not occur prior to the intended design load, calculated through the use of experimental push out test results.

The experimental results of El-Sheikh and McConnel (1993) show a significant increase in the load capacity of the composite grid and an improvement in failure behaviour, resulting

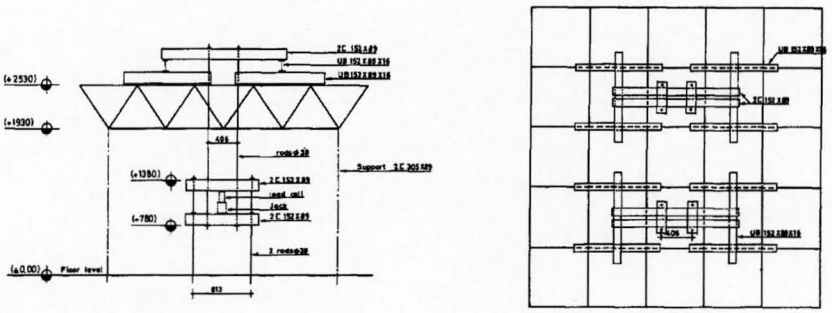

(a) Elevation (b) Plan

Figure 3.21: Articulated load frame used by El-Sheikh and McConnel (1993) to apply UDL to grid.

in a more ductile failure pattern. Although load control was used, post-critical structural resistance was re-established; this is believed to be due to the ductile nature of critical behaviour. In the comparison of the numerical and experimental results of El-Sheikh and McConnel (1993), the following observations are made regarding the numerical analysis method:

- Critical loads are overestimated;
- Post-buckling residual capacity is overestimated, possibly due to the use of load control in analysis;
- The loss of composite action due to shear stud failure is not captured.

The testing undertaken by El-Sheikh and McConnel (1993) is significant as this was the first experimental investigation which considered the affects of semi-rigid connection stiffness and clearly defined the method employed for the application of distributed loading in elastic and post-buckling regimes. Due to omissions regarding material and element cross-section properties, the use of load control, and the use of slender channel sections, the results are not suitable for the purpose of verification. Use of slender cold-formed and hot-rolled channel sections, as compression chord members, introduces significant additional complexity in structural behaviour as local buckling was observed to interact with member flexural buckling.

#### 3.3.4.5 Continuous Chords

El-Sheikh and El-Bakry (1996) undertook the experimental study of the Catruss system, a continuous chord space truss design. The testing undertaken was nominally identical to that undertaken of the Nodus system with composite and non-composite behaviour by El-Sheikh and McConnel (1993) including geometry, loading and support conditions. Three trusses were designed and tested; Truss A was designed with over-sized compression chord members; Truss B was designed with under-sized compression chords to investigate the effects

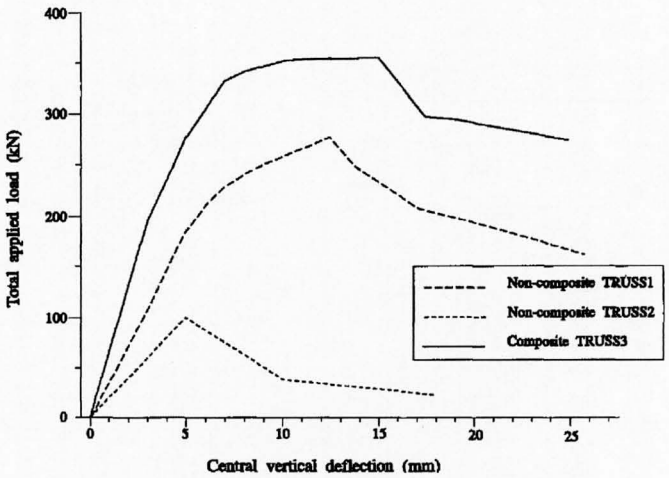


Figure 3.22: Comparison of experimental results for composite and non-composite DLGs (Truss 1-3) (El-Sheikh and McConnel, 1993).

of local member buckling; Truss C was identical to Truss B, but included chord splices in all top and bottom panels to represent a worst case scenario. Experiments were load controlled and consequently the full failure behaviour was not captured.

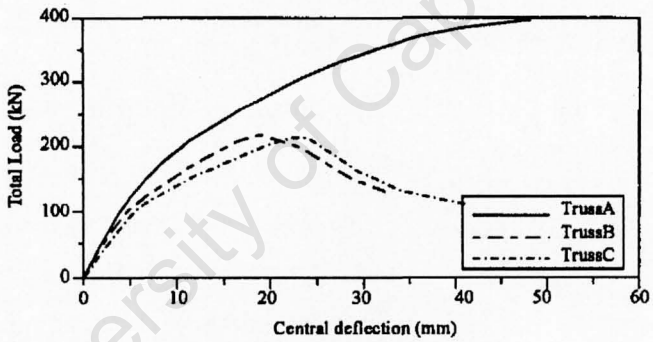


Figure 3.23: Load-displacement behaviour of Catruss DLGs tested under load control by El-Sheikh and El-Bakry (1996).

The results of the experimental testing show significant ductility behaviour which is attributed to the eccentricities and continuity of compression members across joints (see Figure 3.23). The effect of chord splices on grid behaviour appeared to be minimal, resulting only in a slight reduction of structure stiffness. The use of load control is unfortunate as it is possible that the end of the published load displacement curves may signify the point at which a sudden decrease in resistance was encountered.

#### 3.3.4.6 Comments

Comparison of the effectiveness of the methods identified for improving grid behaviour is complex, as the experimental cases considered differ considerably, as do the experimental controls employed.

As with experimental investigations concerned with the establishment of DLG behaviour

(Section 3.3.3) the use of load control results in post-buckling behaviour not following the true failure path. Schmidt et al. (1980), El-Sheikh and McConnel (1993) and El-Sheikh and El-Bakry (1996) all employ load control, however, it is interesting to note the difference in failure behaviour between El-Sheikh and McConnel (1993) and Schmidt et al. (1980). The more ductile critical behaviour of a composite concrete slab-steel DLG, as tested by El-Sheikh and McConnel (1993), allows for the progression of grid failure to extend past the critical resistance and re-establish resistance in the post-buckling regime; this is not the case for the standard DLG tested by Schmidt et al. (1980) (see Figures 3.12b and 3.22).

Use of composite action, as employed by El-Sheikh and McConnel (1993), can be considered to offer the greatest improvement to DLG behaviour. Use of composite action, however, effectively changes the structure type.

The design of DLG structures for tensile yield appears to result in significant nonlinear behaviour prior to the achievement of critical load but post-buckling behaviour is still characterized by sudden and large decreases in structural resistance. The results of Parke (1988) appear to be more promising than those of Schmidt et al. (1980) with respect to the development of chord yield. The grids tested by Parke (1988), however, were designed with oversized compression chord members and therefore the results of Schmidt et al. (1980) are more likely to be indicative of the degree of nonlinearity which can be introduced into actual full scale structures.

Improved DLG collapse behaviour through the use of chord members with eccentric connections, as undertaken by Mwakali (1990), although promising when undertaken on members in isolation, appeared to be difficult to achieve on DLG structures in practice.

The use of 'soft' members, as investigated by Parke (1988), appeared to offer the least promising improvement to DLG collapse behaviour, with one of the two such grids tested failing suddenly.

Continuous chord system grids, as tested by El-Sheikh and El-Bakry (1996), appear to offer significant improvements in grid ductility over non-continuous systems. However, the use of load control did not allow the full failure behaviour to be established.

Connection stiffness was accounted for in the numerical analysis by Parke (1988) and Mwakali (1990) by considering fixed end restraints. El-Sheikh and McConnel (1993) determined the moment-rotation behaviour of connections experimentally and included this in numerical analysis through the use of elements which account for elastic end restraints.

Idealized strut assumptions regarding member behaviour, employed in the numerical analysis of Schmidt et al. (1980), Parke (1988), Mwakali (1990) and El-Sheikh and McConnel (1993) did not account for geometric nonlinearities and were consequently observed to over-estimate post-buckling behaviour where post-buckling behaviour was considered.

## 3.4 Grid Failures

The nature of past grid failures emphasizes the potential for the catastrophic failure of such structures. Two failures are considered, one resulting from under-design and one from overload; however both failures resulted in total collapse. These failures act as a motivation for greater consideration of grid pre-critical nonlinear behaviour in the design of grid structures, so that even if such structures should fail the occupants of the building have time to escape prior to total collapse.

### 3.4.1 Hartford Coliseum Roof, U.S.A.

The failure of the Hartford Civic Centre Coliseum roof in Connecticut, U.S.A. occurred in January 1978, 5 years after the completion of construction. The failure of the structure prompted much research into the design and behaviour of space grid structures. The structure failed suddenly highlighting the catastrophic potential of structures which fail without exhibiting any signs of collapse.

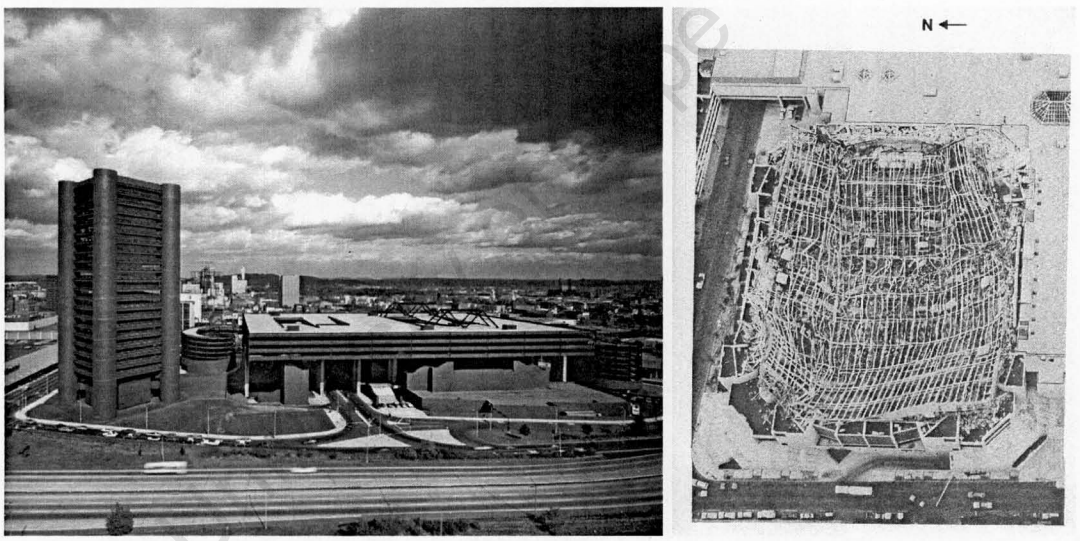


Figure 3.24: Hartford Civic Centre Coliseum (of the Coliseum, 2010) and aerial view of collapsed roof structure(Associates, 1978).

The flat roof structure, of plan dimensions 91.4 x 110m, covered a multi-purpose arena. The roof was corner-supported at four points offset from the grid boundary by 13.7m in both directions. The structure was a novel application of a deep DLG of the SOS configuration (see Figure 3.24). The upper and lower chords, separated by a vertical distance of 6.14m, consisted of a 9.14 x 9.14m grid. The main diagonal web members were 9.14m long and connected the upper and lower chord members. The diagonal web members were additionally braced at mid height by intermediate horizontal members (see Figure 3.25).

Heavy snowfalls preceded the roof failure which failed suddenly. Parke (1988) presents a review of the many articles published regarding the collapse. Research undertaken following the collapse focused on the torsional buckling of compression members, as the compression members used were of cruciform shape, assembled of angle sections welded back to back

(cruciform members are particularly susceptible to torsional instability). It is believed that only flexural buckling of compression members was considered, resulting in a significant under-design of compression member capacity (Parke, 1988).

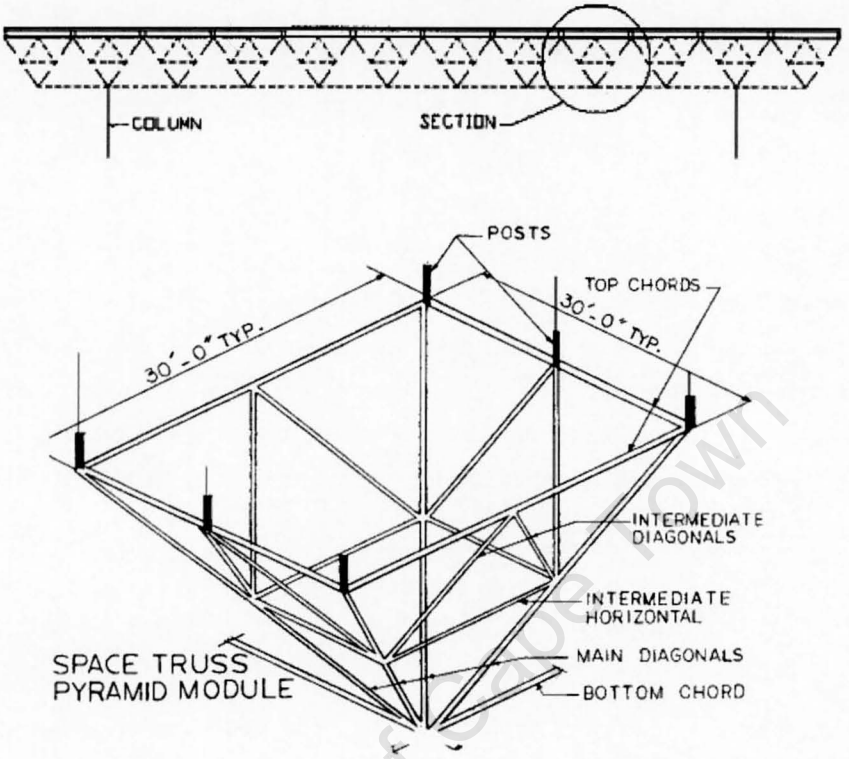


Figure 3.25: Hartford Civic Centre Coliseum Roof, space grid detail (Martin and Delatte, 2001).

Although the failure of the Hartford Civic Centre Coliseum roof resulted from insufficient resistance and not over-load, Parke (1988) comments that even if the structure had been designed correctly this would not have resulted in a different failure behaviour in the case of over-load.



### 3.4.2 Mero Roof, Turkey

The failure of a 28° pitched roof structure covering a 25.0x40.0m plan area constructed of the Mero KK system in Turkey, 2003, further demonstrates the importance of understanding space grid post-buckling behaviour in the design of such structures. Although the failure of the structure was principally due to the under-estimation of snow loads (Caglayan and Yuksel, 2008), the sudden collapse of the structure could have been avoided if the failure behaviour of the structure was considered at the design stage.

In the investigation which followed the collapse, it was discovered that the collapse of the structure was initiated by the rupture of the bolts which connected the node connector with the tubular chord sections (Caglayan and Yuksel, 2008). The bolts in the node connectors were designed for the maximum element loads resulting from an elastic analysis and not the tensile capacity of the sections used. Had bolts been used which mobilized the full

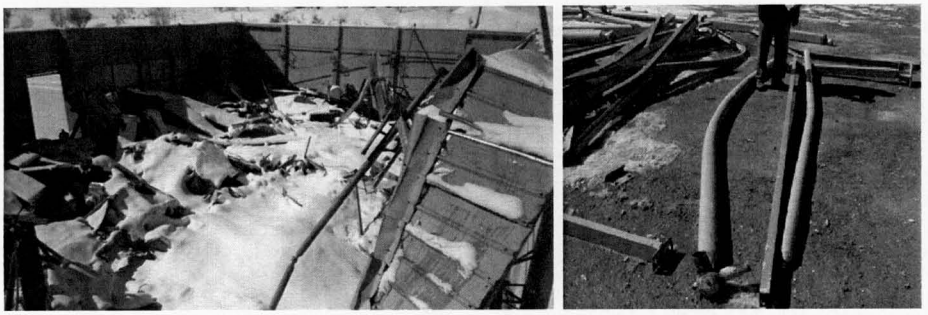

Figure 3.26: Mero roof collapse in Turkey resulting from severe snow load (Caglayan and Yuksel, 2008).

axial capacity of the sections, the capacity of the structure would have been significantly increased and the failure of the structure could potentially have resulted from yielding of the member gross cross-section, resulting in a nonlinear response prior to collapse. Failure through yielding of the cross-section would be characterized by a more ductile and hence gradual failure, providing greater warning for the buildings inhabitants to evacuate.

## 3.5 Conclusions

Owing to the difficulty and costs associated with the experimental testing of the failure behaviour of grid structures, relatively few tests have been undertaken. Various authors have contributed to an initial understanding of the elastic and failure behaviour of such structures; however this has seldom been developed further for application in practice and comparison between different studies is difficult due to the use of different numerical and experimental methods, and the variability of the results. The numerical analysis of grid structures has largely been confined to idealized strut representations of individual member behaviour; most of these studies have neglected geometric nonlinearities. Linearized buckling analysis of grid structures has also been undertaken, but the nature of such analysis has not allowed for observations regarding post-buckling behaviour to be made.

The validation of numerical modelling methods employed in the analysis of DLG structures is important; the work of Collins (1981) appears to be most suitable for such purposes.

Experimental analysis has shown that the failure and elastic behaviour of grid structures fabricated and assembled to general construction tolerances are highly sensitive to inherent geometric and material imperfections. Imperfections are found to direct the failure behaviour away from symmetry, resulting in the non-symmetrical distribution of load, the presence of stress concentrations, and the initiation of grid failure at loads below those predicted by common analysis methods.

The results of experimental analysis performed at larger scales is susceptible to grid geometric and material imperfections while grids tested at smaller scales have tended to be assembled of a single cross-section therefore not representing behaviour of structures with similar relative member proportions used in industry.

Various attempts to improve grid failure behaviour have been undertaken, by introducing pre-critical nonlinear behaviour into the grids' structural load-displacement response. The development of composite action and the incorporation of tensile yield of chord members appear to represent the most significant improvements to the failure behaviour of grid structures.

Although a considerable variety of node connection systems exist for grid structures, which vary in the effective rotational restraint of local members, research of commercial system has largely failed to capture the effect of joint connection stiffness on failure behaviour.

Numerical investigations into the failure behaviour of grid structures have focused on structures constructed with a single member cross-section. Structures constructed with a single cross-section are not representative of real structures; it is therefore possible that real structures, with optimized cross-sections, could experience additional failure modes which have previously been overlooked

Validation of numerical modelling methods can only realistically be achieved for grids which do not diverge significantly from symmetry in their failure and collapse behaviour. Where account of member imperfection is to be undertaken this should be undertaken with a numerical method which has been validated for the case of symmetrical failure.

Considerable room exists for research in the field of the failure behaviour of DLG structures. Experimental and theoretical work has shown that perceptions regarding the so-called inherent safety of redundant structures are not true and that failure of DLG structures generally occurs suddenly without significant warning. The well publicized collapse of grid structures serves as a motivation to account for and design grids which demonstrate significant pre-critical nonlinear behaviour.

# References

Lev Zetlin Associates. Report of the Engineering Investigation Concerning the Causes of the Collapse of the Hartford Coliseum Space Truss Roof on January 18, 1978. Technical report, LZA, 1978. Photo Only.

L. M. Bezerra, C. A. Silv de Freitas, W. T. Matias, and Y. Nagato. Increasing Load Capacity of Steel Space Trusses with End-Flattened Connections. *Journal of Constructional Steel Research*, 65:2197–2206, 2009.

O. Caglayan and E. Yuksel. Experimental and finite element investigations on the collapse of a Mero space truss roof structure A case study. *Engineering Failure Analysis*, 15:458–470, 2008.

Ian Martin Collins. *Collapse Analysis of Double-Layer Grids.* PhD thesis, University of Surrey, 1981.

S. A. L. de Andrade, P. C. G. da S. Vellasco, da Silva J. G. S., de Lima L. R. O., and D'Este A. V. D. Tubular space trusses with simple and reinforced end-flattened nodes-an overview and experiments. *Journal of Constructional Steel Research*, 61:1025–1050, 2005.

A. I. El-Sheikh and H. El-Bakry. Experimental Study of Behaviour of New Space Truss System. *Journal of Structural Engineering*, 122(8):845–853, August 1996.

Ahmed El-Sheikh. Effect of Member Length Imperfections on Triple-Layer Space Trusses. *Engineering Structures*, 19:540–550, 1997.

Ahmed El-Sheikh. Design of Web Members in Space Trusses. *International Journal of Space Structures*, 14(1):25–34, 1999a.

Ahmed El-Sheikh. Effect of Force Limiting Devices on Behaviour of Space Trusses. *Engineering Structures*, 21:34–44, 1999b.

A.I. El-Sheikh and R.E. McConnel. Experimental Study of Behavior of Composite Space Trusses. *Journal of Structural Engineering*, 119:747–766, 1993.

A. Fulop and M. Ivanyi. Experimentally Analyzed Stability and Ductility Behaviour of a Space-Truss Roof System. *Thin-Walled Structures*, 42:309–320, 2004.

M. Malite, C. H. Maiola, R. M. Goncalves, and A. C. Souza. Experimental Analyis of the Structural Performance of Space Trusses Commonly Used in Brazil. *International Journal of Space Structures*, 16(4):253–260, 2001.

Rachel Martin and Norbert J. Delatte. Another Look at Hartford Civic Centre Coliseum Collapse. *Journal of Performance of Constructed Facilities*, 15:31–36, 2001.

J. R. Mwakali. *The Collapse Behaviour of Double-Layer Space Trusses Incorporating Eccentrically Loaded Tee-Section Members.* PhD thesis, University of Surrey, 1990.

Last Days of the Coliseum. Last Days of the Coliseum Media Release, October 2010. URL `http://www.facebook.com/not.php?note_id=169574659722185`. Photograph only.

G. A. R. Parke. *The Behaviour of Space Trusses Incorporating Novel Compression Members.* PhD thesis, University of Surrey, 1988.

Toshitsugu Saka and Yoshiya Taniguchi. Effective Strength of 'Square-and-Diagonal' Double-Layer Grid. *Journal of Structural Engineering*, 118(1):52–72, January 1992.

Toshitsugu Saka and Yoshiya Taniguchi. Buckling Behavior of Square-and-Diagonal Double-Layer Grid. *Journal of Structural Engineering*, 120(4):1088–1102, April 1994.

L. C. Schmidt, P. R. Morgan, and J. A. Clarkson. Space Trusses with Brittle-Type Strut Buckling. *Journal of the Structural Division, Proceeding of the American Society of Civil Engineers*, 102:1479–1492, 1976.

L. C. Schmidt, P. R. Morgan, A. J. O'Meagher, and K. Cogan. Ultimate Load Behaviour of Full-Scale Space Truss. *Proccedings of the Institution of Civil Engineers*, 69:97–109, 1980.

L.C. Schmidt, P. R. Morgan, and A. Hanaor. Ultimate Load Testing of Space Trusses. *Journal of the Structural Division, Proceeding of the American Society of Civil Engineers*, 108:1325–1335, 1982.

Erling A. Smith. Space Truss Nonlinear Analysis. *Journal of Structural Engineering*, 110 (4):688–705, April 1984.

# Chapter 4

# Structural Theory

Failure behaviour of grid structures is largely dependent on the behaviour of individual structural members in the grid. Depending on grid geometry, configuration, and relative member proportions the first member to fail may fail in tension through yielding but the critical load of the structure will generally be reached only when compression failure through yielding or instability initiates. Once the buckling of compression members initiates a decrease in axial load-carrying behaviour is observed which affects the post-buckling behaviour of grid structures.

Owing to the importance of individual compression member failure and post-buckling behaviour in grid structures, a limited review of column buckling theory and an introduction to the analytical post-buckling behaviour of thin walled circular hollow sections is provided, reference is made to the work of Collins (1981) and Mwakali (1990).

Further understanding of elastic grid behaviour is achieved through analogies with continuum plates.



## 4.1 Introduction

Compression members can be divided into three categories depending on their slenderness, $\lambda = l_e/r$, where $l_e$ denotes strut effective length, and $r$ the cross-section radius of gyration. For a pin-ended compression member, columns of length less than the critical length, $l_{cr}$, given by equation 4.1, are defined as 'short' columns and buckle only after their yield stress is reached.

$$l_{cr} = \sqrt{\frac{\pi^2 EI}{\sigma_y A}} \tag{4.1}$$

Columns taller than the critical length, termed 'slender', buckle before the cross-section yields at a critical stress less than the material yield stress. Columns of length equal to the critical length buckle and yield concurrently and are said to have transitional slenderness.

There are three basic types of buckling which a compression member can undergo, namely, flexural buckling, torsional buckling and local buckling of the member cross-section.

Flexural buckling is characterized by a sudden bowing of the member, in the direction of least flexural resistance, when the critical load is reached; torsional buckling is characterized by an axial-rotation of the cross section relative to the supports when the critical load is reached (restricted to doubly symmetric open sections); local buckling is characterized by the development of a wave-like displacement field on individual components which make up the cross section. These buckling types are not mutually exclusive but frequently interact.

## 4.2 Elastic Buckling

Elastic buckling of columns occurs in slender members where the critical buckling stress is less than the yield stress of the material.

The following assumptions are made in the derivation of the critical stress of slender members:

- The material is isotropic, homogeneous and obeys Hooke's law in compression and tension;
- The strut is initially straight and deflections are small;
- Strut loading is concentric;
- Strut ends are pinned.



Derivation of the buckling load for a compression member begins with the governing differential equation (Equation 4.2) of the structural resistance of the strut in its nominally deformed condition where $P$ is the axial load, $EI$ the flexural stiffness, $y$ the horizontal deflection and $x$ the length along the strut. The general solution for a pin ended member is that given in Equation 4.3, where $k = \sqrt{\frac{P}{EI}}$ and $C_1$ and $C_2$ are integration constants.

$$\frac{d^2y}{dx^2} = -\frac{P}{EI}\frac{y}{l} \tag{4.2}$$

$$y = C_1 \sin kx + C_2 \cos kx \tag{4.3}$$

Integration constants are solved for by account of boundary conditions. Substituting a solution to Equation 4.3 back into the governing differential equation (Equation 4.2) allows for the strut critical load to be determined. For a pin ended column the result is the 'Euler' equation, Equation 4.4.

$$P_{cr} = \frac{\pi^2 EI}{l^2} \tag{4.4}$$

The Euler equation holds well for slender columns when compared to experimental results, however, overestimates the critical load for short columns (The Euler equation predicts the load at which horizontal deflection initiates). Consequently various formulae were introduced which account for inelastic behaviour.

## 4.3 Imperfect Strut Behaviour

In practice strut behaviour diverges from the behaviour of a perfect Euler column due to the following factors: residual stresses, initial curvature, eccentricity of load, and end restraint conditions.

### 4.3.1 Residual Stresses

Residual stresses develop in hot-rolled and welded sections from plastic strains due to unevenly distributed heating and cooling. Residual strains result in a decrease of strut critical load. The distribution and magnitude of residual stress is largely dependent on cross-section and cooling history (Mwakali, 1990).



### 4.3.2 Initial Curvature

Rolling Mill tolerances are specified by country-specific codes. The European Committee for Standardization specifies tolerances, dimensions and sectional properties for hot-rolled hollow sections in EN 10210-2:2006. Bow imperfections are typically limited to less than $1/1000$ of the member length and accounted for in calculation through a half sine type distribution.

### 4.3.3 Eccentricity

The effects of load and support eccentricity on the buckling behaviour of compression members are similar to that of initial curvature. The effect of load eccentricity can consequently be expressed as an initial bow curvature which decreases sharply to zero at each end. The Fourier components of the bow imperfection can be taken as:

$$e_0 = \sum a_i \sin \frac{i\pi x}{l} \quad for\ i = 1, 3, 5, ... \tag{4.5}$$

where $a_i = 4e_0/i\pi$.

As the critical load is approached, all but the first term of the series can be neglected and the bow imperfections can be described by a sine curve of magnitude $a_i = 4e_0/\pi$ (Mwakali, 1990).

### 4.3.4 End Restraints

Columns are seldom restrained by connections of a perfectly pinned nature; the concept of effective length was consequently developed. Effective length factors allow for Euler Column behaviour to be extended to columns with alternative end restraints. Effective length factors for combinations of rotationally free, rotationally fixed, translationally free, and translationally fixed end restraint are shown in Figure 4.1.

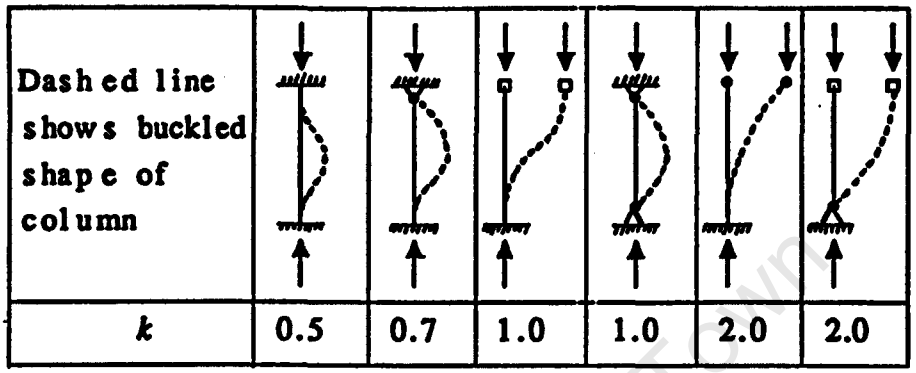


Figure 4.1: Effective lengths of compression members, $k$, with various combinations of common end restraints (Mwakali, 1990).

## 4.4 Inelastic Buckling

Common descriptions of column behaviour, used in practice to account for imperfect behaviour as outlined in Section 4.3, include Rankine's, Tangent Modulus, Secant Modulus and the Perry-Robertson formulae and are widely discussed in the literature. Focus however is paid to the more recent development of the European buckling curves, as employed in the Structural Eurocodes, in evaluating inelastic buckling of compression members due to their potential for incorporation in numerical modelling applications.

### 4.4.1 European Buckling Curves

From 1960 the European Convention for Constructional Steelwork (ECCS) undertook an experimental programme on the behaviour of standard columns. In excess of 1000 columns of various standard cross-sections (I, H, T, U, circular and rectangular hollow sections) and slenderness ratios between 55 and 160 were tested. A probabilistic approach was adopted using both experimental results and theoretical analysis (ESD, 2010). The result of the study was the development of a relationship between strength as a function of reference slenderness for various cross-section groups. Design strength is calculated as the product of the buckling reduction factor, $\chi$, and the cross-section yield force. For the purpose of theoretical analysis a bow imperfection described by a half sine imperfection of magnitude $l/1000$ was considered.

Curves $a_0, a-d$ represent increasing degrees of imperfections; columns are assigned a buckling

curve based on cross-section type, axis about which buckling occurs and material strength. Circular hollow sections are represented by Curve $a$, with the exception of CHS of steel grade S 460 which are represented by curve $a_0$. Figure 4.2 is a graphical representation of the reduction factor, $\chi$, as a function of non-dimensional slenderness, $\overline{\lambda}$, with the numeric representation given by Equation 4.6. $\Phi$ and $\overline{\lambda}$ are given by Equations 4.7 and 4.8 respectively.

$$\chi = 1/[\Phi + (\Phi^2 - \overline{\lambda}^2)^{1/2}] \tag{4.6}$$

$$\Phi = 0.5[1 + a(\overline{\lambda} - 0.2) + \overline{\lambda}^2] \tag{4.7}$$

$$\overline{\lambda} = \sqrt{\frac{Af_y}{N_{cr}}} = \frac{L_{cr}}{i}\frac{1}{\lambda - 1} \quad with \quad \lambda_1 = \pi\sqrt{\frac{A}{f_y}} \tag{4.8}$$

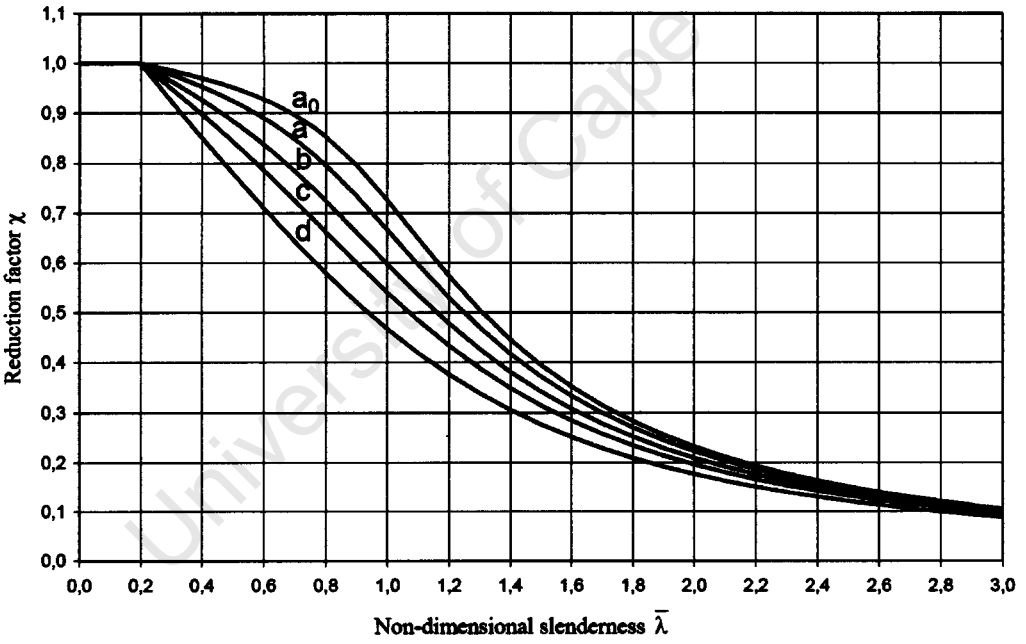




Figure 4.2: European Buckling Curves for flexural buckling of standard structural cross-sections (EC3, 2005).

## 4.5 Post-buckling Behaviour

A theoretical formulation for the resistance of a buckled, thin-walled [1], tube section with pin-ended boundary conditions is given with reference to Collins (1981) and Mwakali (1990).

The resistance of the buckled section is developed for a pin-ended strut of length $L$, area

[1]The thin wall assumption for the derivation of post-buckling strength is sufficient for $R/t < 25$ corresponding to 2% error (Collins, 1981).

$A$, flexural rigidity $EI$ and yield stress $\sigma_y$ which is acted upon by an axial load $P$ which produces an axial shortening $\delta$. Bowing of the strut is assumed symmetric with maximum deflections at the midpoint. A relationship between $P$ and $\delta$ is sought.

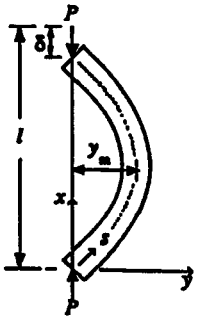


Figure 4.3: Deflected configuration of buckled strut (Mwakali, 1990).

For a slender column which buckles elastically there will initially be very little decrease in load. However, as the column bends the extreme fibres will begin to yield, the bending becomes plastic, load resistance decreases and axial displacement increases.

Axial shortening of the strut is assumed to be the sum of the direct stress, $\delta_a$, and that due to flexure, $\delta_b$, given as:

$$\delta = \delta_a + \delta_b \tag{4.9}$$

where the axial shortening due to direct stress is given as:

$$\delta_a = \frac{PL}{AE} \tag{4.10}$$

and the axial shortening due to bending stress is given by Equation 4.11, where $s$ is the length along the axis of the column and x is the distance along the axis of the undeformed perfect column.

$$\delta_b = \int_0^L (ds - dx) \tag{4.11}$$

It can then be shown, from the geometry of a circle, that:

$$(ds - dx) = \frac{dy}{dx} dx . \frac{1}{2} \frac{dy}{dx} = \frac{1}{2} \left( \frac{dy}{dx} \right)^2 dx \tag{4.12}$$

where $y$ is the transverse deflection and $dy/dx$ is the slope of the deflected shape. The axial shortening can then be expressed as:

$$\delta = \frac{PL}{AE} + \frac{1}{2} \int \left( \frac{dy}{dx} \right)^2 dx \tag{4.13}$$

To integrate this equation, a relationship between $x$ and $y$ is required. It is common to assume a sinusoidal relationship for this purpose (Equation 4.14). Differentiating this equation and substituting into Equation 4.15 allows for the development of an expression for axial shortening given by Equation 4.15. This represents the required $P - \delta$ relationship.

$$y = y_m \sin\left(\frac{\pi x}{L}\right) \tag{4.14}$$

$$\delta = \frac{PL}{AE} + \frac{y_m \pi^2}{4L} \tag{4.15}$$

The unknown strut amplitude $y_m$ can then be calculated assuming equilibrium at mid-strut between the section resisting moment, $M$, and the applied axial force, $P$ (Equation 4.16); where $y_m$ is the eccentricity of strut centreline relative to the undeformed configuration.

$$M = Py_m \tag{4.16}$$

Rewriting Equation 4.15 to consider these equilibrium conditions gives:

$$\delta = \frac{PL}{AE} + \frac{\pi^2}{4L}\left(\frac{M}{P}\right)^2 \tag{4.17}$$

The moment, $M$, is then eliminated by assuming a cross-sectional stress distribution as a function of a geometric parameter, for this case $\theta$, and yield stress $\sigma_y$. For the case of a thin-walled tube, of radius $R$, wall thickness $t$, and a simplified stress distribution, where full plasticity has been developed, the axial load is given by Equation 4.18 with resisting moment given by Equation 4.19, obtained by substituting for $dA = 2Rtd\theta$.

$$P = \int_A \sigma dA = 2Rt\sigma_y(\pi - \theta) = \sigma_y A\left(1 - \frac{\theta}{\pi}\right) \tag{4.18}$$

$$M = \int_A \sigma z dA = 4\sigma_y R^2 t \sin\frac{\theta}{2} \tag{4.19}$$

Elimination of $\theta$ between Equations 4.18 and 4.19 and substitution for $M$ gives:

$$\delta = \frac{PL}{AE} + \frac{1}{L}\left[\frac{\sigma_y A}{P} R\cos\left(\frac{\pi}{2}\frac{P}{\sigma_y A}\right)\right]^2 \tag{4.20}$$

in which the assumption regarding thin wall thickness defines cross-sectional area (Equation 4.21).

$$A = 2\pi Rt \tag{4.21}$$

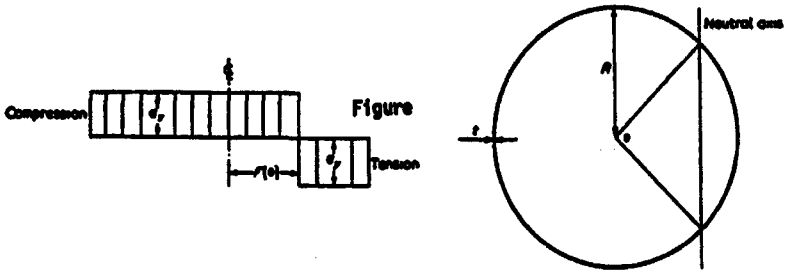


(a) Assumed stress distribution at strut mid-length.

(b) Cross-section parameters.

Figure 4.4: Cross-section stress distribution.

Selection of displacement as the independent variable, and solving for $P$ in Equation 4.20, allows for the load-displacement behaviour of the buckled strut to be plotted using the Euler critical load as the upper bound (see Figure 4.5). Displacement due to axial load initially governs, but begins to decrease as axial load decreases and displacement due to bending begins to dominate.

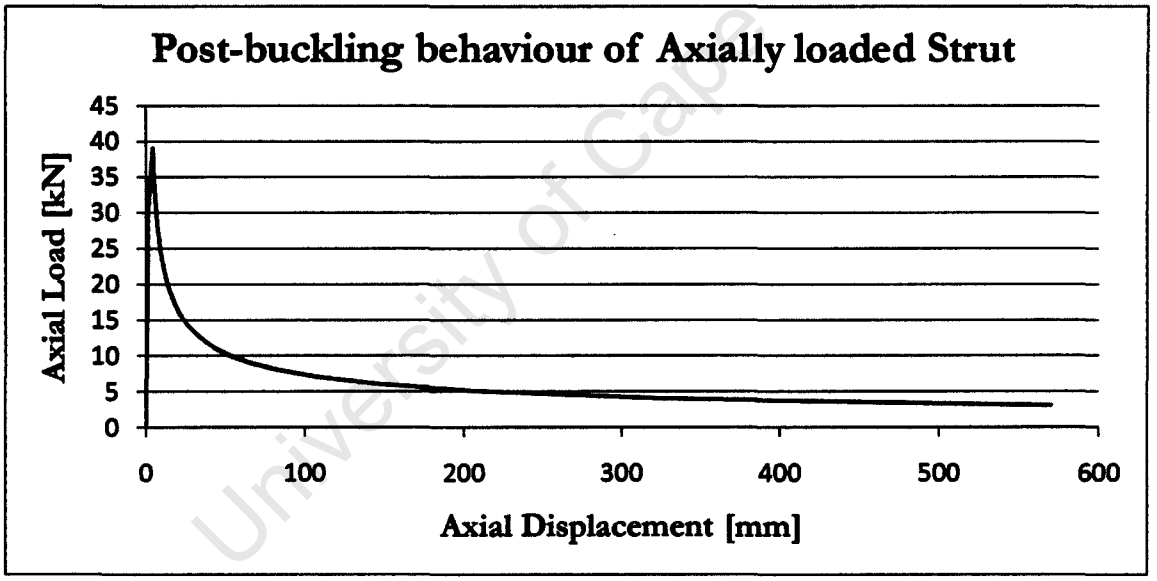


Figure 4.5: Load-displacement behaviour of a thin-walled circular hollow section compression member including elastic and post-buckling regimes.

## 4.6 Analogous Continuum

The multi-directional load-carrying characteristics of grid structures lend themselves to analogies with plates. This analogy is particularly useful for initial design purposes where a complex structure, possibly consisting of thousands of elements, can be relatively accurately approximated by a single (plate) element, with known structural behaviour. From this initial analysis, chord member sizes and grid geometry (chord spacing and grid depth) can be approximated and used as reasonable initial inputs for structural optimization procedures. The analogy is also useful in conceptualizing anticipated grid structure behaviour.

Plates can be divided into two groups:

- isotropic, where elastic properties are identical in all directions
- anisotropic, where there are different elastic properties in different directions

As DLG structures frequently possess different elastic properties in different directions the plate analogy is developed for the anisotropic case, of which isotropic plates are a special case. The derivation of the formulae used in plate analogy is shown below, with reference to Makowski (1981).

This starts from the Woinowsky-Krieger differential equation of the deflected surface of an orthotropic plate, which is valid for all support and loading conditions:

$$D_x \frac{\partial^4 w}{\partial x^4} + 2H \frac{\partial^4 w}{\partial x^2 \partial y^2 w} + D_y = q_0 \tag{4.22}$$

where

$w$ = vertical deflection

$q_0$ = external loading intensity at point considered

$D_y = \frac{E_x h^3}{12(1-\mu^2)}$ = unit flexural stiffness in x-directions

$D_y = \frac{E_y h^3}{12(1-\mu^2)}$ = unit flexural stiffness in y-directions

$2H = D'_x + D'_y + 2(D_{xy} + D_{yx})$

$D_{xy} = \frac{E_x h^3}{24(1+\mu}$, $D_{yx} = \frac{E_y h^3}{24(1+\mu}$

$D'_x = \mu D_x$, $D'_y = \mu D_y$

$E_x, E_y$ = the moduli of elasticity in two mutually perpendicular axes, x and y

$\mu$ = Poisson's ratio

$h$ = plate thickness

A relatively simple analytical solution exists for the vertical deflection of a rectangular plate simply supported on all four sides. This case is therefore used to demonstrate the continuum plate analogy. The solution to this problem was shown, by Navier, to be given by a double trigonometric Fourier series of the form given in Equation 4.23, where a and b are the respective plate dimensions.

$$w = \sum_{m=1,3,5...}^{\infty} \sum_{m=1,3,5...}^{\infty} A_{mn} sin\frac{m\pi x}{a} sin\frac{n\pi y}{b} \tag{4.23}$$

For the special case of uniform loading of magnitude $q_0$ across the plate surface, the coefficient $A_{mn}$ is given as:

$$A_{mn} = \frac{16q_0}{\pi_6} \frac{1}{mn(\frac{m^4}{a^4}D_x + \frac{2m^2n^2}{a^2b^2}H + \frac{n^4}{b^4}D_y)} \tag{4.24}$$

The convergence of the resulting series is rapid and therefore the vertical deflection of the plate as a function of $x$ and $y$ can be approximated relatively accurately by considering only the first term of the series, i.e. m=1, n=1. The vertical deflection is therefore given as:

$$w = \frac{16q_0}{\pi^6} \frac{sin\frac{\pi x}{a} sin\frac{\pi y}{b}}{\frac{D_x}{a^4} + \frac{2H}{a^2b^2} + \frac{D_y}{b^4}} \tag{4.25}$$

By successively differentiating the expression for $w$ (Equation 4.25) the plate vertical deflection, bending moments, torsional moments and shear forces can be obtained (Equations 4.26 to 4.31).

Bending moment in x- and y-direction

$$M_x = -(D_x \frac{\partial^2 w}{\partial x^2} + D'_x \frac{\partial^2 w}{\partial y^2}) \tag{4.26}$$

$$M_y = -(D_y \frac{\partial^2 w}{\partial y^2} + D'_y \frac{\partial^2 w}{\partial x^2}) \tag{4.27}$$

Torsional moment in x- and y-direction

$$M_{xy} = 2D_{xy} \frac{\partial^2 2}{\partial x \partial y} \tag{4.28}$$

$$M_{xy} = -2D_{yx} \frac{\partial^2 2}{\partial x \partial y} \tag{4.29}$$

Shearing forces on x and y faces

$$Q_x = \frac{\partial M_x}{\partial x} - \frac{\partial M_{yx}}{\partial y} \tag{4.30}$$

$$Q_y = \frac{\partial M_y}{\partial y} + \frac{\partial M_{xy}}{\partial x} \tag{4.31}$$

**Notes on above equations** i)In practice the Poisson term may be dropped with little effect on accuracy. ii) In SLGs with rigid connections additional attention will need to be paid to the effects of torsional moments; however, this will not be considered here as the effect of torsional moments on DLG grids is minimal. iii) Additional formulations for $A_{mn}$ may be used for alternate loading conditions; see Makowski (1981, Chapter 5).

Extending the above formulae, which are for plates, to two-way spanning grids can be achieved using the notion of unit flexural rigidity. Unit flexural rigidity of a single-layer, rectangular, two-way grid, with members perpendicular to the grid edges, dimensions $a$ x $b$, respective spacing of beams running in x and y directions of $b_1$ and $a_1$ and flexural rigidities $EI_y$ and $EI_x$ can be obtained using Equations 4.32 and 4.33.

$$D_x = \frac{EI_x}{b_1} \tag{4.32}$$

$$D_y = \frac{EI_y}{a_1} \tag{4.33}$$

Further extending the formulae from two-way plates to approximate the behaviour of two-way DLGs can be achieved by dividing the bending moment of the equivalent SLG by the depth of the DLG. The determination of deflections in the DLG requires knowledge of the flexural rigidity. Flexural rigidity $EI$ can be approximated using an approximate grid second moment of area $I_{approx}$ as given in Equation 4.34.

$$I_{approx} = \frac{A_T A_B}{A_T + A_B} h^2 \tag{4.34}$$

$A_T$ and $A_B$ are the cross-sectional areas of the top and bottom chords respectively and $h$ is the effective height of the DLG.

The above method ignores the influence of web member stiffness on global stiffness. Forces in inclined web members, $D$, can be approximated by calculating the component of shear force on the inclined plane at the equivalent point in the SLG with:

$$D = S.cosec(\alpha) \tag{4.35}$$

where $\alpha$ is the inclination angle of the diagonal web member with the horizontal.

The plate analogy can further be applied to other grid geometries including diagonal configurations see Makowski (1981, Chapter 5).

## 4.7 Structural and Static Redundancy

One of the initial reasons that space trusses gained so much popularity, in addition to their simple and quick construction, was their perceived safety. The large degree of static redundancy present in space grids resulted in a perception, by some, that these structures could

easily redistribute load upon localized failure, due to the numerous alternative load paths which could be adopted. Although this behaviour may be true for internal web members it is not the case for the most highly loaded members in the structure. Chord members in compression, which typically carry the highest loading in space grids, demonstrate unstable buckling behaviour which on initiation results in a brittle successive collapse of the structure (El-Sheikh, 1997). Structural redundancy should be distinguished from static redundancy in that structural redundancy refers to the number of structural members which can be removed before collapse of the structure initiates.

### 4.7.1 Kinematic Stability

The understanding of static and kinematic indeterminacy is central to an understanding of the mechanics of pinned structures. The performance of pinned structures is a good guide to the behaviour of similar rigidly connected structures (Pellegrino and Calladine, 1986), consequently the understanding developed of such pin jointed structures can be extended to similar structures with fixed connections.

Static determinacy of a structure relates the number of unknowns in a structure to the number of equilibrium equations. If the number of unknowns is equal to the number of equilibrium equations, the structure is said to be statically determinate. Structural determinacy is commonly defined by Maxwell's Rule given, for three-dimensional frameworks adequately secured to foundations, by Equation 4.36; where $b$ is the total number of bars and $J$ is the number of internal joints.

$$b = 3J \tag{4.36}$$

If a load is applied to the structure the resulting internal stress distribution is unique. It should be noted, however, that a statically determinate structure may be kinematically indeterminate; this is not captured in Maxwell's Rule.

Kinematic, also referred to as geometric, stability defines whether a structure is susceptible to mechanism-type displacement, where mechanism displacement refers to in-extensional deformation. If the geometry of a given group of bars is not unique then the structure is said to be kinematically indeterminate.

Mechanism-type displacement can be divided into infinitesimal and finite mechanisms. For finite mechanisms, joints can move freely for a finite distance with no change in bar length. For infinitesimal mechanisms, however, there are small changes to bar length and the structure is said to 'tighten up' when the mechanism is mobilized, introducing a state of self-stress into the structure. Pellegrino and Calladine (1986) describe a matrix method which can be used to identify if a structure is susceptible to in-extensional displacement mechanisms.

The method developed by Pellegrino and Calladine (1986) was extended by Savassi et al. (2004) who describe the further development and the application of these matrix methods

to double-layer grids. The method developed was used to assess how kinematic instability can be avoided through modification to grid layout. In many cases mechanism behaviour can be prevented by the addition of only a few bars.

Saka and Taniguchi (1994) investigated the effect of edge beams on restraining the kinematic instability of SOD and DOS grids (see Section 3.3.3.4). Saka and Taniguchi (1994) showed that edge beams were an effective means of preventing kinematic stability in DOS grids, Saka and Taniguchi (1994) also showed there is a threshold value of connection stiffness which restrains kinematic instability.

## 4.8 Conclusions

The growth in understanding of the behaviour the flexural buckling phenomena has allowed for more accurate predictions of column critical stress and loads to be made for short, intermediate and long columns. The European Buckling Curves are based on the assumption of an initial bow imperfection and have found wide application in design codes. The assumption of an initial half sine, or bow imperfection, in predicting the buckling behaviour of imperfect columns is a common practice and is consequently acceptable for use in overcoming the problem of bifurcation in nonlinear failure analysis of grid structures, as introduced in Chapter 6.

A theoretical basis for the post-buckling behaviour of compression members exists, based on an assumed cross-sectional stress distribution. The special case of the post-buckling behaviour of thin-walled tubes is considered but may be extended to other cross-sections. Post-buckling behaviour varies depending on member slenderness.

Analogies between continuum plates and DLGs may be exploited for initial design purposes and may be configured to account for anisotropic grid stiffness.

Higher order deformations of grid structures may occur for grids assembled of the pyramid module due to the kinematic instability of this configuration. In practice higher order deformations of grid structures are restrained by boundary conditions, boundary members, and the rotational stiffness of connections. Numerical analysis of grid structures of pyramid base modules and pinned connections may consequently result in singularity errors.

# References

Eurocode 3: Design of Steel Structures - Part 1.1: General Rules and Rules for Buildings BS-EN 1993-1-1:2005, 2005.

ESDEP Course Notes, 2010. URL `http://www.fgg.uni-lj.si/kmk/ESDEP/master/wg07/10510.htm#SEC_5`.

Ian Martin Collins. *Collapse Analysis of Double-Layer Grids.* PhD thesis, University of Surrey, 1981.

Ahmed El-Sheikh. Effect of Member Length Imperfections on Triple-Layer Space Trusses. *Engineering Structures*, 19:540–550, 1997.

Z. S. Makowski, editor. *Analysis, Design and Construction of Double-Layer Grids.* Applied Science Publishers Ltd, 1981.

J. R. Mwakali. *The Collapse Behaviour of Double-Layer Space Trusses Incorporating Eccentrically Loaded Tee-Section Members.* PhD thesis, University of Surrey, 1990.

S. Pellegrino and C. R. Calladine. Matrix Analysis of Statically and Kinematically Indeterminate Frameworks. *International Journal of Solids and Structures*, 22(4):409–428, 1986.

Toshitsugu Saka and Yoshiya Taniguchi. Buckling Behavior of Square-and-Diagonal Double-Layer Grid. *Journal of Structural Engineering*, 120(4):1088–1102, April 1994.

W. Savassi, R. M. Goncalves, and A. S. C. de Souza. On Kinematic Stability of Double-Layer Grid Space Structures. In *IASS Synopsium 2004 Montpellier*, 2004.

# Chapter 5

# Finite Element Analysis

An introduction numerical analysis based on the finite element method, relevant to the analysis of grid structures, follows.



## 5.1 Analysis Methods

The Finite Element Method is an approximate numerical method for solving partial differential equations. This is used to develop approximate solutions for continuum problems in structural engineering mechanics.

The basic methods commonly employed in the static analysis of structures vary in complexity and can be categorized by increasing complexity[1] as follows:

- Linear analysis;
- Geometrical nonlinear analysis;
- Material nonlinear analysis;
- Coupled material and geometrical nonlinear analysis.

In addition to linear and nonlinear analysis methods Eigen value type analysis methods need also be considered as a means to capture the stability and dynamic behaviour of structures (Simulia, 2010b).

### 5.1.1 Linear Elastic Analysis

Linear elastic analysis of grid structures assumes a perfect structure with a linear response to axial force. In statically determinate structures bar forces are dependent on the need to

[1] Relative complexity of geometric and material nonlinear analysis is highly dependent on the application and materials considered

satisfy internal equilibrium; member geometric imperfections can consequently be considered to have no influence on the distribution of member forces through the structure. This is not the case for grid structures. Grid structures possess high degrees of static indeterminacy and therefore imperfections in bar geometry can affect the distribution of bar forces between members (Marsh, 2000).

Where the design of a grid structure is dependent on the behaviour of the chord members, overloading of these members may result in sudden failure. It is therefore important to include member imperfection in linear analyses of grid structures so that a more realistic load distribution can be established throughout the structure. The effect of overloading particular members can only be determined through a full nonlinear analysis. The use of 'pseudo loads' to approximate the effects of temperature or initial member lack of fit may also be undertaken.

### 5.1.2 Stability Analysis

Eigen value solution methods are used for both buckling and dynamic modal shape type problems. For buckling problems the roots of the stiffness equation, $F = Kd$, can be solved for, by setting the determinant of the structure stiffness matrix, $K$, to zero, where $F$ is the external force vector and $d$ the displacement vector (Simulia, 2010c). Eigen value extraction methods can be incorporated into finite element codes relatively easily and the calculations are not computationally expensive.

For buckling problems solved by Eigen value extraction methods (also referred to as linearized buckling) the Eigen value represents the factor of safety of the system to buckling relative to the applied loading, while the resulting Eigen vectors represent the relative buckled mode shapes. Depending on the type of elements (and their respective degrees of freedom) the Eigen value solution will pick up various buckling modes. In the general case, where beam elements are used (six degrees-of-freedom at each node), both local and global buckling modes will be identified, while if truss elements are used (three degrees-of-freedom at each node), only global buckling modes will be identified. The buckling of individual members is influenced by the rotational behaviour of the connecting nodes at a local scale while global buckling is influenced by geometric instability at a global scale and can therefore be resolved in terms of nodal displacement only.

For the buckling analysis of structures Eigen values and their associated vectors need to be determined for various loading conditions as the resulting Eigen values and vectors are dependent on the externally applied load configuration, and the pre-existing internal stress and strain state (Simulia, 2010a).

In addition to indentifying the critical load of structures, linearized buckling analysis can also be used to identify kinematic instability of structures identified by an Eigen value approximately equal to zero.

#### 5.1.2.1 Initial Imperfections

The mode shapes compiled from Eigen vectors can additionally be used to seed geometry imperfections into a finite element model reference configuration for the purpose of nonlinear analysis. In such a case, multiple dominant buckled mode shapes are scaled appropriately, superimposed on each other, and then applied as the initial geometry for subsequent steps in the analysis (Simulia, 2010a). Introducing imperfections into the initial geometry of grid structures is particularly important as bifurcation behaviour of individual members dominate the failure of such structures. Failure of perfect beams under axial loading can only be accounted for in nonlinear analysis through empirical stress-strain relations.

### 5.1.3 Nonlinear Analysis

Grid structures are susceptible to material and geometric nonlinear behaviour and both forms of nonlinearity should be considered in the analysis of such structures (Koushky et al., 2007). This is especially true when grid structures are loaded towards their limit points and when the post-buckling behaviour or progressive collapse mechanisms are to be investigated.



#### 5.1.3.1 Material Nonlinearity

Material nonlinear behaviour of typical construction materials results from nonlinear stress-strain relationships, which may include the effects of: material yielding; cracking; crushing; and time-related effects including creep and relaxation.

Material models used to describe the nonlinear behaviour of steel need to capture the plasticity of the material and its hardening, where hardening describes the change in yield surface with successive yielding such that conditions for subsequent yielding may be established (Koushky et al., 2007).

Isotropic or work hardening material behaviour (Figure 5.1) assumes that the yield surface remains centred about the initial stress state and expands in size with plastic strain. Kinematic hardening assumes that the yield surface remains constant in size but translates in stress space with yielding. The Bauchinger's effect is captured in kinematic hardening which accounts for cyclic loading effects. Isotropic hardening is generally used for static analysis.

#### 5.1.3.2 Geometric Nonlinearity

Geometric nonlinear effects, including buckling and other plastic changes to structural configuration, can significantly change the equilibrium position of space grid structures and the distribution of load and stress within a structure. Geometric nonlinearity is consequently of particular importance for collapse behaviour where large displacements and rotations are encountered. Geometric imperfections generally amplify the effect of geometrical nonlinear behaviour (Malla and Serrette, 1996). It is therefore important that the effect of geometrical

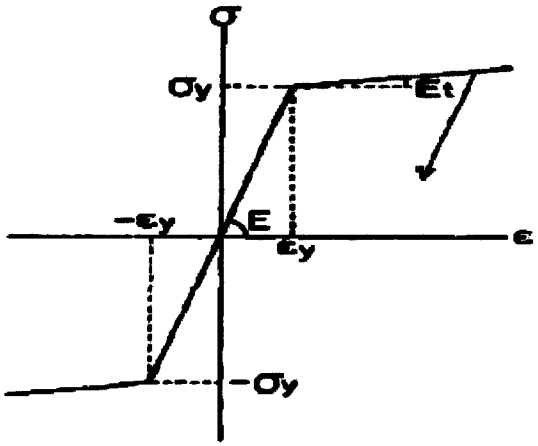


Figure 5.1: Stress-strain relationship for isotropic hardening (Koushky et al., 2007).

nonlinearity is considered for the collapse analysis of structures.

### 5.1.4 Nonlinear Solution Schemes

For application of the finite element method to nonlinear problems the method has been adapted and additional calculation methods and formulations have been introduced. An overview of nonlinear solution schemes employed in finite element analysis and used to pass limit points in the progression of numerical analysis, resulting from nonlinear material and geometrical behaviour, is presented with reference to Crisfield (1991) and Memon and Su (2004). The application of displacement control to nonlinear analysis is also considered.

#### 5.1.4.1 Overview

Nonlinear solution methods are frequently approached through incremental load stepping procedures. This allows the equilibrium path of the structure, under load, to be traced with a load-displacement plot and consequently includes $P-\delta$ effects (effect of load moving with structure). In the progression of an incremental nonlinear analysis, local or global limit points may be encountered. The progression of solutions past these points represents a problem to numerical stability in finite element formulations for the case of load controlled analysis. Numerical instability occurs, since for a given load the position along the load-displacement plot is not unique (Simulia, 2010c). Arc-length control is a numerical solution method which searches for incremental convergence along a predefined path, thereby avoiding ambiguity in load displacement space.

In practice the modified Newton-Raphson Method is used to capture nonlinear behaviour while the Riks and other similar methods are used to progress past limit points. The Riks method is a combination of the modified Newton-Raphson (incremental and iterative) solution strategy and arc-length control, and consequently allows for the progression past limit points. Incremental and iterative strategies are first introduced separately followed by a

description of the combination of these solution methods as the modified Newton-Raphson Method. A description of Arc-length control then follows.

#### 5.1.4.2 Incremental Solution Schemes

An incremental solution scheme requires that the incremental load applied in each load step, be multiplied by the tangent stiffness matrix at that point, such that the displacement associated with that load step is obtained (see Figure 5.2). In this form the tangent stiffness matrix, $K_t$, replaces the function of the stiffness matrix in linear analysis. The incremental solution requires the repeated application of Equation 5.1 where $W$ = Load, and $w$ = displacement.

$$\Delta w = \frac{dW}{dw}^{-1} \Delta W = K_t^{-1} \Delta W \tag{5.1}$$

The incremental solution is only evaluated at discrete points however; the approximated behaviour therefore diverges from the exact solution.



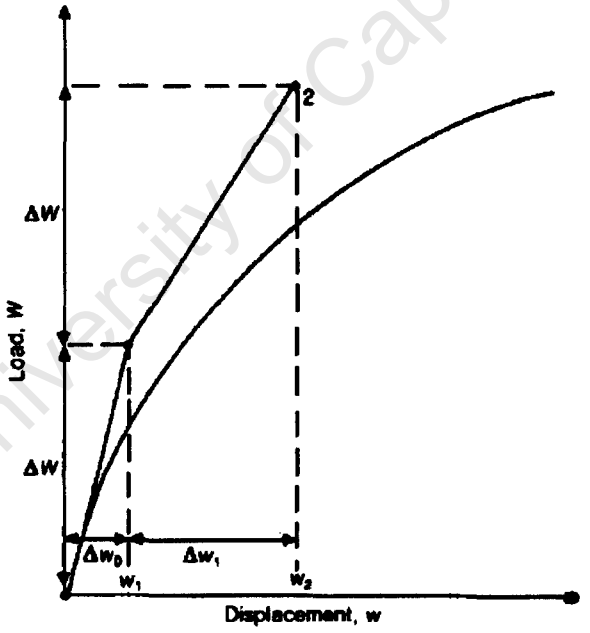


Figure 5.2: Incremental Solution Scheme (Crisfield, 1991, Chapter 1).

#### 5.1.4.3 Iterative Solution Scheme

An iterative solution scheme is used to solve the load-displacement relationship for a given load using an expanded Taylor series expression. In this case all terms of the load-displacement relationship are taken to one side of the equation and set equal to a constant, $g$, which is in turn set equal to zero. The iterative procedure is then set up by taking the truncated Taylor series expansion of $g$ (see Equation 5.2):

$$g_n \approx g_0 + \frac{dg_0}{dw}\delta w + (\frac{1}{2}\frac{d^2 g_0}{dw^2}(\delta w)^2) \tag{5.2}$$

where the term $dg_0/dw$ indicates the differential of $g$ w.r.t. displacement, $w$, calculated at 0. If an initial estimate for $w_0$ is given, for which $g_0(w_0) \neq 0$, and if the bracketed higher order terms are neglected, then by setting $g_n = 0$, the Taylor series can be simplified as follows:

$$\delta w_0 = -(\frac{dg_0}{dw})^{-1} g_0(w_0) \tag{5.3}$$

from which a new estimate of $w$ is given as:

$$w_1 = w_0 + \delta w_0 \tag{5.4}$$

Iterating the above process results in quadratic convergence of displacement, $w$, for a given load, $W$. Such iterative solution schemes, however, become inefficient if large load steps are implemented. An accurate solution for load-displacement behaviour can consequently be obtained by merging incremental and iterative solution methods. This is given by the modified Newton-Raphson Method.

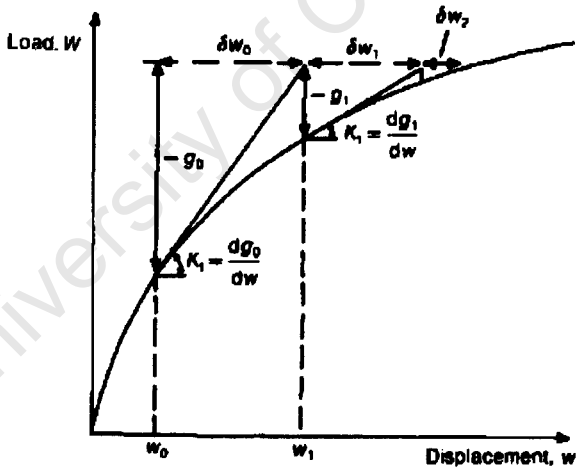


Figure 5.3: Iterative Solution Scheme (Crisfield, 1991, Chapter 1).

#### 5.1.4.4 Incremental and Iterative Solution Schemes

A combined incremental and iterative solution scheme, commonly referred to as the modified Newton-Raphson Method, combines the advantages of an iterative solution scheme's convergence with the advantages of small load increments associated with incremental schemes, and allows the nonlinear equilibrium response of a structure to be traced efficiently (the equilibrium path). In this case the 'tangential incremental solution' is used as the predictor providing the initial starting solution, $w_0$, for the iterative solution which is then repeated until the total load has been introduced in load increments (see Figure 5.4).

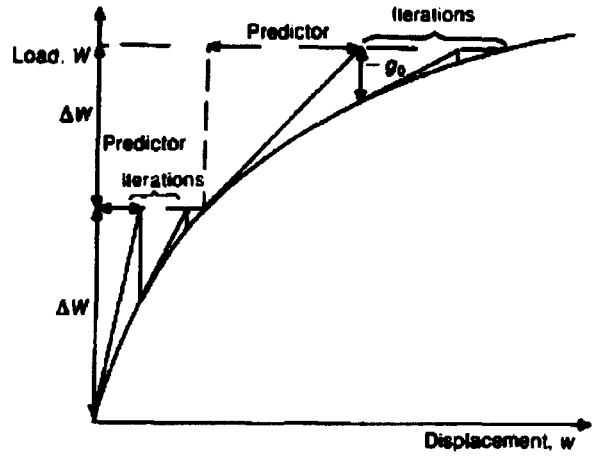


Figure 5.4: Modified Newton-Raphson (incremental and iterative) Solution Scheme (Crisfield, 1991, Chapter 1).

#### 5.1.4.5 Arc-length Control

Optimized methods of selecting load step size are termed arc-length control or Riks methods. Such methods allow the numerical solution of nonlinear finite element models to progress past local maxima or minima in load-displacement space. This is achieved by forcing the equilibrium solution for each load increment to be searched for along a predefined path until convergence is achieved, thereby avoiding any ambiguity in load displacement space. A general overview of arc-length methods is provided with reference to Memon and Su (2004).

For load and displacement controlled methods, load and displacement are kept constant for each increment respectively, but for methods employing arc-length control a load-factor is introduced which is modified for each iteration such that the solution follows a specified path, such as a circular arc (see Figure 5.5). Since the load factor is treated as a separate variable, this then becomes an additional unknown in the equilibrium equations. This requires an additional constraint equation, for finite element implementation, which is expressed in terms of current displacement, load factor, and arc-length. In the case of varying arc-length, arc-length is re-evaluated at the beginning of each load increment. Arc-length and the current tangent modulus are used to compute the incremental displacements at which solutions for the load-factor are required.

Simplification of the constraint equations results in a quadratic equation whose roots are used to determine the load factor. The load factor is computed according to the rate of convergence of the solution process. If convergence is not achieved within a predefined number of iterations the load increment is reduced.

### 5.1.5 Displacement Control

When a solution is required to progress past limit points, an alternative to using load controlled solution methods is to formulate the calculation process in terms of incremental displacements (Simulia, 2010c). This is in contrast to the use of incremental load steps used

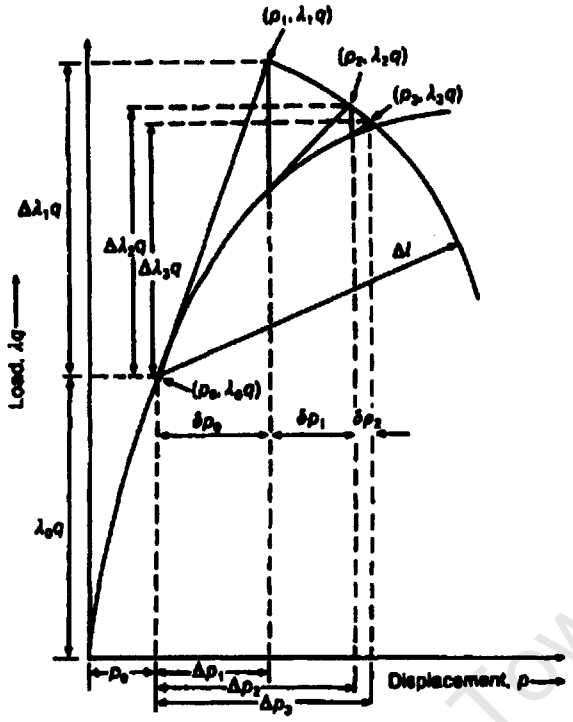


Figure 5.5: Arc-length control, or modified Riks methods, force equilibrium for each load increment to be found along a specified path. This allows for the numerical solution to progress pass maxima and minima in load factor-displacement space (Crisfield, 1991, Chapter 9).

with Riks methods. By defining the solution process in terms of displacement the point along the displacement curve is unique. Displacement controlled methods can generally be used in FEM implementations for problems where similar displacement control would be used in experimental testing. The use of displacement controlled methods can, however, break down if the structure exhibits snap-back behaviour or if the displacement behaviour exhibits sudden changes in load-displacement response (Crisfield, 1991).

Displacement control is best suited to problems where the maximum displacement is readily identified and where the point selected for displacement control is indicative of the behaviour of the rest of the structure.

## 5.2 Formex Configuration

The development of structural analysis has seen great improvement in areas such as non-linear capabilities, material constitutive descriptions and solution methods. The ability to pre-process information for submission to a finite element code, however, has often lagged behind (Nooshin and Peter, 2000). In practice pre-processing also represents one of the processes most susceptible to modelling errors. The repetitive nature of grid structures, with hundreds of members in a regular pattern, lends itself to more concise methods of describing structure geometry than individually defining each bar and node by their coordinates. Formex configuration is a method which addresses these problems by describing complex

structure geometry concisely in a few lines of code using the software package Formian 2 (Nooshin and Peter, 2000). The package has various commands which allow for the mirroring and array of bar elements as well as other more complex functions for use in describing space structures. Importantly, Formian 2 allows for the automatic generation of input files for propriety finite element codes including, geometry, element type, member cross-section, material, supports, constraint and loading properties.

Although the use of Formian 2, for the pre-processing of geometry for grid structure analysis, initially appeared very attractive, it was found to be more appropriate for use in design applications. Numerical model inputs created in Formian 2 are restricted to simple elastic descriptions of DLG structures. Formex configuration was therefore not employed in the research presented.

## 5.3 Abaqus

The Abaqus finite element code is widely used for nonlinear analysis in engineering research and industrial applications. The aspects of theory employed in the code, and used for analysis in this research, including the governing equations, solution procedures, dynamic analysis, quasi-static analysis, linear buckling analysis, Euler-Bernoulli beam elements, coupling elements and incremental plasticity, are widely accepted and have been validated against experimental behaviour. Where theory relating to the finite element method is presented in this document this is due to its importance with respect to application, a more rigorous representation of the theory employed in the Abaqus finite element code can be found in Simulia (2010c).



## 5.4 Conclusion

The high structural indeterminacy of grid structures results in member imperfections having a significant effect on elastic load distribution. The adequate numerical representation of grid structure nonlinear behaviour can only be achieved through combined geometric and material nonlinear analysis. Problems encountered in numerical analysis when passing limit points can effectively be overcome through the use of optimized methods, combining the modified Newton-Raphson and arc-length control solution schemes, or by use of displacement controlled analysis. Eigen vectors, resulting from buckling analysis and representing buckled mode shapes can be used to seed initial imperfections in nonlinear models which are susceptible to bifurcation behaviour. Linearized buckling analysis can be used to identify kinematic instability of structures.

# References

M. A. Crisfield. *Non-Linear Finite Element Analysis Of Solids And Structures Essentials.* John Wiley & Sons, 1991.

A. L. Koushky, G. Dehdashti, and A. Fiouz. Nonlinear Analysis of Double-Layer Grids with Composite Nodes under Symmetric and Unsymmetrical Gravity Loads. *International Journal of Space Structures*, 22:133–140, 2007.

Ramesh B. Malla and Reynaud L. Serrette. Double-Layer Grids: Review of Static and Thermal Analyis Methods. *Journal of Structural Engineering*, 122(8):873–881, August 1996.

Cedric Marsh. Some Observations on Designing Double-Layer Grids. *International Journal of Space Structures*, 15(3 and 4):225–231, 2000.

Bashir-Ahmed Memon and Xiao-zu Su. Arc-length technique for nonlinear finite element analysis. *Journal of Zhejiang University SCIENCE*, 5:618–628, 2004.

Hoshyar Nooshin and Disney Peter. Formex Configuration Processing I. *International Journal of Space Structures*, 15:1–51, 2000.

Simulia. *Abaqus Analysis User's Manual.* Simulia Corp., version 6.10 edition, 2010a.

Simulia. *Abaqus/CAE User's Manual.* Simulia Corp., version 6.10 edition, 2010b.

Simulia. *Abaqus Theory Manual.* Simulia Corp., version 6.10 edition, 2010c.

# Chapter 6

# Analysis Method

Collapse analysis of grid structures was undertaken with Abaqus 6.10. The Abaqus finite element code was selected as it proved to be the most versatile FEA software available to the author. The scripting capabilities of Abaqus were most useful in developing parametric studies.

An overview of analysis types and their respective advantages precedes an outline of the implementation of the Abaqus software to the collapse analysis of grid structures including consideration of, element types, material behaviour, boundary conditions, loading, symmetry and scripting. Although the analysis method and the validation of this analysis method are considered separately (see Chapter 7), the analysis method was developed through continuous comparison of numerical results with experimental results and therefore reference is made to Chapter 7 where relevant.



## 6.1 Grid Analysis

The numerical analysis of grid structure collapse is a geometrical and material nonlinear problem which additionally undergoes individual member buckling and global softening behaviour.

In general structural engineering applications the critical load of structures susceptible to instability is typically obtained through a linearized buckling analysis, however, as the full failure path of grid structures was to be investigated a full nonlinear analysis approach was adopted where both the geometric and material nonlinearities could be included. The failure of grid structures results from individual member failure and consequently this needed to be adequately modelled. Individual member failure in grid structures is characterized by bifurcation; consequently the finite element representation of the problem needed to be defined in such a way that there was no ambiguity in the displacement behaviour of individual member failure. To this purpose initial half-sine imperfections were seeded into the reference geometry at a member level (see Section 6.2.1.1).

### 6.1.1 Analysis Procedures

Five types of implicit integration finite element analysis procedures and one explicit integration analysis procedure exist in Abaqus which demonstrated potential for the application to the failure analysis of grid structures. A brief overview of these methods follows with reference to Simulia (2010a). The Riks Method represents the only load controlled analysis procedure capable of passing limit points in the structural response resulting from nonlinear analysis, all other analysis methods available in Abaqus require displacement control in order to capture critical and post-buckling behaviour of grid structures (see Section 7.3). All analysis procedures considered allow for nonlinear effects including, large displacements and rotations, and material and boundary nonlinearity.

**General Static Analysis** is the default static stress analysis in Abaqus which is employed where effects of inertia and time dependent material behaviour can be ignored.

**Static Analysis with Stabilization** can be used for applications where the solution to a general static analysis becomes unstable. To overcome such a problem, stabilization may be introduced into the solution process to allow progression of the solution. Stabilization is introduced through structural damping or energy dissipation. Applied damping and energy dissipation are required to be sufficiently large to prevent instantaneous buckling or collapse but should be sufficiently small as not to significantly affect the structural failure path.

**Static Riks Analysis** is used where instability resulting from buckling or collapse is encountered in the analysis and the structure consequently experiences global softening behaviour. Riks analysis allows for unstable structures to be analyzed under load control and allows for any arrangement of load to be considered. The Riks algorithm follows the equilibrium path of the structure and allows for the progression of the numerical solution past limit points in the structural response. The load applied in such an analysis does not follow a prescribed history but is included as part of the solution process. The load distribution is defined as a function of a single parameter, the Load Proportionality Factor, and loading is consequently scaled in a relative manner through the analysis.

**Quasi-Static Dynamic Analysis** is a dynamic analysis procedure in which the acceleration and velocity terms can generally be neglected and the focus of the analysis is on the final static response of the structure. The advantage of a quasi-static analysis over a general static analysis is that the effects of inertia are introduced to stabilize local instabilities resulting from buckling or collapse behaviour.

**Dynamic Analysis** uses time integration to calculate the transient dynamic response of a structural system. Dynamic analysis procedures are used where the immediate and

continuous structural response to dynamic loading (impact or vibration) is of interest and consequently the acceleration and velocity terms are of great significance.

**Explicit Integration Analysis** procedures can also be used, however, due to the small time steps required the computational time required for the analysis of static grid structure behaviour was found to be significantly larger than a comparable implicit analysis. Explicit integration analysis procedures were therefore not considered to be appropriate for the collapse analysis of grid structures.

The types of analysis procedures available in Abaqus all have their respective strengths and weaknesses with regard to their application to the collapse analysis of grid structures. The selection of the most appropriate analysis procedure was therefore undertaken through comparison between numerical results and the experimental results of Collins (1981) (see Chapter 7) and through consideration of the major difficulties associated with modelling grid behaviour.

### 6.1.2 Analysis Procedure Selection

The two major difficulties encountered in the analysis of grid structures were the occurrence of softening behaviour and sudden decreases in load resistance. The effectiveness of the previously introduced analysis procedures at capturing softening behaviour and sudden decreases in load resistance consequently defined which methods were most appropriate for the collapse analysis of grid structures.

#### 6.1.2.1 Softening Behaviour

As grid structures enter the post-buckling regime, global softening behaviour is generally encountered. For the analysis to continue past the critical point and into the post-buckling regime a solution procedure needed to be used which could account for such behaviour.

Both load and displacement controlled analysis are appropriate for capturing critical grid behaviour when the Riks and General Static Analysis procedures are used respectively (see Chapter 5). The Riks Method, however, develops the equilibrium response of a structure and therefore does not allow for grid structure post-buckling behaviour to fully develop and be identified (see Section 7.3). Displacement controlled analysis procedures were therefore considered to be more appropriate for the analysis of grid structures, as this allowed for the full failure path of grid structures to be developed and observed (see Sections 3.3 and 7.4.2); a displacement controlled analysis procedure was consequently adopted for grid analysis.

#### 6.1.2.2 Discontinuous Solution

To account for sudden decreases in structural resistance for displacement controlled analyses, as has been observed to frequently occur in the collapse of grid structures (see Sections

3.3.3.2, 3.3.4.1 and 3.3.4.2) a dynamic solution strategy was adopted and the displacement was applied in a linear ramp pattern over an appropriately long step time (displacement should be applied at a rate which is significantly lower than the dominant natural frequencies of the structure) so that the resulting solution represented the answer to the static problem, referred to as a quasi-static solution. By using a dynamic solution method for a static problem, greater stability was achieved through the application of numerical damping and the introduction of the effects of inertia.

#### 6.1.2.3 Summary

Due to the global softening behaviour and sudden decreases in load resistance frequently observed in the post-buckling behaviour of grid structures a displacement controlled quasi-static (dynamic) analysis procedure was found to most accurately capture the post-buckling behaviour of grid structures; provided the applied displacement was ramped linearly over a sufficiently lengthy time period relative to the dominant natural frequencies of the structure.

### 6.1.3 Solution Controls

Due to the highly discontinuous nature of grid structure collapse it was found that selected standard solution controls in Abaqus needed to be adjusted to allow for the analyses to run to completion. These solution controls do not significantly vary the solution but can result in improved computational efficiency.

#### 6.1.3.1 Convergence Criteria

Solution controls in Abaqus are frequently defined with respect to convergence of the solution, where this refers to a balance between external forces (forces or reactions at boundaries) and internal forces (internal forces resulting from the internal stress field). The difference between the internal and external forces is termed the force residual. Where the force residual is equal to zero the structure is in static equilibrium, however, for nonlinear problems the force residual is seldom equal to zero and therefore a maximum allowable residual error is defined, relative to the average member force, to judge convergence.

For the analysis of most nonlinear engineering problems the accuracy of the solution will generally be sufficient if convergence is accepted when the residual error is less than 0.5% for each increment (Simulia, 2010b). Due to the high indeterminacy of grid structures, however, it was found that the maximum allowable residual error applied to displacement and rotation fields needed to be reduced to 0.1%, in selected instances to ensure the numerical stability of the solution. A maximum allowable residual error of 0.1% was consequently adopted for all analyses undertaken.

#### 6.1.3.2 Time Incrementation

In addition to the use of a dynamic solver, 'Time Incrementation Controls' $I_0$ and $I_R$ were modified to account for the sometimes highly discontinuous nature of the solution. This was done to avoid premature cutbacks in increment time.

The incrementation control, $I_0$, determines the number of equilibrium iterations allowed before the residual is checked, so as not to be increasing in two consecutive iterations, while the incrementation control, $I_R$, specifies the number of iterations after which the logarithmic rate of convergence is checked.

The solution controls for convergence were set to the following values: $I_0 = 14$ and $I_R = 16$ for the purpose of the analyses undertaken; these are modified from the Abaqus default settings of $I_0 = 4$ and $I_R = 8$.

### 6.1.4 Solution Incrementation

Step time was found not to affect the solution, provided the step time was significantly larger than the first natural frequency of the structure. A step time of 20s was found to be adequate for the analysis of grids considered in the parametric study.

Initial increment size and the maximum allowable increment size were found to significantly affect the resolution of the solution path in both the elastic and post-buckling regimes. The maximum allowable increment size was found to influence the failure path, in selected cases, if it was not kept sufficiently small; this was largely due to its effect on stress and displacement fields during elastic loading. The initial increment and maximum increment time were consequently set to be equal with a value between 0.05-0.15s, and were varied when difficulties in convergence were encountered.



## 6.2 FEM Implementation

Justification for elements, material behaviour, boundary conditions and loading used in the analysis of grid structures is provided and their verification sought. The implementations of model parameters are discussed where applicable.

### 6.2.1 Elements

#### 6.2.1.1 Beam Elements

Euler-Bernoulli beam elements (Element code B33, in Abaqus) were used in the analysis of grid structures for this investigation. The use of beam elements to model member behaviour was initially considered and later proved to be sufficient as the focus of the study was on global structural behaviour. Members in grid structures are not generally placed under

high shear stresses and therefore decoupling of shear and bending moments, as considered for Timoshenko beam elements, was not required. The use of beam elements neglects the local instability effects of individual members and pipe section ovalization, which can be captured through the use of shell elements. The considerable increase in computational expense associated with the use of shell elements, however, proved not to be justifiable as little difference between the failure of members discretized with shell and beam elements was observed.

**Beam Imperfections** Grid failure behaviour is characterized by bifurcation; consequently numerical models were defined in such a way that there was no ambiguity in the displacement behaviour of individual member failure. To this purpose initial imperfections were seeded into the grid reference geometry in the form of a half sine wave displacement from the perfect geometry at the member level (imperfection magnitudes are expressed as the product of an imperfection factor and the geometric length of the perfect strut geometry). Initial member imperfections needed to account for all reductions in member capacity. Member imperfections were considered for all member groups which could potentially experience compression in the elastic regime. Imperfections were seeded in the vertical plane to limit influence on failure behaviour and were symmetrical about the grid centre (see Figure 6.1).

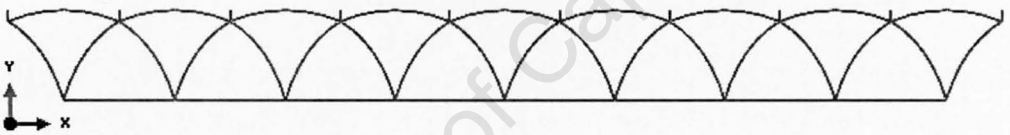


Figure 6.1: Elevation of grid with seed imperfections shown; imperfection scaled x25.

**Member Discretization** As individual compression members were seeded with an initial half-sine imperfection, the number of elements required to adequately capture the failure behaviour of such members in axial compression was consequently determined by comparing observed load displacement behaviour to failure, while varying the number of beam elements along the member length. Convergence of the failure path in load displacement space was found for 12 elements or more and consequently this value was used in further models. Convergence of the first Eigen value, resulting from a buckling analysis of a perfectly straight end fixed compression member, was also found to converge when 12 or more beam elements were used along the length of the member. The finite element buckling solution was found to underestimate the critical load by 0.14% when compared to the Euler critical load. Timoshenko beam elements were found to give higher errors for the critical buckling load.

#### 6.2.1.2 Connector Elements

In practice connection behaviour is seldom perfectly pinned or fixed but exhibits a degree of rotational stiffness which lies between these bounds. The rotational stiffness of connections has a significant effect on individual member and global structural behaviour and consequently needed to be considered. Connection rotational behaviour is usually nonlinear and

is typically expressed in the form of moment rotation curves. Due to the large number of connections in grid structures, however, a simple linear elastic representation of connection rotational behaviour was adopted. Connection behaviour was represented in the numerical models through the use of connection elements in Abaqus. A built-up connection was employed consisting of the translational component **join** and rotational component **cardan**. Connection stiffness was defined for each degree of freedom (DOF) about a local axis. Initially the local DOF corresponding to member torsion was set to rigid, however, greater numerical stability was observed by setting this stiffness equal to the stiffness value associated with the local DOF corresponding to member bending.

**Implementation** Two approaches to the implementation of connector elements were considered. Initially connectors were modelled as a combination of rigid elements and an offset elastic connector as per Vaeghi Amir and Davoodi (2002) (see Figure 6.2). This representation of the grid connector was, however, found not to be suitable as the connector rotation no longer occurred about the intersection of the member centrelines. This effectively changed the structural behaviour of the connector as can be seen in the kinematic instability of a single triangular pyramid module, a geometric configuration which is kinematically stable. Due to the change in structural behaviour resulting from a connector implementation as suggested by Vaeghi Amir and Davoodi (2002), it was decided to model connector behaviour at the coincident point of the member centrelines. This resulted in the kinematic stability of a triangular pyramid module as would be expected. Consequently the connector rotational stiffness as considered for the purpose of this investigation considers the entire connector behaviour, including end rigidity, as would be observed in the common Moment-Rotation description of connector behaviour.



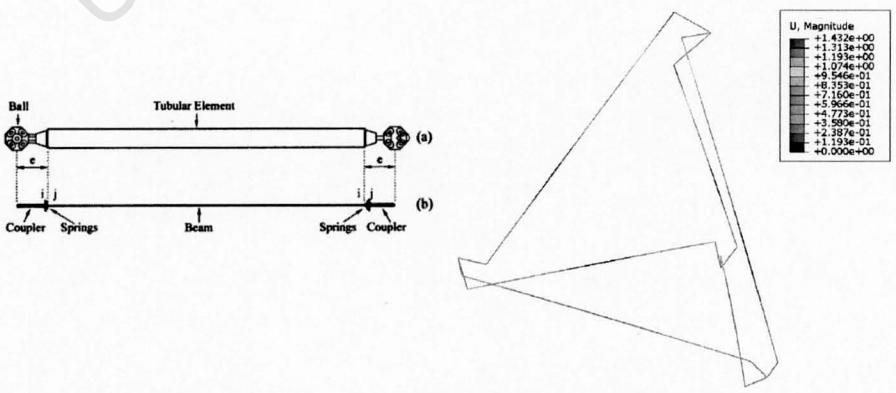


(a) Connector implementation schematic. (b) Kinematic instability of three sided pyramid module.

Figure 6.2: Connector implementation of Vaeghi Amir and Davoodi (2002) and the associated misrepresentation of a three sided pyramid module's behaviour.

### 6.2.2 Material Behaviour

A linear elastic, perfectly plastic description of material behaviour was used. Solland (1999) recommends that for the collapse analysis of steel jacket offshore structures material behaviour is limited to the yield plateau of common structural steels and therefore strain hardening effects should not be considered. This is as, for compression members prior to collapse, strains in buckled members are generally limited to the range $0.3\% - 0.5\%$, and for tension members ductility criteria will limit strains before strain hardening becomes significant. Similar behaviour was observed in the analysis of DLG structures.

The use of linear elastic, perfectly plastic material behaviour was justified through comparison of the numerical results with experimental results (see Section 7.2.3). It was found that the inclusion of strain hardening material behaviour in the numerical analysis resulted in a strain hardening of the global structural behaviour in the post-buckled regime which was not consistent with experimental results.

### 6.2.3 Boundary Conditions

Simply supported boundary conditions were applied as translation and equation constraints at the corner support nodes; no rotational restraints were enforced. This method of applying boundary conditions was found to be most consistent with the experimental work of Collins (1981) (see Figure 7.2) and additionally ensured symmetrical displacement of corner nodes. Simply supported conditions were achieved by applying positive and negative vertical restraint at all support nodes (direction of Y axis) and through equation constraints which enforced symmetry of support displacement in the horizontal plane, about XY and YZ vertical planes. For the case of pinned DOS grids, further equation constraints were applied to ensure kinematic stability (see Section 8.2.2.1).



### 6.2.4 Loading

Flat grid structures are most commonly employed as roofing structures. Consequently the loading pattern dominating the static global response of such structures is a distributed load corresponding to rain water or snow loading for example. This is as opposed to a concentrated load which may dominate the behaviour of local members.

It is preferential to analyze the failure behaviour of structures under a representative loading pattern. A uniformly distributed load (UDL) would be such a representative load distribution for grid structures. Displacement control is, however, typically applied to analyses where a single displacement boundary condition is applied to a single point or to a group of nodes where the node group undergoes equal displacement; this is not the case for grid structures.

One method of applying a UDL under displacement control is through the development of an articulated load frame as was undertaken in the experimental analysis of El-Sheikh and McConnel (1993); however, this type of setup is limited to two points or grids of load points

of multiples of 2 and symmetric about 2 horizontal axes (i.e. 2x2, 2x4, 4x4 etc.). The equal distribution of load when using an articulated frame is achieved through the ability of each arm to rotate individually and through a balance of load on each arm.

The finite element representation of such an articulated load frame was initially attempted. Results from using such a frame can be seen in Figure 6.3. Equal distribution of load when passing limit points; however, broke down as rotation of the load frame did not occur sufficiently quickly. The use of such a frame in a finite element analysis introduced significant additional complexity into the model and was consequently disregarded.

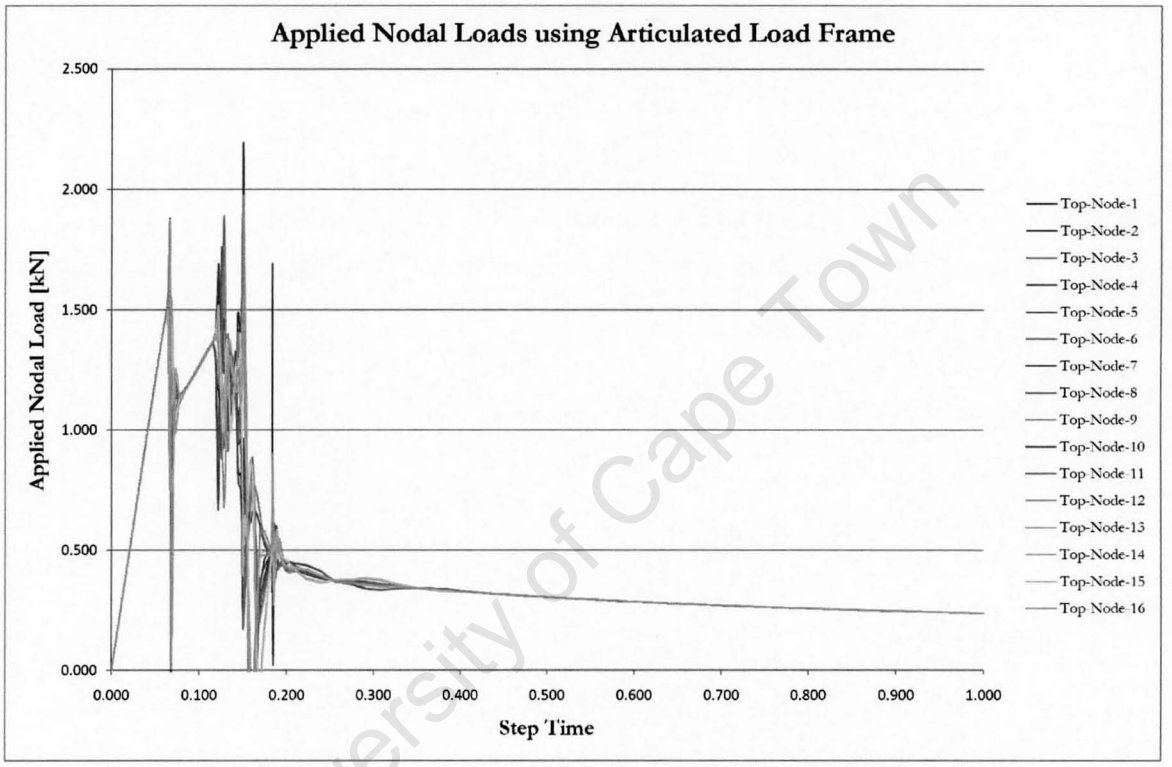


Figure 6.3: Load-displacement behaviour of a SOS grid with distributed loading applied with FEA implementation of an articulated load frame.



An alternate method of equally distributing load applied in a finite element model under displacement control was consequently developed by employing a combination of the following Abaqus elements and constraints:

- The translational connector element **link** which constrains displacement along the axis between two nodes, also referred to as a pinned rigid link;
- The **continuum distributing** coupling constraint, typically used to constrain multiple shell element nodes to a single point, distributes load at a reference node to connected coupling nodes achieved through a moment and force balance (see Section 6.2.4;
- And the **equation constraint**, used to constrain specific DOF in an equation form.

In this setup a 'Control-Node', located at the centre of mass of the load points, and other secondary nodes directly below each load point were created in the same horizontal plane.

The 'Control-Node' was connected to the secondary nodes with the **distributing coupling constraint** and the secondary nodes were in turn connected to the load nodes with the **link connector** elements. An additional two **equation constraints** were then defined for each connector elements to constrain horizontal movement of the secondary node to that of the load node, this was done to ensure that the axial load transferred from the secondary node to the load node was always applied in the vertical plane. The control node remained at the centre of mass of the grid load points throughout the analysis as the loading considered was only applied in the vertical plane and grid horizontal displacement was symmetric about two axes. This setup consequently allowed a single displacement boundary condition to be applied at the 'Control-Node' for which the resulting reaction could be monitored. An added benefit of this method of load application was that any combination of load points, symmetrically distributed about the control node, in plan, could be accommodated.

**Distributing coupling element** distributes load between a reference node and multiple coupling nodes. Admissible distribution of force must satisfy Equations 6.1 and 6.2 (Simulia, 2010b):

$$\sum_n F^n = F^R \tag{6.1}$$

$$\sum_n x^n \times F^n = M^R + x^R \times F^R \tag{6.2}$$

where $F^R$ and $M^R$ are the force and moment at the reference node, $F^n$ is the statically admissible force distribution amongst the coupling nodes and $x^R$ and $x^n$ are the positions of the reference and coupling nodes respectively.



### 6.2.5 Symmetric Collapse

The symmetrical failure path of a grid structure generally represents the upper bound of grid critical behaviour, as multiple members symmetrical about the point of maximum deflection fail together, and the lower bound of post-buckling behaviour, as grid failure is distributed throughout the model and consequently fewer alternate load paths remain available (see Figure 9.31).

Although in practice the symmetrical failure of grid structures is highly unlikely, due to inherent imperfections present in assembled grid structure geometry and local geometric and material imperfections at a member level, it was initially decided that the symmetrical failure path of the grid structures would be investigated. This was as the symmetrical failure of grid structures allows for better comparison between different grid structures as failures occur at a larger scale across the grid; this is in contrast to non-symmetrical failures where failure tends to concentrate about the point of initial failure. It was additionally thought that an investigation into the symmetrical failure of grid structures would simplify implementation

in a finite element model, as the distribution of imperfection within the model would not need to be considered.

The subject of symmetry and divergence from symmetry in the analysis of grid structures was a recurring theme. Every aspect of the numerical models considered, including geometry, boundary conditions, member sizes, seeded imperfections and loading, were symmetric and consequently a symmetrical failure path was expected. The failure path of the grid structures analyzed, however, tended to diverge from a symmetrical failure path. The reason for the divergence from the symmetrical failure path was thought to be due to the allowable residual at the end of each increment in the analysis procedure adopted, but this could not be proven. Tolerated errors and step sizes were significantly reduced in an attempt to force the finite element model to maintain a symmetrical failure path, but this was not achieved; this behaviour further highlights the sensitivity of DLG structures to imperfections.

Symmetry of grid structure failure behaviour was therefore enforced through the use of equation constraints for cases where the full geometry was considered (see Section 8.6.3).

## 6.3 Grid Symmetric Quarter Models

The symmetric nature of grid geometry lends itself to the use of symmetry in the analysis of such structures. For the case of uniformly distributed load one quarter of the full grid geometry was used for analysis purposes. The symmetric division of grid geometry was carefully considered to ensure ease of implementation. The use of symmetry in analysis requires the implementation of appropriate boundary conditions along the lines of symmetry, while the method of load application employed for full grid models required slight modification.

### 6.3.1 Lines of Symmetry

The division of SOS and DOS geometry into symmetric sub assemblies, as employed in all subsequent analyses which make use of grid symmetry, is presented. Careful consideration of grid division was undertaken to minimise the number of members which are located on the lines of symmetry. For the case of members which do lie on the lines of symmetry member cross sections were reduced such that the resulting member stiffness and resistance was reduced by 50%.

#### 6.3.1.1 SOS Grid

Lines of symmetry which extend from the middle of one edge to the middle of the opposite edge are considered for the symmetric description of SOS geometry dividing the grid structure into square quarters in plan (see Figure 6.4). Although certain lower chord members are located on the lines of symmetry, these members number significantly less than the alternate symmetric configurations.

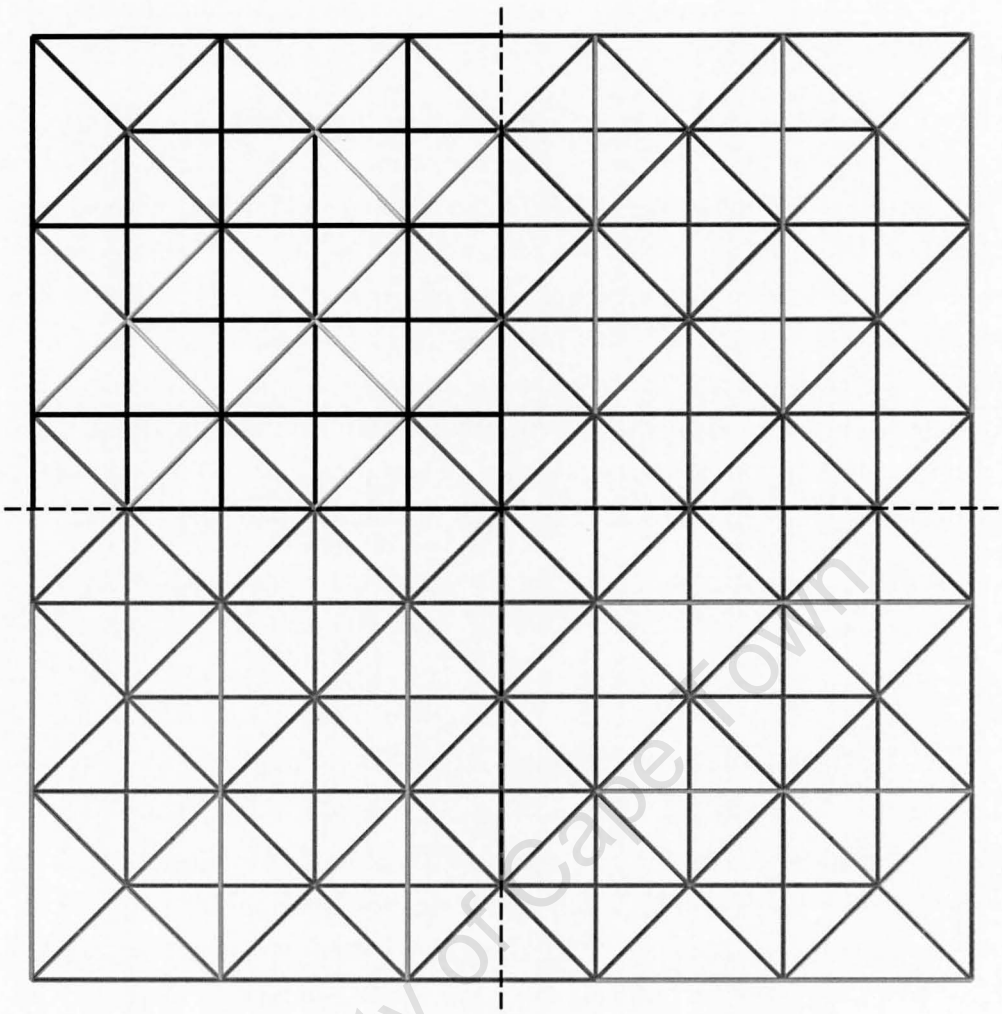

Figure 6.4: Plan view of SOS quarter model (colour) as fraction of full model (gray scale).



#### 6.3.1.2 DOS Grid

Lines of symmetry which extend between opposite supports are considered for the symmetric description of DOS geometry dividing the grid structure into triangular quarters in plan (see Figure 6.5). The symmetric configuration of DOS grids considered does not result in any members lying along the lines of symmetry.

### 6.3.2 Boundary Conditions

Symmetric restraints were applied along the lines of symmetry by restricting selected rotational and displacement degrees of freedom (see Figure 6.6 (SOS grids) and Figure 6.7 (DOS grids)) while the single corner support included in each symmetric quarter model was defined in the vertical direction only and constraint equations used to enforced symmetry of support displacement in the horizontal plane, about XY and YZ vertical planes, simulating simply supported conditions. For nodes on the lines of symmetry, displacement perpendicular to the line of horizontal symmetry, rotation about the horizontal line of symmetry and rotation

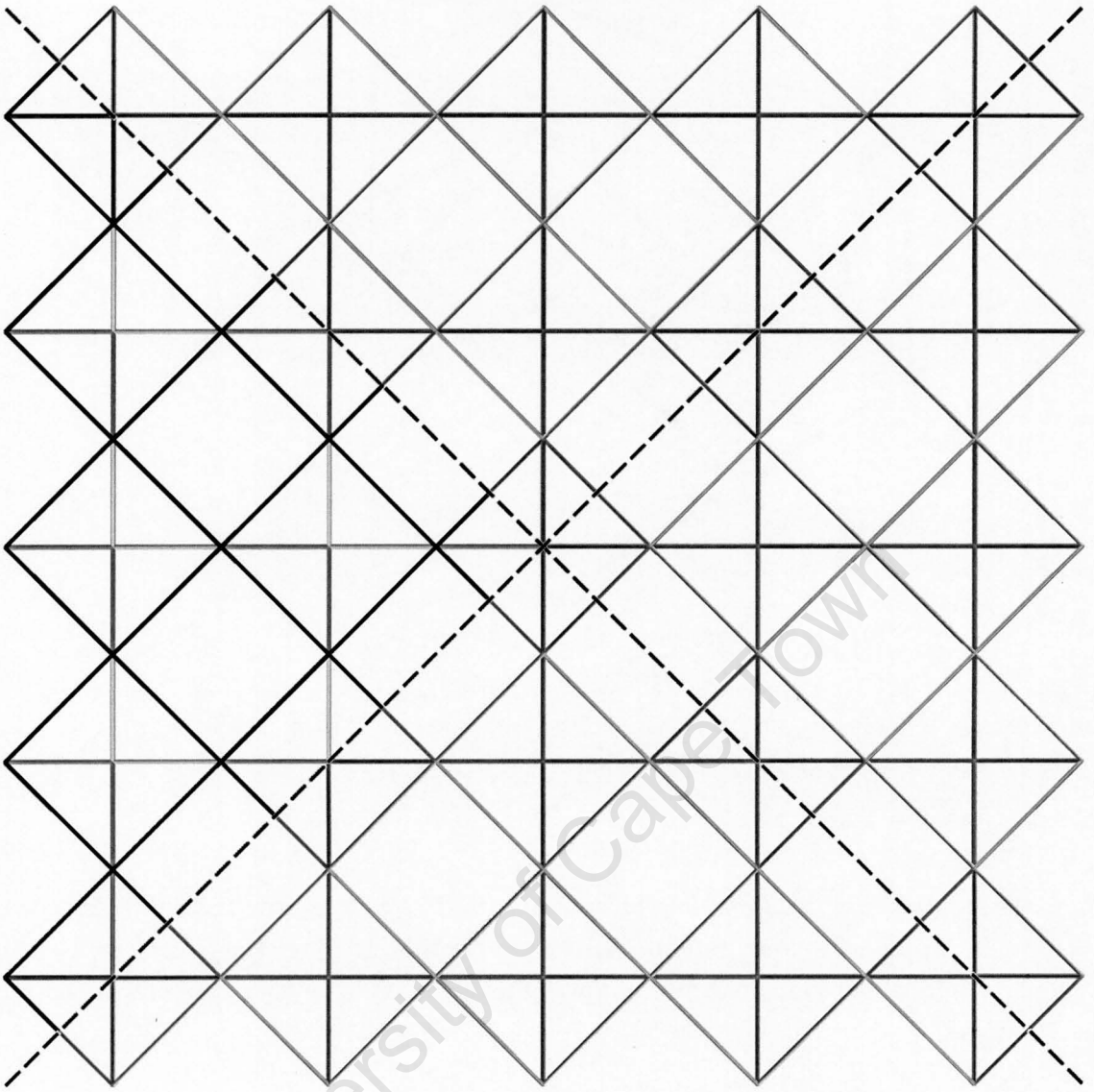

Figure 6.5: Plan view of DOS quarter model (colour) as fraction of full model (gray scale).



about the vertical axis were restricted.

### 6.3.3 Loading

For the case of applying distributed loading to symmetric quarter models the same method presented in Section 6.2.4 can be used, however the centre of mass of the load points is no longer located at the centre of the grid and therefore the control node will also not be at the grid centre. Displacement of the control node however still represents the average displacement of loaded nodes in the quarter model and therefore represents the average displacement of the loaded nodes for the complete model too. In comparing load-displacement behaviour between quarter and full descriptions of grid geometry the load applied to the quarter model should be multiplied by a factor of 4.

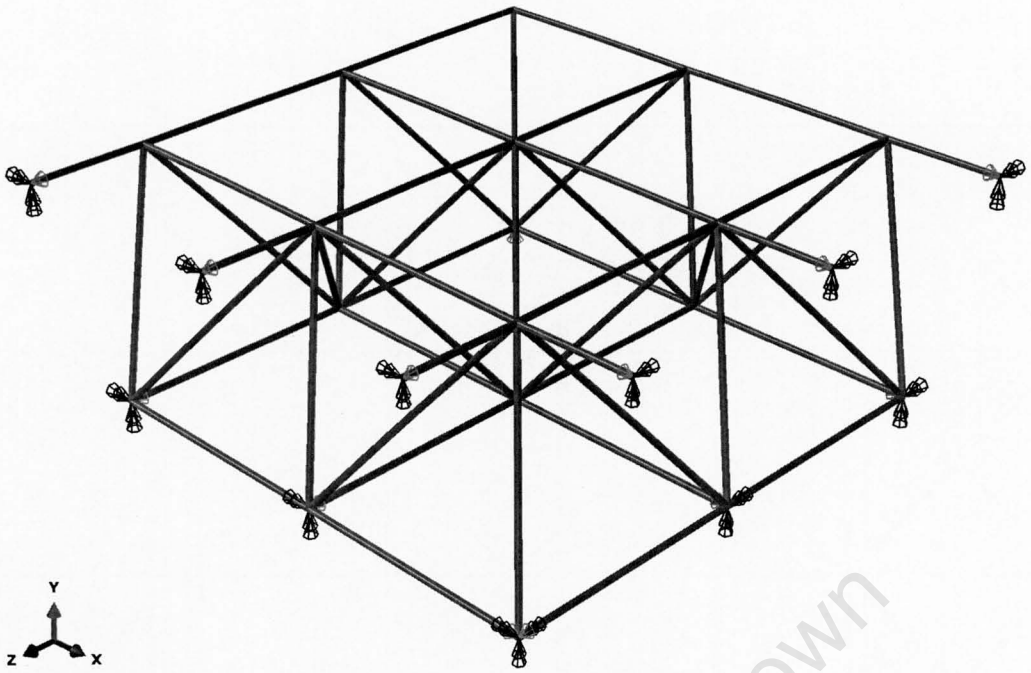


Figure 6.6: Rotational (blue) and displacement (orange) boundary conditions applied to SOS quarter model.

### 6.3.4 Failure Path

Where symmetry was employed for the analysis of grid structures, by considering the symmetric quarter model representation of grid geometry, problems relating to divergence from symmetry were not encountered; this is due to the reduction in ambiguity of potential failure paths.

## 6.4 Scripting

Analysis pre-processing was undertaken with Python, an object-orientated programming language. Abaqus CAE interfaces with Python and allows for the parameterization of model information. This allowed for multiple successive jobs to be batched from a parameterized Python script. Abaqus CAE generates the input for the Abaqus Standard finite element code, based on instructions in the Python script, and submits the input to Abaqus standard (the implicit integration finite element code). The use of Python scripting with Abaqus additionally allowed for jobs to be submitted without the use of the Graphical User Interface, reducing computational demands and therefore resulting in a reduction to job run times.

The historical approach to numerical modelling has been to directly write text based input files. This was initially the approach adopted, however, Python proved to be significantly more powerful and less complex. Not all Abaqus features are however supported by Abaqus CAE and therefore the direct approach to input processing is sometimes required [1].

[1]Seeding member imperfection as multiples of Eigen vector deformation results from a linear buckling analysis is an example of a feature which requires modification of the Abaqus input file

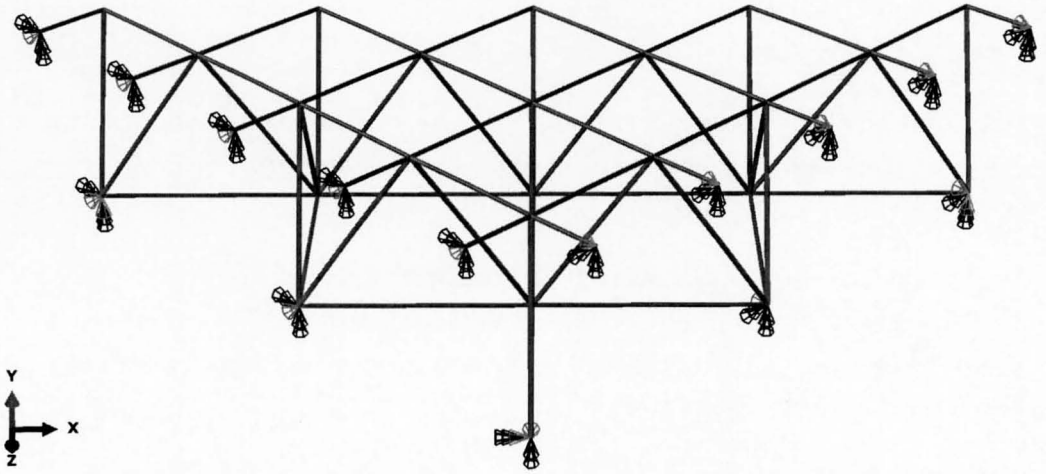


Figure 6.7: Rotational (blue) and displacement (orange) boundary conditions applied to DOS quarter model.

The ability for Abaqus to interface with Python allowed for the feasible application of Abaqus to a parameter study of the size considered for this research. The number of models considered would not otherwise have been possible if attempted by conventional means and would have been susceptible to input errors. The use of a single parameterized input acts to reduce modelling errors as all models are derived from the same set of coded instructions.



## 6.5 Modelling Method and Solution Strategy - Summary

The modelling method and solution strategy as adopted for the collapse analysis of grid structures undertaken for the presented research is summarized as follows:

- Structural members were modelled with Euler-Bernoulli, 2-noded, cubic elements; 12 elements were defined along the length of each member; Cross-sections were integrated during the analysis to account for variations in member stiffness through the analysis;
- Elastic, perfectly plastic material behaviour was defined through Young's Modulus, Poison's Ratio and yield stress material parameters;
- Geometric imperfections were introduced to compression members in the vertical plane of the reference geometry, in the form of a half-sine imperfection, with the magnitude of imperfection specified by EC3 (2005) as $L/250$ for the purpose of plastic analysis;
- Simple support conditions were applied as translation and equation constraints at corner supports, translation was constrained in the vertical direction and symmetry of support nodes in the horizontal plane was enforced through equation constraints;
- For the case of the symmetric models, boundary conditions were applied at nodes on the planes of symmetry by restricting displacement perpendicular to the plane of symmetry and by restricting rotation about the line of symmetry and about the vertical axis;

- Gravitational loading was applied in Step 1, a general static step, through the application of a gravitational acceleration of $9.81 m.s^{-2}$;
- Distributed or point loading was applied as a displacement in Step 2, an implicit dynamic quasi-static displacement controlled step, and ramped linearly through the step;
- Where loading was applied as a UDL, this was achieved by applying a prescribed displacement to a reference node; load was then distributed from this node to the top chord nodes using a distributing couple element, link connection elements and equation constraints;
- Time Incrementation Solution Controls were modified, to $I_0 = 14$ and $I_R = 16$, to account for the discontinuous nature of the solution;
- The solution controls, for convergence acceptance criteria, of displacement and rotation fields were modified, between a range of 0.1-0.5% of the residual error, to account for the high indeterminacy of grid structures;
- A total step time of 20s was employed for Step 2. This was found to be sufficiently long relative to the dominant natural frequencies of the DLGs considered as increasing total step time resulted in no significant change to grid behaviour;
- Initial and maximum increment sizes were varied to achieve convergence of the solution. Initial and maximum increment sizes were kept to approximately $1/200$ of the step time to ensure that both the elastic and post-buckling structural responses were captured at an adequate resolution;
- All inputs were parameterized with Python to allow for parametric investigation and to mitigate input errors.

# References

Eurocode 3: Design of Steel Structures - Part 1.1: General Rules and Rules for Buildings BS-EN 1993-1-1:2005, 2005.

Ian Martin Collins. *Collapse Analysis of Double-Layer Grids.* PhD thesis, University of Surrey, 1981.

A.I. El-Sheikh and R.E. McConnel. Experimental Study of Behavior of Composite Space Trusses. *Journal of Structural Engineering*, 119:747–766, 1993.

Simulia. *Abaqus Analysis User's Manual.* Simulia Corp., version 6.10 edition, 2010a.

Simulia. *Abaqus Theory Manual.* Simulia Corp., version 6.10 edition, 2010b.

Gunnar Solland, editor. *Ultiguide: Best Practice Guidelines for use of Non-Linear Analysis Methods in Documentation of Ultimate Limit States for Jacket Type Offshore Structures.* DNV-SINTEF-BOMEL, 1999.

J. Vaeghi Amir and M. R. Davoodi. Modelling the Semi-Rigid Behaviour of the Mero Jointing System. In *Space Structures 5, Volume 1*, 2002.

# Chapter 7

# Validation

This chapter documents the validation of a finite element model, compiled for and analyzed with the Abaqus code, of the collapse of a simple corner supported, 5x5 module, DLG, with SOS configuration and mansard edge detail under two-point loading. Validation was targeted through the comparison of the numerical model results with the results of physical experiments presented by Collins (1981) and motivation for the use of displacement controlled analysis is also provided. The extension of numerical model validation to cases including semi-rigid connections and uniformly distributed loading was then undertaken; the effectiveness of DLG parameterization used in subsequent analyses was assessed through consideration of model scale. A model for an alternate DOS DLG geometric configuration was additionally validated. Finally the description of grid plastic behaviour is assessed and the effectiveness of employing grid symmetry for the purpose of analysis investigated.



## 7.1 Introduction

The validation of finite element models through comparison of the numerical results with the results of experimentally analyzed physical models is critical to establish confidence in the results obtained from numerical modelling. It is imperative that the modelling method validated against experimental data is employed as strictly as possible in further analyses.

The review of literature on the experimental analysis of grid structures revealed that the most appropriate experimental results for the validation of numerical DLG collapse analysis were the experimental results presented by Collins (1981). Validation of the collapse analysis method presented in Chapter 6 is therefore undertaken through comparison with these results. The differences between displacement and load controlled analysis methods are then considered through comparison between the results of similar load and displacement controlled grid collapse analyses.

The extension of numerical model validation to the case of grid structures with semi-rigid connections is sought through comparison of grid structures with connection stiffnesses which range between upper (fixed) and lower (pinned) bounds. The suitability of the method

described in Chapter 6 for applying uniformly distributed loading to grid structures under displacement control is assessed.

The effectiveness of the DLG parameterization in subsequent analyses is then considered by investigating the effect of scale on grid behaviour for various failure mechanisms. The effect of scale on grid behaviour is subsequently used to size a comparable DOS grid configuration. Validation of the DOS grid is targeted through critical comparison with similar SOS grid experimental results. The plastic description of material behaviour employed and the nonlinear geometric analysis is assessed through consideration of loading, unloading and reloading cycles.

The use of symmetric boundary conditions allows for a full double-layer grid to be analysed under uniformly distributed loading by considering only one quarter of the total structure geometry. The effectiveness of the symmetric quarter model, including associated boundary conditions and method of load application, is assessed through comparison of the quarter and full DLG results for both SOS and DOS configurations.

Structural behaviour and critical output values are compared between physical and numerical models. Where variations are encountered these are accounted for as best as possible. All the results presented are for the final modelling method proposed and are adopted for analyses undertaken in subsequent chapters.



## 7.2 SOS Grid Analysis Validation

The review of available literature revealed that the most appropriate and comprehensive experimental results available for the purpose of validating numerical models, capturing the failure behaviour of DLGs, were those of Collins (1981) (see Chapter 3). The experimental objective of Collins (1981) was to develop a set of experimental results of the failure behaviour of DLG structures to validate similar numerical models, consequently significant attention was paid to minimizing unknowns in the experimental set-up such that discrepancies in results could largely be attributed to the numerical representation of the problem. Collins (1981) conducted his experimental analysis with displacement control so that the full structural failure path could be observed, the appropriateness of this statement is considered through the comparison of results from load and displacement controlled analyses (see Section 7.3).

Although great care was taken by Collins (1981) in the design and assembly of the grids and experimental equipment to limit experimental unknowns, there were material parameters which were not clearly defined in "Collapse Analysis of Double-Layer Grids "(Collins, 1981) and consequently require further attention as part of this validation process.

### 7.2.1 Collins' Grids

Collins (1981) investigated the failure behaviour of four, 5x5 SOS module, mansard edge

detail, corner-supported, rigidly connected grids constructed of steel CHS with the purpose of validating a numerical collapse analysis method based on idealized strut behaviour. Four grids of nominally identical geometry were tested to failure under various load configurations (see Figure 7.1). Loading was applied for each grid at two nodes at the upper chord level by actuators which additionally controlled the progression of the experiment in terms of displacement.

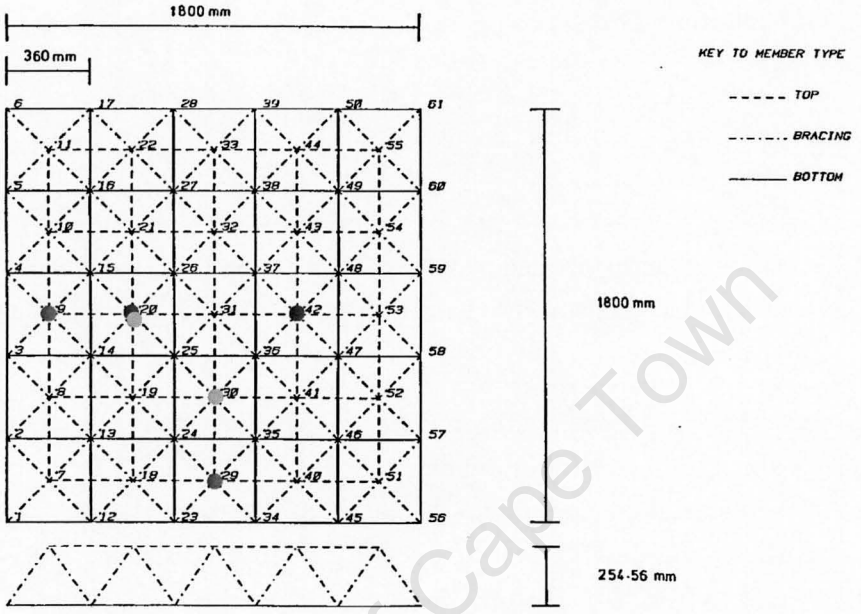


Figure 7.1: Plan of grids as tested by Collins (1981) with loaded nodes shown, Grid No.1 (green), Grid No.2 (red) and Grid No.3 (blue).

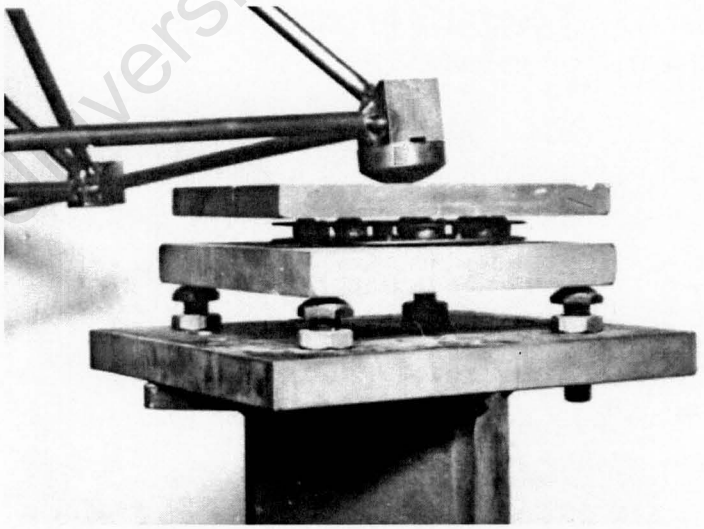

Figure 7.2: Support detail for Collins' (1981) grids.

### 7.2.2 Validation Method

Experimental results, as reported by Collins (1981), were used to validate the finite element models, analyzed with the Abaqus finite element code, according to the modelling method

presented in Chapter 6. Attention was paid to Grid No. 1 (Collins, 1981) as the experimental results of this grid are best suited to the validation of the numerical analysis; this is as symmetry about the loading axes in plan was relatively closely maintained throughout the test. The results of the experimental analysis of Grids No. 2, 3 and 4 were characterized by a divergence from symmetry (Divergence from a symmetric failure path is governed by the random distribution of imperfections throughout the structure which is beyond the scope of the work presented). Validation was sort through comparison of load-displacement behaviours and deformed geometries.

#### 7.2.2.1 Material and Member Behaviour

FE representation of Collins' (1981) grids required further consideration of material behaviour, which was not clearly defined by Collins (1981), and the magnitude of initial member imperfections; an input parameter for the specific nonlinear analysis method proposed.

**Yield Stress;** although tension and compression tests were undertaken of individual members, there was confusion regarding different batches of steel used by Collins (1981) as is demonstrated in reported member failure loads which are above the yield stress determined in testing. Although Collins (1981) conducted extensive testing of individual members, Collins (1981) had to resort to using critical loads observed in experimental analysis for the numerical analysis for this reason.

**Imperfection Magnitude;** is a parameter required for the type of nonlinear analysis proposed in Chapter 6, it is influenced by fabrication and assembly tolerances and should be calibrated with experimental behaviour where possible.

For the case considered, individual member behaviour is dependent on the member material yield stress and the member initial imperfection. It was therefore decided to vary yield stress and initial imperfection values in the failure analysis of Collins' Grid No. 1 to determine appropriate values for these parameters through comparison with the experimental grid behaviour.

Individual member behaviour was consequently initially modelled in Abaqus and an appropriate initial approximation of member imperfection and yield stress was adopted, based on comparison with the experimentally measured critical member stresses reported by Collins (1981).

Variation of these two parameters was then undertaken for the grid analysis, within reasonable ranges, to test the sensitivity of the structure to these parameters and identify the values which best defined the experimental work of Collins (1981). The magnitude of bow imperfection proposed in EC3 (2005) for plastic nonlinear analysis of $L/250$ for members corresponding to buckling curve $a$ was used to guide this selection.

Results of the numerical analysis method were then compared to the experimental results of

Collins (1981).

The effect of plastic material behaviour was additionally investigated to determine if strain hardening occurred for the strain ranges encountered in DLG collapse. This was done by varying the degree of strain hardening defined in the elastic plastic material model describing steel behaviour and comparing the experimental and numerical results.

### 7.2.3 Results and Discussion

A comparison between the failure behaviour as documented by Collins (1981) and that observed in the results of numerical analysis undertaken with Abaqus is made.

#### 7.2.3.1 Parameter Variation

Parameters not explicitly defined in the experimental work of Collins (1981) were calibrated through parameter variation and comparison of load displacement behaviour. The sensitivity of selected parameters was investigated where deemed necessary and an appropriate model for material behaviour selected.

**Yield strength and Initial Imperfection** Combinations of imperfection magnitude and yield stress were varied together. Failure paths, in load displacement space, for the independent variation of yield stress (Figure 7.3) and initial imperfection (Figure 7.4) are shown.

It can be seen from the resulting load-displacement responses that the material yield stress affects the post-buckling residual strength of the grids, while a combination of material yield stress and imperfection determine the critical structure resistance. This observation allowed for an appropriate value of yield strength to first be identified, followed by the identification of an appropriate value of initial imperfection.

A yield stress of $340MPa$ and an initial member imperfection of $L/769$ were found to most accurately define the experimental setup of Collins (1981) for the FE model considered.

**Plastic Material Behaviour** An elastic, perfectly plastic material behaviour was found to be most representative of the material used by Collins (1981) in the strain range considered. Material hardening behaviour was found to result in an increase in post buckling grid residual strength with displacement. This was not consistent with experimental results.

**Discrepancies** A moderate discrepancy in the gradient of the load-displacement response in the elastic regime of structure behaviour was observed between the experimental and analytical results. The experimental grid tested was found to be less stiff when compared to the results of numerical model analysis. Owing to this observation a further parameter investigation was undertaken where the material's Young's modulus was varied in a range

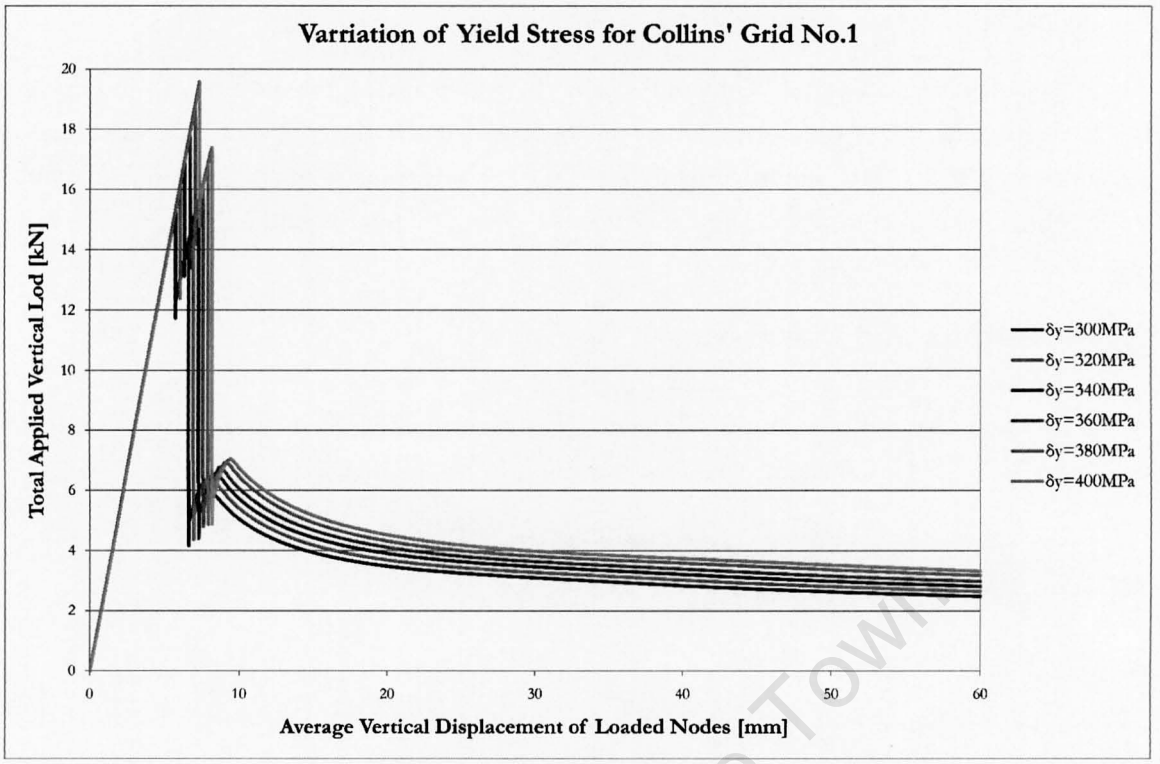


Figure 7.3: Load-displacement behaviour of Grid No. 1 for variation of material yield stress.

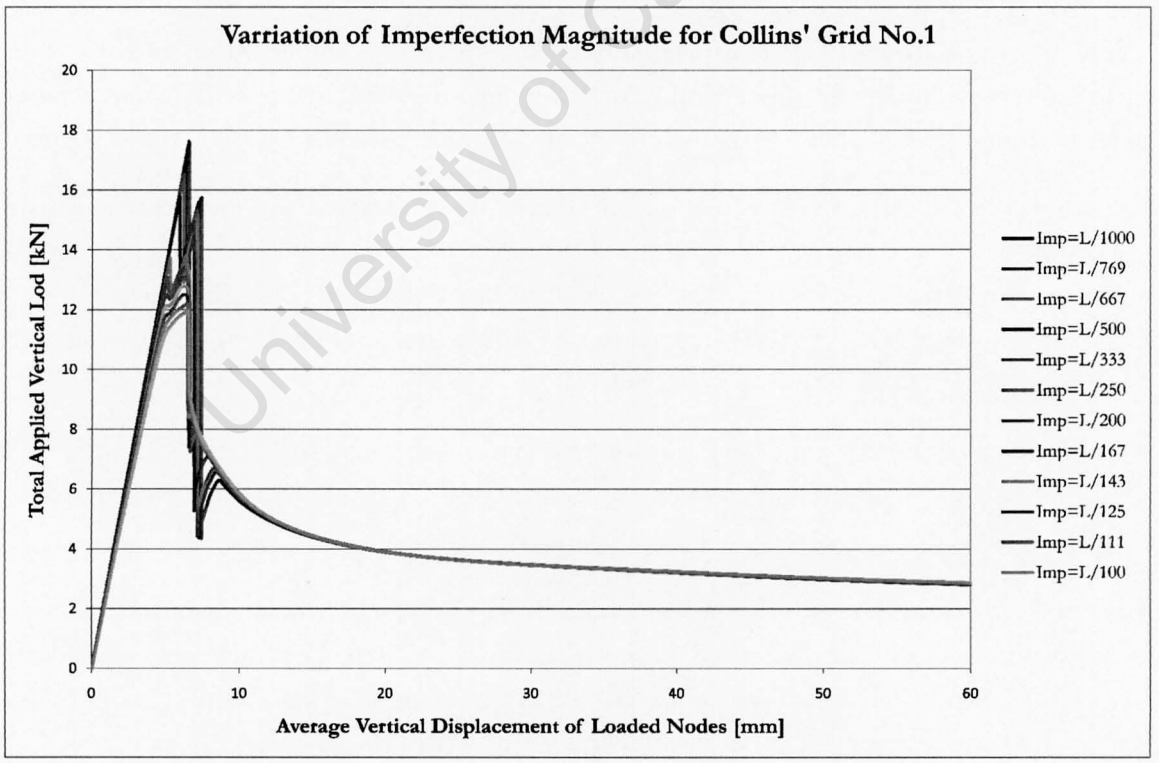


Figure 7.4: Load-displacement behaviour of Grid No.1 for variation of initial half-sine imperfection magnitude.

consistent with steel ($190 - 210GPa$). No significant change to the behaviour of the grid in the elastic region was observed and consequently the original value, as defined by Collins (1981), of $204.8GPa$ was adopted.

The discrepancy in the grid elastic stiffness was consequently believed to be most likely attributed to nonlinear connection behaviour, the numerical and experimental grid response were observed to be initially equal but varied with increasing grid displacement. The effect of this nonlinear connection behaviour was however not believed to have a significant influence on grid behaviour as grid collapse, characterized by a sudden decrease in grid resistance, initiated at approximately equivalent values of grid displacement for both experimental and numerical cases.

#### 7.2.3.2 Grid No. 1

A description of grid failure behaviour observed in the FEA results precedes a comparison of load-displacement behaviour for FE and experimental analyses.

**Description of Failure** The failure mechanism associated with Grid No.1 was compression yielding of top chords. Failure initiated in the two top edge chords at mid-span and spread inwards. As the top chords buckled, load was redistributed from the edge chords to the adjacent set of parallel chords, as was observed in the first instances of softening behaviour in the load-displacement plot. When the second pair of top chord members buckled a significant and sudden reduction in grid load resistance was observed for a minimal increase in vertical displacement, since load was not adequately redistributed in time to the centre chord member. A slight hardening regime followed as load was distributed to the centre top chord, but this member quickly buckled and softening resumed, levelling off into the post-buckling residual strength. Successive buckling of adjacent chord pairs resulted in the development of a plastic hinge in the grid about which further rotation occurred.

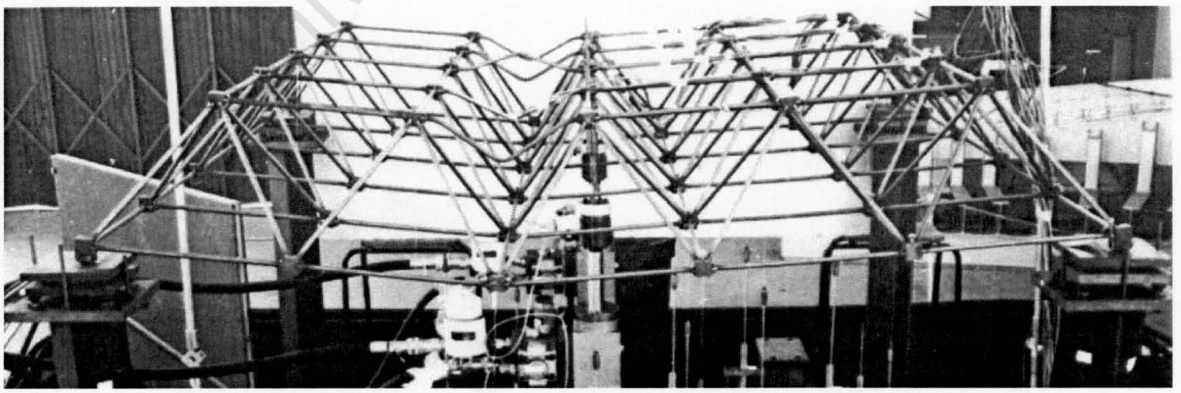

Figure 7.5: Failure condition of Collins' Grid No.1 (Collins, 1981).

Although much of the grid's load resistance was lost due to buckling, the residual strength of the buckled chord members and the tensile strength of the bottom chord members were able to continue supporting load in the post-buckling regime. The failure mechanism identified in the experimental test was captured very closely by the numerical model as can clearly be seen in the comparison of Figures 7.5 and 7.6.

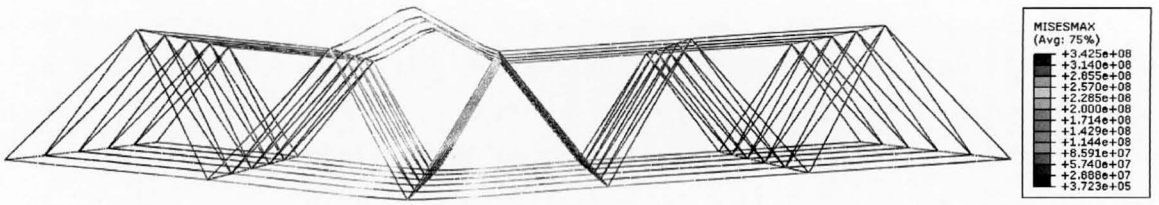


Figure 7.6: FEA results for Collins' (1981) Grid No.1 failure condition, with superimposed maximum von Mises section stresses (displacement scale 1:1).

**Load-displacement Behaviour** Load-displacement and deformed geometry plots, for the experimental and numerical analyses of the collapsed structures, show good correlation between results for critical values and residual strength behaviour. Individual buckling events can be identified in the load-displacement plot resulting from the numerical analysis but only a single buckling event is observed in the experimental plot. The observed discrepancy may be a result of sampling frequency in the experimental test or may result from dynamic effects not captured by the numerical model, but this is not considered to be significant as it does not appear to influence the critical load, the failure path, or the residual strength of the structure.

It should be noted that the experimental results show a small divergence from symmetry towards the grid critical load; this was attributed to the premature yielding of one of the bottom chord members (Collins, 1981), however, symmetry in load-displacement space was re-established as the failure progressed further. The symmetry of displacement for the loaded nodes about the load axes was enforced as a constraint in the numerical model and was consequently maintained throughout the analysis. The divergence from symmetry observed in the experimental results was small and was consequently not significant in its effect on the global structural behaviour.



### 7.2.4 Comments

Very good correlation between experimental and numerical results of the collapse behaviour of a DLG structure with SOS configuration was observed. The numerical method proposed in Chapter 6 is therefore considered to be appropriate for the analysis of SOS DLG collapse under point loading.

## 7.3 Displacement vs. Load Control

Both the experimental and FE results presented for the validation of Grid No. 1 have been obtained under displacement control, i.e. progression of the analysis is obtained by applying small increments of displacement and recording the resulting reaction force at the node where displacement is applied. Displacement control is an efficient method of solution control where a single point on a structure is loaded or where multiple points are loaded and have the same displacement behaviour. Load control of structural collapse analyses is,

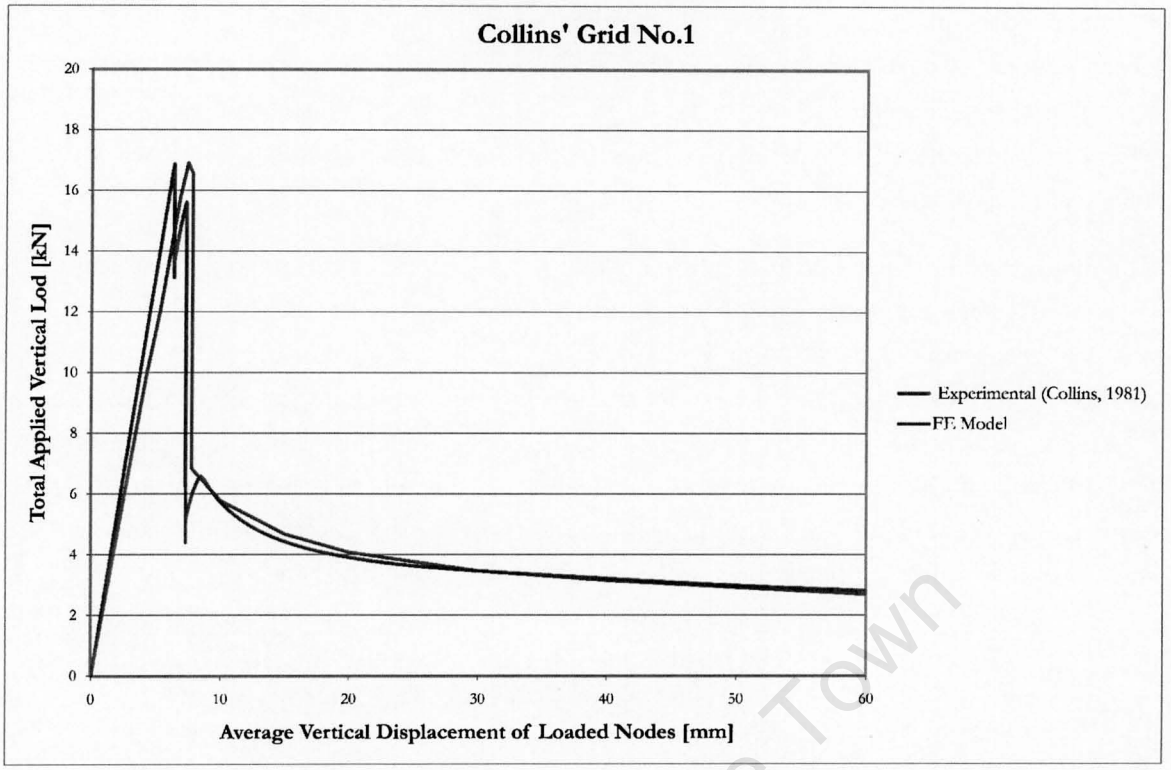


Figure 7.7: Load-displacement behaviour of Collins' (1981) Grid No.1 and FE model results.

however, preferable for general applications as it allows for random load distributions to be analyzed. The differences between load and displacement controlled analyses are investigated and observations made on the effectiveness of these two means of analysis control in their application to the collapse analysis of grid structures.

### 7.3.1 Investigation Method

The effectiveness of load control for capturing the failure behaviour and residual strength of grid structures was investigated by comparing results from the FE model of Grid No. 1 under displacement control and load control. The case of displacement control was considered with reference to the collapse analysis method presented in Chapter 6 while load control was implemented through use of the Riks analysis procedure in Abaqus (see Section 5.1.4).

### 7.3.2 Results and Discussion

Comparison of the load-displacement responses for load and displacement controlled analyses reveals the problem associated with application of load control to the collapse analysis of grid structures (see Figure 7.8).

Both load and displacement controlled nonlinear analyses are implemented through an incremental iterative solution scheme and consequently follow respective equilibrium paths as convergence of equilibrium is required for each increment. The difference between load and displacement controlled analyses, however, is that a displacement controlled analysis follows

a predefined displacement path while the displacement path of a load controlled analysis is not defined. Consequently, the sudden decrease in load resistance of grid structures observed in the collapse behaviour of Grid No. 1, results in the equilibrium path associated with the load controlled analysis diverging from the equilibrium path associated with the displacement controlled analysis.

The divergence of the two load-displacement responses occurred after the grid critical loads, associated with subsequent sets of top chords failing, was reached and a sudden decrease in grid resistance was observed. For the case of the load controlled analysis the applied load had to be significantly reduced for equilibrium to be maintained under load control, resulting in a reduced displacement, and the analysis did not continue into the post-buckling regime. For the case of the displacement controlled analysis the reaction force resulting from the applied displacement reduces significantly as the top chords fail and the analysis continues such that post-buckling behaviour is observed.

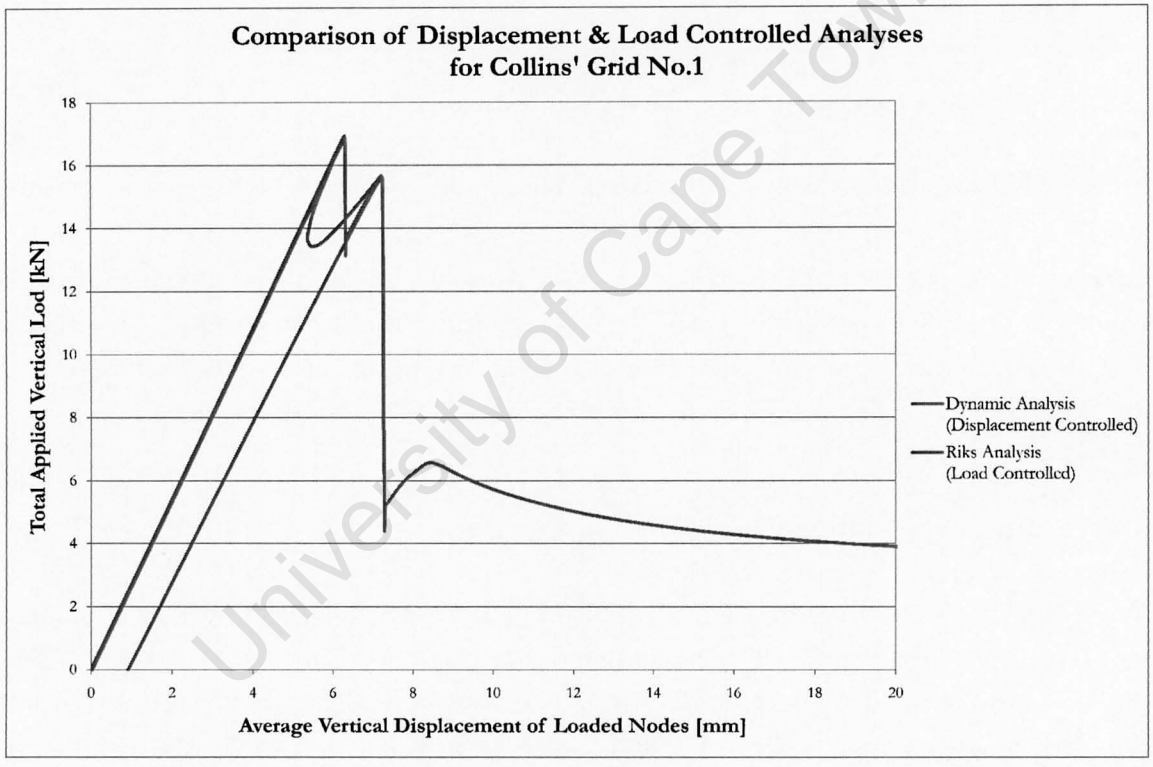




Figure 7.8: Comparison of load-displacement behaviour of load and displacement controlled analyses. Load controlled analysis was undertaken using the Modified Riks Method and the displacement controlled analysis was undertaken as a quasi-static dynamic analysis.

### 7.3.3 Comments

Load control can be used effectively to determine the critical load of grid structures; however, it fails to identify the post-buckling behaviour of such structures adequately. Displacement control should therefore be employed for capturing the full failure path of grid structures including post-buckling behaviour, this is consistent with the reasoning of Collins (1981), Parke (1988) and Mwakali (1990) (see Chapter 3).

## 7.4 Extension of Grid Analysis Validation

Validation achieved for the DLG of SOS configuration, with rigid connections, under two-point loading is extended to the cases of semi-rigid connections by varying the connection properties of the numerical model of Grid No. 1. The case of distributed loading is also investigated through comparison of nodal load histories. An inverted Grid No.1 configuration is considered (5x5, SOS DLG, with cornice edge detail) for the case of distributed loading as there is less ambiguity in the failure path of this geometric configuration.

### 7.4.1 Connection Stiffness

In most practical applications structural connections do not exhibit perfectly fixed or pinned behaviour but rather behave in a semi-rigid manner. It is therefore desirable to investigate the influence of connector stiffness on grid behaviour. Connector stiffness was idealized through the use of elastic rotational connections at member ends, although this can be easily modified to account for nonlinear spring behaviour associated with specific connections, with an associated increase in computational cost.

#### 7.4.1.1 Validation Method

The finite element model for Grid No. 1, as validated in the previous section, was modified to include the effect of connector rigidity. The validity of this modified model was then considered through critical comparison with the results of the previous rigidly connected model. Similar models with connector stiffnesses varying between pinned and fixed bounds were analyzed and then compared. For the case of pinned connections, a connection stiffness approaching but not equal to $0N.m.rad^{-1}$ was used; this was found to ensure numerical stability of the solution.

#### 7.4.1.2 Results and Discussion

Comparison between the results of the rigidly connected model and the semi-rigidly connected models for Grid No. 1 demonstrate that, with increasing connector rotational stiffness, the behaviour of the semi-rigidly connected model approaches that of the upper bound of grid behaviour represented by the rigidly connected model. At the lower bound, with decreasing connector rigidity, the semi-rigid model approaches the behaviour of a pinned structure. This can be seen by the reduction of the grid critical load capacity. Figure 7.9 demonstrates the result of varying connector stiffness on global grid behaviour. The grids' load-displacement responses, for varying connection stiffnesses, are similar as the same flexural failure mechanism is observed for all the cases considered[1].

[1]It is possible that for certain cases variation of connection stiffness may result in a change of grid failure mechanism.

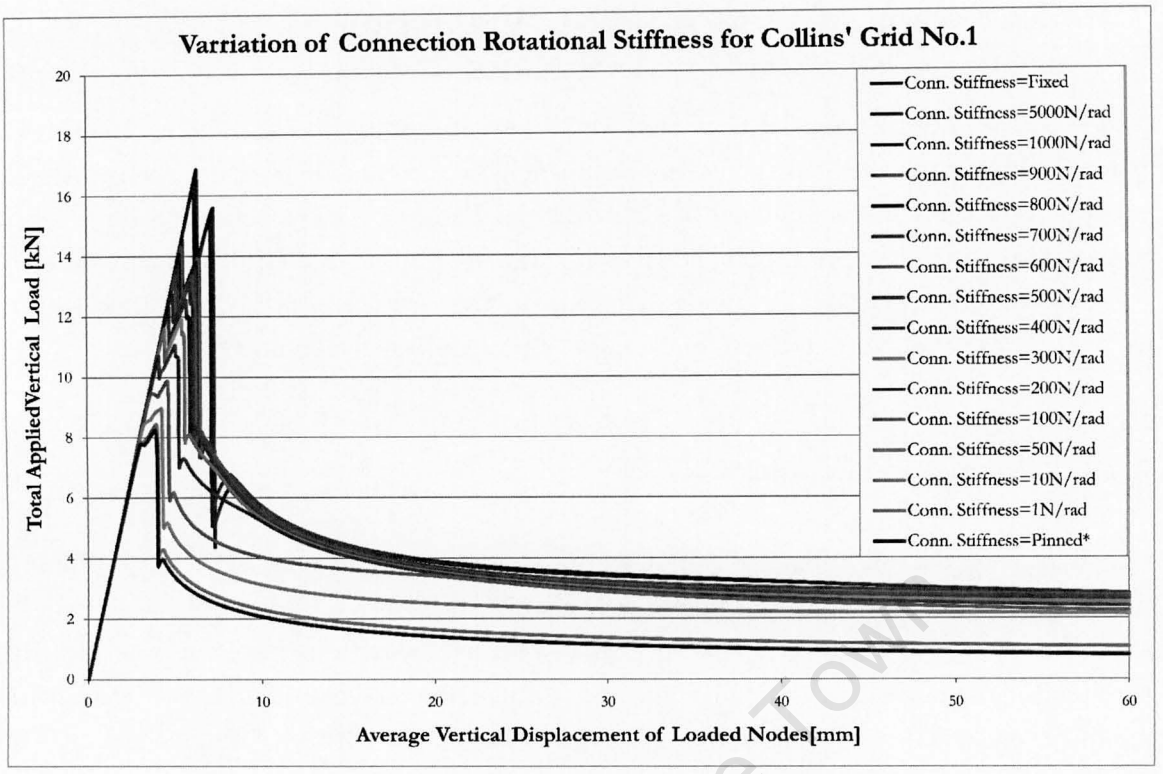


Figure 7.9: Load-displacement behaviour for variation of connection rotational stiffness.



#### 7.4.1.3 Comments

The effect observed, on global grid behaviour, of employing linear springs as semi-rigid connection elements is as was expected. Grid global load-displacement behaviour converged at lower and upper bounds. The use of linear springs in defining FE models of grid behaviour is consequently an improvement over existing pinned and fixed descriptions, as the full range of connection behaviour can be accurately accounted for. FE analysis of specific node connections can be further accounted for through non-linear descriptions of node behaviour, but this is not considered for the work presented.

### 7.4.2 Distributed Loading

The analysis of an inverted Grid No.1 configuration was undertaken to validate the suitability of the method, described in Chapter 6, for the application of distributed loading under displacement control. Grid geometry was selected to reduce ambiguity in the failure behaviour of the grid structure.

#### 7.4.2.1 Validation Method

An inverted Grid No.1 structure (5x5, SOS DLG, with cornice edge detail) was used for the purpose of validating the application of a UDL under displacement control as there was less ambiguity observed in the failure path of such a structure when compared to a 5x5 grid with

mansard edge detail. Load was applied at the level of the top chords at 36 points. The load-step time response at each point of load application was recorded and compared. The *load-step time* behaviour for all loaded nodes should be observed to be equivalent for the proposed method of distributed load-application to be validated.

#### 7.4.2.2 Results and Discussion

The *load-step time* response resulting from the collapse analysis of the 5x5 module, DLG of SOS configuration showed that the load applied to each of the top chord nodes remained equal relative to the other nodes throughout the analysis (see Figure 7.15); consideration of the load-step time responses in XZ plane additionally confirmed that load was only applied in the vertical direction. The method defined in Chapter 6 is therefore considered to be acceptable for applying a UDL in a displacement controlled analysis.

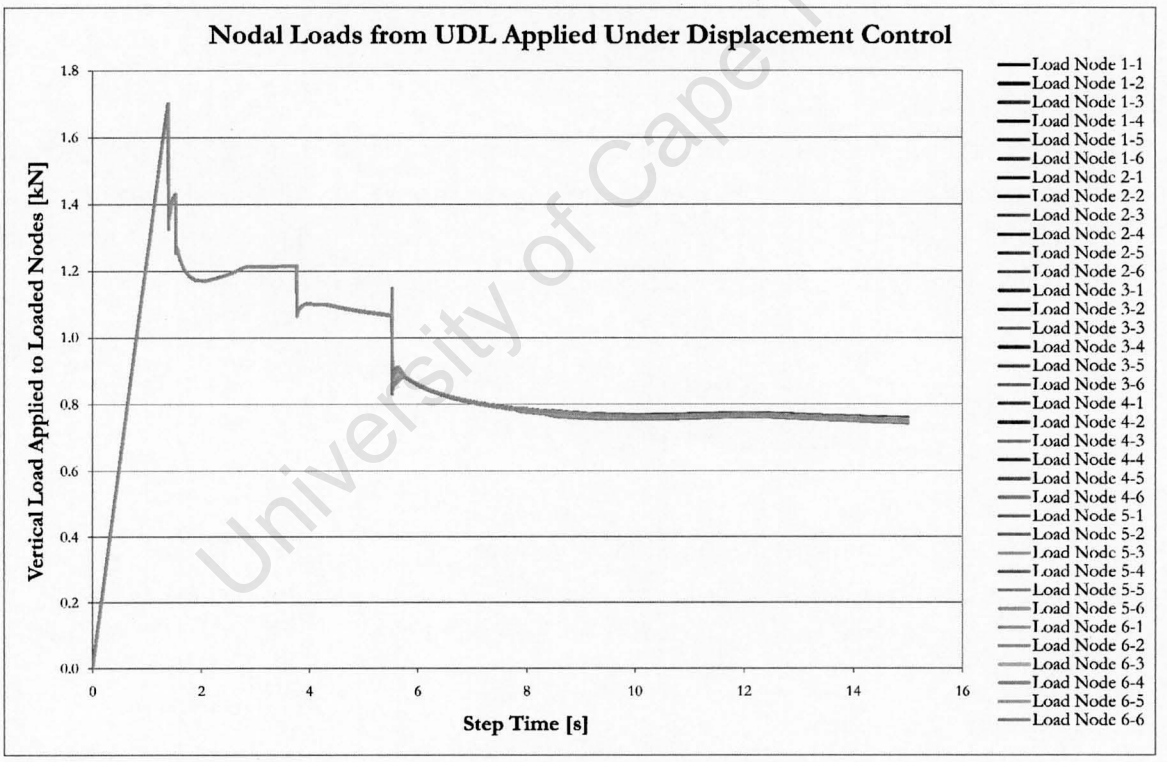


Figure 7.10: Nodal loads for UDL applied to 6x6 SOS, DLG structure in displacement controlled analysis.

### 7.4.3 Comments

Validation of the numerical collapse analysis was extended to the cases of semi-rigid connections and distributed loading, significant confidence can be associated with these results.

## 7.5 Parameter Validation (Scale Effect)

Web Angle, Connection Stiffness, Top Chord Member, Web Resistance Ratio and Chord Area Ratio parameters are to be used to parameterize DLG structures in subsequent analyses (see Section 8.4). In order to determine if the parameterization of the grid structures to be considered accurately captures the behaviour of these structures the effect of grid scale is considered. Validation of grid behaviour additionally allows for a suitable comparison to be made between DLG grids of other geometric configurations.

The behaviour of scaled grid structures has further implications, because if accurate parameterization is achieved, the results of the grids considered can be extended to scale equivalents of grids analyzed in this investigation. The effect of scale on DOS grid behaviour is considered initially in this section although the comparison of DOS and SOS grids is only introduced in Section 7.6.



### 7.5.1 Validation Method

For the purpose of validating the parametric representation of DLG grids considered in this study similar grids, varying in scale, were analyzed and the load-displacement results compared. The effect of a scaling factor, $B$, was considered on local member resistance, elastic stiffness and grid geometric dimensions.

#### 7.5.1.1 Grid Geometry

All global geometric dimensions are scaled by scale factor $B$. As both span and depth are scaled proportionally span:depth is maintained constant and consequently grid global geometry is not expected to have any effect on grid stiffness.

#### 7.5.1.2 Local Member Stiffness

Elastic stiffness of an axial member is a function of $EA/L$. The relative stiffness between members determines the relative distribution of load. By scaling member cross section by scaling factor $B$ member elastic stiffness is expected to remain unchanged and hence the distribution of load between members is also expected to remain proportional.

As both member elastic stiffness and span:depth was expected to remain constant between grids, the load-displacement behaviour of scaled equivalent grids were expected to be identical in the respective elastic regimes.

#### 7.5.1.3 Local Member Resistance

The effect of scale on predominantly axially loaded members was considered in the context of member resistance to buckling, tension yielding and compression yielding.

**Buckling** Simple Euler theory shows that the elastic buckling resistance of a axially loaded compression member ($P_{cr}$) is a function of member cross section, $A$, and member slenderness, $\lambda$, and is proportional to $A/\lambda^2$ where $\lambda = l/r$ (See equations 7.1 and Section 4.2). Consequently the $A/\lambda^2$ parameter was scaled by factor $B$ for similar members resulting in member buckling resistance being proportionally to $B$ too.

$$P_{cr} = \frac{A\pi^2 E}{(l/r)^2} \tag{7.1}$$

**Compression and Tensile Yielding** Member resistance to compression and tensile yielding can be taken to be proportional to the member cross sectional area if connection effects are disregarded. Consequently by scaling member cross section area, $A$, by scale factor $B$ ensured that member compression and tensile yielding remained proportional to $B$.

**Application** Scaling of CHS member resistance was achieved by first scaling member cross section, $A$, by scale factor $B$ and then scaling member OD such that the $A/\lambda^2$ parameter remained proportional to global scaling parameter $B$. Scaling member cross sections with this method ensures member resistance to elastic buckling, plastic failure in compression and tension are scaled proportionally.

#### 7.5.1.4 Global Behaviour

The effect of the previously defined method of scaling grid stiffness, member resistance and geometry by scale factor $B$ is expected to be as follows:

- Member forces will remain proportional to total applied load;
- Displacement will remain proportional to applied load;
- Member resistance will increases by factor $B$;
- Structure critical load will therefore increases by a factor $B$.

#### 7.5.1.5 Investigation

By comparing elastic, critical and post-buckling behaviour of similar grids, scaled by factor $B$, with the predicted behaviour (see Section 7.5.1.4), the effectiveness of the structure pa-

| Parameterization Error [%] | | | | | | |
|---|---|---|---|---|---|---|
| Failure | Flexure | | Shear | | Yield | |
| Grid Type | SOS | DOS | SOS | DOS | SOS | DOS |
| $B = 1$ | - | - | - | - | - | - |
| $B = 2$ | 0.235 | 0.447 | 0.223 | 0.326 | -0.008 | 0.169 |
| $B = 5$ | 0.327 | 0.567 | 0.458 | 0.402 | -0.104 | 0.217 |
| $B = 10$ | 0.462 | 0.585 | 0.480 | 0.414 | -0.153 | 0.222 |

Table 7.1: Error between observed and predicted results for critical load of SOS and DOS DLG structures.

rameterization can be established. The effectiveness of grid parameterization can be assessed further by taking account of different failure mechanisms[2].

For the purpose of evaluating the effectiveness of grid parameterization, the 5x5 SOS grid employed in Section 7.4.2 and the 5x5 DOS grid employed in Section 7.6 were scaled by scale factor, $B = 1, 2, 5, 10$. The case of uniformly distributed loading was considered for both grids.

In addition to the case of uniform section sizes for the SOS and DOS grid members (which results in grid flexural failure), cases with reduced corner web member and bottom chord member cross-section sizes were additionally considered to account for shear and yielding failure of grid structures respectively. Shear failure was achieved by replacing corner web members with standard web members while yielding failure was achieved by reducing bottom chord member cross-section area and buckling resistance by 50%.

The effectiveness of the SOS and DOS grid parameterization is to be assessed by comparing FE model results to expected results obtained through the application of analytical reasoning to the collapse analysis results for grids with scale factor $B = 1$.



### 7.5.2 Results

Load-displacement results for the investigation of the effect of scale on grid behaviour are shown in Figures 7.11 and 7.12 (flexural failure) and Figures 7.18 to 7.21 (shear and yielding failure). The results are in good correlation with the effect of grid scale predicted by analytical means. The error associated with the grid parameterization is expressed as the percentage difference between the scaled FE model result and the predicted result. The grid critical load (Table 7.1) and the total energy added to the systems (integral of load-displacement curve) (Table 7.2) are used to compare results. The parameterization error observed falls within the range -0.2% to +1.2% for both critical load and total energy comparisons.

[2]Failure mechanisms are described with reference to global behaviour. Flexural failure refers to failure of top chords in compression, shear failure refers to compression failure of web members in proximity to supports and yielding failure refers to tensile failure of bottom chords (see Section 9.3 for description of grid failure mechanisms).

| Parameterization Error [%] | | | | | | |
|---|---|---|---|---|---|---|
| Failure | Flexure | | Shear | | Yield | |
| Grid Type | SOS | DOS | SOS | DOS | SOS | DOS |
| $B = 1$ | - | - | - | - | - | - |
| $B = 2$ | 0.646 | 0.660 | 0.389 | -0.201 | 0.243 | 0.188 |
| $B = 5$ | 0.823 | 0.842 | 0.525 | -0.130 | 0.212 | 0.337 |
| $B = 10$ | 0.998 | 1.217 | 0.503 | -0.035 | 0.273 | 0.431 |

Table 7.2: Error between observed and predicted results for total energy applied to SOS and DOS DLG structures.

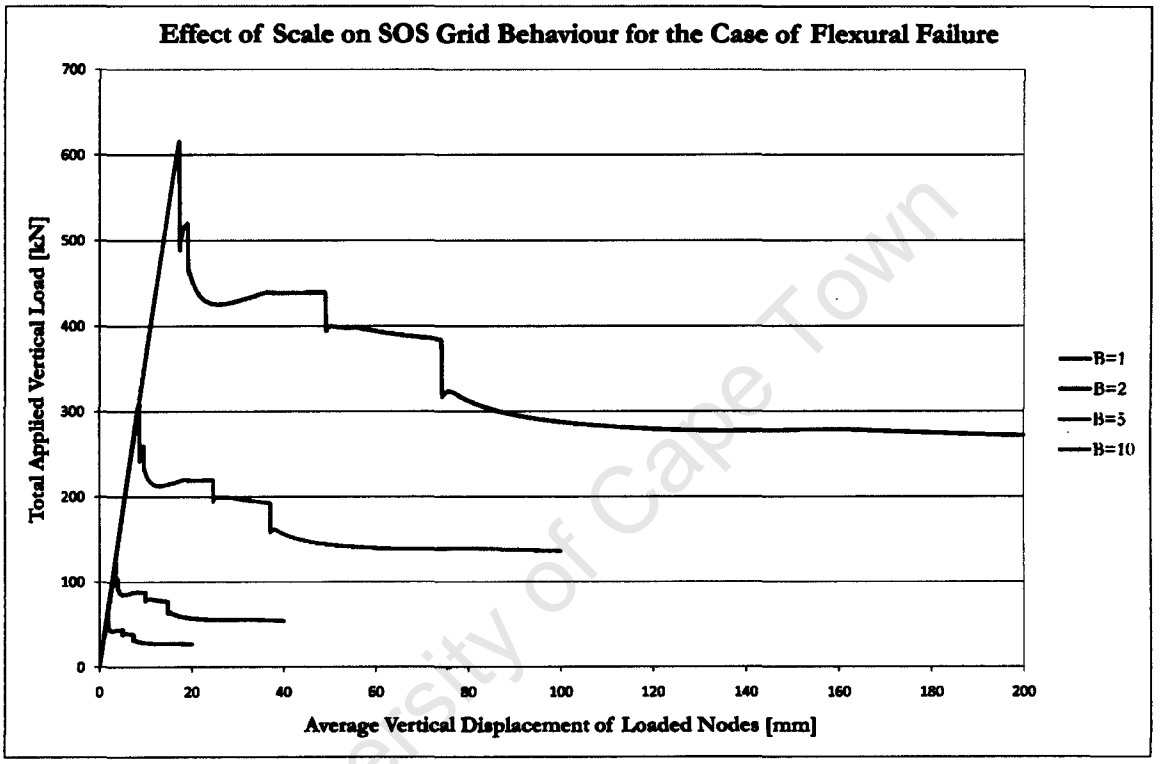


Figure 7.11: Load-displacement behaviour of equivalent scaled SOS grids which fail in flexure.

### 7.5.3 Comments

The good correlation between observed and predicted grid load-displacement behaviour for all failure mechanisms demonstrates that the parameterization considered accurately captures all aspects of DLG behaviour. The results of analyses undertaken can therefore additionally be taken to be accurately representative of grid behaviour for similar larger or smaller scaled grids.

## 7.6 Alternate Grid Configuration

Validation of alternate DLG configurations through comparison with experimental results was not possible as such information was not available. A DOS grid of similar proportions to previous 5x5, SOS grid configurations with cornice edge detail was therefore modelled in Abaqus, according to the same methodology as previously employed and validated, to allow

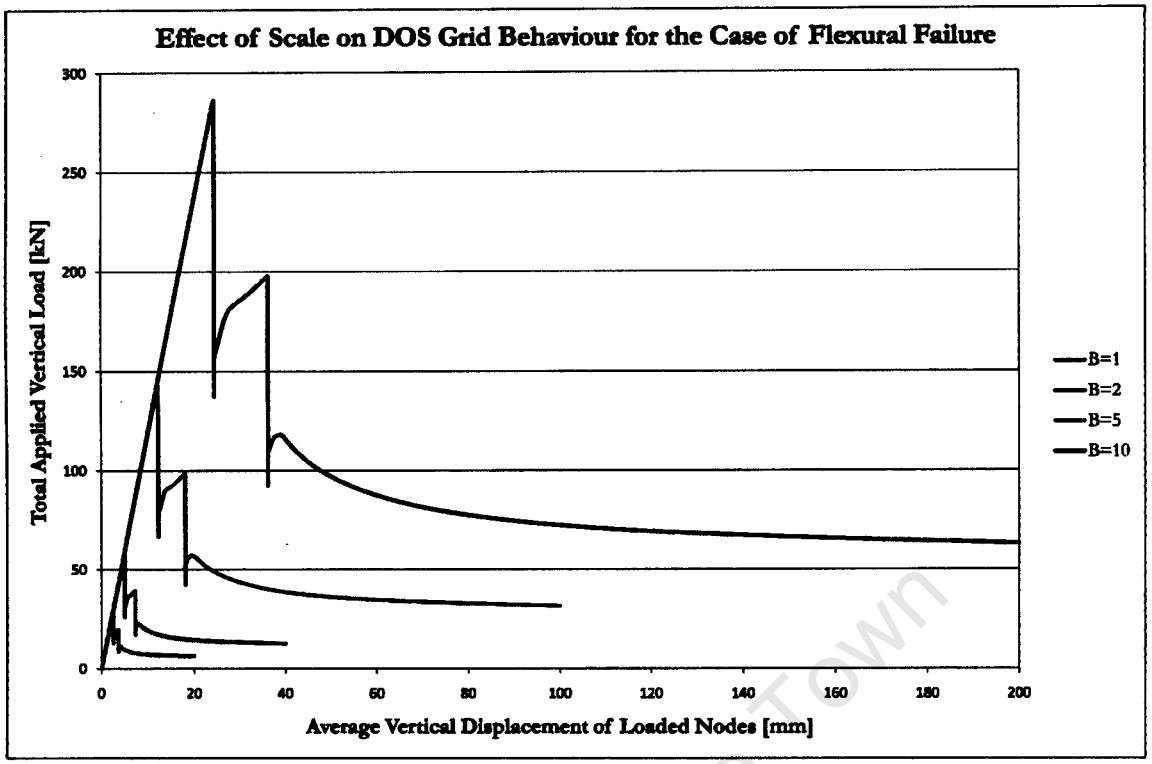


Figure 7.12: Load-displacement behaviour of equivalent scaled DOS grids which fail in flexure.

for critical comparison of DOS and SOS grid collapse results. The DOS, DLG structure modelled was configured such that the span between supports and grid depth were consistent with previous SOS grids. Results of SOS and DOS grid analyses were additionally compared with approximate analytical expressions of grid behaviour.

### 7.6.1 Basis for Comparison

The differences in geometric configuration of SOS and DOS DLGs do not readily lend themselves to direct comparison. Comparison of grid behaviour for differing grid geometries is best undertaken if the grids span the same area and are of equivalent depth such that differences in behaviour can be attributed to grid configuration; consequently it was decided to maintain grid extent and grid depth constant between SOS and DOS grids.

#### 7.6.1.1 Grid Span

A 5x5, DOS grid, with cornice edge detail and top chord geometry equivalent to that of the SOS grid was originally developed and scaled by factor $B = 0.7072$, reducing grid span from 2.036m to 1.440m and member length from 0.360m to 0.255m. By varying the member cross section concurrently the top chord density ($mm^2/m$) was kept constant between SOS and DOS grids while spanning the same area. Member resistance was scaled by keeping the member $A/\lambda^2$ ratio consistent (see Section 7.5).

#### 7.6.1.2 Grid Depth

Grid depth was kept constant between SOS and DOS grids by varying the web angle of DOS grids. Web angle of DOS grids was increased from 45° to 54.74°. The change in web angle effects the transfer of global shear forces between top and bottom chords, however as the comparison of SOS and DOS grids is considered for the case of global flexural failure this is not believed to significantly influence the resulting grid behaviour.

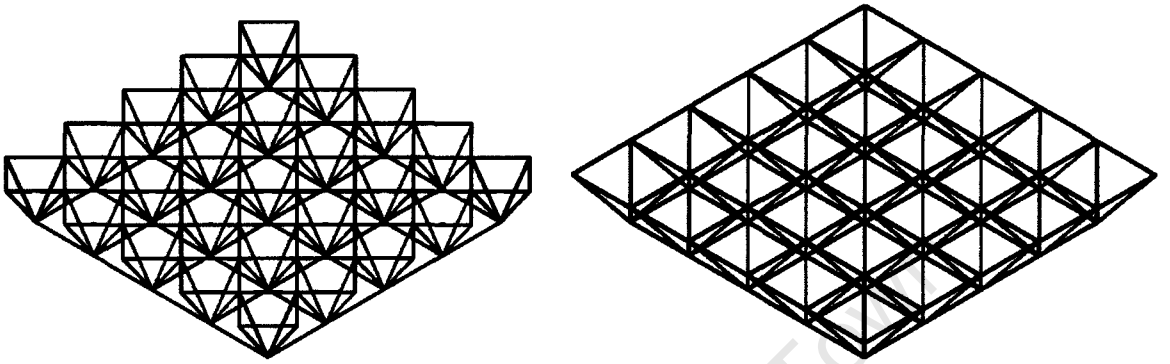

Figure 7.13: Comparison of 5x5 SOS and DOS DLG configurations with cornice edge detail; grids span equal areas.



### 7.6.2 Validation Method

The load displacement results of DOS and SOS grids, as considered in Section 7.5, are compared to each other and to analytical descriptions of grid resistance. SOS and DOS grids analyzed are subjected to uniformly distributed loading. Comparison between SOS and DOS grids is made with reference to grid elastic stiffness, grid critical load, initiation of failure and post-buckling behaviour.

### 7.6.3 Results and Discussion

Comparison between the load-displacement responses of SOS and DOS grids did not reveal any unexpected behaviour. The DOS grid proves to be less stiff than the SOS grid while the critical load resisted by the DOS grid is less than that resisted by the SOS grid. The DOS grid considered was expected to be less stiff than the similar SOS grid due to the diagonal orientation of top chord members and reduced bottom chord density. The critical load resisted by the DOS grid was expected to be less than that resisted by the similar SOS grid due to the increased distance top chord members span in the DOS grid (between opposite corners). Both grids were observed to fail in flexure. In the DOS grid, failure initiated through top-chord buckling at the grid centre; this was expected due to the spanning direction of top chord members in DOS grids.

Comparison of FE results with behaviour predicted by analytical means proved to be unsuccessful. The use of a combination of approximate values of grid stiffness, analytical

descriptions of grid displacement and moment distribution, and individual member resistance was not consistent with FE results. The analogy between DLG and plate behaviour, although useful for understanding grid behaviour, did not prove to accurately predict grid elastic behaviour for the case considered. Analytical descriptions of SOS DLG structures proved to under estimate grid stiffness, while the effect of the spanning direction of DOS grid top chord members could not be adequately accounted for. The differences between FE results and analytical results are believed to be partly due to the small horizontal extent of the grids considered, i.e. edge effects influence results.

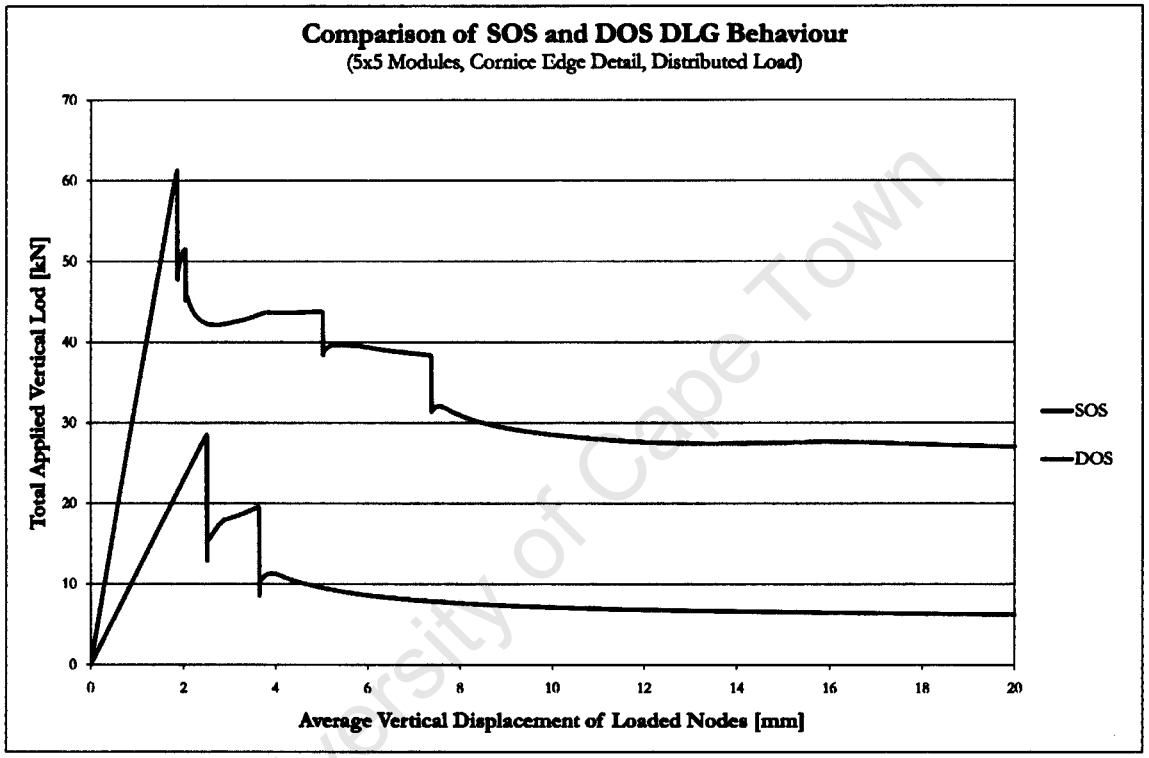


Figure 7.14: Comparison of SOS and DOS DLG load-displacement behaviour.



### 7.6.4 Comments

Although a rigorous means of validating the numerical model describing DOS, DLG collapse behaviour was not evident, comparison of the load-displacement behaviours for DOS and SOS grids showed that the same method used for collapse analysis of SOS DLGs can be applied to DOS grid structures which exhibit generally similar behaviour. The confidence associated with the previous validation of the numerical method for analysing SOS, DLG collapse behaviour combined with the logical agreement between DOS and SOS load-displacement behaviour are therefore believed to be sufficient to justify further use of the numerical analysis method proposed in Chapter 6 for DOS grids.

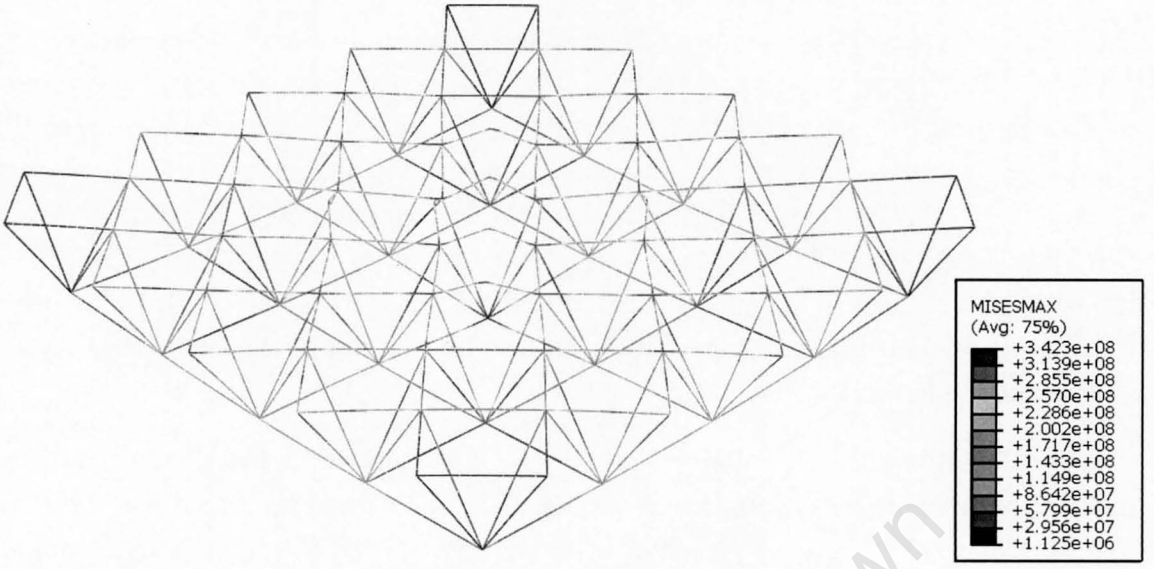


Figure 7.15: Displaced shape of DOS DLG in post-buckling regime; maximum von Mises section stresses superimposed.

## 7.7 Post-buckling Load Resistance

In order to verify that the load-displacement path of DLG structures in the post-buckling regime is representative of grid load resistance, a grid in the post-buckling regime is unloaded and reloaded and the result critically assessed.

### 7.7.1 Investigation Method

A 5x5, SOS grid, with cornice edge detail under uniformly distribute loading (as considered in Section 7.4.2) is subjected to an average loaded node displacement of 10.0mm in a displacement controlled analysis step (50% of displacement applied in previous analyses) such that the structure deforms and moves into the post-buckling regime. The displacement boundary condition is then removed and the structure is allowed to return to the resulting equilibrium configuration in a Static, General Analysis step. The structure is then displaced further in a second load displacement controlled analysis step such that a total displacement of 20.0mm is achieved (equivalent to final displacement applied in previous analyses) and the load-displacement results compared to previous analyses.

Plasticity theory predicts that the grid load-displacement behaviour for unloading and reloading should be equivalent and equal to the virgin load-displacement behaviour. As the grid experiences plastic deformation prior to unloading and reloading the grid stiffness is expected to decrease. Validation of grid plasticity behaviour and the representation of grid post critical resistance will therefore be achieved if load-displacement behaviour for unloading and reloading are equivalent and represent a decrease in grid stiffness.

### 7.7.2 Results and Discussion

The load-displacement behaviour of a SOS DLG under uniformly distributed loading is shown in Figure 7.16. The structure is initially loaded to a displacement of 10.0mm (curve a-b), the displacement boundary condition is then removed and the boundary force consequently decreases immediately to zero (curve b-c). The release of the displacement condition results in the upward displacement of the grid back to the new equilibrium position of an average nodal displacement of 7.44mm (curve c-d). On initiation of reloading the grid displaces linearly until the previous load-displacement curve is intersected (curve d-b) after which the grid offers no further resistance and the structure deforms without any increase in load application (curve b-e).

When the DLG is reloaded failure re-initiates at an equal load and displacement to that observed prior to initial loading being suspended. The load-displacement curve of DLG grids considered is therefore representative of grid post-buckling load resistance (residual load resistance). The grid global reloading and virgin loading behaviour are both linear, as is predicted by plasticity theory, the gradient differs between reloading and virgin loading due to a reduction in stiffness associated with deformed grid configuration.

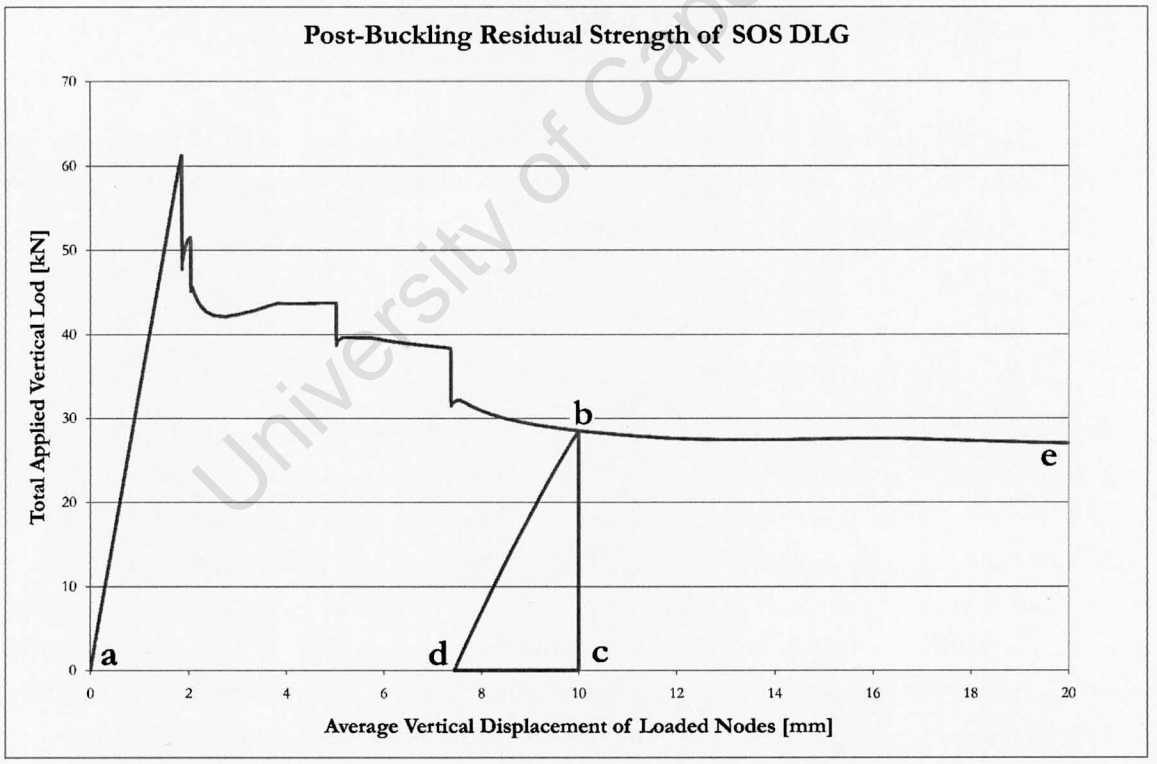


Figure 7.16: Loading, unloading and reloading of SOS DLG under uniformly distributed load.

### 7.7.3 Comments

Load-displacement behaviour of DLG collapse represents the residual post-buckling strength of DLG structures. FE models considered are able to take account of grid plastic behaviour

and correctly represent loading, unloading and reloading cycles.

## 7.8 Symmetric Models

To take advantage of the symmetric nature of grid geometry and loading considered in this study, a symmetric quarter model was developed for SOS and DOS DLG structures. In order to validate the symmetric quarter models including the representation of: grid geometry on lines of symmetry; boundary conditions; and application of distributed loading, the results for the symmetric quarter models are compared with results for a similar full model.

### 7.8.1 Investigation Method

Symmetric quarter model representations, developed as per the method described in Section 6.3, of the SOS and DOS grids modelled in Section 7.5, for the case of flexural failure and $B = 1$, are analyzed and compared with the results of the full model analysis. Comparison is made of grid critical loads and the grid load-displacement response.



### 7.8.2 Results and Discussion

Critical behaviour observed between symmetric quarter and full models is nominally identical, while small differences in load-displacement behaviour in the post buckling regime are observed for SOS and DOS grids (see Figure 7.17). The difference between the total energy applied to displace the symmetric quarter and full models is -0.60% and -2.99% for SOS and DOS grids respectively. The discrepancy between the models' behaviour is believed to be due to a nominal divergence from symmetric behaviour for the case of the full models. The similarity between the load-displacement behaviours is consequently sufficient to validate the symmetric quarter models for SOS and DOS grids under uniformly distributed load.

### 7.8.3 Comments

Good correlation has been observed between FE models which account for the full grid geometry and reduced symmetric quarter FE models which take advantage of grid symmetry. The use of symmetry in the analysis of grid behaviour results in a significant computational saving (the number of elements in FE model is reduced by 75%) and increased simplicity as symmetry of failure behaviour is generally maintained. Caution however needs to be applied in the use of symmetry in the analysis of grid behaviour as failure mechanisms associated with the instability of a pyramid module are inherently restrained.

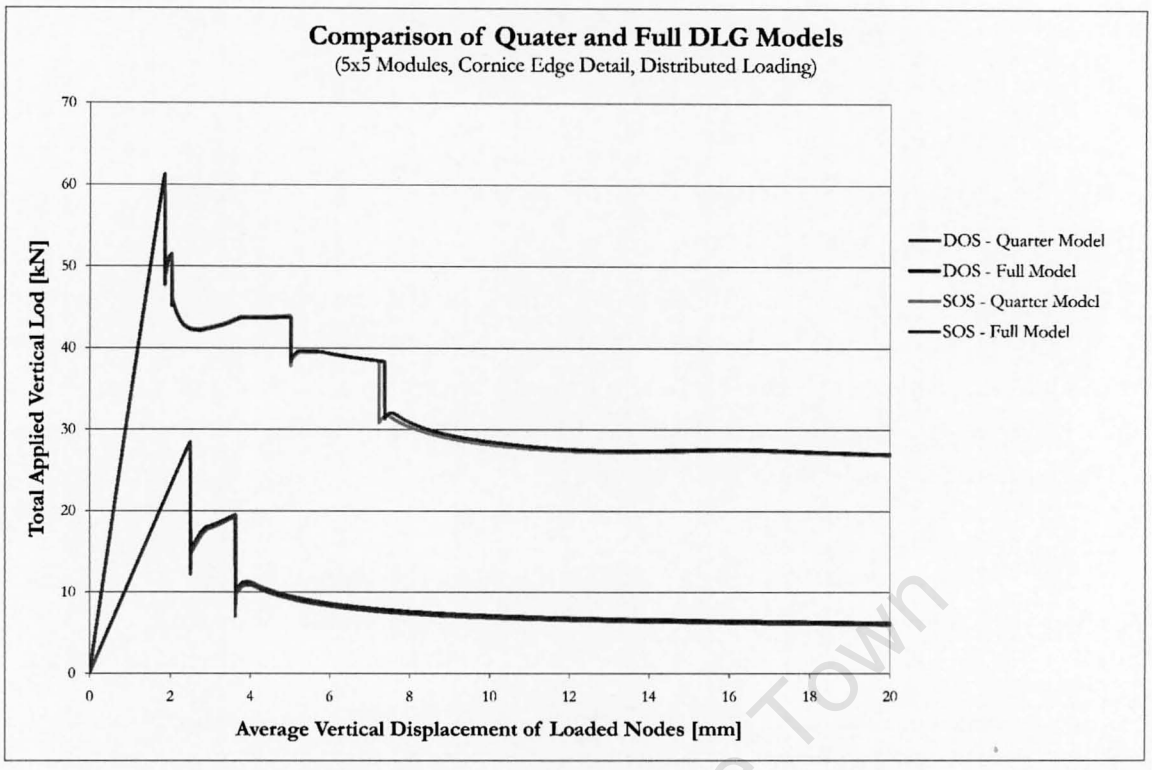


Figure 7.17: Comparison of load-displacement behaviour of SOS and DOS DLGs for full and symmetric quarter FE models.



## 7.9 Conclusions

A good correlation between experimental and numerical results was achieved. The largest source of discrepancy between numerical and experimental behaviour was due to the divergence from symmetry observed in the failure paths of the experimental results at the point of first buckling.

The critical load resisted by the grids analyzed by Collins (1981) was found to be dominated by the combination of material yield stress and initial imperfection magnitude while material yield stress was found to dominate post-buckling residual strength. As there was uncertainty regarding the actual yield strength of the material used in the experimental grid tests, various combinations of initial member imperfection magnitude and material yield stress were investigated and appropriate values were selected.

The comparison between numerical and experimental results developed a better understanding of the numerical model behaviour and the sensitivity of the structure to parameters which were not explicitly defined in the experimental work of Collins (1981). Greater insight into the grid behaviour was obtained by observing and identifying the global grid response to the variation of individual parameters.

Displacement control of the failure analysis of grid structures was shown to be more appropriate than load control in identifying the structural failure paths.

Validation of the numerical method for the rigidly connected structure, presented by Collins

(1981), was extended to a similar grid with semi-rigid linear elastic connection behaviour, between upper and lower bounds of connection stiffness.

Displacement control of the failure analysis of a grid under two point loads was extended to the failure analysis of grids under uniformly distributed loading while employing displacement control.

The grid parameterization employed was verified through comparison of load-displacement behaviour of scaled equivalent grids which accounted for flexural, shear and yielding failure mechanisms. The $A/\lambda^2$ parameter was used to scale member resistance.

Validation of the analysis method used for SOS grids was extended to an alternate DLG, of DOS grid configuration.

Post-buckling load-displacement behaviour obtained in displacement controlled analyses was shown to be representative of grid post-buckling residual strength.

Symmetric quarter models of SOS and DOS grid configurations were shown to give equivalent results to numerical models which accounted for the full grid geometry at a significant computational saving.

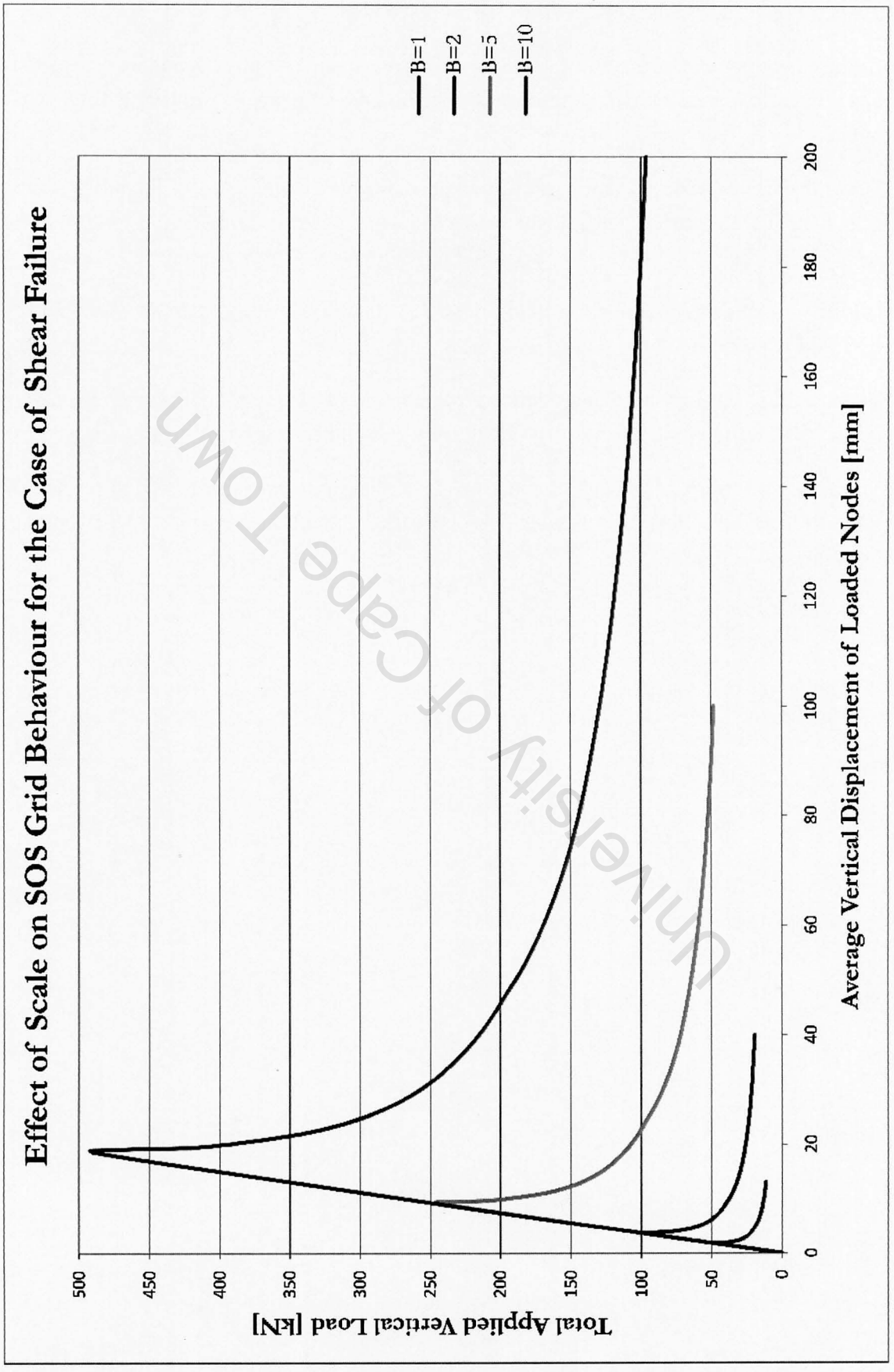


Figure 7.18: Load-displacement behaviour of equivalent scaled SOS grids which fail in shear.

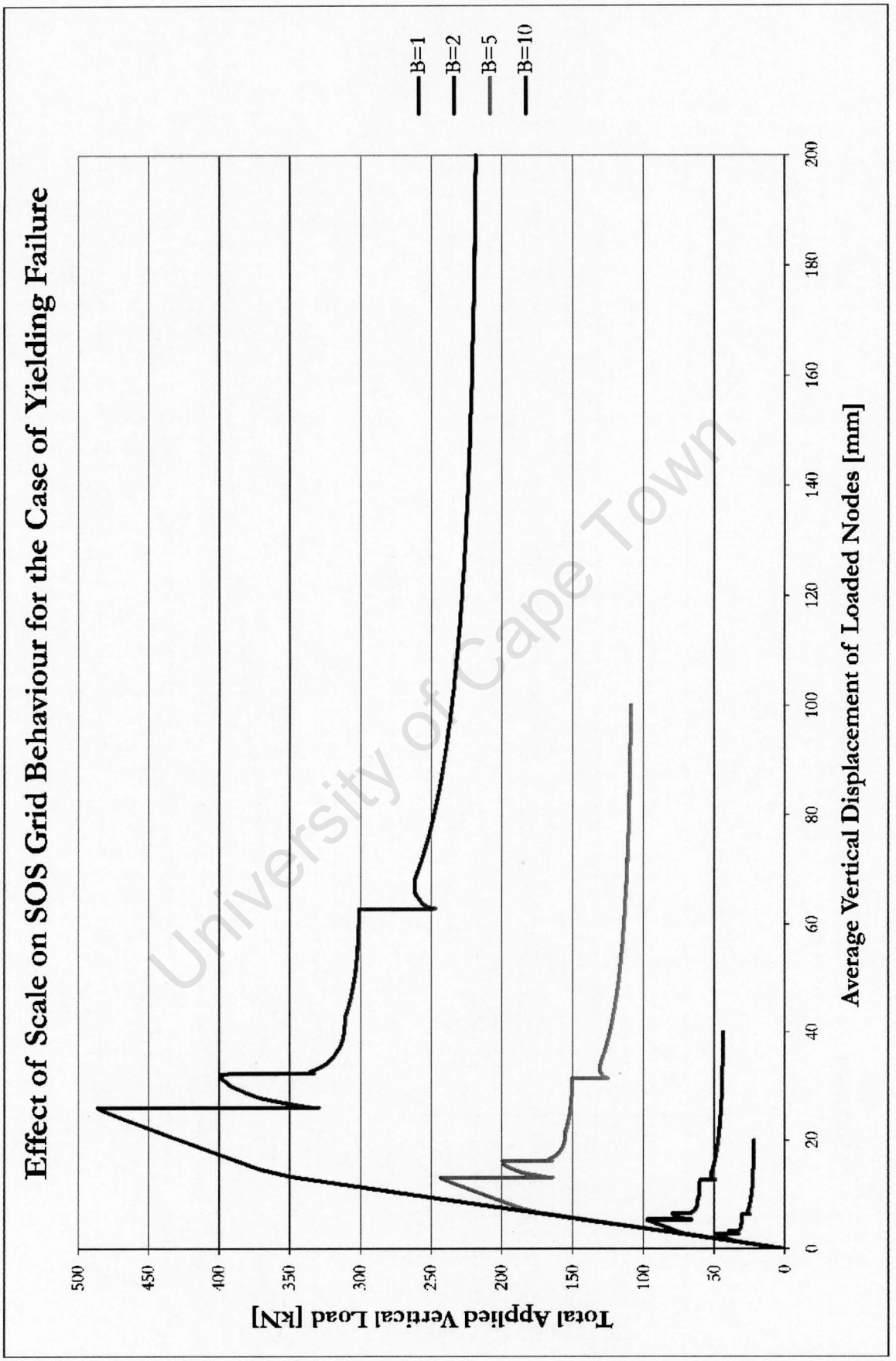




Figure 7.19: Load-displacement behaviour of equivalent scaled SOS grids which experience yielding failure.

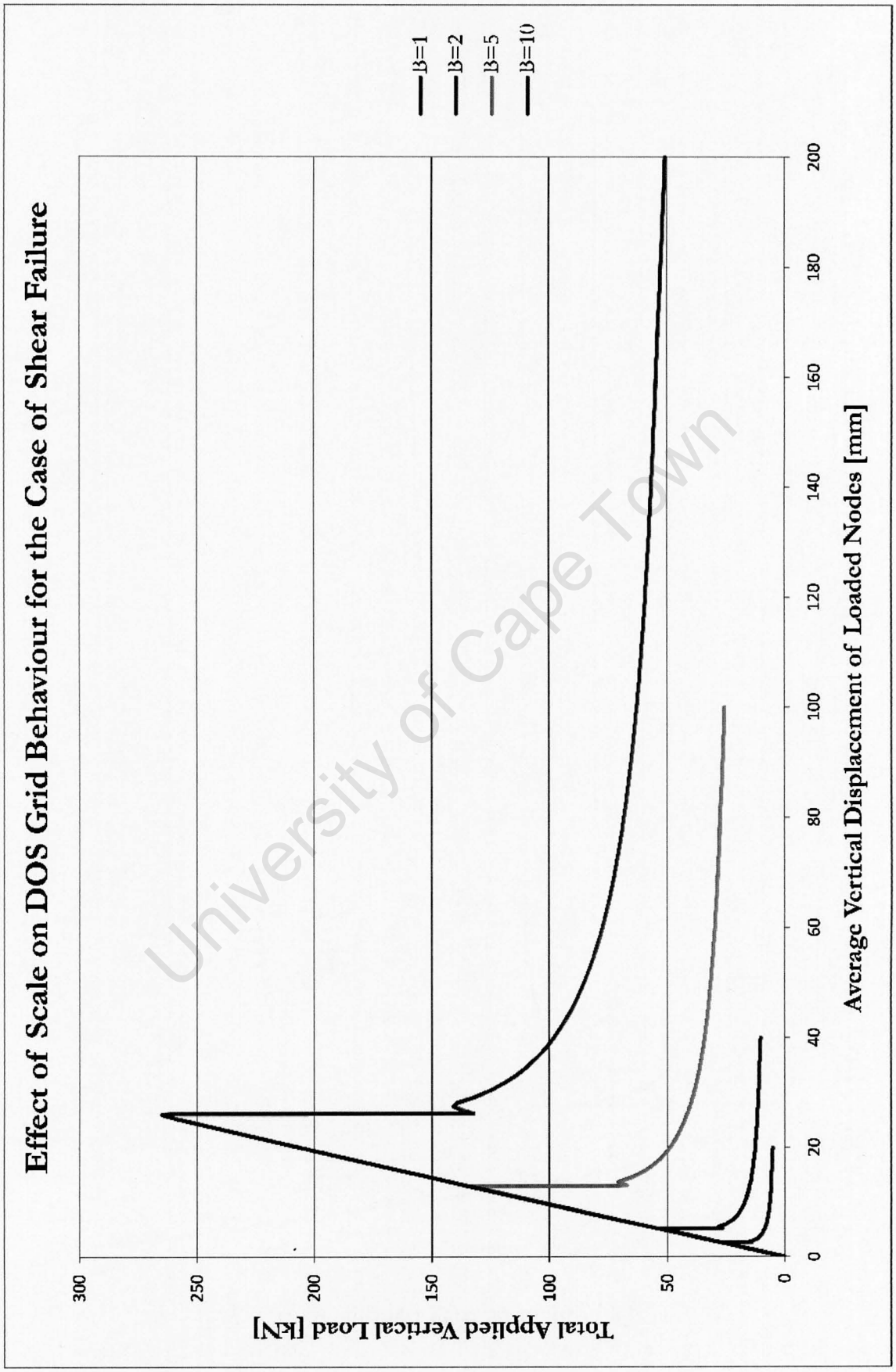




Figure 7.20: Load-displacement behaviour of equivalent scaled DOS grids which fail in shear.

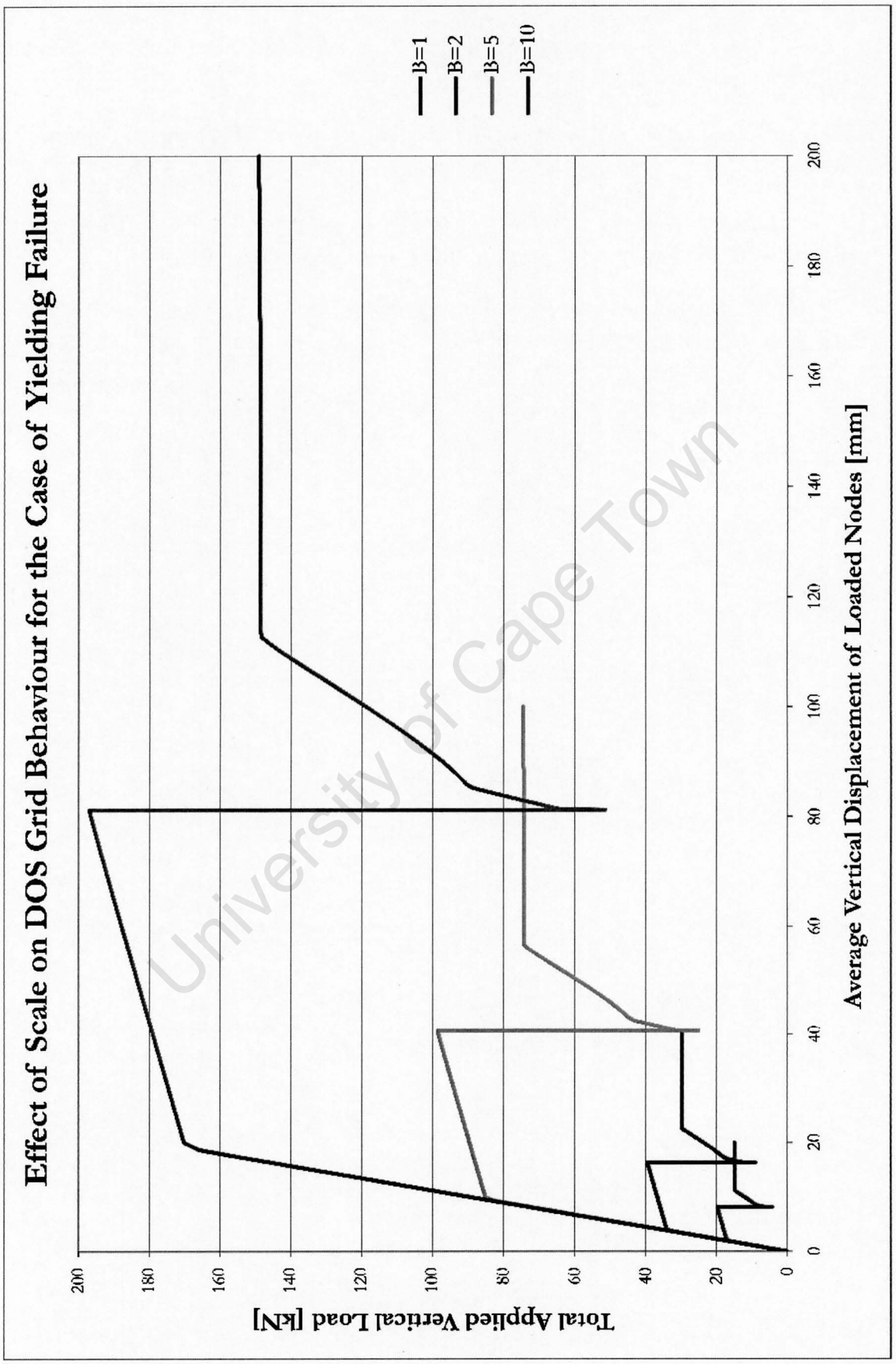


Figure 7.21: Load-displacement behaviour of equivalent scaled DOS grids which experience yielding failure.

## References

Eurocode 3: Design of Steel Structures - Part 1.1: General Rules and Rules for Buildings BS-EN 1993-1-1:2005, 2005.

Ian Martin Collins. *Collapse Analysis of Double-Layer Grids.* PhD thesis, University of Surrey, 1981.

J. R. Mwakali. *The Collapse Behaviour of Double-Layer Space Trusses Incorporating Eccentrically Loaded Tee-Section Members.* PhD thesis, University of Surrey, 1990.

G. A. R. Parke. *The Behaviour of Space Trusses Incorporating Novel Compression Members.* PhD thesis, University of Surrey, 1988.

# Chapter 8

# Investigation Method

## 8.1 Introduction

A parameter study was undertaken to develop the full spectrum of DLG collapse behaviour, for grids of the SOS and DOS configurations. The study of DLG collapse behaviour was undertaken to determine if improvements to grid ductility behaviour could be achieved for specific combinations of common structural and geometric parameters and identify and categorize grid failure and collapse behaviour. The DLG structures considered were square in plan and spanned 20m between supports; a cornice edge detail was selected as this resulted in a structure less susceptible to local failure in the vicinity of the supports. All aspects of the structures considered were symmetrical in plan about two axes, including seeded imperfections. FE analysis of the DLG structures was therefore undertaken utilizing this symmetry; one quarter of the full structure geometry was considered for numerical analysis.

The symmetrical failure pattern, resulting from the symmetric definition of DLG structure considered, represents a good basis for comparing grid behaviour as failure is well distributed through the structure. The symmetric failure of DLG structures can additionally be used as a control to which further study on the effect of initial imperfections on grid failure and collapse behaviour may be compared.

The methodology employed for the selection of individual parameters and parameter combinations considered for the parametric study are discussed. A summary of individual parameter values used in the analysis is provided.

## 8.2 Grid Geometry

Grid geometry and design was initially defined for the SOS DLGs considered. Grid geometry for the DOS DLGs was subsequently selected to allow for the greatest level of comparability between the two structural configurations.

### 8.2.1 SOS Grid

The SOS grid configuration considered for the purpose of the parameter study was a 9x9 module, square grid in plan, with chord length of 2.500m and a cornice edge detail. The plan dimensions of the grid were consequently 22.500 x 22.500m with a clear span between adjacent supports of 20.000m. The grid geometry to be analyzed was selected as a compromise between analyzing large scale structures and computational efficiency. The grid geometry was selected as it was considered to be of an appropriate size to capture the flexural failure mechanism for the parameter ranges considered and provide comprehensive insight into the post-buckling behaviour of such grid structures.

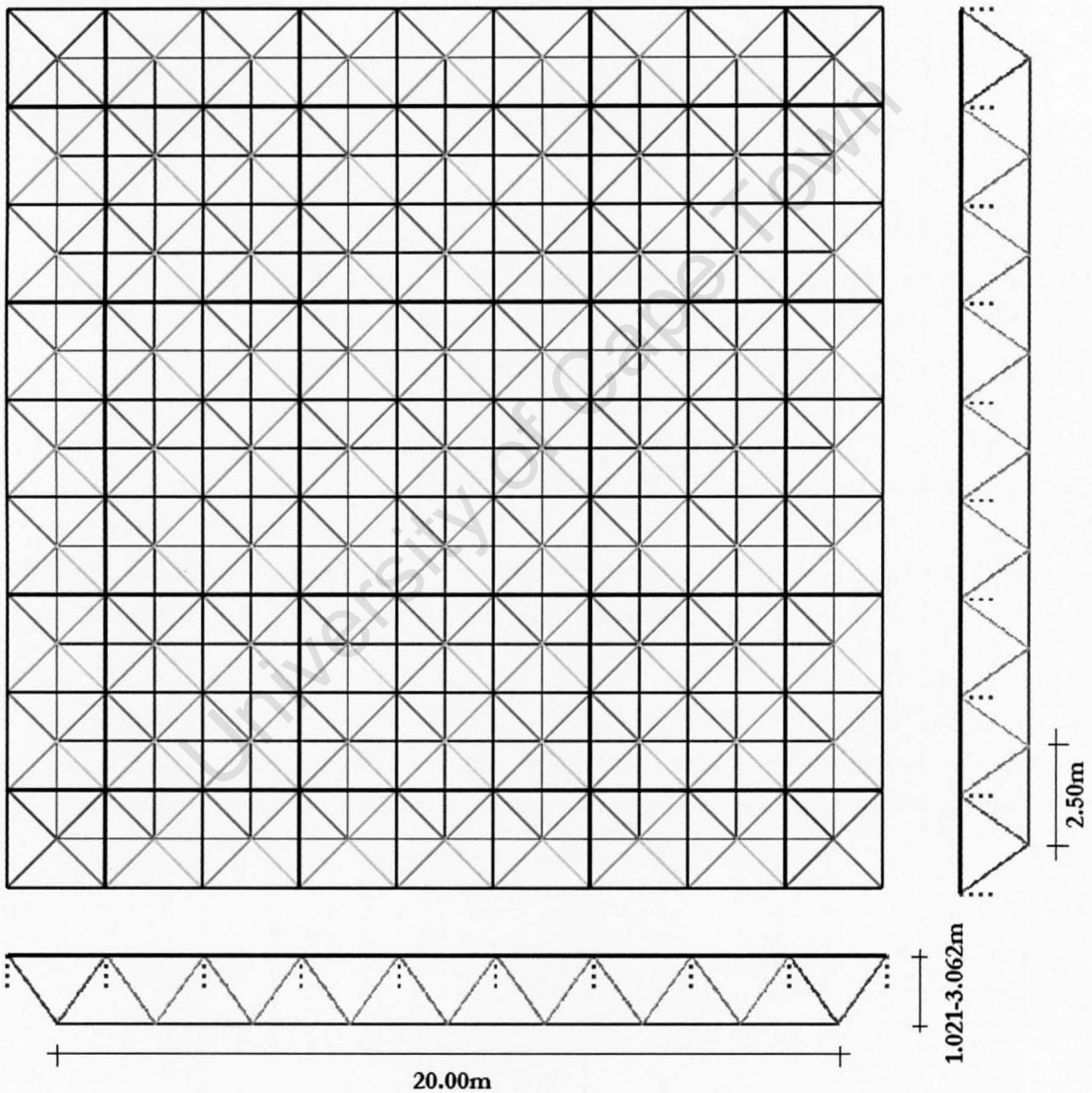


Figure 8.1: 9x9, SOS, DLG considered for the parameter study.

A grid geometry consisting of an odd number of top compression chord members was favoured as this allowed for greater symmetry of the failure path; in such cases the initial failure of top compression members (buckling or yielding) is confined to the centre-most members on each span. Furthermore, the grid geometry consisting of 9x9 modules was selected as such

| Grid | Modules | Span | Depth | Chord Length | Web Angle | Load Points |
|---|---|---|---|---|---|---|
| SOS | 9x9 | 20.0m | 1.768m | 2.500m | 45.00° | 100 |
| Configuration-A | 9x9 | 20.0m | 1.768m | 1.768m | 54.735° | 180 |
| Configuration-B | 7x7 | 20.0m | 1.768m | 2.357m | 46.686° | 112 |

Table 8.1: Comparison of SOS and possible DOS configurations A and B.

a grid was particularly well suited to possible future investigation on the effects of aspect ratio on grid behaviour (9x3, 9x6, 12x9 and 18x9 modules give aspect ratios of 3:1, 3:2, 4:3 and 2:1 respectively).

The Cornice edge detail was selected and support provided at the level of the bottom chords as this allowed for supports to be inset from the grid periphery. Inset of supports from the grid edge has been shown to result in DLG structures which are less susceptible to local failure in the regions surrounding supports.

The 2.500m chord member length was selected as this allowed for the grid to span an area 20.000 x 20.000m. This is considered to be at the lower end of areas typically spanned by grids supported along all sides, but is of a representative size for corner-supported grids. Furthermore, grid structure critical and post-buckling behaviour can be scaled in specific instances. This allows the results of the grids analyzed to be extended to additional cases.



#### 8.2.1.1 Kinematic Stability

Kinematic instability of the SOS DLGs was considered by undertaking a series of linearized buckling analyses, with the subspace method in Abaqus, of models consisting of the full SOS grid geometry.

Kinematic instability of the SOS grids was not observed in the linearized buckling analyses performed on full geometry models of these structures. Kinematic stability of SOS grids with pinned connections was adequately provided by boundary conditions, while kinematic stability of SOS grids with semi-rigid and rigid connections was additionally provide by connection rigidity. As the SOS grids are deemed to be kinematically stable the behaviour of the symmetric quarter models is considered to be equivalent to the behaviour of the full models (implementation of the symmetric quarter model boundary conditions consequently do not hide any kinematically unstable deformation modes).

### 8.2.2 DOS Grid

Comparison between SOS and DOS DLG structures was sought to highlight the differences in behaviour of these two grid configurations. Owing to the differences in geometry between SOS and DOS grids, the parameterization employed did not result in directly equivalent structures. Grid span:depth ratio was not equivalent between SOS and DOS grids for a given web angle, and an equivalent grid span between SOS and DOS grids could not be achieved while maintaining equal top chord member lengths.

The significance of grid depth and span on grid stiffness has been acknowledged; DOS grid depth and span was consequently set equal to the span and depth of the equivalent SOS grids. Equivalent grid depth and span was achieved by scaling the DOS grid module dimensions and adjusting the DOS grid web angle respectively. As symmetric grid failure behaviour was to be investigated, an uneven number of modules at the level of the top chords were selected. This approach to defining DOS grid geometry resulted in two admissible DOS DLG configurations which were compared with the previously defined SOS grid configuration in order to determine the most suitable DOS grid configuration for the parameter study presented (see Table 8.1).

DOS grid Configuration-A was characterized by an equivalent number of modules to the SOS grids, while DOS grid Configuration-B was characterized by greater compatibility of web angle and number of load points between the SOS and DOS grids.

As: no significant differences in structural behaviour were anticipated to result from the number of modules employed within the range of grid span:depth ratios considered; significantly more load points were associated with Configuration-A; and the effect of web angle is expected to have an effect on force distribution in grid web members, Configuration-B was selected as the DOS grid geometry to be employed in the parameter study.

The DOS grid geometry proposed as Configuration-B was achieved as follows:

- A 7x7 module, DOS grid, with a cornice edge detail and module size of 2.50m (as employed for the SOS grids) was configured which resulted in a grid with a horizontal extent of 24.749m x 24.749m spanning an area of 21.213m x 21.213m between adjacent supports;
- Member cross-sections were assigned to the DOS grid which were equivalent to the cross-sections used for the SOS grids (member resistance was not scaled to account for increased length of DOS grid bottom chords);
- DOS grid geometry and member cross-sections were scaled by a factor of **0.9428** with the method previously validated (see Section 7.5) resulting in a grid which spanned 20.000m between adjacent supports;
- DOS grid depth was configured to be equivalent to SOS grid depth by increasing the DOS web angle from 45° to 46.686°;
- DOS web member cross sections were scaled, by adjusting cross section OD and thickness, such that the member $A/\lambda^2$ parameter remained constant with the increase in grid depth.

Scaling of grid geometry retained the top chord cross-section area and resistance density and therefore maintained maximum compatibility between scaled equivalent DOS grids and between SOS and DOS grids. The DOS DLGs have 112 loading points compared to 100 for the SOS DLGs; this is not believed to effect grid behaviour as comparison between grids is

undertaken with respect to total applied load. A small difference between SOS and DOS grid angle exists; although this is believed to affect distribution of forces in web members a small difference in the grid web angle has a less significant effect on global grid behaviour than a difference in grid depth which would result if grid web angle was equal between SOS and DOS grids.

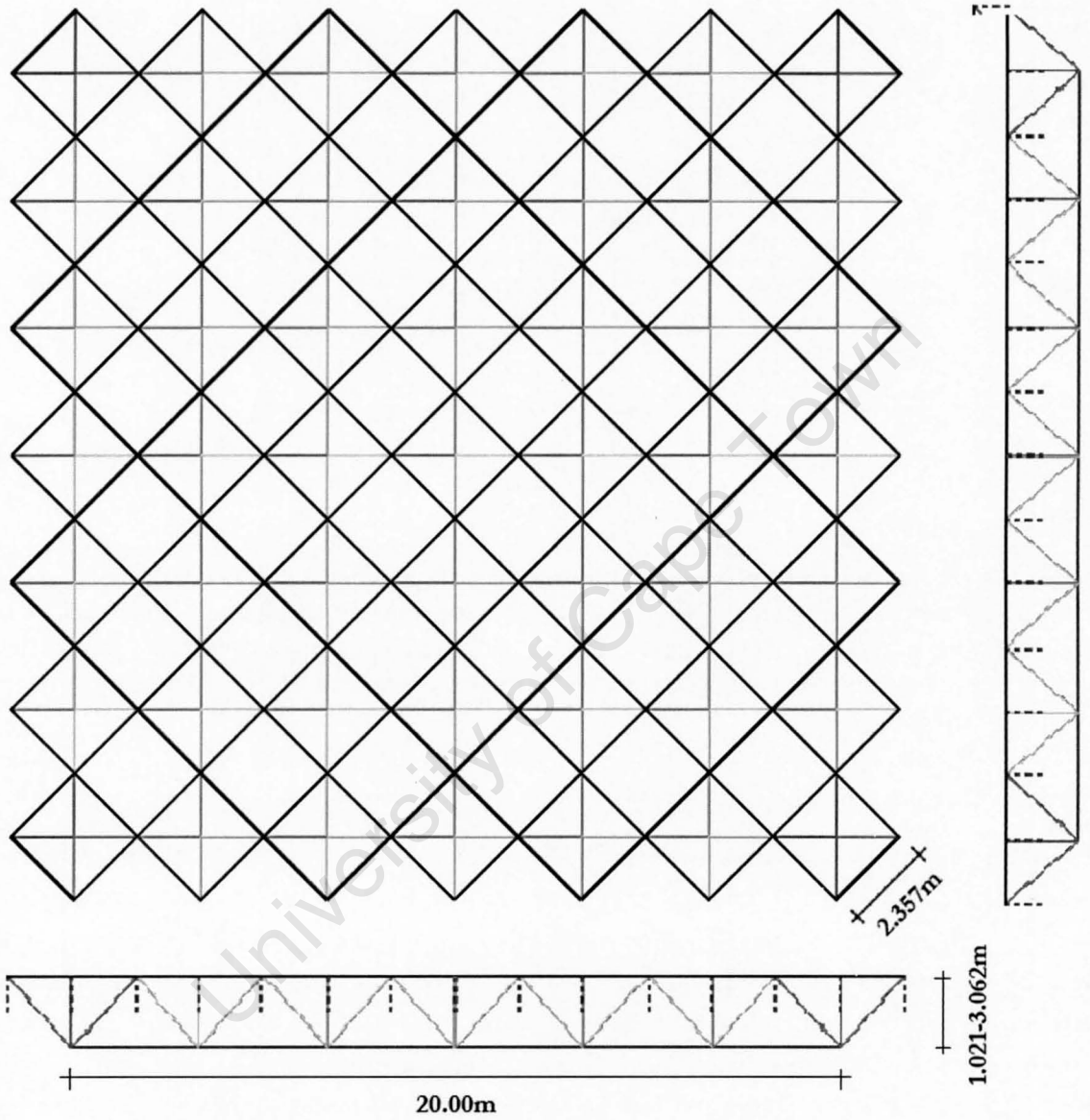


Figure 8.2: 7x7, DOS, DLG considered for the parameter study.

#### 8.2.2.1 Kinematic Stability

Kinematic instability of the DOS DLGs was considered by undertaking a series of linearized buckling analyses, with the subspace method in Abaqus, of models consisting of the full DOS grid geometry.

The symmetric quarter model of the DOS DLGs did not demonstrate kinematic instability (see Figure 8.4); however, kinematic instability of the full DOS grids was observed (i.e. kinematic instability was sufficiently restrained by symmetric boundary conditions) (see Figure

8.3). Kinematic instability of the full model was consequently investigated such that results of the parameter study could be applied to real cases. Restraint of kinematic instability was assessed within the context of physical experimental analysis of DLG structures.

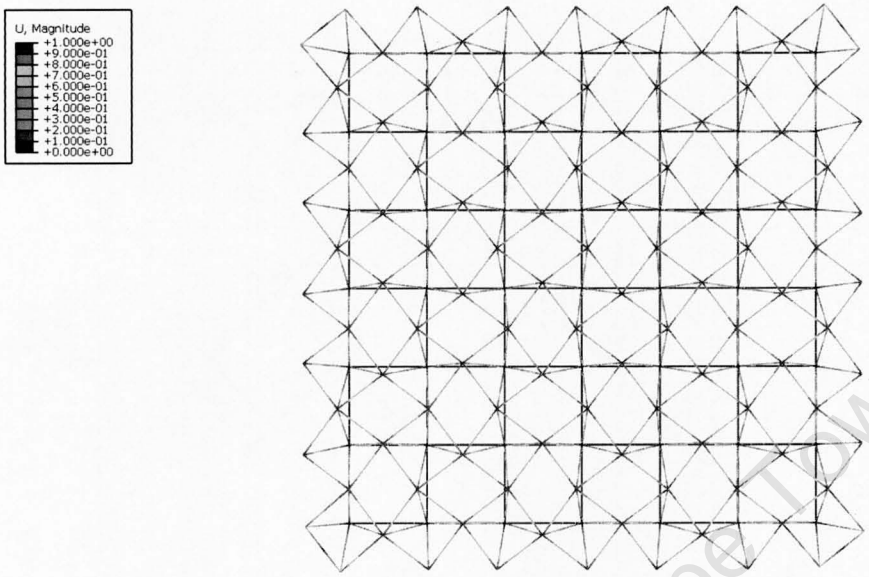


Figure 8.3: Eigen vector displacement obtained from buckling analysis, occurring at 7.5% of the DLG self-weight loading (scale x0.25). The kinematic instability of the DOS DLG configuration, associated with the instability of the pyramid module, is clearly visible when appropriate constraints on displacement are neglected; restraint often applied in the form of a boundary beam.



In practice kinematic stability of pinned DOS configurations is typically ensured through the use of an edge beam around the grid periphery, at the level of the upper chords. The use of an edge beam for the DOS grids considered, however, should be avoided as this would change the structural behaviour of the grid. An edge beam spans the shorter distance between adjacent supports while the main compression members of DOS grids span between opposite corners. Additionally, as the number of members required for an edge beam for the given DOS geometric configuration is even, there would be further implications regarding the symmetry of the failure.

Consequently a compromise between representivity of structural behaviour and ensuring kinematic stability should be targeted. Restraint of kinematic instability for the experimental analysis of DOS DLGs with pinned connections should be achieved through the use of: an edge beam which extends across the first two modules adjacent to each corner at the level of the top chords; and the use of boundary conditions to constrain displacement of the four top, central, edge, nodes in the direction between adjacent supports. Use of the partial edge beam and displacement constraints were shown to restrain kinematic instability for the DOS DLGs considered, through FE analysis of full DOS grid geometry; application of either one of these constraints to grid displacement in isolation was not observed to result in kinematic stability.

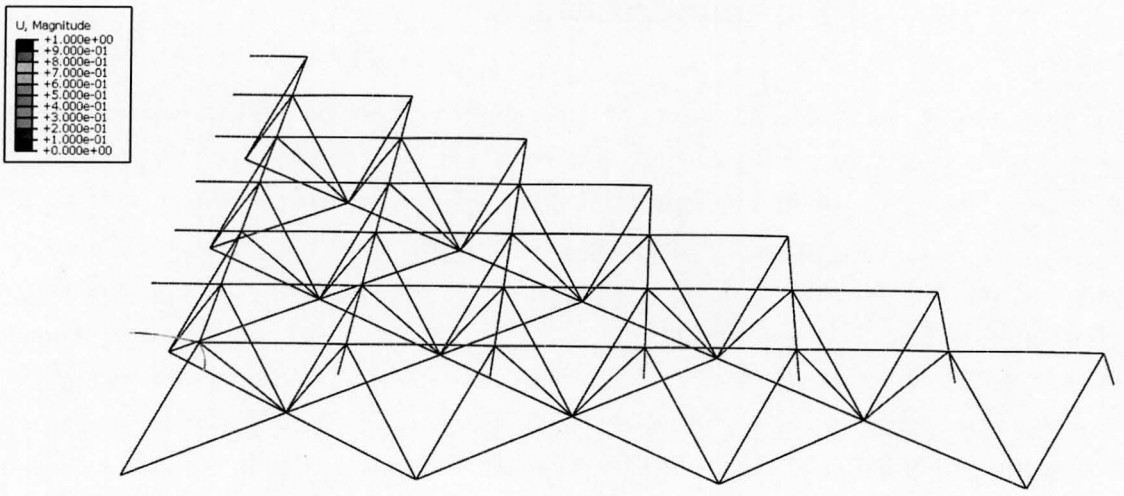


Figure 8.4: First Eigen vector field for buckled deformation of symmetric quarter model of DOS DLG, occurring at 1392% of applied gravity loading (scale x0.25). The kinematic instability of the DOS grid configuration is restrained by the symmetric boundary conditions

## 8.3 Design

In order to ensure that the SOS and DOS grids considered were of representative section sizes and proportion, an initial grid design was undertaken using EC3 (2005). Loading was in accordance with EC1 (2002) for inaccessible roofs; a 1kPa UDL was consequently adopted and applied at the top nodes.

A second-order elastic analysis was undertaken with PROKON frame analysis software and members were sized accordingly (this was repeated until member size convergence was obtained). For the purpose of design and member sizing, four member groups were considered: top chords, bottom chords, web members, and support web members (four web members at each support). Members were checked for tensile capacity, compression buckling and compression yielding; reductions in member capacity due to connections and reduced end cross-sections were not considered. An effective length of $0.85L$ was adopted, this is consistent with industry practice for fixed connections in grid structures (Ramaswamy et al., 2002).

The following member sizes, of steel grade S355, were obtained:

- Top chords: 102 x 3.5 CHS
- Bottom chords: 63 x 4.5 CHS
- Web members: 76 x 62.5 CHS
- Support web members: 89 x 3.0 CHS

And were used as a basis for the grid parameterization to be considered for the parametric study.

## 8.4 Structural Parameterization

Parameters to be included in the study were carefully considered. Sufficient parameters and discrete parameter values were needed to develop the full spectrum of behaviour of such structures. Owing to the high computational cost of grid structure collapse analysis however, the number of parameters which could be considered was limited. Parameters to be considered needed to be independent so as to allow the response of a single parameter to be investigated and needed to be varied concurrently with other parameters to detect parameter interaction in terms of structural behaviour. Parameters to be included were selected through consideration of the analytical representation of grid elastic behaviour and through comparison with previous studies. Parameters selected were kept within representative limits so that the behaviour observed was consistent with typical grid structure behaviour.

The following parameters were selected:

- Span:Depth (governed by web angle);
- Connection Rotational Stiffness;
- Top Chord Resistance (defined but not used for the parameter study)
- Web:Top Chord Resistance;
- Chord Area Ratio.



A description of these parameters and how they were varied for the purpose of the parametric study follows. The Span:Depth parameter is considered to be a geometric parameter, due to its effect on grid depth, while all other parameters are considered to be structural parameters. Connection Stiffness and Cross-Section parameters are grouped together as these structural parameters affect the compression behaviour of grid structures, these parameters are consequently expressed in terms of member $A/\lambda^2$ ratio. The Chord Area Ratio parameter affects the tensile behaviour of grid structures and this parameter is consequently principally expressed with respect to member cross-section area, as the member cross-section area is also captured in the member $A/\lambda^2$ ratio (due to the method employed in scaling members) and as stress reversal may occur in the post-critical regime of grid behaviour the Chord Area Ratio parameter was also expressed in terms of the member $A/\lambda^2$ ratio.

**Note on Transition from Stocky to Slender Members** The behaviour of compression members varies with slenderness (see Chapter 4). Slender column resistance is governed by the member slenderness ratio while stocky column resistance is governed by the member cross-sectional area. The parameterization of the structures considered with respect to member $A/\lambda^2$ allowed for both stocky and slender member resistance to be varied concurrently.

### 8.4.1 Span:Depth

SOS and DOS DLG spans were to remain constant for all grids considered in the parameter study. Span:Depth was consequently varied by changing grid depth which was achieved through variation of grid web angle.

The grid web angle was defined as the acute angle, expressed in degrees (°), between chord and web members and measured in the vertical plane. For a constant span, variation of the span:depth ratio results in a change of grid depth which results in a change in grid stiffness and web member length; distribution of global shear forces between top and bottom chords is also affected.

The Span:Depth parameter was varied while maintaining the $A/\lambda^2$ parameter constant for web members. This was achieved by varying the outer diameter (OD) and wall thickness (t) of the web members.

It was anticipated that variation of the grid depth would affect the global bending stiffness by the factor $depth^2$ according to the Parallel Axis Theorem, where $I = I_{own\ axis} + a.depth^2$. Consequently three discrete values of the Span:Depth parameter were considered sufficient to develop trends with Span:Depth as the independent variable.

The three discrete values of the Span:Depth parameter selected were: 19.6, 11.3 and 6.5. Variation of Span:Depth parameter was achieved by employing the following grid web angle values: for SOS grids 30°, 45° and 60°; and for DOS grids 31.482°, 46.686° and 61.439°. The values of the Span:Depth parameter employed are believed to cover the range of web angle values commonly used in practice while the span:depth ratios are consistent with the recommendations of West (1967) (span:depth=20 for continuous edge support, span:depth=12 for corner support).

### 8.4.2 Connection Stiffness

Connection stiffness was defined as the rotational stiffness of connections restraining top chord, bottom chord, web and corner web members; expressed as a percentage, relative to pinned (0%) and fixed (100%) connections and interpolated between these bounds.

Relative connection stiffness affects the buckling resistance of compression chord and web members. Connection stiffness also affects post-buckling behaviour at a member and grid level. The restraint provided to an individual member in isolation with end connections is dependent on the ratio of the beam bending stiffness and the connection rotational stiffness. The extent of restraint applied to a member in a structural system is, however, more complex as it is additionally dependent on the restraint offered by the surrounding structural members. For this reason relative connection stiffness was assessed at a member level.

Connection Stiffness was assessed by compression test to failure of initially bowed members representative of top chord, bottom chord, web and corner web members used in the DOS and SOS grids by FE analysis. An initial member bow imperfection of $L/250$ was employed

as was to be considered in subsequent DLG collapse analyses. A total of 33 members were tested for the SOS grids and 29 for the DOS grids [1 top chord, 4 bottom chords, 4 reduced bottom chords (SOS grid only, due to symmetry considerations), 12 web members, 12 corner web members]. Comparison of member critical values for various rotational stiffness values allowed for rotational stiffness values of semi-rigid connections corresponding to 33% and 66% of the critical load to be selected for each member (see Figure 8.5).

Discrete values of the Connection Stiffness parameter corresponding to pinned (0%), semi-rigid (33% and 66%) and fixed (100%) connection rotational behaviours were considered. The Connection Stiffness parameter values considered cover the range of possible connection restraint.

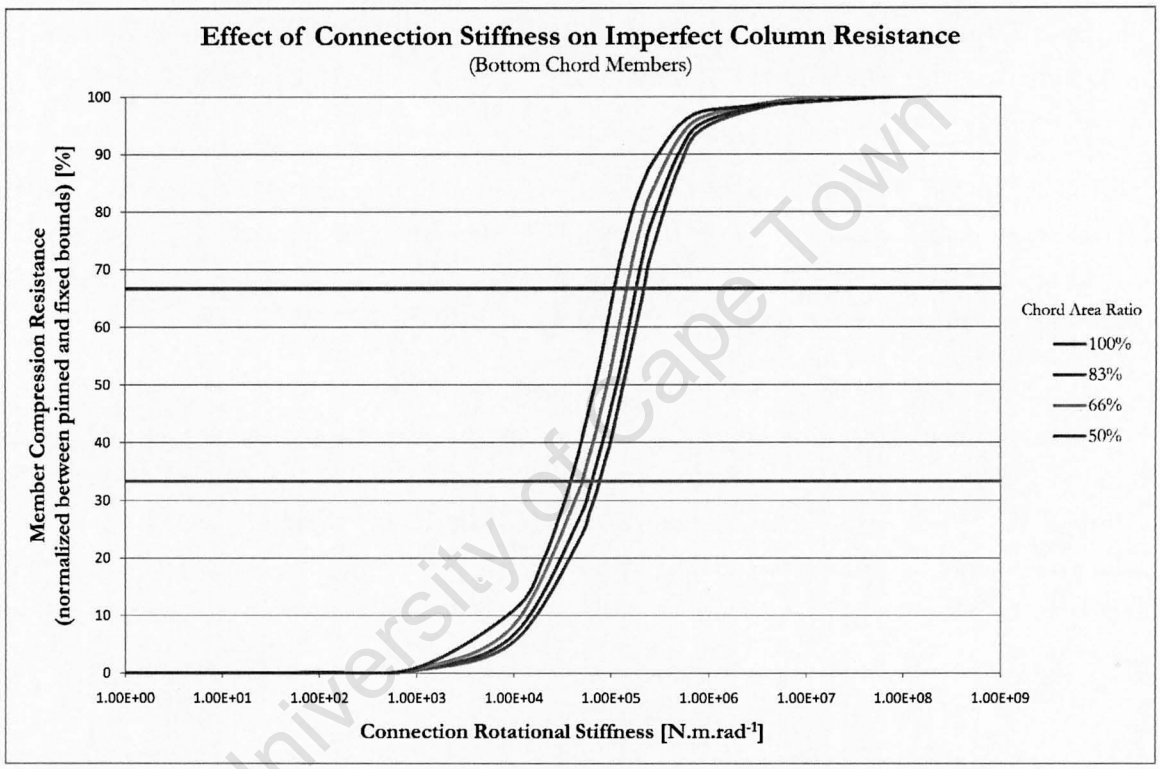




Figure 8.5: The effect of connection stiffness on the critical load of compression members, varying in flexural stiffness, with initial half-sine imperfection of magnitude $L/250$.

### 8.4.3 Top Chord Resistance

The Top Chord Resistance parameter was defined as the $A/\lambda^2$ parameter of the top chord members, considering the case of fixed end connections.

Top chord slenderness is influenced by both member cross-section and member end restraints. To this extent the primary means of varying the top chord parameter was by variation of the connection stiffness. However, to account for a wider range of the top chord parameter, various top chord cross-sections could be considered by variation of member OD and thickness.

Due to computational limitations, only one value of the Top Chord parameter was considered.

The member section employed resulted in a range of top chord slenderness ratios between 40 and 80 being considered, due to variation of the connection stiffness. The slenderness ratios considered cover the range of slender to stocky compression member behaviour.

### 8.4.4 Web:Top Chord Resistance

The Web:Top Chord Resistance parameter was defined as the ratio of web and top chords $A/\lambda^2$ parameter values, expressed as a percentage. The Web:Top Chord Resistance parameter principally defines the ratio of top chord and web member resistance.

The Web:Top Chord Resistance parameter directly affects web member stability. Buckling of slender web members may interact with or even precede buckling of compression chord members. The Web:Top Chord Resistance parameter was varied by changing the web member OD and wall thickness.

Five discrete values of the Web:Top Chord Resistance parameter were considered, 33%, 50%, 66%, 83% and 100%. The range of web slenderness considered is believed to be representative of values typically used in practice and includes stocky, intermediate and slender members.



### 8.4.5 Chord Area Ratio

The Chord Area Ratio parameter was defined as the ratio of member cross-sectional area between bottom and top chord members, expressed as a percentage. The Chord Area Ratio was however defined with respect to the $A/\lambda^2$ parameter as stress inversion, at a member level, was observed in the post-critical regime resulting in bottom chord buckling.

The Chord Area Ratio parameter directly affects the degree to which yielding of the tension chord members can take place prior to the initiation of top chord member buckling. Variation of the Chord Area Ratio parameter was achieved by changing the bottom chord $A/\lambda^2$ and cross-sectional area parameters proportionally through variation of the member OD and wall thickness.

Four discrete values of the Chord Area parameter were considered, 50%, 66%, 83% and 100%. This was believed to represent the range of typical values used in practice. Although the same Chord Area Ratio parameter values are applied to SOS and DOS grids, attention is drawn to the reduced bottom chord density and increased bottom chord length of DOS grids in comparison with SOS grids. This results in the effective bottom:top cross-sectional chord area ratio of DOS grids being approximately half that of comparable SOS grids and reduced compression buckling resistance of DOS bottom chord members relative to SOS grids.

## 8.5 Additional Considerations

### 8.5.1 Support Web Members

The focus of the parametric study undertaken is on the global failure behaviour of grid structures. Local failure of support web members was therefore not considered to be desirable. For this reason support web member resistance was increased by a factor of 4 relative to internal web members, assessed by scaling the member $A/\lambda^2$ parameter. This ensured that support web members would not fail even as failure of the structure progressed in the post-critical regime.

### 8.5.2 Members on Lines of Symmetry

Members which were coincident with lines of symmetry enforced for the purposes of symmetric modelling, namely selected bottom chord members in SOS grids, were accounted for by halving their respective resistances. This reduction to the member resistance was achieved by keeping member slenderness constant and changing member cross-section area. The members' respective $A/\lambda^2$ parameter values were therefore reduced by half, as was member axial resistance.



### 8.5.3 Grid Reference

The large number of grids considered necessitated a consistent referencing system to easily identify grids and the respective parameter values employed. The following referencing system was consequently adopted, with respect to the parameter definitions provided in Section 8.4:

**Grid Type-Span:Depth-Chord Area Ratio-Web:Top Chord Resist.-Connection Stiff.**

Which, when applied to a particular grid, selected at random, will appear as 'SOS-19.6-100-83-66' for example.

### 8.5.4 Parameter Variation

Structural behaviour is commonly a function of the interaction of numerous parameters. Consequently all possible combinations of the defined parameters were considered. This allowed for maximum flexibility in the comparison of results. Interaction of the parameters can be observed in the results by varying the combinations of parameter and parameter discrete values simultaneously. The total number of models analyzed, $N$, can therefore be expressed by Equation 8.1 where $n_i$ is the number of discrete variables for the $i^{th}$ parameter.

$$N = (n_1) \cdot (n_2) \cdot ..... \cdot (n_i) \tag{8.1}$$

For the purpose of the parametric study, two grid configurations, and five structural and geometric

parameters were considered, each consisting of one to four discrete parameter values, resulting in a total of 480 models ($N$ = 2(geometric configurations) x 3(Span:Depth) x 1(Top Chord Resistance) x 4(Connection Stiffness) x 4(Chord Area Ratio) x 4 (Web:Top Chord Resistance) parameter values).

## 8.6 Grid Analysis

Aspects of the parametric study relevant to the nonlinear analysis of grid structures are considered including, initial imperfection magnitude, applied displacement and symmetry considerations.

### 8.6.1 Initial Imperfections

The magnitude of the half sine imperfections employed for the nonlinear analysis of grid structures considered was consistent with the recommendations of EC3 (2005) for the nonlinear plastic analysis of structures. A half sine imperfection of magnitude $L/250$ was applied at a member level for all member groups which experience compression forces in the elastic regime; where $L$ is the individual member length between end nodes.

### 8.6.2 Applied Displacement

Analysis of the grid structures considered was undertaken with displacement control, as detailed in Chapter 6 . The displacement applied to all structures at the grid control point was 0.800m, this equates to an applied displacement of $L/25$ for the SOS and DOS grids. This displacement represents the average displacement applied to all nodes; consequently, multiplying the total applied force by this displacement gives the total energy added to the system. Maximum nodal displacements may therefore be much greater than the displacement applied to the control node (average displacement). Displacements are defined relative to the reference (undeformed configuration).

Grids would have ideally been tested to complete collapse; the point where the structure no longer offers any resistance to the application of displacement. However, this was not feasible as the application of large displacements resulted in even greater computational cost while problems tended to arise with convergence of the numerical solution when very large rotations were encountered. The magnitude of displacement applied was selected as it was sufficient to observe the critical behaviour and the development of the post-critical behaviour, for the structures considered, without excessive computational cost. DOS grids were generally observed to be less stiff than SOS grids; consequently, for a given displacement, which exceeded the critical displacement, SOS grids exhibit greater development of post-buckling behaviour.

### 8.6.3 Symmetry Constraints

Numerical analysis of DLG collapse behaviour, where the full grid geometry was considered, was susceptible to divergence from symmetric failure path; however, divergence from a symmetric failure path for the case of symmetric quarter models was significantly less common. As symmetrical failure of the grids was to be investigated, where a divergence from grid symmetry was observed in the failure path, symmetry was enforced through the use of displacement constraints. Displacement constraints were used to set the vertical displacement of nodes, symmetrical about the grid centre, equal to each other.

## 8.7 Summary of Grid Detail

Grid details used to define the numerical models of SOS and DOS grids are listed. The description of grid detail is divided to include Constants, aspects of the numerical model description which remain unchanged for all cases considered, and Variables, where a range of discrete values are employed and varied for the purpose of the parametric study.

### 8.7.1 Constants

#### 8.7.1.1 Material Properties

- Material: Steel (S355)
- Elastic Modulus: 210x10$^9$Pa
- Poison's Ratio: 0.3
- Density: 7850$kg.m^{-3}$
- Yield Stress: 355MPa
- Constitutive Behaviour: Elastic-Perfectly Plastic

#### 8.7.1.2 Grid Geometry and Loading

**SOS grid**

- Span: 20.000m x 20.000m
- Plan dimensions: 22.500m x 22.500m
- Aspect ratio: 1:1
- Chord Length: 2.500m
- Grid Type: Square-on-Square
- Edge Detail: Cornice
- Boundary Conditions: Simple Corner Supports (at level of bottom chords)
- Loading: All Top Nodes (100 points)

**DOS grid**

- Span: 20.000m x 20.000m
- Plan dimensions: 23.333m x 23.333m
- Aspect ratio: 1:1
- Chord Length: 2.357m
- Grid Type: Diagonal-on-Square
- Edge Detail: Cornice
- Boundary Conditions: Simple Corner Supports (at level of bottom chords)
- Loading: All Top Nodes (112 points)

#### 8.7.1.3 Elements and Connections

- Element Groups

  Group 1: Top Chords

  Group 2: Bottom Chords

  Group 3: Web Members

  Group 4: Support Web Members

- Section type, chord and web members: Circular hollow sections
- Section type, support web members: Circular hollow sections
- Connection Behaviour

  Translation: Rigid (d.o.f. 1,2,3)

  Rotation: Linear Elastic (d.o.f. 4,5,6)

- Top Chord: 40
- Initial Imperfection Magnitude: $L$x0.004 (L/250)

### 8.7.2 Variables

- Span Depth: 6.5, 11.3, 19.6
- Connection Stiffness: 0% (pinned), 33%, 66% and 100% (fixed)
- Web:Top Chord Resistance: 33%, 50%, 66%, 83% and 100%
- Chord Area Ratio 50%, 66%, 83% and 100%

### 8.7.3 Input Values

Input values used to vary grid geometry and structure as functions of Span:Depth, Connection Stiffness, Web:Top Chord Resistance and Chord Area Ratio parameters are listed.

#### 8.7.3.1 Span:Depth (Web Angle)

As the span of grids considered was kept constant, the Span:Depth parameter defined grid depth. Grid Depth was maintained constant between SOS and DOS grids by variation of the grid web angle (see Table 8.2).

#### 8.7.3.2 Connection Stiffness

Connection stiffness values employed for the range of Connection Stiffness parameter values and member types are shown in Tables 8.6 (TopChords), 8.7 (Bottom Chords), 8.8 (Webs) and 8.9 (Corner Webs).

#### 8.7.3.3 Top Chord

The Top Chord Cross-Section parameter was not varied as part of the parametric study. The Top Chord Cross-Section parameter only defined the CHS member used for the grid top chord members. For a Top Chord Cross-Section parameter value of 40, a CHS with an OD of $91.819mm$ and wall thickness of $3.500mm$ was specified.

#### 8.7.3.4 Web:Top Chord Resistance

The Web:Top Chord Resistance parameter defined the CHS member used for the grid web members, the web member cross-section employed was however also dependent on the Span:Depth parameter. For Web:Top Chord Resistance and Span:Depth parameter values between $33\% - 100\%$ and 6.5-19.6 the CHS ODs and wall thickness for internal web members and ODs for support member solid bars were specified as shown in Tables 8.4 and 8.5 for SOS and DOS DLGsrespectively.

#### 8.7.3.5 Geometric Configuration

| Grid Type | Span:Depth [-] | Web Angle [°] | Grid Depth [m] | Top Chord Length [m] | Span [m] |
|---|---|---|---|---|---|
| SOS | 19.596 | 30.000 | 1.021 | 2.500 | 20.000 |
| | 11.314 | 45.000 | 1.768 | 2.500 | 20.000 |
| | 6.532 | 60.000 | 3.062 | 2.500 | 20.000 |
| DOS | 19.596 | 31.482 | 1.021 | 2.357 | 20.000 |
| | 11.314 | 46.686 | 1.768 | 2.357 | 20.000 |
| | 6.532 | 61.439 | 3.062 | 2.357 | 20.000 |

Table 8.2: Linear elastic spring stiffnesses employed for connections and varied as a function of the Connection Stiffness parameter.

#### 8.7.3.6 Member Cross-section Sizes

| Bottom Chord Member Sections (SOS and DOS Grids) | | | | |
|---|---|---|---|---|
| Chord Area Ratio | SOS Grids | | DOS Grids | |
| | OD [mm] | Wall Thickness [mm] | OD [mm] | Wall Thickness [mm] |
| 50% | 90.119 | 1.749 | 85.063 | 1.749 |
| 50% reduced | 89.258 | 0.874 | n.a. | n.a. |
| 66% | 90.689 | 2.332 | 85.633 | 2.332 |
| 66% reduced | 89.546 | 1.166 | n.a. | n.a. |
| 83% | 91.256 | 2.916 | 86.199 | 2.916 |
| 83% reduced | 89.834 | 1.457 | n.a. | n.a. |
| 100% | 91.819 | 3.500 | 86.670 | 3.500 |
| 100% reduced | 90.120 | 1.749 | n.a. | n.a. |

Table 8.3: SOS and DOS grid bottom chord sections, employed as a function of the Chord Area Ratio parameter.

| Internal Web Member Sections (SOS and DOS Grids) | | | | | |
|---|---|---|---|---|---|
| Span: Depth | Web:Top Chord Resistance | SOS Grids | | DOS Grids | |
| | | OD [mm] | Wall Thickness [mm] | OD [mm] | Wall Thickness [mm] |
| 19.6 | 50% | 74.279 | 2.143 | 75.249 | 1.989 |
| | 66% | 74.970 | 2.858 | 75.893 | 2.653 |
| | 83% | 75.674 | 3.574 | 76.530 | 3.317 |
| | 100% | 76.332 | 4.291 | 77.162 | 3.983 |
| 11.3 | 50% | 90.119 | 1.749 | 92.694 | 1.600 |
| | 66% | 90.689 | 2.322 | 93.217 | 2.133 |
| | 83% | 91.256 | 2.916 | 93.737 | 2.667 |
| | 100% | 91.819 | 3.500 | 94.253 | 3.201 |
| 6.5 | 50% | 126.230 | 1.237 | 131.838 | 1.115 |
| | 66% | 126.638 | 1.649 | 132.207 | 1.486 |
| | 83% | 127.044 | 2.061 | 132.573 | 1.858 |
| | 100% | 127.449 | 2.473 | 132.939 | 2.230 |

Table 8.4: SOS grid web member sections, employed as functions of Span:Depth and Web:Top Chord Resistance parameters.

| Corner Web Member Sections (SOS and DOS Grids) | | | | | |
|---|---|---|---|---|---|
| Span: Depth | Web:Top Chord Resistance | SOS Grids | | DOS Grids | |
| | | OD [mm] | Wall Thickness [mm] | OD [mm] | Wall Thickness [mm] |
| 19.6 | 50% | 80.279 | 8.628 | 80.580 | 8.001 |
| | 66% | 82.807 | 11.572 | 83.219 | 10.719 |
| | 83% | 85.259 | 14.578 | 85.522 | 13.486 |
| | 100% | 87.643 | 17.671 | 87.765 | 16.316 |
| 11.3 | 50% | 95.125 | 7.017 | 97.296 | 6.413 |
| | 66% | 97.268 | 9.379 | 99.273 | 8.658 |
| | 83% | 99.364 | 11.762 | 101.211 | 10.737 |
| | 100% | 101.468 | 14.173 | 103.113 | 12.926 |
| 6.5 | 50% | 129.852 | 4.950 | 135.113 | 4.461 |
| | 66% | 131.430 | 6.604 | 136.544 | 5.951 |
| | 83% | 132.988 | 8.261 | 137.959 | 7.443 |
| | 100% | 134.528 | 9.923 | 139.360 | 8.938 |

Table 8.5: DOS grid web member sections, employed as functions of Span:Depth and Web:Top Chord Resistance parameters.

#### 8.7.3.7 Connection Stiffnesses

| Top Chord Member Connection Stiffness (SOS and DOS Grids) | | |
|---|---|---|
| Connection Stiffness | Spring Stiffness $[N.m.rad^{-1}]$ | |
| | SOS Grids | DOS Grids |
| 33% | $7.637 \times 10^4$ | $6.798 \times 10^4$ |
| 66% | $2.159 \times 10^5$ | $1.918 \times 10^5$ |

Table 8.6: Linear elastic spring stiffnesses employed for top chord member connections and varied as a function of the Connection Stiffness parameter.

| Bottom Chord Member Connection Stiffness (SOS and DOS Grids) | | | |
|---|---|---|---|
| Chord Area Ratio | Connection Stiffness | Spring Stiffness $[N.m.rad^{-1}]$ | |
| | | SOS Grids | DOS Grids |
| 50% | 33% | $3.819 \times 10^4$ | $3.727 \times 10^4$ |
| | 33% reduced | $1.910 \times 10^4$ | n.a. |
| | 66% | $1.080 \times 10^5$ | $1.164 \times 10^5$ |
| | 66% reduced | $5.400 \times 10^4$ | n.a. |
| 66% | 33% | $5.091 \times 10^4$ | $4.969 \times 10^4$ |
| | 33% reduced | $2.546 \times 10^4$ | n.a. |
| | 66% | $1.439 \times 10^5$ | $1.552 \times 10^5$ |
| | 66% reduced | $9.199 \times 10^4$ | n.a. |
| 83% | 33% | $6.365 \times 10^4$ | $6.210 \times 10^4$ |
| | 33% reduced | $3.183 \times 10^4$ | n.a. |
| | 66% | $1.799 \times 10^5$ | $1.940 \times 10^5$ |
| | 66% reduced | $8.999 \times 10^4$ | n.a. |
| 100% | 33% | $7.637 \times 10^4$ | $7.450 \times 10^4$ |
| | 33% reduced | $3.819 \times 10^4$ | n.a. |
| | 66% | $2.159 \times 10^5$ | $2.327 \times 10^5$ |
| | 66% reduced | $1.080 \times 10^5$ | n.a. |

Table 8.7: Linear elastic spring stiffnesses employed for bottom chord member connections and varied as a function of the Connection Stiffness parameter.

| Internal Web Member Connection Stiffness (SOS and DOS Grids) | | | | |
|---|---|---|---|---|
| Span: Depth | Web:Top Chord Resistance | Connection Stiffness | Spring Stiffness $[N.m.rad^{-1}]$ | |
| | | | SOS Grids | DOS Grids |
| 19.6 | 50% | 33% | $3.132x10^4$ | $2.998x10^4$ |
| | | 66% | $8.790x10^4$ | $8.419x10^4$ |
| | 66% | 33% | $4.176x10^4$ | $3.997x10^4$ |
| | | 66% | $1.172x10^5$ | $1.122x10^5$ |
| | 83% | 33% | $5.219x10^4$ | $4.995x10^4$ |
| | | 66% | $1.465x10^5$ | $1.403x10^5$ |
| | 100% | 33% | $6.262x10^4$ | $5.994x10^4$ |
| | | 66% | $1.758x10^5$ | $1.683x10^5$ |
| 11.3 | 50% | 33% | $3.819x10^4$ | $3.713x10^4$ |
| | | 66% | $1.080x10^5$ | $1.057x10^5$ |
| | 66% | 33% | $5.091x10^4$ | $4.808x10^4$ |
| | | 66% | $1.440x10^5$ | $1.407x10^5$ |
| | 83% | 33% | $6.364x10^4$ | $6.191x10^4$ |
| | | 66% | $1.800x10^5$ | $1.774x10^5$ |
| | 100% | 33% | $7.637x10^4$ | $7.417x10^4$ |
| | | 66% | $2.159x10^5$ | $2.100x10^5$ |
| 6.5 | 50% | 33% | $5.340x10^4$ | $5.256x10^4$ |
| | | 66% | $1.541x10^5$ | $1.521x10^5$ |
| | 66% | 33% | $7.120x10^4$ | $7.009x10^4$ |
| | | 66% | $2.054x10^5$ | $2.041x10^5$ |
| | 83% | 33% | $8.900x10^4$ | $8.771x10^4$ |
| | | 66% | $2.567x10^5$ | $2.595x10^5$ |
| | 100% | 33% | $1.068x10^5$ | $1.051x10^5$ |
| | | 66% | $3.081x10^5$ | $3.043x10^5$ |

Table 8.8: Linear elastic spring stiffnesses employed for web member connections and varied as a function of the Connection Stiffness parameter.

| Corner Web Member Connection Stiffness (SOS and DOS Grids) | | | | |
|---|---|---|---|---|
| Span: Depth | Web:Top Chord Resistance | Connection Stiffness Parameter | Spring Stiffness $[N.m.rad^{-1}]$ | |
| | | | SOS Grids | DOS Grids |
| 19.6 | 50% | 33% | $1.250x10^5$ | $1.197x10^5$ |
| | | 66% | $3.510x10^5$ | $3.363x10^5$ |
| | 66% | 33% | $1.664x10^5$ | $1.594x10^5$ |
| | | 66% | $4.674x10^5$ | $4.478x10^5$ |
| | 83% | 33% | $2.046x10^5$ | $1.989x10^5$ |
| | | 66% | $5.829x10^5$ | $5.588x10^5$ |
| | 100% | 33% | $2.455x10^5$ | $2.365x10^5$ |
| | | 66% | $6.971x10^5$ | $6.689x10^5$ |
| 11.3 | 50% | 33% | $1.526x10^5$ | $1.482x10^5$ |
| | | 66% | $4.316x10^5$ | $4.199x10^5$ |
| | 66% | 33% | $2.033x10^5$ | $1.975x10^5$ |
| | | 66% | $5.752x10^5$ | $5.594x10^5$ |
| | 83% | 33% | $2.540x10^5$ | $2.467x10^5$ |
| | | 66% | $7.184x10^5$ | $6.988x10^5$ |
| | 100% | 33% | $3.044x10^5$ | $2.958x10^5$ |
| | | 66% | $8.610x10^5$ | $8.379x10^5$ |
| 6.5 | 50% | 33% | $2.136x10^5$ | $2.118x10^5$ |
| | | 66% | $6.163x10^5$ | $6.667x10^5$ |
| | 66% | 33% | $2.846x10^5$ | $2.802x10^5$ |
| | | 66% | $8.216x10^5$ | $8.490x10^5$ |
| | 83% | 33% | $3.557x10^5$ | $3.502x10^5$ |
| | | 66% | $1.027x10^5$ | $1.014x10^6$ |
| | 100% | 33% | $4.269x10^5$ | $4.202x10^6$ |
| | | 66% | $1.232x10^6$ | $1.217x10^6$ |

Table 8.9: Linear elastic spring stiffnesses employed for corner web member connections and varied as a function of the Connection Stiffness parameter.

# References

Eurocode 1: Actions on Structures Part1-1: General Actions - Densities, Self-Weight, Imposed Loads for Buildings, 2002.

Eurocode 3: Design of Steel Structures - Part 1.1: General Rules and Rules for Buildings BS-EN 1993-1-1:2005, 2005.

G. S. Ramaswamy, M. Eekhout, and G. R. Suresh. *Analysis, design and construction of steel space frames.* Thomas Telford, 2002.

F. E. S. West. as cited by Makowski (1981) . A study of the efficiency of double-layer grid structures. Master's thesis, University of Surrey, 1967.

# Chapter 9

# Results and Discussion

## 9.1 Introduction

The results of the numerical model collapse analysis, of SOS and DOS DLG structures under uniformly distributed loading, are presented and discussed. In total 480 structures were analyzed as part of the study (240 SOS grids and 240 DOS grids).

Grid failure and collapse mechanisms were identified in the results of the grids analyzed; grid load-displacement responses, and incremental displacement and stress fields were used for this purpose. Trends in structural behaviour were initially assessed in terms of the individual structural parameters considered. Cross-comparison of the results then allowed for the effect of parameter interaction to additionally be identified. Where favourable trends in grid plastic behaviour were observed these were identified and are discussed in greater detail.



### 9.1.1 Sub-division of DLG Behaviour

Three regimes of grid behaviour were identified for the purposes of presenting and post processing the results of the numerical model collapse analysis. The three regimes of DLG behaviour selected were defined as follows:

- Pre-critical behaviour, subdivided further into:
  - Grid elastic behaviour, characterized by a linear elastic response where deformations are fully recoverable; and
  - Grid plastic behaviour, characterized by a continued hardening response, where bottom chord or web member tensile yielding results in non-recoverable deformation.
- Critical behaviour, characterized by the onset of grid softening behaviour, governed by flexure or shear failure mechanisms; and
- Post-critical behaviour (also referred to as post-buckling behaviour), characterized by: gradual decreases in structural resistance associated with the failure of multiple non-critical members; a sudden decrease in structural resistance associated with the failure of critical members; or the development of grid plastic hinges.

Owing to the large amount of data generated, only representative load displacement curves and graphics are presented for the purposes of identifying and categorizing grid behaviour; the full set of load-displacement and deformed geometry plots, superimposed with Maximum von Mises stresses, are included on the accompanying CD.

### 9.1.2 Post-Processing and Comparison of Results

Comparison of the load-displacement curves of similar grids, through parameter variation, provided the greatest insight into grid behaviour. The use of load-displacement curves was, however, limited in its application to comparison of numerous grids concurrently. The use of energy applied to grids in the form of work done, $W = F.d$ (represented in this case as the integral of the load-displacement response), was found to be effective for the comparison of multiple grids concurrently and allowed for trends in grid behaviour to be identified.

Trends in grid behaviour were established through the comparison of quantifiable aspects of structural behaviour, identified through post-processing of grid load-displacement data, for each of the three grid behaviour regimes considered. Quantifiable representations of grid behaviour, extracted from the load-displacement response of DLG collapse analysis and used for comparison of similar DLGs included:

- Grid elastic stiffness;
- Grid critical load resistance;
- Ratio of grid plastic to critical energy fractions;
- Grid average post-critical resistance;
- Ratio of grid average post-critical to critical load resistance.



### 9.1.3 Design Resistance

For the case of the initial SOS grid design, comparison between numerical collapse analyses and design resistances was undertaken to demonstrate the potential for significant reductions in grid capacity resulting from non-symmetrical failure patterns, although this should not be taken to be generally representative of DLG structures. For this comparison design resistance was calculated in accordance with Eurocode 3; and both symmetrical and unsymmetrical failure paths were considered for the purpose of numerical analysis.

## 9.2 Pre-critical Behaviour

Results demonstrating behaviour observed prior to the onset of grid global softening behaviour are introduced and discussed. Attention was paid to the development of pre-critical nonlinear behaviour (plastic behaviour) resulting from tensile chord yielding due to its favourable effect on grid behaviour.

### 9.2.1 Elastic Behaviour

Flexural stiffness of DLG structures was found to define grid elastic behaviour, as was expected. DLG flexural stiffness was observed to increase with Chord Area and Connection Stiffness parameters while

flexural stiffness decreased with increasing values of the Span:Depth parameter. The Web:Top Chord Resistance parameter was not observed to have a significant effect on DLG elastic behaviour, within the range of parameter values considered. The stiffness of web members can therefore be said not to contribute to DLG flexural stiffness. DOS grids were found to be less stiff than comparable SOS grids due their comparatively less dense bottom chord arrangement and the larger top chord span between opposite supports (see Figure 9.3 for a typical comparison of the load-displacement responses of SOS and DOS grids).

Load distribution in the elastic regime, of maximum compressive stresses, was found to be a good proxy for the location of critical members. This is attributed to the generally high elastic stiffness of DLG structures and their resulting initial linear elastic response. The distribution of stress in the elastic regime is consequently considered for SOS and DOS grid configurations.

#### 9.2.1.1 Elastic Stress Distribution in SOS Grids

The rectilinear arrangement of the top and bottom chord members in SOS grids resulted in structures which spanned between adjacent supports. The most highly stressed compressive and tensile members were consequently found to be at the midspan, between adjacent supports, on the grid periphery (see Figure 9.1).

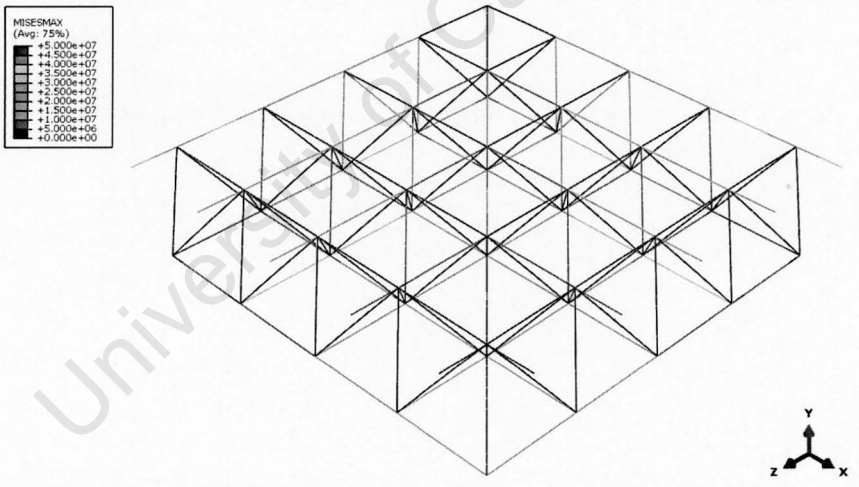


Figure 9.1: Typical elastic distribution of maximum von Mises section stress ($N.m^{-2}$) in SOS DLG resulting from self-weight; grid $SOS - 11.3 - 50 - 83 - 0$ shown.

#### 9.2.1.2 Elastic Stress Distribution in DOS Grids

The diagonal orientation of the top chord members in DOS grids, relative to the supports, resulted in structures which spanned between opposite supports at the level of the top chords and spanned between adjacent supports at the level of the lower chords. The most highly stressed compressive members were consequently found at the level of the top chords, midspan between opposite supports, while the most highly stressed tensile members were found at the level of the bottom chords, midspan between adjacent supports (see Figure 9.2).

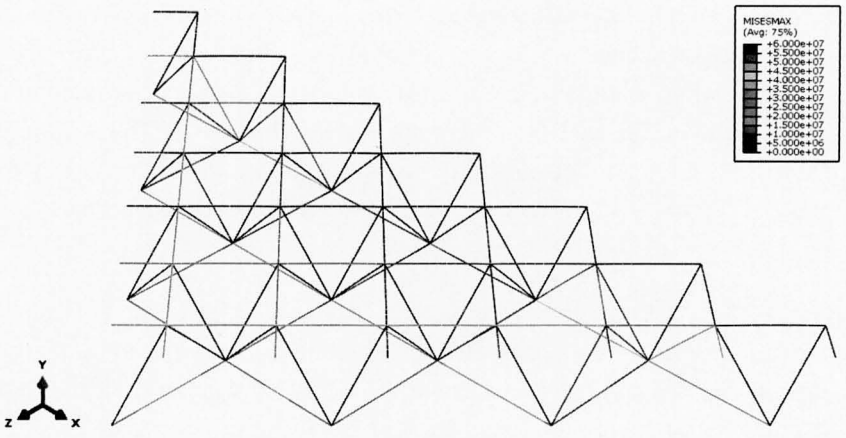


Figure 9.2: Typical elastic distribution of maximum von Mises section stress ($N.m^{-2}$) in DOS DLG resulting from self-weight; grid $DOS - 11.3 - 50 - 83 - 0$ shown.

### 9.2.2 Plastic Behaviour

Plastic behaviour of DLG structures on a macro scale resulted from the tensile yielding of bottom chord or web members prior to the onset of grid critical behaviour (see Figure 9.4). The potential for pre-critical plastic deformation of DLG structures is generally considered desirable as increased deflection is evident prior to failure. Plastic pre-critical deformation behaviour in the load-displacement response of DLG structures provides warning of imminent collapse (see the load-displacement behaviour of grid $DOS - 11.3 - 50 - 83 - 0$ relative to similar SOS grid in Figure 9.3).

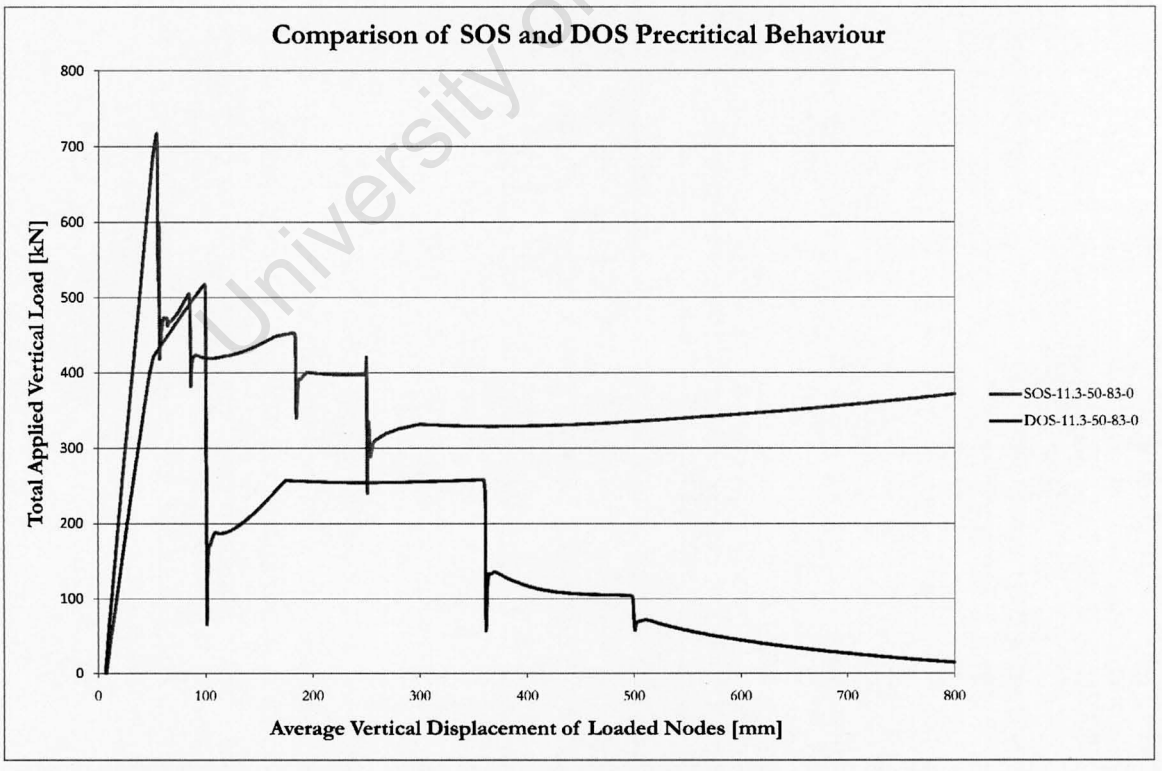


Figure 9.3: Plastic pre-critical behaviour of DOS DLG, resulting from tensile chord yielding, is evident in the comparison of similar SOS and DOS grids.

Plastic behaviour of DLG structures was identified in the load-displacement response of such structures by a decrease in grid stiffness. This decrease in stiffness was consistent with elastic perfectly

plastic material model used for steel and considered for the purpose of analysis. Due to this material behaviour, the yielding of members resulted in the stiffness of these members being subtracted from the grid stiffness as $\Delta\sigma/\Delta\epsilon \rightarrow 0$, where $\Delta$ is the change in stress, $\sigma$, and strain, $\epsilon$. The grid global stiffness consequently decreased and grid global deflections increased for a unit load increment. Where successive changes to grid stiffness were encountered prior to the critical load, this was attributed to yielding of successive sets of bottom chord members adjacent to each other (see points $B_1$ and $B_2$ in Figure 9.5).

Web member yielding was observed for low values of the Web:Top Chord Resistance parameter; in such cases tensile web members adjacent to support web members were observed to yield resulting in global pre-critical plastic deformation as was observed for tensile chord yielding (see load-displacement response of grids $DOS-19.6-83-33-33$ and $DOS-11.3-83-33-33$ in Figure 9.9). Web member yielding was only observed for DOS grids due to the reduced web member area associated with such grid configurations.

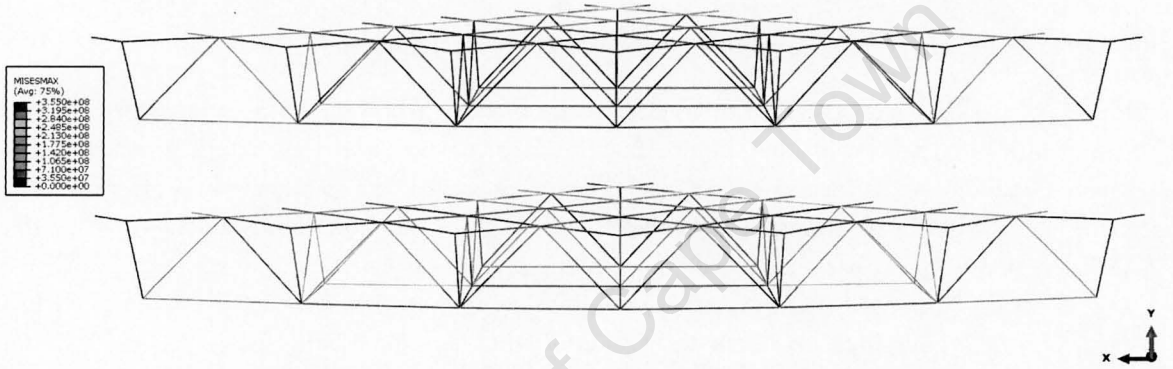


Figure 9.4: Comparison of bottom chord yielding (top) and web yielding (bottom) behaviour between similar DOS grids (grids $DOS-11.3-50-100-66$ and $DOS-11.3-50-33-66$ respectively).



#### 9.2.2.1 Means of Comparison

The extent of grid plastic behaviour observed was assessed independently of grid load resistance, to facilitate comparison between grid structure variations. Plastic behaviour observed in the collapse analysis results was therefore assessed relative to the grid elastic deformation energy and was expressed as the ratio of plastic to critical energy fractions (see Figure 9.5). For the purpose of post-processing load-displacement data, from finite element model results, the onset of plastic behaviour was identified with the following logic (point references refer to Figure 9.5):

1. The grid critical load was identified as the maximum load encountered prior to the onset of softening behaviour (Point C).

2. In the pre-critical regime, the incremental gradient of the load-displacement response was evaluated for each increment (Between points A-C).

3. If the gradient of the load-displacement curve for the current increment was <66% of the equivalent gradient from the previous increment[1], then the reaction force of the previous increment was compared with the grid critical load.

[1]The value of 66% was calibrated through comparison with grid load-displacement responses.

4. If the previous increment's reaction force was less than 90% of the grid critical load[2], yielding of the structure was identified (i.e. if Applied Load at $B_1$ <90% of Applied Load at C, yielding is identified at $B_1$).

5. If no yielding of the structure was identified before the grid critical load was achieved, the structure was considered to pass directly from the elastic to the post-buckling regime.

#### 9.2.2.2 Parameterized Behaviour

Significant plastic behaviour was not observed for the SOS grid configurations considered (see Figure A.1) due to the high effective bottom chord densities associated with the SOS grid configuration. DOS grids however, demonstrated significant plastic deformation for certain parameter combinations; the extent to which DOS grids were able to plastically deform prior to the onset of critical behaviour is shown in Figure 9.6. SOS DLGs would be expected to exhibit similar pre-critical plastic behaviour to DOS grids if comparable effective bottom chord areas were employed.

Initiation of yielding behaviour in grid structures was observed to be dependent on the ratio of bottom to top chord area (defined by the Chord Area Ratio parameter) while the extent to which plastic behaviour was allowed to develop in grid structures was found to be dependent on the stability of the structure during plastic deformation (defined primarily by: the Web:Top Chord Resistance parameter; the Connection Stiffness parameter and; to a lesser extent the Span:Depth parameter). Stability of a grid structure during plastic deformation was observed to be dependent on the avoidance of shear and flexural failure mechanisms (for a description of DLG failure mechanisms see Section 9.3). The development of grid plastic behaviour can therefore be said to be dependent on the ratio of bottom chord resistance to critical top chord and web member resistance.

DOS grid plastic behaviour was considered with respect to the grid parameterization considered and the limitations imposed by shear and flexural failure; reference is made to grid load-displacement behaviour and the parameterized plot of DOS grid critical load:

**Chord Area** The initiation of plastic behaviour observed in the DOS structures considered was found to be inversely proportional to the Chord Area parameter (see Figure 9.7); this is attributed to the affect of the Chord Area parameter on grid stiffness and consequently the onset of bottom chord yielding. As the ratio of bottom to top chord area decreased, grid yielding behaviour was observed to initiate at lower total applied grid loads. The degree of yielding behaviour was also observed to increase with decreasing bottom chord area (see Figure 9.6), this is as yielding initiated when critical top chord and web members were in a lower stress range and consequently prolonged stability of the grid structure resulted under plastic deformation.

**Connection Stiffness** Connection stiffness was not observed to influence the initiation of plastic behaviour; this is as the Connection Stiffness parameter did not affect the tensile resistance of bottom chord members. Connection Stiffness was however observed to influence stability of DOS structures during plastic deformation due to its effect on top chord and web member resistance. As connection stiffness was increased, top chord and web member resistance increased, stability of the grid structures was maintained to increased values of total applied grid load (see Figure 9.8) and increased grid plastic behaviour was observed (see Figure 9.6).

[2]This ensured that grid critical behaviour was not confused with grid plasticity behaviour.

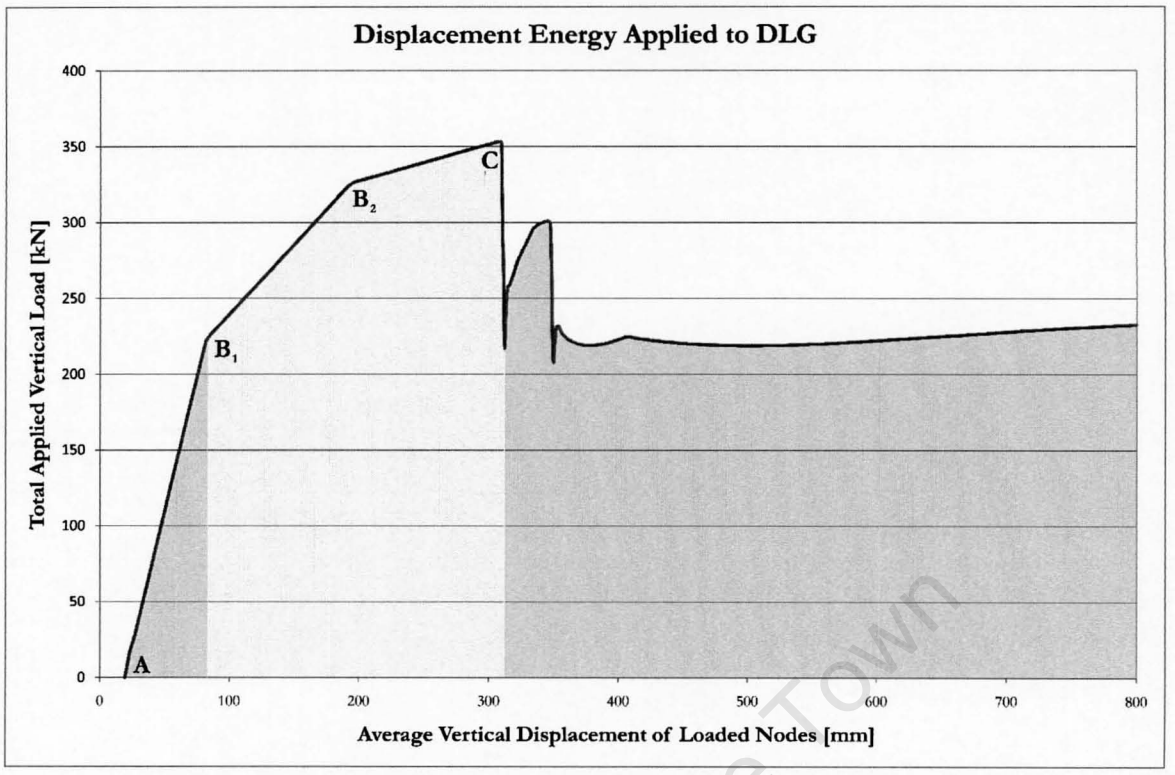


Figure 9.5: Elastic, plastic and post-critical energy fractions of total energy applied to DLGs in the form of displacement (blue, yellow and green respectively). Critical energy is defined as the sum of elastic and plastic energy fractions. Successive yielding of bottom chord member groups identified by change in pre-critical stiffness at locations $B_1$ and $B_2$.

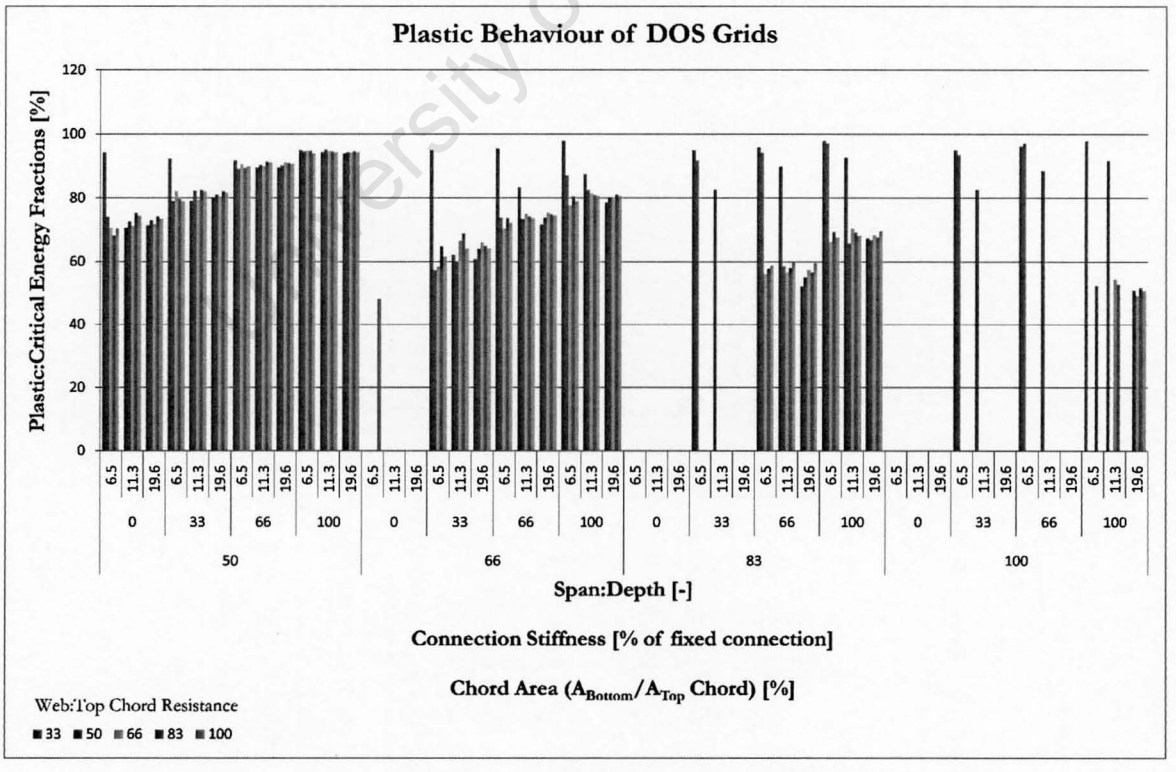


Figure 9.6: The extent of DOS DLG plastic deformation, resulting from bottom chord yielding, was observed to be dependent on initiation of plastic behaviour (inversely proportional to the Chord Area parameter) and the stability of the grid during plastic deformation (proportional to Connection Stiffness and Web:Top Chord Resistance parameters).

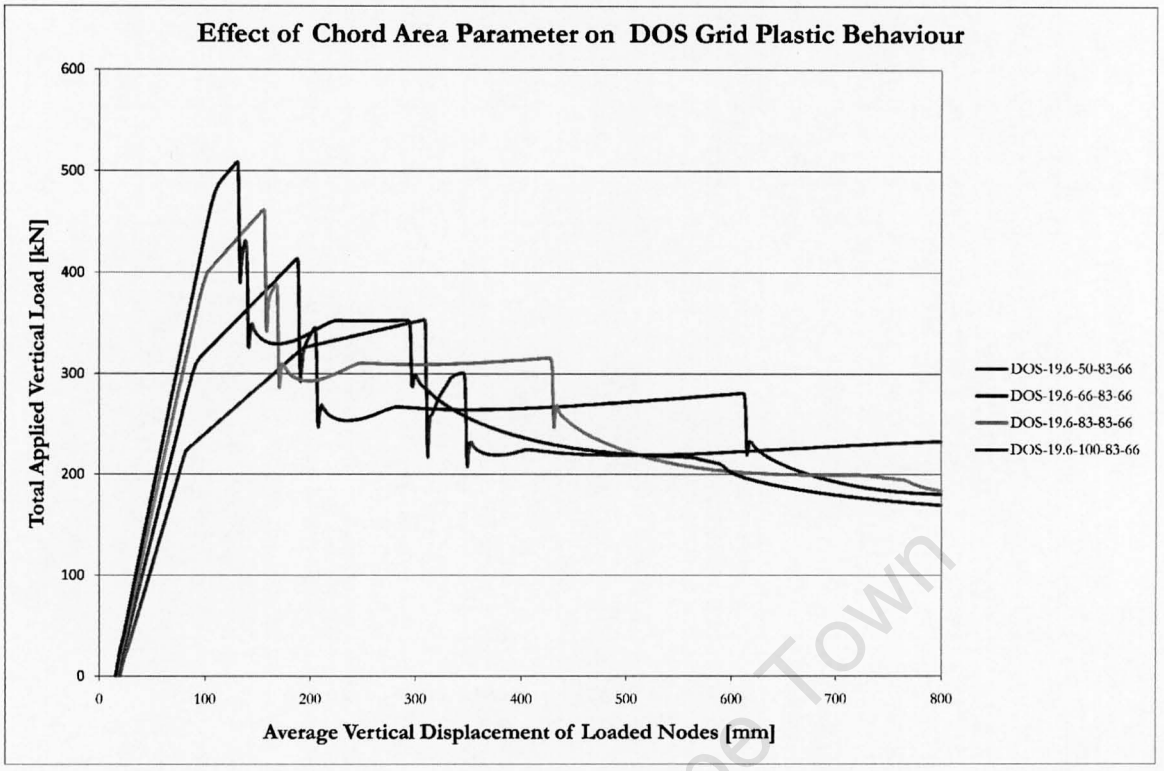


Figure 9.7: The initiation and the extent of DOS grid plastic deformation were observed to be inversely proportional to the Chord Area Ratio parameter.

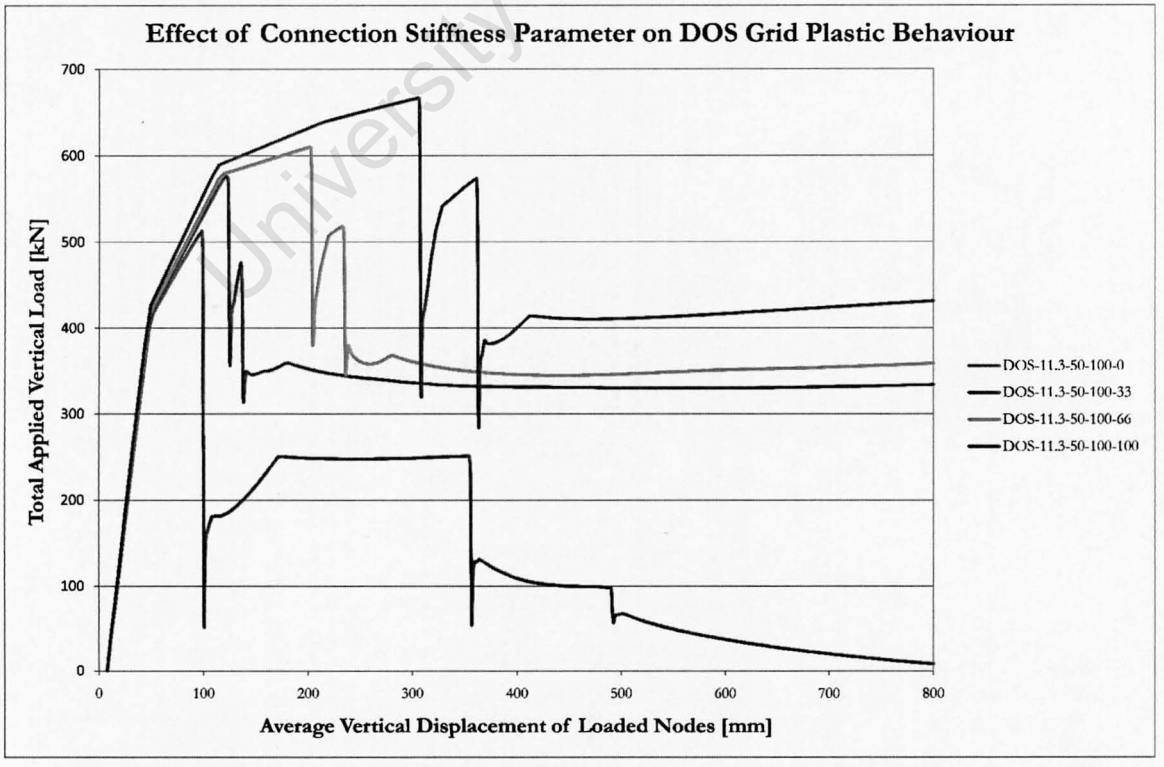


Figure 9.8: Increasing stability of DOS grid plastic deformation was observed for increasing values of the Connection Stiffness parameter.

**Span:Depth and Web:Top Chord Resistance** parameters were not observed to have a significant effect on grid flexural plasticity behaviour but were observed to affect web member yielding behaviour. Web member yielding behaviour was governed by web member resistance (defined by the Web:Top Chord Resistance parameter) and shear force distribution (defined by the Span:Depth parameter).

As the Span:Depth parameter decreased, DLG flexural stiffness increased while grid shear stiffness remained unchanged; concurrently as the Span:Depth parameter decreased shear load distribution changed, for a given applied load the component of the grid global shear load associated with grid bending decreased. Grid structures with decreasing values of the Span:Depth and Web:Top Chord Reistance parameters were consequently most susceptible to web member yielding behaviour.

Global plastic behaviour resulting from web yielding was observed for grids represented by Chord Area Ratio parameter values of 83% and 100%, Connection Stiffness parameter values of 33% and 66%, Span:Depth parameter values of 6.5 and 11.3, and Web:Top Chord Resistance parameter values of 33% and 50% (for Span:Depth of 6.5 only), see Figure 9.9). The Connection Stiffness and Chord Area Ratio parameters affected web member yielding behaviour due to their influence on web member stability and bottom chord yielding respectively.



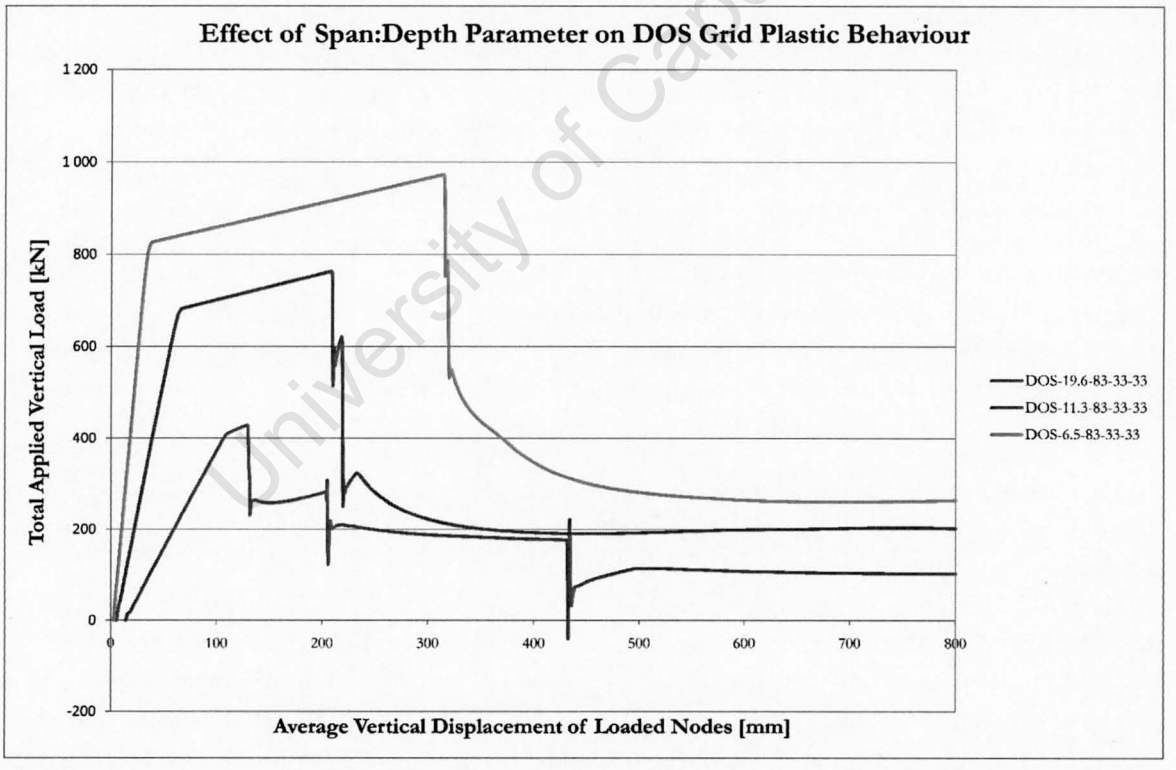


Figure 9.9: The Span:Depth parameter was observed to affect the distribution of force through DLG structures. The Span:Depth parameter consequently affected grid failure mechanism and pre-critical plastic stability too. Grid $DOS - 6.5 - 83 - 33 - 33$ failed in flexure, grids $DOS - 11.3 - 83 - 33 - 33$ and $DOS - 19.6 - 83 - 33 - 33$ experience web yielding and failed in shear. Increased stability under plastic deformation was observed for decreasing values of the Span:Depth parameter.

### 9.2.3 Discussion

Elastic behaviour of grid structures observed in the load-displacement responses of the grids analyzed was consistent with expectations. A general increase in grid flexural stiffness was observed for increasing Chord Area Ratio and Connection Stiffness parameters while a decrease in flexural stiffness was observed for increasing values of the Span:Depth parameter. The Web:Top Chord Resistance parameter was not observed to effect grid stiffness and did not influence elastic stress distribution in SOS and DOS DLG structures. SOS grids were observed to have a higher flexural stiffness than DOS grids.

Plasticity behaviour of DOS grid structures was observed to predominantly result from tensile yielding of chord members; however selected cases of web tensile yielding were also observed to result in similar grid plastic deformation. The stability of grid plastic behaviour resulting from web failure however is questionable as load was redistributed to surrounding critical members which can result in sudden decreases in grid resistance. Development of grid plastic behaviour resulting from web member failure was consequently not considered to represent an improvement in grid behaviour.

Significant plasticity behaviour was observed for the majority of DOS grid configurations analyzed but only in relatively few of the SOS grid configurations analyzed. The differences observed between SOS and DOS grid structure pre-critical behaviour is attributed to: the effective bottom:top chord area ratios (for the case of grid flexural yielding behaviour); and the effective web member area ratios (for the case of grid shear yielding behaviour). DOS grids have a less dense configuration of bottom chord and web members, relative to SOS grids, and therefore bottom chords and web members in DOS grids are able to yield prior to the initiation of shear or flexural failure mechanisms. For the case of grid flexural yielding SOS grids would be expected to demonstrate similar behaviour to DOS grids if equivalent effective bottom:top chord areas were employed; the reduced chord spacing in DOS grids is however believed to be a more practical means of reducing the effective chord area ratio.

Initiation of plastic behaviour was found to be dependent on the Chord Area parameter (provided shear and flexure failure mechanisms were avoided prior to yielding) while the development of grid plastic deformation of DOS grids was limited by the stability of top chord and web compression members. Plastic behaviour of grid structures can therefore be said to be inversely dependent on the ratio of bottom chord resistance to critical member resistance.

The nonlinear load-displacement responses observed in DOS pre-critical yielding behaviour, which resulted from bottom chord yielding, are desirable from a structural design and safety perspective as it provides warning of grid damage prior to grid collapse. The extent of nonlinear behaviour observed in selected DOS grids is significant, see Figure 9.10, and is comparable to the improvements achieved by Parke (1988) on SOS grids (see Section 3.3.4.1). The work undertaken by Parke (1988), however, achieved yielding behaviour by increasing the resistance of compression chord members. The work presented shows that yielding behaviour can also be achieved by reducing tension member resistance, through adoption of grid configurations which employ less dense bottom chord arrangements, this is believed to be a more practical means of achieving yielding behaviour in 'real structures' as excessively over-designed compression members or excessively under-designed tension members are not required.

## 9.3 Critical Behaviour

Results demonstrating DLG critical behaviour are introduced and discussed. Failure mechanisms observed in the results of grid structure analysis are presented and provide a basis for the subsequent

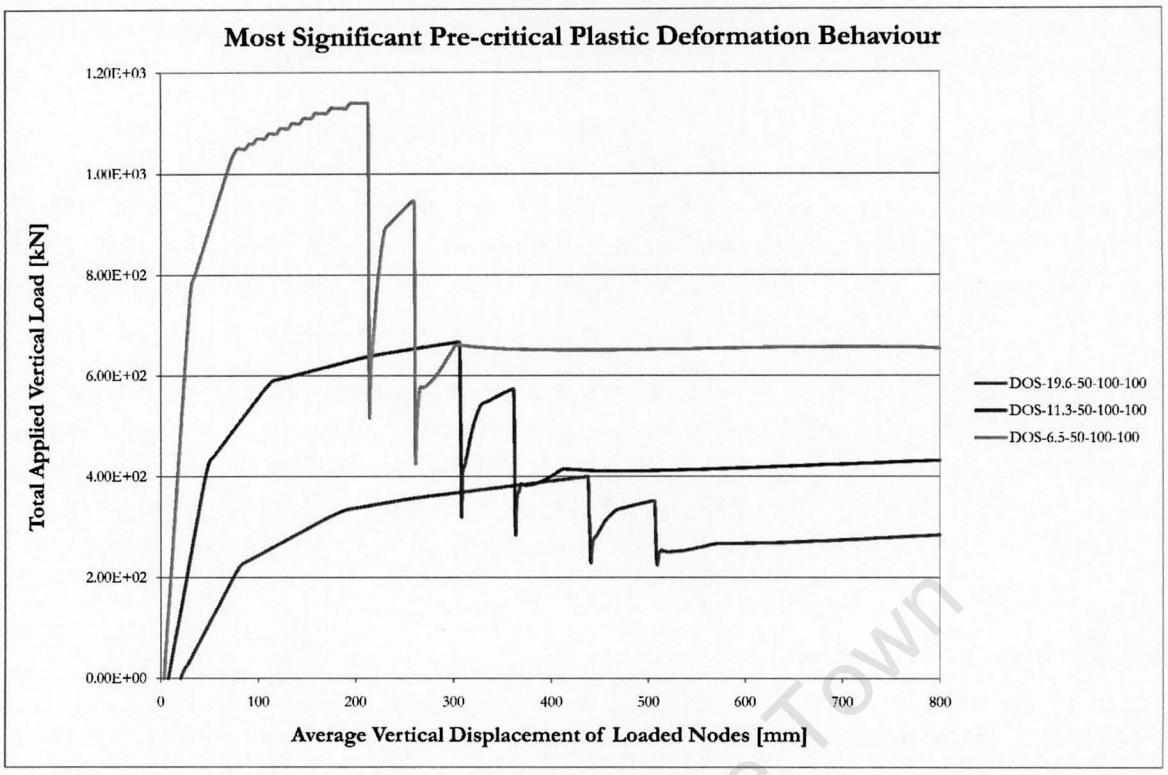


Figure 9.10: Load-displacement behaviour of DOS grids which were observed to have the highest values of plastic:elastic energy ratio. All grids shown have approximately equal values of plastic:elastic energy ratio; flexural plastic behaviour was not observed to be significantly affected by the Span:Depth parameter.

parameterized description of DLG critical behaviour.

### 9.3.1 Failure Mechanisms

Failure mechanisms of DLG structures, defined with respect to grid critical behaviour and observed in the results of the SOS and DOS grids analyzed, are introduced. Two distinct types of grid failure were observed: grid flexural and grid shear failure. Failure mechanisms were defined according to the grid global behaviour, analogous with plate behaviour, rather than the failure behaviour of individual members. The failure of individual members was through compression instability, or compressive or tensile yielding. Grid shear failure was generally observed to limit the structural resistance of DLGs, as the resulting failures were localized and did not allow for significant load redistribution or the full resistance associated with grid flexure to be developed.

#### 9.3.1.1 Grid Shear Failure

DLG shear failure refers to the failure of grid web members in compression, through buckling or yielding. Shear failure behaviour was observed where loads applied transverse to the grid (global shear loads) resulted in web member forces, located near to the supports, being higher than the chord member forces, resulting from grid global bending moments, relative to their respective member capacities. Generally as grid Span:Depth and Web:Top Chord Resistance parameters decreased, grid shear failure was observed to become more likely. The grids analyzed were designed so that the support web members would not fail throughout the post-buckling analysis. Consequently, where

grid shear failure occurred, this took place at the web members adjacent to the support web members (see Figures 9.11 and 9.12).

The shear failure behaviours of DLGs of SOS and DOS configuration were observed to be very similar. DOS grids were initially expected to be more susceptible to shear failure owing to: the reduced number of web members in DOS grids; and the reduced restraint applied to web members by chord members in DOS grids (bottom chord members in DOS grids are more slender than similar members in comparable SOS grids); however SOS grids were observed to fail more often in shear than DOS grids.

The increased flexural resistance of SOS grids was the reason that such structures were observed to be more likely to fail in shear than DOS grids. Increased flexural resistance of SOS grids resulted in increased grid shear loads, while yielding behaviour of DOS grids limited grid shear loads. Hence even though DOS grids had a less dense distribution of web members than SOS grids, DOS grids were not observed to be as susceptible to shear failure mechanisms as SOS grids.

#### 9.3.1.2 Grid Flexural Failure

DLG flexural failure refers to the failure of grid compression chord members, through buckling or yielding; such failure behaviour was observed where global bending moments resulted in chord member forces that were larger than support web member forces, resulting from applied shear loading, relative to individual member capacities. Consequently, as the grid Span:Depth parameter increased, and provided web members were sufficiently stocky, grid flexural failure dominated.

Initiation of flexural failure of DLG structures was consistent with the elastic distribution of member forces within the DLG structure. The flexural failure of the SOS grid configurations consequently initiated in the top chord members, located at the grid edge, midspan between adjacent supports, while the flexural failure of the DOS grid configurations initiated in the top chords, located at the grid centre, midspan between opposite supports (see Figures 9.13 and 9.14).

### 9.3.2 Means of Comparison

The ultimate resistance of various DLG structures was relatively easily compared through consideration of grid critical load. The degree of nonlinearity encountered prior to the critical load has previously been used to compare the nature of critical behaviour of such structures (see Section 9.2).

DLG critical load was defined as the first peak encountered in the load-displacement response of the collapse analysis of such structures. Similar logic was applied for the purposes of post-processing the numerical results. Plots of grid critical load were developed for each parameter so that the dependence of critical load could be established for each parameter considered and extended to account for parameter interaction.

### 9.3.3 Parameterized Behaviour

The critical behaviour of the SOS and DOS DLGs analyzed was investigated with respect to the parameterization of the structures considered, reference is made to plots of critical load as functions of Web:Top Chord Resistance and Span:Depth parameters as these parameter were observed to affect grid failure mechanism. Plots of grid critical resistance allow for general trends in grid behaviour

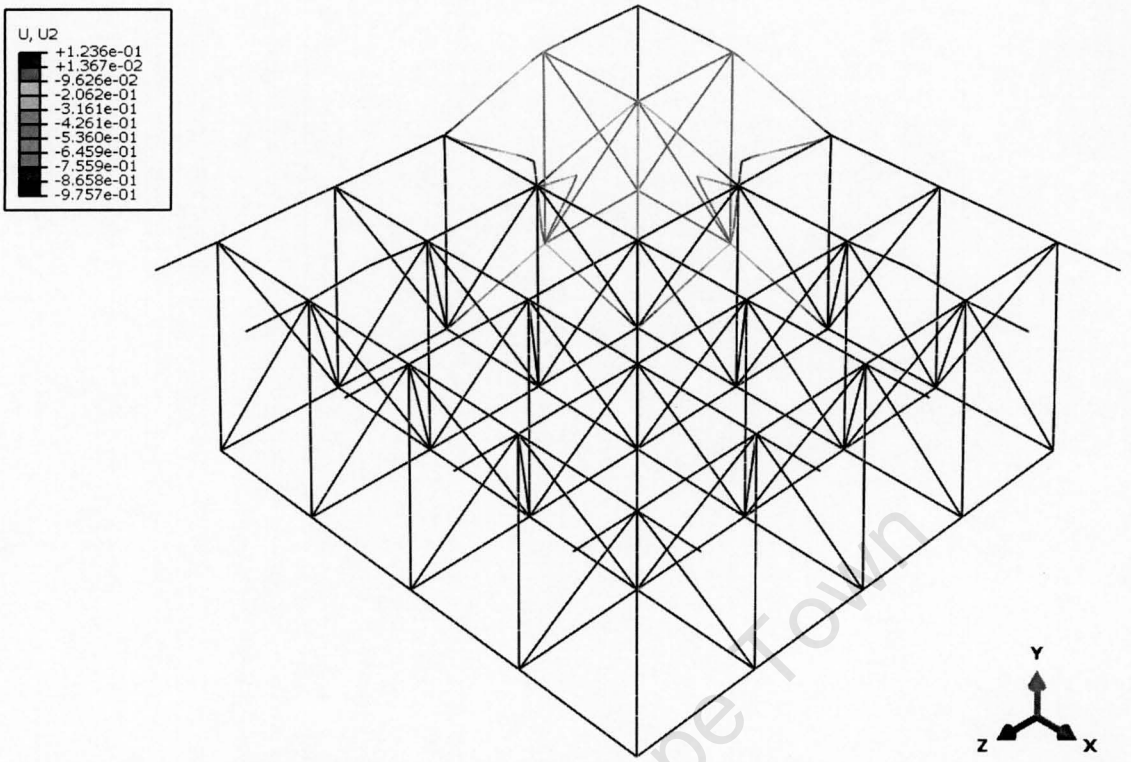


Figure 9.11: Vertical displacement (U2) field of SOS grid shear failure and collapse, grid $SOS - 6.5 - 66 - 50 - 66$ shown.



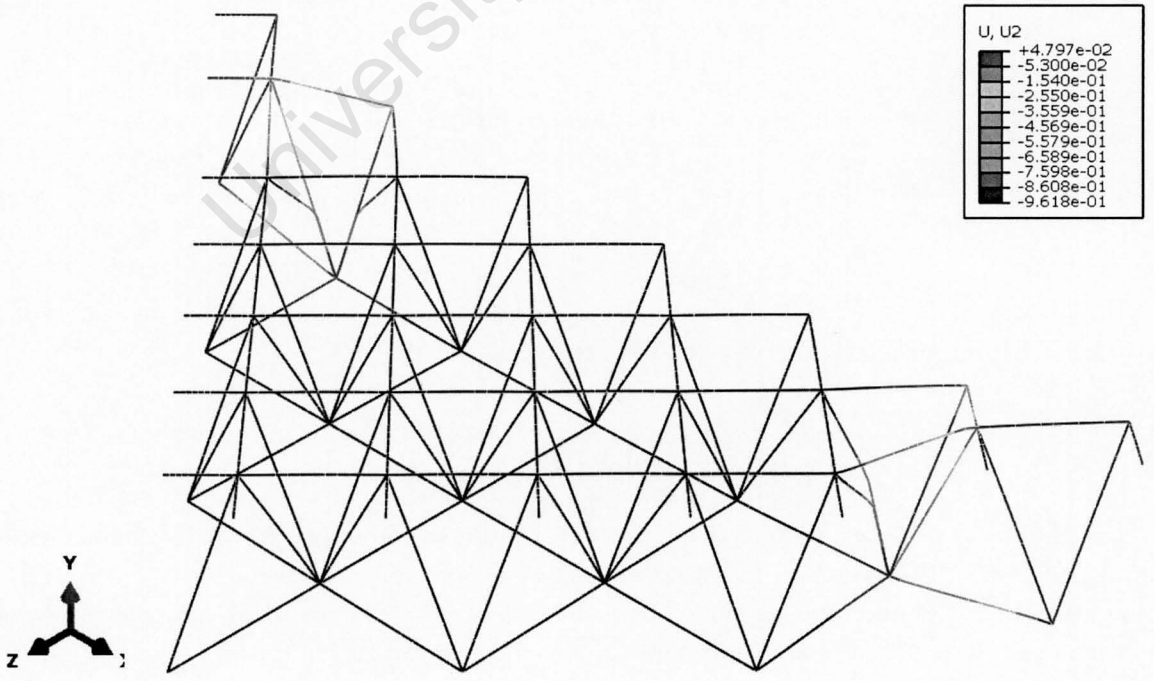


Figure 9.12: Vertical displacement (U2) field of DOS grid shear failure and collapse, grid $DOS - 11.3 - 40 - 100 - 66 - 0$ shown.

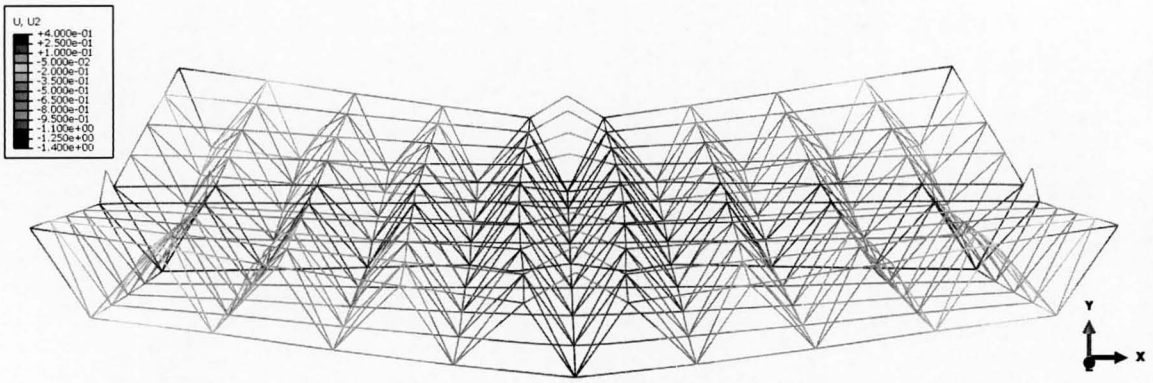


Figure 9.13: Vertical displacement (U2) field of SOS grid flexural failure, grid $SOS-11.3-100-66-66$ shown.

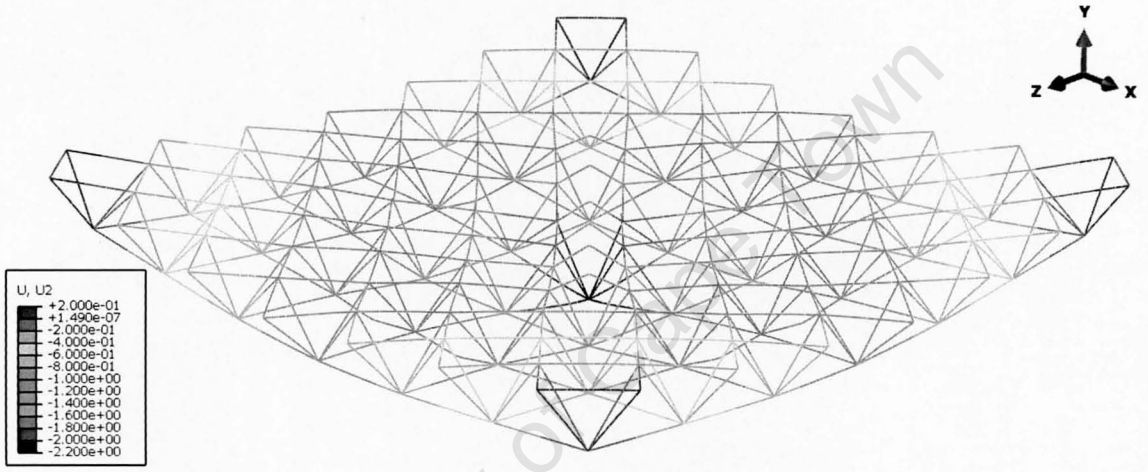


Figure 9.14: Vertical displacement (U2) field of DOS grid flexural failure, grid $DOS-11.3-100-66-66$ shown.

to be identified, these are included in Appendix A as Figures A.3 to A.10. Caution was however applied, in determining failure mechanisms from critical load plots as similar grids with negligible differences in critical load, were observed to have different failure mechanisms. Figure 9.15 provides a clear overview of SOS and DOS DLG critical behaviour.

#### 9.3.3.1 Effect of Web:Top Chord Resistance

The effect of the Web:Top Chord Resistance parameter on DLG critical load was due to its effect on web member axial resistance, and consequently the grid failure mechanism.

Figure 9.16 shows the relationship between the Web:Top Chord Resistance parameter, failure mechanism and critical DLG resistance for SOS and DOS configurations. Grid structures with a Web:Top Chord Resistance parameter values of 33% were observed to be most susceptible to shear failure. An increase in grid critical load was consequently observed between Web:Top Chord Resistance parameter values of 33% and 50%. The Web:Top Chord Resistance parameter was not observed to have a significant effect on grid critical behaviour for grid structures which failed in flexure.

In selected cases a nominal decrease in grid critical resistance was observed for increasing values of the Web:Top Chord Resistance parameter: this was attributed to the greater flexibility of such structure

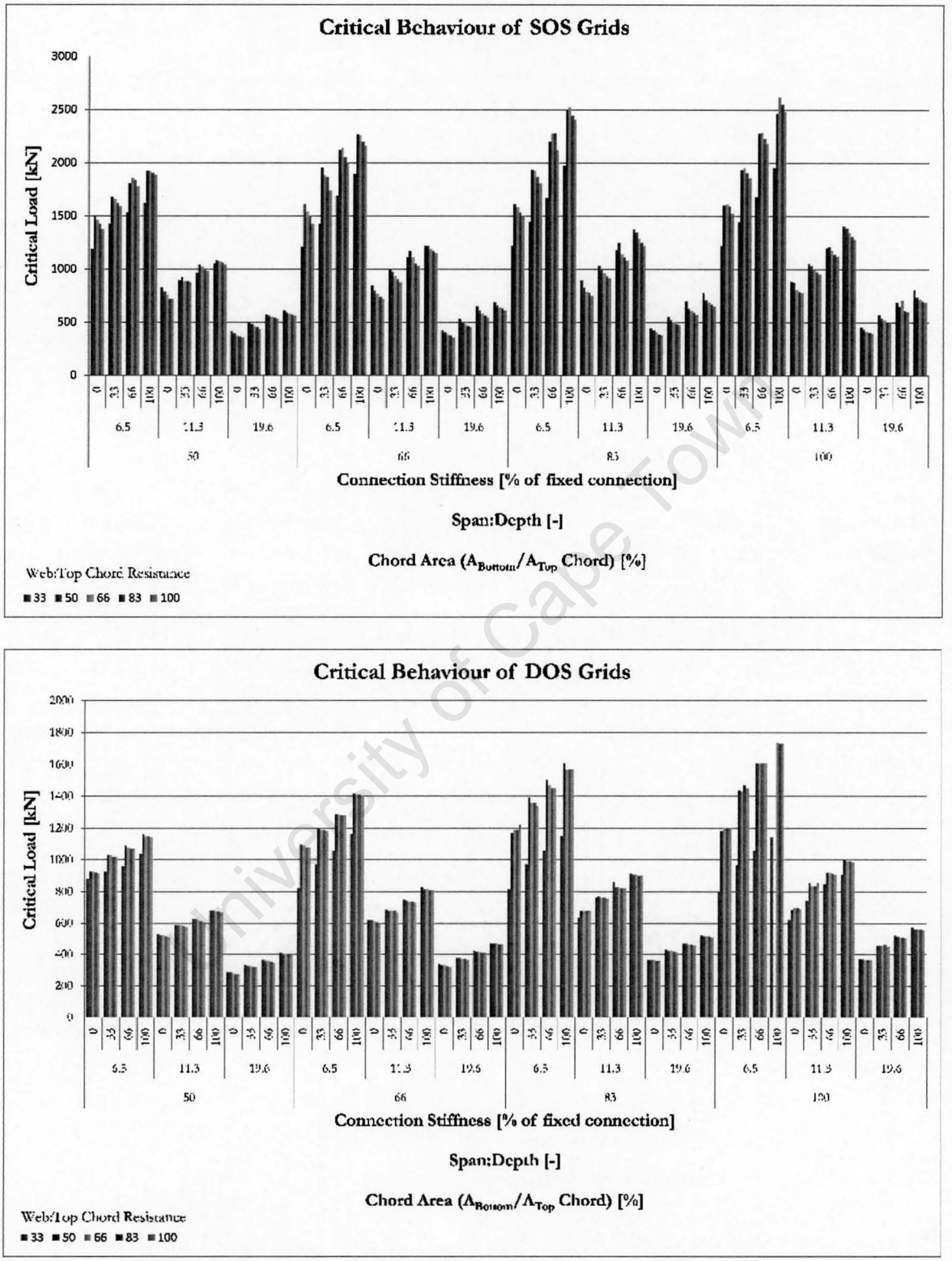




Figure 9.15: DLG critical load resistance dependence on grid parameterization considered. Increases in grid critical load observed for: increasing values of the Connection Stiffness and Chord Area parameters; and decreasing values of the Span:Depth parameter.

and the resulting potential for redistribution of load.

#### 9.3.3.2 Effect of Chord Area Ratio

The effect of the Chord Area Ratio parameter on the DLG critical load was due to its influence on grid bending stiffness, and initiation of grid yielding behaviour.

For both SOS and DOS grids a general linear increase in grid critical resistance was observed for increasing values of the Chord Area Ratio parameter, for grids which failed in flexure (see Figures A.5 and A.6). No increase in the grid critical load was observed between similar DLGs where slender web members were considered (low values of Web:Top Chord Resistance parameter); this was consistent with the shear failure of such grids.

The increase of grid critical resistance with increasing values of the Chord Area Ratio parameter was consistent with analytical approximations of grid stiffness.

#### 9.3.3.3 Effect of Span:Depth

The effect of the Span:Depth parameter on DLG critical resistance was due to its influence on the grid bending stiffness as the Span:Depth parameter defined grid depth (grid span was maintained constant).

A significant increase in grid critical resistance was observed with decreasing values of the Span:Depth parameter (see Figures 9.17, A.7 and A.8). This increase in DLG critical load resistance, with increasing grid depth, was in the form of a second-order polynomial consistent with the increase in stiffness prescribed by the parallel axis theorem (see Section 4.6). The critical load results of similar grids, plotted in series of increasing Span:Depth parameter values, were well banded; the reduction in grid resistance associated with shear failure is clearly visible for grids with a Span:Depth parameter value of 6.5 (see Figure 9.17).

Grid bending resistance was developed through a force couple in top and bottom chord members separated by the grid depth. As the grid depth increased, the force in top and bottom chords required to develop a given bending resistance decreased. Consequently, for the parameterized case considered, as grid depth increased, resistance to flexural failure increased, and resistance to shear failure remained constant (Ratio of web resistance to top chord resistance was maintained constant for varying grid depth). Consequently, grids of low Span:Depth parameter values were more susceptible to grid shear failure, in comparison with flexural failure, than equivalent grids of high Span:Depth parameter values.

#### 9.3.3.4 Effect of Connection Stiffness

The effect of the Connection Stiffness parameter on DLG critical load was due to its influence on member restraint, and consequently member capacity. As connection stiffness was defined as a function of individual member resistance, variation of the Connection Stiffness parameter was not observed to result in a change to grid failure mode.

A linear increase in DLG critical load resistance was observed with increasing values of the Connection Stiffness parameter, where grids failed in flexure (see Figures A.9 and A.10). This increase in grid critical load was due to the increased resistance to buckling of the top chord members with increasing

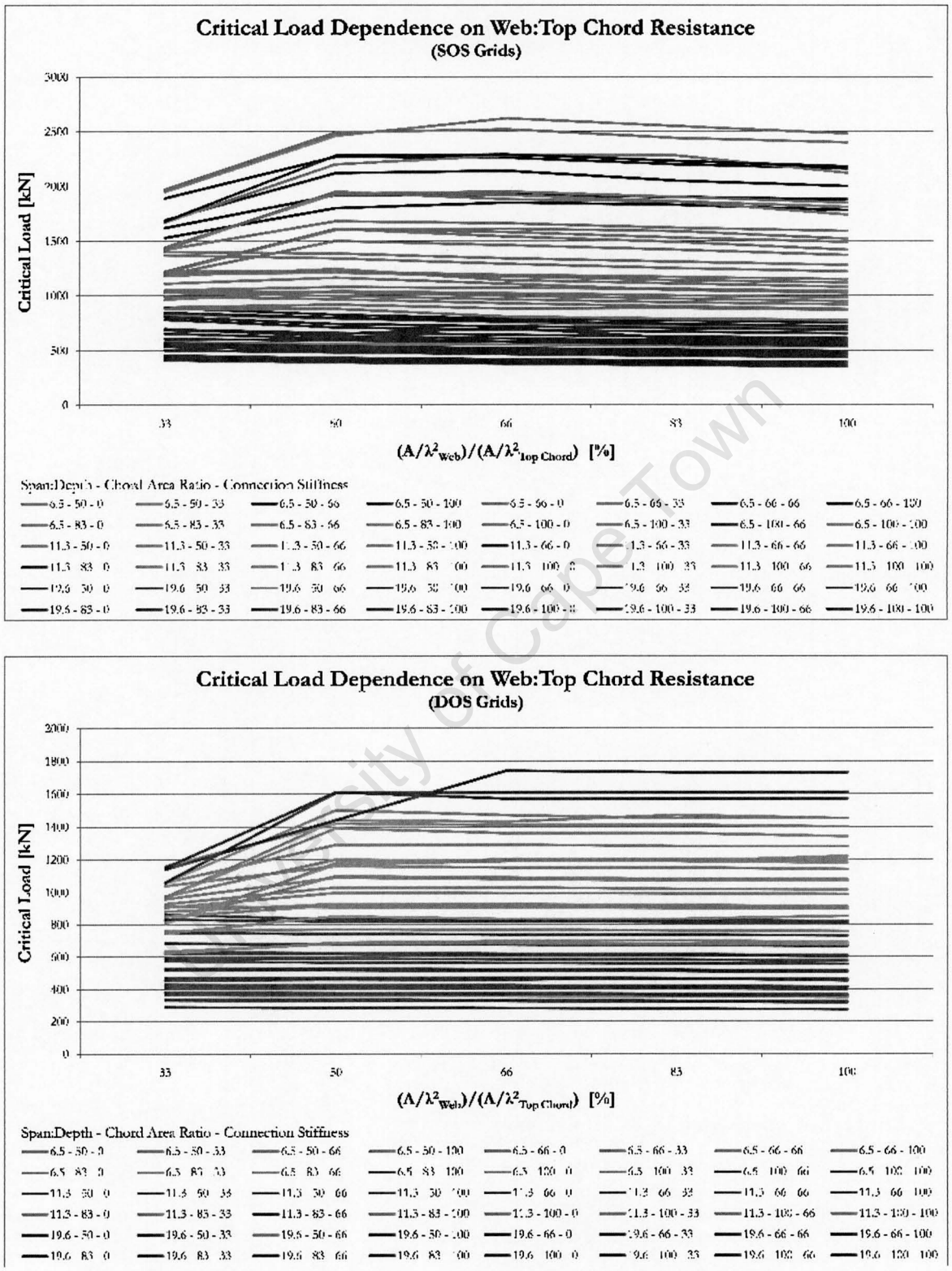


Figure 9.16: Critical load dependence on Web:Top Chord Resistance parameter. Decreases in grid resistance due to grid shear failure are evident for Web:Top Chord Resistance parameter values of 33% (green); and 33% and 50% (red).

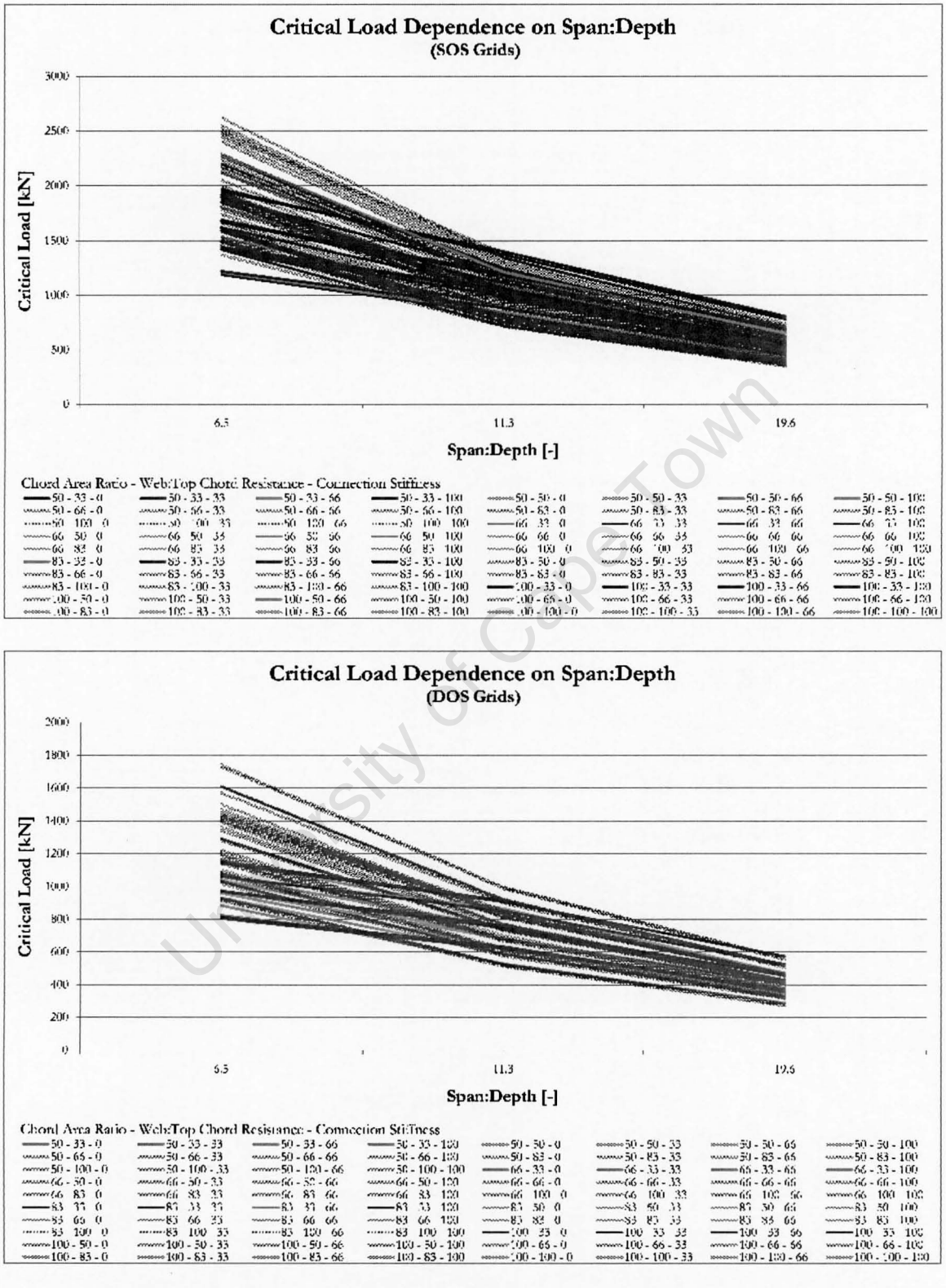


Figure 9.17: DLG critical load resistance dependence on Span:Depth parameter. Decreases in grid critical load due to shear failure are evident for Span:Depth parameter values of: 6.5 (orange); 6.5 and 11.3 (red); and 6.5, 11.3 and 19.6 (green).

rotational restraint. A linear increase in grid critical load was expected due to the way that grid connection resistance was defined, relative to individual member resistance, and the way in which appropriate values of the Connection Stiffness parameter were determined.

The critical load of grids which failed in shear was governed by the axial resistance of web members. Consequently, a linear relationship between grid critical resistance and the Connection Stiffness parameter was expected, where the same failure mechanism was encountered, and was observed in the results of collapse analyses.

### 9.3.4 Discussion

The critical behaviour of SOS and DOS grids was observed and identified. Results obtained for grid critical load were found to be significantly affected by the Span:Depth and Web:Top Chord Resistance parameters due to their effect on grid failure mechanism and Span:Depth, Chord Area and Connection Stiffness parameters due to their effect on member resistance and grid stiffness.

Web:Top Chord Resistance and Span:Depth parameters were observed to affect the ratio of web member load to web member resistance, while maintaining grid flexural resistance constant, and consequently affected the grid failure mechanism. Shear failure was observed to dominate for grids with slender web members (defined by Web:Top Chord resistance and Connection Stiffness parameters) and low values of the Span:Depth parameter. In all cases considered, grid critical load resistance resulted from compression failure of individual members through yielding or buckling, even where tensile chord yielding behaviour was initially observed.

The trends observed in grid critical load for the SOS and DOS grids failing in flexure were as predicted by elastic analytical behaviour, with the exception of the effect of the Web:Top Chord Resistance parameter which was not observed to affect grid critical resistance at all. SOS grids proved to be more susceptible to shear failure than DOS grids which was due to the greater shear loads achieved in SOS grids.

The variability observed in the pre-critical and critical behaviour results for the SOS and DOS grids considered highlights the importance of including material and geometric nonlinearity in the numerical analysis of grid structures. The importance of avoiding shear failure mechanisms in design is additionally evident in the significant reductions observed in grid critical load where web member resistance was reduced; and web member yielding did not take place.

## 9.4 Post-critical Behaviour

Results demonstrating the post-critical behaviour of the DLG structures considered are introduced and discussed. Post-critical behaviour was assessed both in terms of the residual strength of failed DLGs and the collapse behaviour of DLGs.

Post-critical structural capacity was dependent on the potential of a structure to redistribute load away from the damaged components of the structure. Post-critical behaviour was, consequently, observed to be dependent on the location of the initial failure, which was in turn dependent on the initial failure mechanism and the type of grid configuration (SOS or DOS). The identification of collapse mechanisms, observed in the results of the collapse analyses, serves as an introduction to the latter identification of trends in post-critical DLG resistance and collapse behaviour presented with respect to the structural parameterization considered.

### 9.4.1 Collapse Mechanisms

The post-critical behaviour of DLG structures was frequently observed to be consistent with initial flexural and shear failure mechanisms; however, significant interaction of compression chord, web member and bottom chord member failure in the post-critical regime was also observed. Comparison of load-displacement behaviour, deformed geometry, and stress distribution for the grids analyzed revealed these three distinct grid post-critical behaviours. Additional observations on post-critical behaviour were also made and are discussed.

The post-critical behaviour of grid structures was observed to be more varied than the critical behaviour of such structures. The variability of the post-critical behaviour of grid structures relates to the nature of incremental collapse with successive changes to grid stiffness and spanning directions and the resulting load redistribution.

#### 9.4.1.1 Shear Failure and Collapse

SOS and DOS grids with low Web:Top Chord Resistance and Span:Depth parameter values were predisposed to shear failure (see Section 9.3). Typical grid shear collapse behaviour was characterized by a sudden decrease in grid structural resistance as web members adjacent to the supports buckled (see load-displacement response for grid SOS-11.3-83-33-33 in Figure 9.18), although grid plastic behaviour was observed to precede shear failure in selected cases. The residual strength of grids having failed in shear was observed to be dependent on the buckled web member capacity, which was in turn dependent on the web slenderness ratio (captured by Web:Top Chord Resistance and Connection Stiffness parameters).

Owing to the location of shear failure initiation, adjacent to the supports in corner-supported DLGs, the post-critical behaviours of SOS and DOS grids which failed in shear were characterized by limited re-establishment of structural resistance or complete collapse due to the limited presence of alternate load paths.

For SOS grids, initial failure occurred in web members on the grid periphery orientated towards the adjacent corner and resulted in load redistribution to adjacent web members on the grid diagonal, the inverse was observed for DOS grids. Subsequent failure of web members was characterized by the re-establishment of structural resistance as the top and bottom chord members were observed to span across failed web members.

#### 9.4.1.2 Flexural Failure and Shear Collapse

The interaction of web member failure with initial flexural failure, in the post-critical regime of DLG structure behaviour, was attributed to load redistribution following initial top chord member failure. The failure of multiple non-critical web members associated with flexural failure-shear collapse interaction resulted in a more gradual decrease of grid load resistance when compared with flexural failure and collapse behaviour, as seen in the comparison of the load-displacement response of grids $SOS - 11.3 - 83 - 66 - 33$ and $SOS - 11.3 - 83 - 100 - 33$ in Figure 9.18 (see also Section 9.4.1.3). The flexural failure of SOS and DOS grids initiated at different locations; consequently, the nature of flexural failure and shear collapse behaviour of SOS and DOS grids were different.

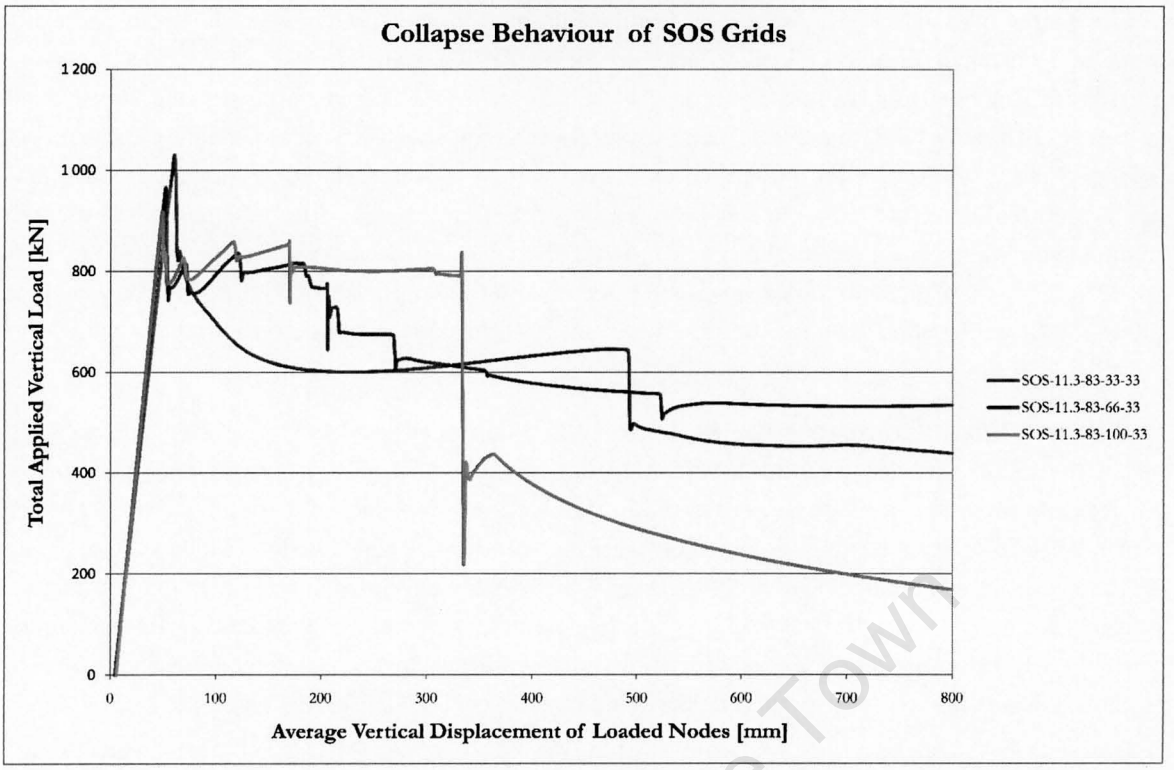


Figure 9.18: Load displacement behaviour of SOS grids with varying values of the Web:Top Chord Resistance parameter. Three distinct post-critical failure behaviours relating to shear failure and collapse ($SOS - 11.3 - 83 - 33 - 33$), flexural failure with post-critical shear failure interaction ($SOS - 11.3 - 83 - 66 - 33$) and flexural failure and collapse ($SOS - 11.3 - 83 - 100 - 33$) were observed.



**SOS grids** The failure of top chord members resulting from the flexural failure of SOS grids was observed to result in a change to the way SOS grids resisted applied load. Undamaged SOS grids spanned between adjacent corners, but once failure of the top chord members between adjacent chords initiated, SOS grids were observed to change span direction to between opposite corners. This load redistribution resulted in an increase to web member forces on the diagonal and consequently failure of these members initiated (see Figure 9.19). Global shear collapse in the post-critical regime, following initial flexural failure, was observed to be characterized by multiple successive web member failures resulting in a gradual decrease in grid load resistance.

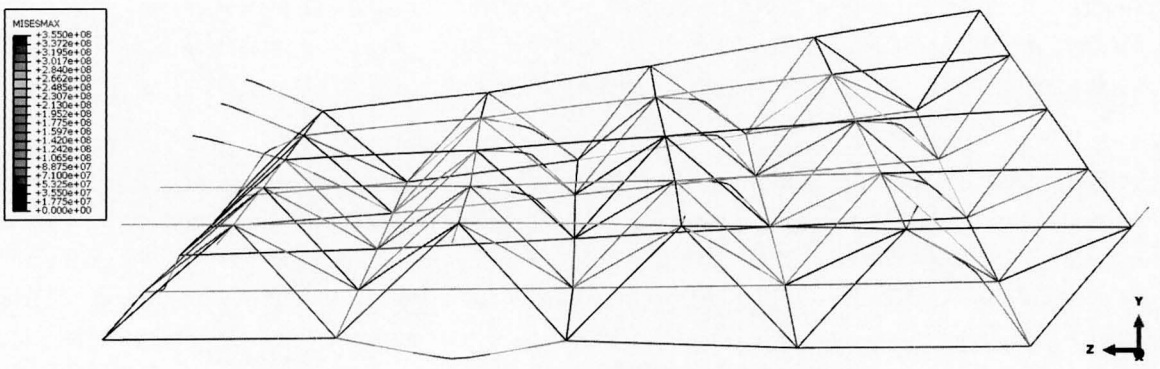


Figure 9.19: Initial flexural failure of SOS DLG followed by web member failure on grid diagonal associated with redistribution of load away from grid periphery.

**DOS grids** As with SOS grids, initial flexural failure of top compression chords at the grid centre resulted in a redistribution of load to adjacent members. In DOS grids, however, the failure line progressed diagonally outwards from the grid centre towards the grid corners. Once several sets of top chord members symmetrical about the grid centre failed, load was redistributed towards the grid periphery. Failure of the central compression members altered the load carrying behaviour of the structure; the structure no longer spanned between opposite supports but behaved as a corner supported-plate with a hole in the centre. The redistribution of load resulted in the most highly loaded members being located near midspan between adjacent supports. The redistribution of global shear forces resulted in successive failure of multiple web members at the grid periphery.

**Bottom Chord Compression Failure** Where initial flexural failure was encountered, the redistribution of load and structural stiffness in the grid post-critical regime caused the grid to span in alternate directions from those considered in the elastic regime. In such cases the parts of the grid which failed were supported and spanned between parts of the grid which had not failed. Consequently hogging moments at a global level were observed which resulted in bottom chord member compression and in selected cases the flexural buckling of the, generally more slender, bottom chord members (see Figure 9.20). Bottom chord failure was observed to result in further load redistribution, for SOS grids this was observed to prevent the development of flexural collapse, see Section 9.4.1.3.

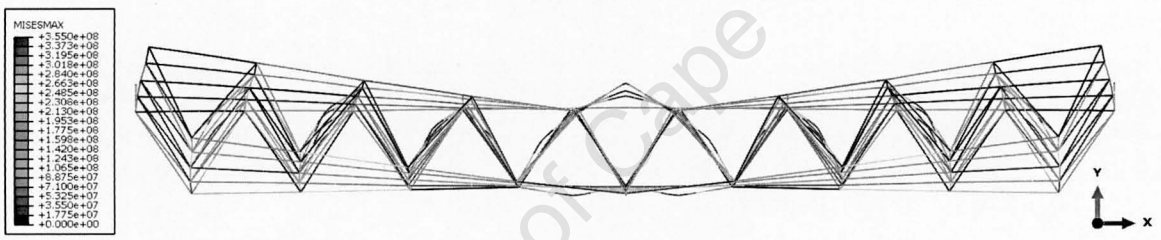


Figure 9.20: Bottom chord compression instability due to redistribution of load in DLG following initial flexural failure, grid $SOS-11.3-66-66-0$ shown

### 9.4.1.3 Flexural Failure and Collapse

Interaction between shear and flexural failure mechanisms was not observed in the post-critical behaviour of SOS grids with high values of Web:Top Chord Resistance, Connection Stiffness and Chord Area Ratio parameters. Post-critical behaviour of such grids was consequently characterized by the failure of multiple adjacent top chord members resulting in the development of a plastic hinge across the grid. Flexural collapse of DOS DLGs was not observed due to the effect of corner supports on the DOS grid displacement field. Flexural failure of DOS grids is said to represent a non-developable displacement field.

**SOS Grids** Once initial compression failure occurred, of the top chord members located at the midspan between adjacent supports, load was redistributed to adjacent chord members and the failure line progressed towards the grid centre. The progression of the failure front towards the grid centre resulted in the development of a plastic hinge across the structure about which further rotation occurred. The development of the plastic hinge across the structure divided the structure into four rigid panels, was characterized by large vertical displacements, and resulted in a sudden decrease in structural resistance being observed (see load-displacement response of grid $SOS-11.3-83-100-33$ in Figure 9.18). The residual resistance observed was consistent with the post-buckling residual resistance of the individual compression members spanning the yield lines. Bottom chord buckling

was observed to prevent flexural collapse as this resulted in load redistribution away from top chord members.

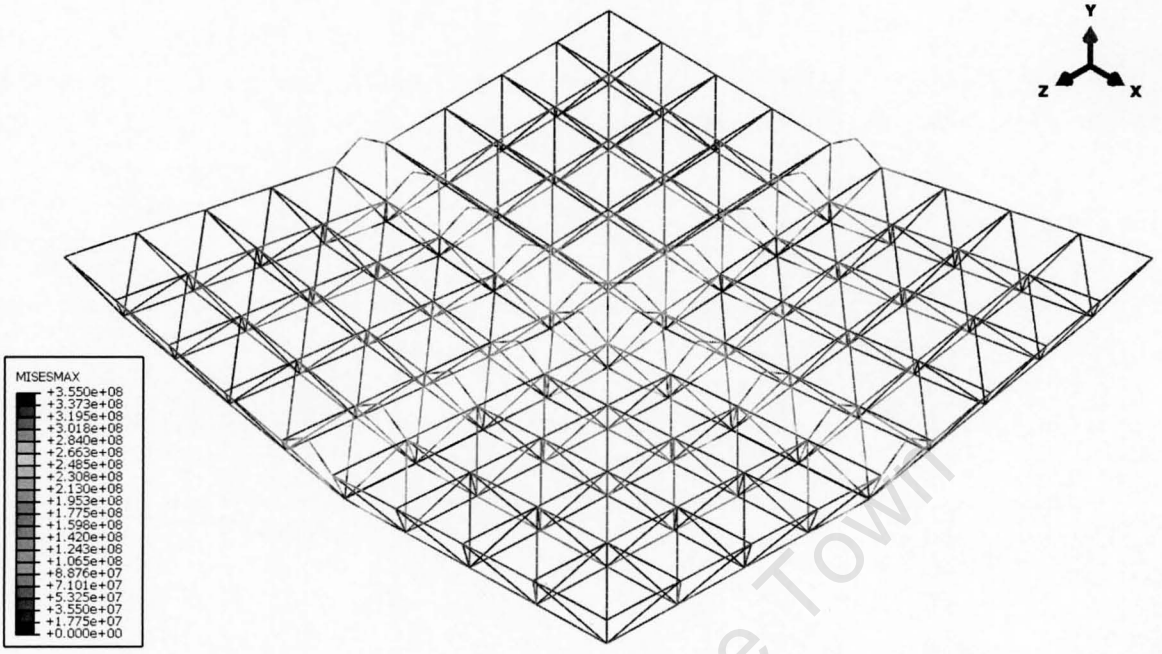


Figure 9.21: Flexural failure and collapse through development of yield line of failed top chord members, perpendicular to grid edges; DLG $SOS-11.3-100-83-66$ shown, with maximum von Mises stresses superimposed.



**DOS grids** The diagonal orientation of DOS DLG top chord members, combined with corner supports, prevented the development of a failure line of top chord members across DOS corner-supported grids; flexural collapse of DOS grids was consequently not observed.

DOS grids with high values of Web:Top Chord Resistance, Connection Stiffness and Chord Area Ratio parameters were characterized by load redistribution in top chords which was observed to result in the failure of multiple other top chord members, as web member failure was avoided. Flexure failure of multiple top chord members in DOS grids resulted in a more gradual decrease in grid load resistance than flexural failure and collapse of SOS grids.

### 9.4.2 Means of Comparison

The post-critical behaviour of DLG structures proved to be significantly more difficult to quantify than critical behaviour. Inspection of load-displacement responses and deformed geometry plots, of collapse behaviour, provided the greatest insight into individual grid behaviour and allowed for comparison between similar grids; however, these differences were not quantifiable. Post-processing of grid load-displacement results was undertaken to quantify grid collapse behaviour for the purposes of comparison. Comparison was undertaken with respect to grid post-critical resistance and post-critical behaviour. Post-critical load resistance was used to assess grid post-buckling residual strength while the ratio of post-buckling to critical resistance was used to assess collapse behaviour.

#### 9.4.2.1 Post-Critical Residual Strength

In order to quantify the residual strength of failed grid structures the concept of average post-critical resistance was considered.

The following logic was used to post-process grid load-displacement responses for the purpose of determining DLG average post-critical resistance:

- The grid critical load was identified by the onset of first softening behaviour;
- The applied displacement required to achieve the grid critical load was identified, and post-critical displacement calculated (800mm-critical displacement);
- The integral of the post-critical load-displacement curve was computed (post-critical energy)[3];
- The average post-critical grid resistance was calculated as the quotient of post-critical energy and post-critical displacement;

#### 9.4.2.2 Collapse Behaviour

For the purpose of quantifying the collapse behaviour of DLG structures, it was found that the ratio of the average post-critical load resistance to critical load resistance best captured the trends in post-buckling behaviour. Alternate methods of quantifying grid behaviour tended to include effects of grid stiffness and grid plasticity and were consequently not suitable for the comparison of post-critical behaviour. Average post-critical resistance and critical load values, as determined in Sections 9.4.2.1 and 9.3.2 respectively, were used for this purpose.

### 9.4.3 Parameterized Residual Strength Behaviour

The post-critical residual strength of the SOS and DOS grids analyzed is investigated. Reference is made to parameterized charts of average post-critical resistance for the purpose of demonstrating the distribution observed in post-critical grid resistance and identifying trends in such behaviour (see Figures A.11 to A.18). Post-critical behaviour was observed to be significantly less predictable than critical behaviour; this was attributed to the redistribution of load resulting from successive member failures. The effect of collapse mechanisms on grid post-critical residual strength is considered in greater detail in Section 9.4.4.

Post-critical residual strength of DLGs which failed in flexure was developed through the same mechanism as undamaged DLG resistance however was dependent on the residual axial resistance of buckled members. Span:Depth and Connection Stiffness parameters consequently had the greatest effect on DLG post-buckling load resistance; the top chord cross section was not changed in the parameter study.

[3]Where the load-displacement response was characterized by negative load values these were not included in the integral of the load-displacement curve. Negative load values in the load-displacement response of grid analysis indicate periods of momentary instability where a supporting force is required to achieve equilibrium in the structure

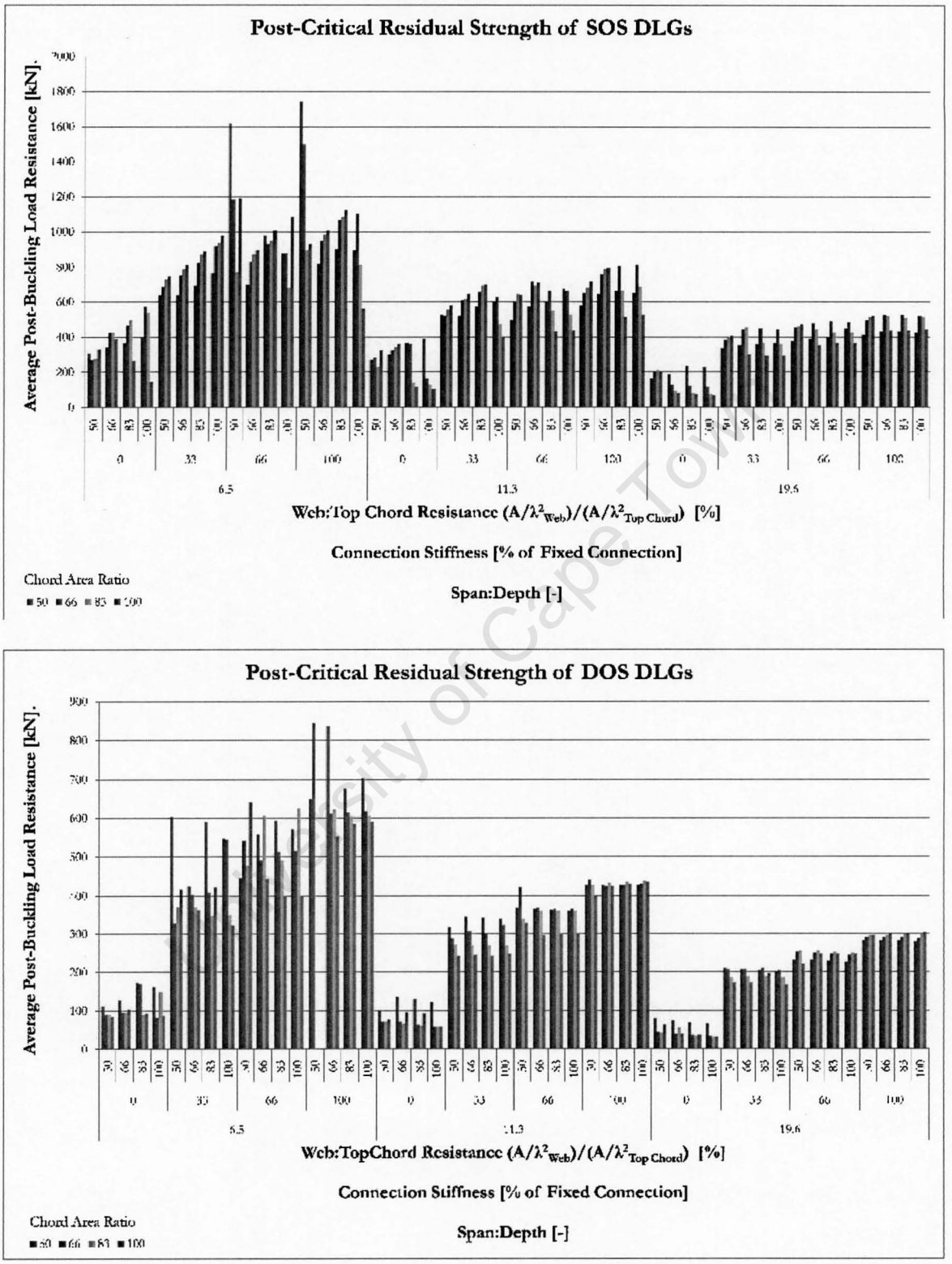


Figure 9.22: DLG post-critical load resistance dependence on grid parameterization considered. Increases in grid post-critical load resistance observed for increasing values of the Connection Stiffness parameter and decreasing values of the Span:Depth parameter.

#### 9.4.3.1 Effect of Web:Top Chord Resistance and Chord Area Ratio

A small increase in post-critical grid resistance was observed for increasing values of Web:Top Chord Resistance, this was due to the increased resistance to web failure in the post-buckling regime where web failure was observed to interact with initial flexural failure.

Where Web:Top Resistance and Chord Area Ratio parameters were observed to have a more significant affect on post-critical behaviour this was due to the development of the flexural collapse mechanism in SOS grids. High parameter values for Web:Top Chord Resistance and Chord Area Ratio resulted in flexural collapse as shear failure and bottom chord compression failure were consequently avoided. A decrease in average post-critical resistance was observed for grids which experienced flexural collapse, this is as flexural collapse resulted in significant decreases in grid resistance (see Figure 9.23).

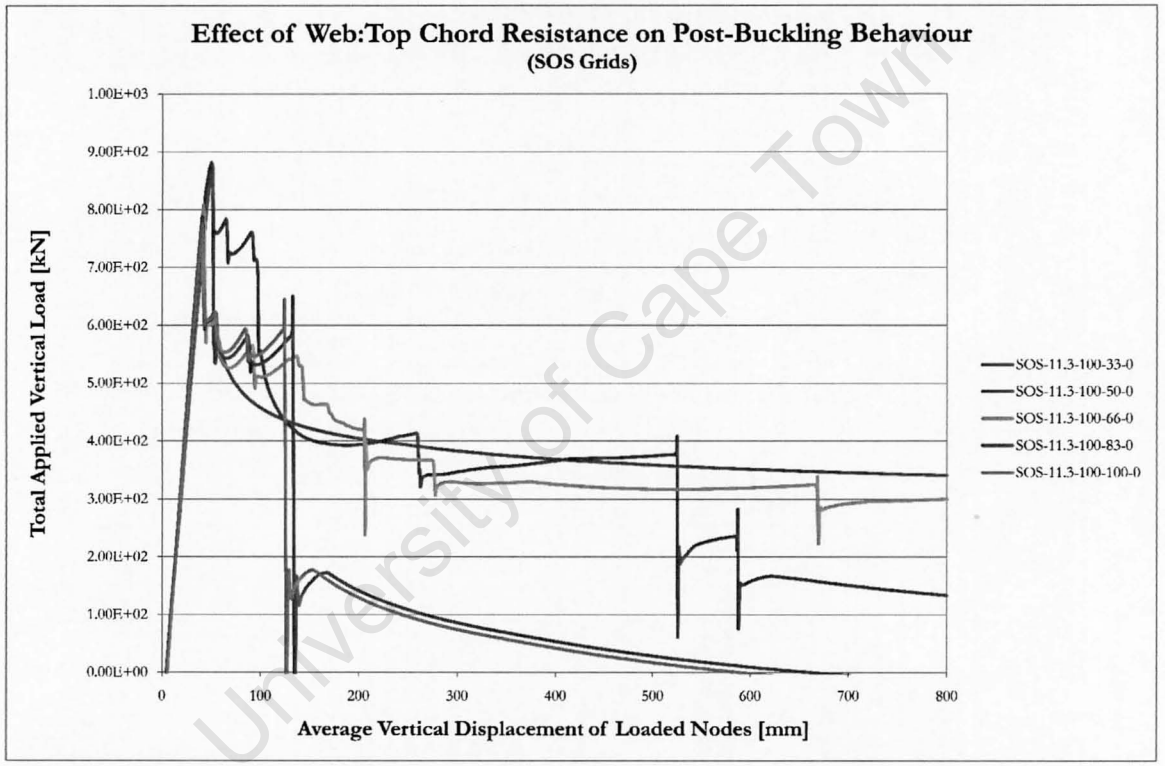




Figure 9.23: Sudden decreases in grid post-critical load resistance associated with flexural collapse of SOS grid configuration (grids $SOS-11.3-100-83-0$ and $SOS-11.3-100-100-0$) shown.

#### 9.4.3.2 Effect of Span:Depth

A near linear increase in grid post-critical residual strength was observed for increasing grid depth, i.e. decreasing values of Span:Depth parameter. This is attributed to the nature of grid flexural resistance which was developed as a force couple between top and bottom chords; as only the top chord resistance decreased following grid flexural failure the relationship between post-critical resistance and the Span:Depth parameter was not exponential, as for the case of critical resistance, but approached a linear relationship, see Figure 9.24. A similar relationship between Span:Depth and post-buckling resistance was observed for both SOS and DOS grids.

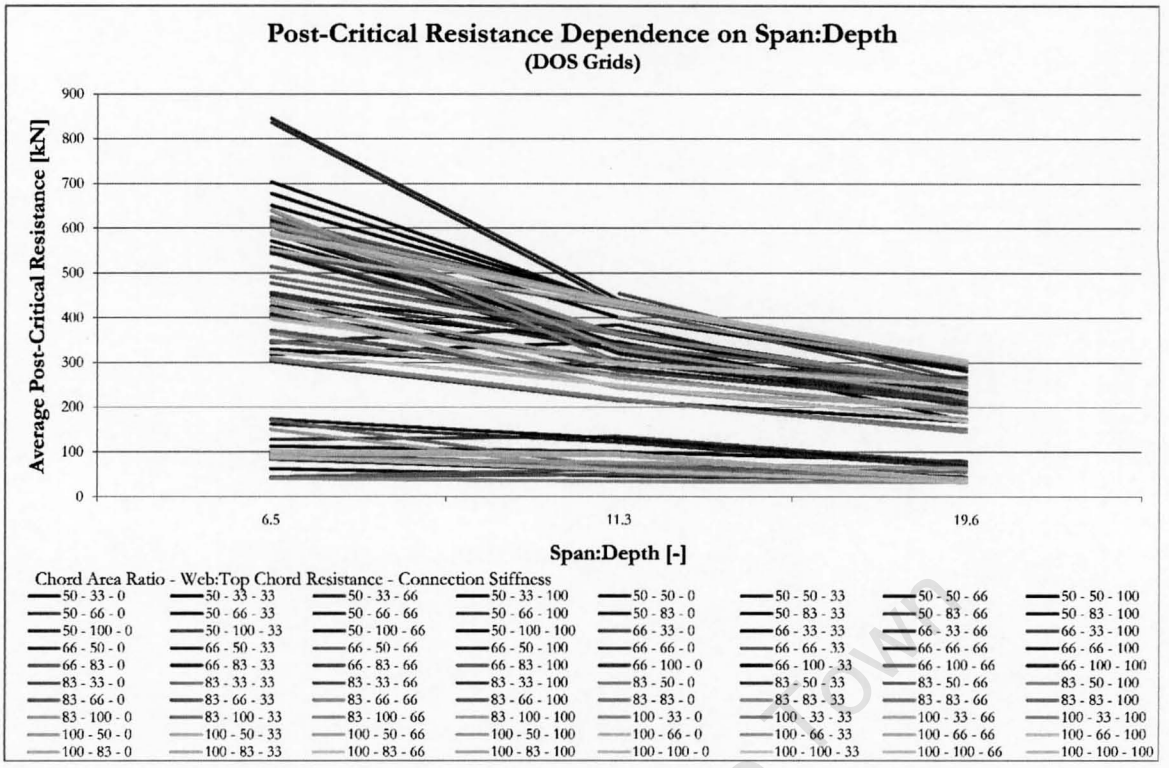


Figure 9.24: Average post-critical load resistance of DOS DLGs; an approximately linear decrease in grid average post-critical resistance was observed for increasing values of Span:Depth parameter.



#### 9.4.3.3 Effect of Connection Stiffness

A significant increase in grid post-critical residual strength was observed between Connection Stiffness parameter values of 0% and 33% while a linear increase in post-critical load resistance was observed for grids with Connection Stiffness parameter values of 33%-100%. These trends in post-critical residual strength were also evident in the load-displacement behaviour of DLGs; grids with connection stiffness parameter values of 33%, 66% and 100% tended to result in similar post-critical residual strengths while grids with pinned connections resulted in a reduced residual grid strength (see Figure 9.25). The reduced post-critical resistance of grids with a connection stiffness parameter value of 0% was attributed to the failure behaviour of top chord members in such cases. Grids with a connection stiffness parameter value of 0% represented the case of slender top chord members (i.e. failure occurred through buckling as opposed to yielding); consequently failure of grids with pinned connections occurred significantly more quickly. The linear increase in post-critical residual resistance of grids with Connection stiffness parameter values of 33%-100% was attributed to increased post-buckling resistance of individual top chord members.

#### 9.4.3.4 Effect of Geometric Configuration

DOS grids were observed to have a reduced post-critical load resistance in comparison with SOS grids. The lower post-critical resistance of DOS grids was attributed to the less dense distribution of bottom chord members in DOS grids and the associated reduction in grid stiffness. SOS grids were susceptible to significant reductions in post-critical load resistance for high values of Connection Stiffness, Web:Top Chord Resistance and Chord Area parameter values, this was attributed to the flexural collapse mechanism. Reductions in post-critical resistance were not observed for similar DOS

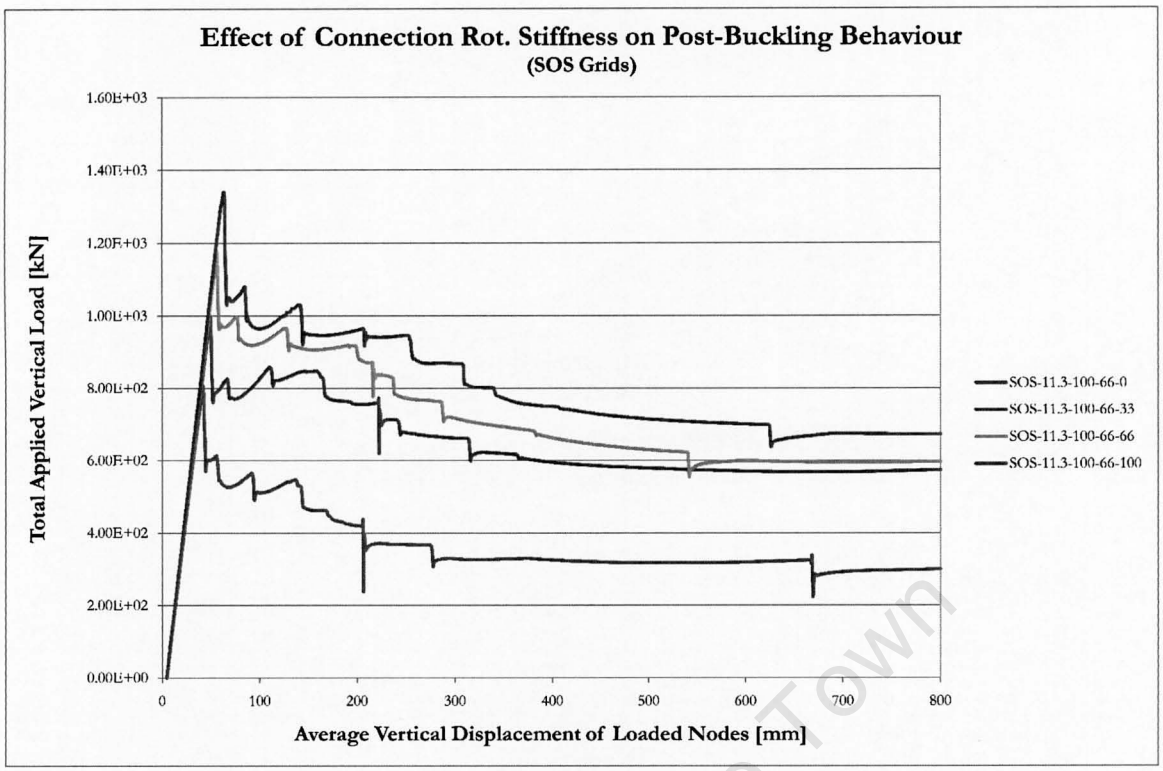


Figure 9.25: Post-critical behaviour of DLG grids approached a similar resistance for Connection Stiffness parameter values of 33%, 66% and 100%. Grids with pinned connections (Connection Stiffness parameter value 0%) showed a significant reduction in post-critical resistance when compared to similar grids with increased connection stiffness.

grids as the displacement field associated with flexural collapse in DOS grids was not developable, flexural collapse of DOS grids was impeded by the corner supports.

The average value of DLG average post-critical resistance for DOS grids was approximately 52% of the average post-critical resistance for SOS grids.

### 9.4.4 Parameterized Collapse Behaviour

Comparison is made between grid post-critical resistance and grid critical resistance in order to evaluate the nature of DLG collapse. Although only a limited number of grids demonstrated increased grid resistance after initial failure, see Section 9.4.4.7, the rate at which DLG post-critical resistance decreased is believed to be indicative of the collapse behaviour of grid structures. The ratio of average post-critical resistance to critical resistance was therefore considered. Reference is made to parameterized charts of average post-critical:critical resistance for the purpose of demonstrating the distribution observed in post-critical grid behaviour and identifying trends in such behaviour (see Figures A.19 to A.26). High values of post-critical:critical load resistance were observed to be indicative of more gradual collapse behaviour, and were consequently preferred due to structural safety considerations.

Web:Top Chord Resistance and Chord Area Ratio parameters were not observed to have a major effect on grid post-critical behaviour except where combinations of these parameters resulted in the flexural collapse of SOS grids; the effect of flexural collapse was consequently considered independently. Variation in collapse behaviour resulted either directly from the variation of structural and

geometric parameters or indirectly due to a change in failure mechanism. Grids which failed in shear and grids which experienced flexural collapse were observed to have low values of post-critical:critical load resistance when compared to similar grids which experienced flexural failure and post-critical shear collapse interaction.

#### 9.4.4.1 Effect of Web:Top Chord Resistance

SOS and DOS grid post-critical behaviour was observed to respond similarly to variation of the Web:Top Chord Resistance parameter, except for the cases of grid flexural collapse. Web:Top Chord Resistance was observed to influence post-critical behaviour most significantly through its affect on collapse mechanism.

SOS and DOS DLGs with a Web:Top Chord Resistance parameter value of 33% and a Span:Depth parameter value of 19.6, were observed to be the DLGs most susceptible to shear failure (see Section 9.3.3.1). A sudden decrease in post-critical load resistance was observed for grids which failed in shear; post-critical behaviour following shear failure was not observed to be significantly affected by pre-critical yielding behaviour.

A small variation of post-critical:critical load resistance was observed for variation of Web:Top Chord Resistance. As post-buckling behaviour of DLGs which initially failed in flexure was characterized by successive web member failure, grids with increasing values of the Web:Top Chord Resistance parameter were observed to collapse in a more gradual manner; provided flexural collapse did not result from increase web resistance.

Where the post-critical:critical load resistance was observed to vary most significantly for SOS grids failed in flexure, this was due to the development of the flexural collapse mechanism; see Section 9.4.4.3.

#### 9.4.4.2 Effect of Chord Area Ratio

Collapse behaviour was not observed to be significantly affected by the Chord Area Ratio parameter; this can be seen in the tightly banded nature of the load-displacement behaviour, in post-critical regime, of similar grids with varying Chord Area Ratio parameter values (see Figure 9.7). A general decrease in post-critical:critical load resistance was observed for increasing values of the Chord Area Ratio parameter, for both SOS and DOS grids; this was attributed to the accompanying increase in grid critical resistance. DLG collapse behaviour can therefore be described as occurring more suddenly for increasing values of the Chord Area Ratio parameter.

Where the post-critical:critical load resistance was observed to vary significantly for SOS grids with the Chord Area Ratio parameter this was due to the development of the flexural collapse mechanism; see Section 9.4.4.3.

#### 9.4.4.3 Effect of Web and Bottom Chord Resistance on Flexural Collapse

The flexural collapse mechanism was characterized by a significant reduction in post-critical resistance. Grids with Web:Top Chord resistance values of 83% and 100% and Chord Area Ratio parameter values of 83% and 100% were the grids most likely to collapse in flexure due to their avoidance of web failure and bottom chord buckling in the post-critical regime respectively.

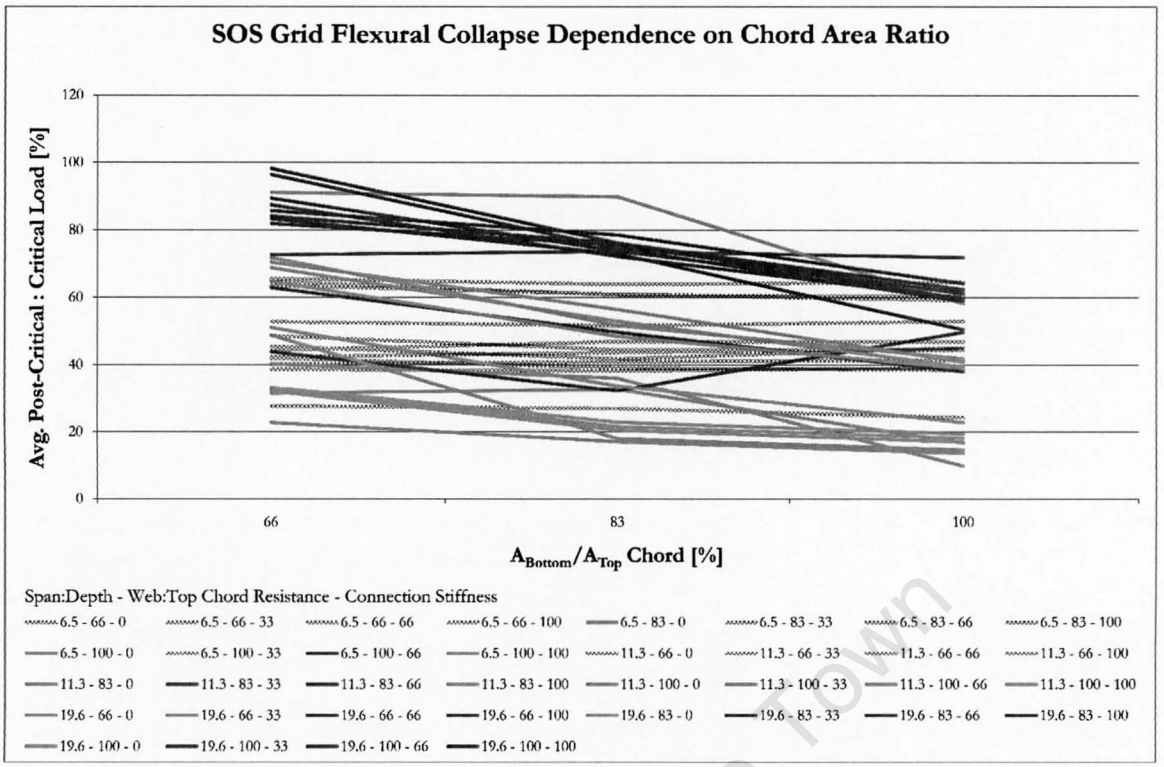


Figure 9.26: Flexural collapse behaviour dependence on Chord Area Ratio parameter for SOS DLGs. Flexural collapse was observed for DLGs with Chord Area Ratio parameter values of: 100% (Orange); 100% and 83% (Red); 100%, 83% and 66% (Green); 83% (Purple) and; 66% (Pink).

SOS DLGs with lower values of the Chord Area Ratio parameter were observed to be subject to bottom chord compression instability following load redistribution in collapsing grid structures and consequently did not result in flexural collapse. Compression failure of bottom chord members resulted in further redistribution of load which halted further top chord failures and the development of grid plastic hinges associated with grid flexural collapse.

Grids which collapsed in flexure were characterized by a significant decrease in grid post-critical:critical load resistance relative to similar grids which failed in flexure and experienced post-critical shear failure interaction. Flexural collapse of DLG structures should consequently be avoided. Figure 9.26 demonstrates the relationship between flexural collapse and post critical:critical grid resistance as a function of the Chord Area Ratio parameter; a step in the curve of post-critical:critical resistance is observed where flexural collapse is observed with increasing values of the Chord Area parameter.

#### 9.4.4.4 Effect of Span:Depth

The effect of the Span:Depth parameter on grid collapse behaviour was attributed to its influence on the ratio of elastic grid stiffness and grid post-critical stiffness.

A near linear reduction in grid post-buckling resistance was observed for increasing values of the Span:Depth parameter while an exponential decrease in grid resistance was observed for increasing values of the Span:Depth parameter. The post-critical:critical load resistance description of grid post-critical behaviour was consequently observed to increase significantly for increasing values of the Span:Depth parameter (see Figure 9.28). This increase in the grid post-critical:critical load resistance parameter is indicative of the more sudden failure behaviour of grids with low values of

the Span:Depth parameter.

#### 9.4.4.5 Effect of Connection Stiffness

Connection Stiffness affected grid post-critical behaviour through its influence on individual member critical and post-buckling behaviour.

A significant increase in post-critical load resistance was observed between Connection Stiffness parameter values of 0% and 33% (see Figure A.25 (SOS grids) and A.26 (DOS grids)) which was not consistent with grid behaviour for Connection Stiffness parameter values of 33%-100%. This change in post-critical behaviour was not a result of failure mechanism but was due to the failure behaviour of the slender top chord members.

As both critical and post-critical resistances were observed to increase with an increase of the connection stiffness parameter the post-critical:critical load resistance description of grid post-critical behaviour was observed to be approximately linear for Connection Stiffness parameter values between 33% and 100%. Comparison of critical and post-critical behaviour of grids with pinned connections demonstrated a significant reduction for both values when compared with similar grids of increasing connection stiffness. The low values of post-critical:critical load resistance for grids with a Connection Stiffness parameter of 0% indicates that grids with slender top chord members are significantly more susceptible to sudden collapse than grids with stocky top chord members. A general improvement in grid failure behaviour was observed for increasing values of connection stiffness.

#### 9.4.4.6 Effect of Geometric Configuration

The ratio of Post-critical to Critical Load Resistance was generally lower for DOS grids than for SOS grids. The critical load which DOS grids were able to support was in many cases limited by yielding of bottom chord members however the flexural failure of top chord members in DOS grids resulted in more significant decreases in post-critical load resistance, see Figure 9.29.

Although the post-critical resistance of SOS grids was in many cases reduced due to the development of grid plastic hinges associated with flexural collapse, the average value of post-critical:critical load resistance observed for SOS grids was higher than for DOS grids; 52.6% and 38% respectively. SOS grids can therefore be considered to demonstrate better post-critical behaviour than similar DOS grids, provided flexural collapse mechanisms are avoided.

#### 9.4.4.7 Increases above Critical Structural Resistance

Post-critical increases in structural resistance were observed in selected instances for the case of SOS grids with a Span:Depth parameter value of 19.6; no significant increases to DOS grid post-critical resistance were identified. Post-critical increases in structural resistance represent the case of improved structural safety as collapse does not automatically follow initial failure but requires a further increase in load above the grid ultimate resistance.

For the case of SOS grids, increases in structural resistance above the critical grid resistance were observed for selected grids which failed and collapsed in flexure (see Figure 9.30). The increase in post-critical resistance above the critical resistance however was due to flexural failure interaction with bottom chord instability. For grids of increasing depth, bottom chord buckling prevented the

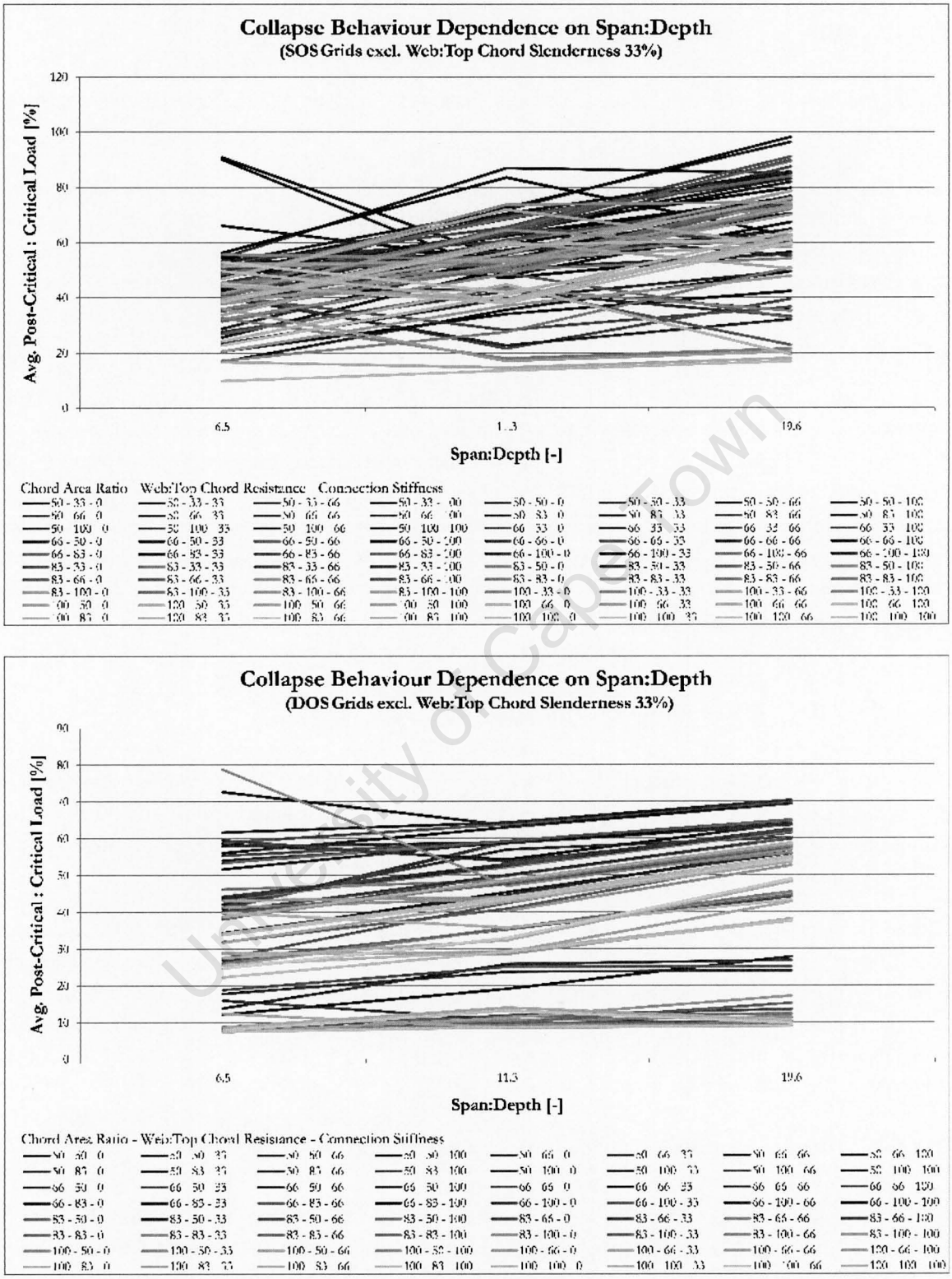


Figure 9.27: Effect of the Span:Depth parameter on DLG collapse behaviour. Increasingly gradual collapse behaviour was observed for increasing values of Span:Depth parameter for both SOS and DOS grid configurations. Variation of grid collapse behaviour with Span:Depth parameter is due to nature of post-buckling residual strength mechanism.

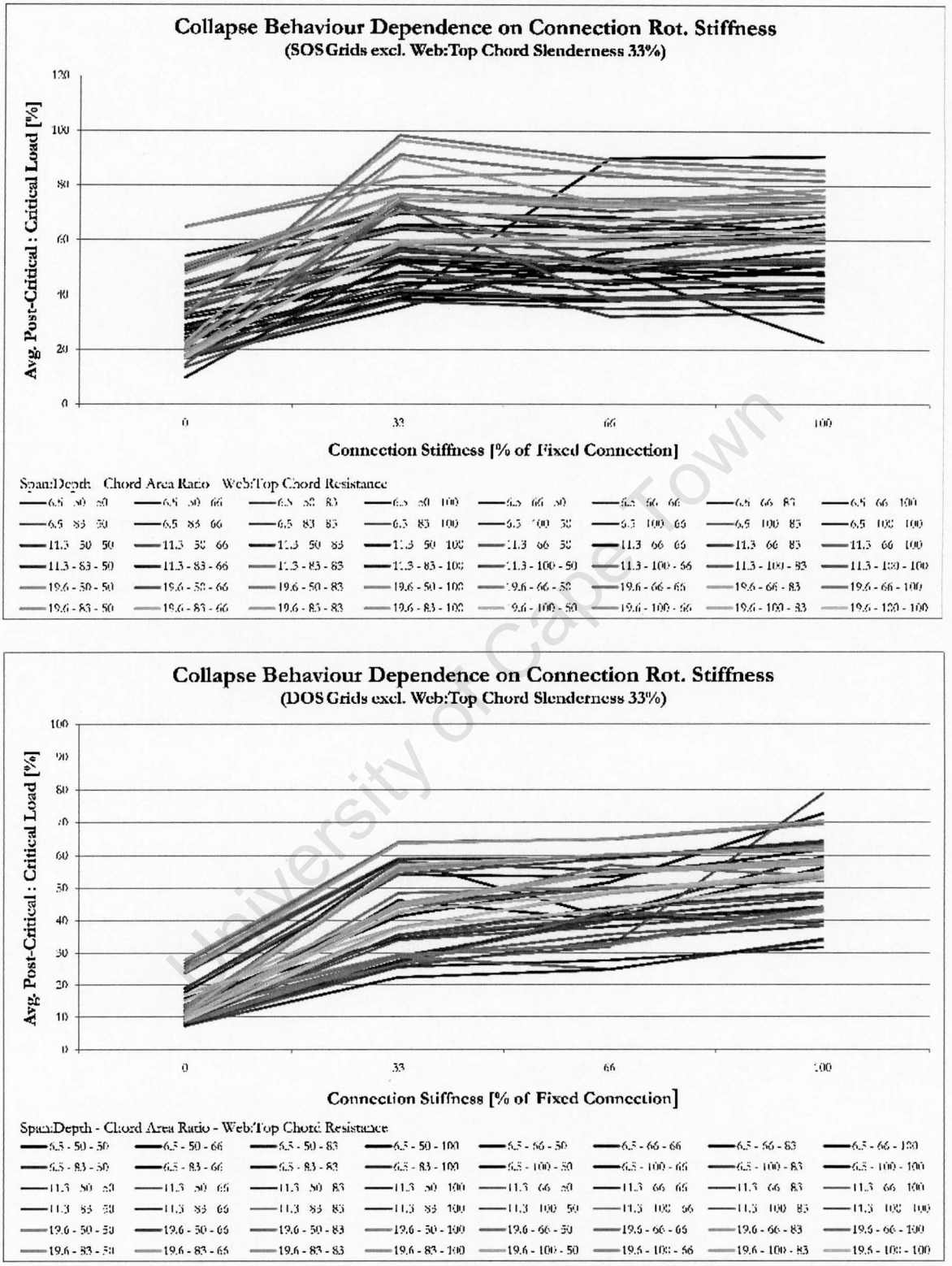


Figure 9.28: Effect of the Connection Stiffness parameter on DLG collapse behaviour; collapse of DLGs with slender top chord members (Connection Stiffness parameter value of 0%) was observed to be sudden, represented by a low value of post-critical:critical load resistance, in comparison with grids with stocky top chord members.

Consideration of a non-symmetric failure resulted in a significant decrease in grid critical load, although this value was similar to the yield load for the case of symmetrical grid failure. The applicability of Design codes for assessing grid resistance should not be assessed on this isolated case; further investigation is consequently required.

## 9.6 Summary of DLG Behaviour

The effects of the structural and geometric parameters, considered in the presented study of DLG collapse behaviour, are summarized for pre-critical, critical and post-critical regimes of grid behaviour.

#### 9.6.0.1 Web:Top Chord Resistance

The Web:Top Chord Resistance parameter was not observed to affect DLG flexural stiffness and consequently did not affect grid elastic behaviour. The Web:Top Chord Resistance parameter was observed to influence the degree of plasticity behaviour resulting from tensile chord yielding experienced prior to the onset of critical behaviour through its affect on grid stability under plastic deformation. The Web:Top Chord Resistance parameter was, however, observed to have a significant effect on grid failure mechanisms. DLGs with low values of the Web:Top Chord Resistance parameters were susceptible to shear failure and were also observed to result in web member yielding behaviour. The Web:Top Chord Resistance parameter was observed to only have a slight influence on post-critical grid behaviour; this was due to its effect on shear failure interaction with initial flexural failure.

#### 9.6.0.2 Chord Area Ratio

An increase of the Chord Area Ratio parameter was accompanied by an increase in grid stiffness for both SOS and DOS grids. For SOS and DOS grids failing in flexure a linear increase in critical load was observed for increasing values of the Chord Area Ratio parameter. The Chord Area Ratio parameter was not observed to affect resistance to shear failure. The Chord Area Ratio parameter was observed to have the greatest affect on grid plastic behaviour defining the initiation of tensile chord member yielding while the degree of grid plastic deformation was observed to be inversely proportional to the Chord Area Ratio parameter. The Chord Area Ratio parameter was not observed to have a significant effect on post-critical behaviour except for its influence on the development of the flexural collapse mechanism in SOS grids. More sudden collapse behaviour was observed for increasing values of the Chord Area Ratio parameter due to the accompanying increase in DLG critical load.

#### 9.6.0.3 Span:Depth

The Span:Depth parameter was observed to have a significant effect on grid elastic stiffness and consequently grid critical load, where failure occurred in flexure. The Span:Depth parameter was observed to influence grid failure mechanism; grids with decreasing values of the Span:Depth parameter were observed to be more susceptible to shear failure. Increased probability of shear failure resulted from the increasing flexural resistance of DLGs and decreased component of global shear load for decreasing values of Span:Depth. An exponential decrease in grid critical resistance was observed for increasing values of the Span:Depth parameter, while an approximately linear decrease in DLG post-critical

resistance was observed for increasing values of the Span:Depth parameter. DLG collapse behaviour was consequently observed to become increasingly sudden for decreasing values of the Span:Depth parameter.

#### 9.6.0.4 Connection Stiffness

A small increase in grid elastic stiffness was observed for increasing Connection Stiffness parameter values for SOS and DOS grids while a linear increase in grid critical load was observed for increasing values of Connection Stiffness, this was consistent with the definition of the Connection Stiffness parameter adopted. A linear increase in post-critical grid resistance was observed for Connection Stiffness parameter values of 33%-100%. A significant reduction in post-critical grid resistance and post-critical:critical load resistance, representative of sudden post-critical collapse behaviour, was observed for a Connection Stiffness parameter value of 0%; this was consistent with the resulting slender description of Top Chord members in such cases.

## 9.7 Comments

DOS DLG pre-critical behaviour, for DLGs with low values of the Chord Area Ratio parameter, represents a significant improvement over similar SOS DLG behaviour due to the plastic deformation behaviour resulting from bottom chord yielding. DOS DLG critical behaviour was additionally observed to be less susceptible to shear failure than SOS DLGs. Post-critical behaviour of SOS grids was however, observed to be less sudden than DOS grids and SOS grids were generally observed to have a higher post-critical residual strength than DOS grids, for the case of initial flexural failure and post-critical shear failure interaction. Consequently DOS grids can generally be said to have demonstrated the preferred DLG pre-critical behaviour while SOS grids demonstrated the preferred post-critical behaviour.

As the most significant concern regarding the behaviour of DLG structures related to the propensity of DLGs to fail without warning it is argued that the DOS grid configuration is preferential to the SOS configuration for application to corner supported DLGs.

# References

G. A. R. Parke. *The Behaviour of Space Trusses Incorporating Novel Compression Members.* PhD thesis, University of Surrey, 1988.

# Chapter 10

# Conclusion and Recommendations

Concluding remarks on the collapse behaviour of DLG structures are provided; this is accompanied by a summary of trends observed in DLG behaviour. Recommendations for the design and analysis of DLG structures are presented and areas for future research are highlighted.



## 10.1 Conclusion

Nonlinear analysis of DLG structures, to determine the complete failure behaviour of such structures, was successfully undertaken by applying initial imperfections at a member level and implementing displacement control. A method of applying distributed loading to DLG structures under displacement control was developed and implemented. SOS and DOS DLG structures were parameterized and their behaviour investigated.

The behaviour of DOS DLG configurations, with low bottom:top chord area ratios, was shown to exhibit significant stable, nonlinear, pre-critical behaviour resulting from the yielding of bottom chord members. The yielding behaviour observed for DOS structures was believed to be equally effective as the use of 'soft' chord members or 'over designed' top chord members, employed by other researchers, in improving pre-critical and critical behaviour. The less dense distribution of bottom chord members in the DOS configuration is an effective and simple means of introducing pre-critical yielding behaviour in DLG structures which provides warning of structural damage prior to structural collapse. The DOS DLG configuration, and potentially other DLG configurations, with less dense bottom chord arrangements, therefore represent attractive structural configurations for design purposes, provided dominant loading is applied in one direction only.

Connection stiffness and Span:Depth parameters were observed to have the greatest effect on DLG post-critical behaviour. A general improvement in post-critical behaviour, characterized by the retention of structural load-carrying resistance, was observed for increasing connection stiffness and increasing Span:Depth parameters.

The failure of the DLG structures considered was observed to be followed by increased post-critical resistance in only a few instances and a trend in such behaviour was not established. Although exceeding the critical load of all the other structures considered results in collapse, the post-critical behaviour observed is indicative of the nature of collapse.

SOS grids were observed to demonstrate the preferred post-critical behaviour; however, DOS grids

were observed to demonstrate the preferred DLG pre-critical behaviour. The most significant concern regarding the behaviour of DLG structures has been their propensity to fail without warning. DOS grids, consequently, represent the most suitable DLG configuration considered for corner supported DLG structures.

The results presented in this study are for the case of symmetric failure. In 'real' DLG structures symmetrical failure is not observed due to the sensitivity of such structures to imperfections. The results presented, therefore, provide a means of evaluating the effects of the identified structural and geometric parameters on an idealized failure; idealized failure and collapse behaviour of DLG structures is, however, believed to be indicative of the behaviour of similar 'real' structures.

### 10.1.1 Trends in DLG Behaviour

DLG behaviour resulting from the collapse analyses was divided into three regimes for the purpose of comparison: pre-critical behaviour, comprising linear elastic and plastic behaviour; critical behaviour; and post-critical behaviour. Critical and post-critical behaviour was observed to vary as a result of failure mechanism, collapse mechanism and as a direct result of the variation of structural and geometric parameters.

#### 10.1.1.1 Pre-critical Behaviour

Pre-critical behaviour was dominated by plastic yielding behaviour of DOS DLG configurations. Significant plastic deformation of SOS grids was not observed; this was attributed to the denser layout of bottom chord members in SOS grids relative to DOS grids.

DLG pre-critical behaviour, observed in the results of DLG collapse analysis, was summarized as follows:

- DOS grids were less stiff than comparable SOS grids.
- Grid stiffness increased with the Connection Stiffness and Chord Area Ratio parameters.
- Grid stiffness decreased with the Span:Depth parameter.
- Web members did not affect grid flexural stiffness.
- DOS grid configurations allowed for the development of significant nonlinear behaviour prior to the onset of grid failure.
- Initiation of grid plastic deformation was inversely proportional to the Chord Area Ratio parameter.
- Stability of DLG plastic deformation was dependent on the avoidance of shear and flexure failure mechanisms, plastic deformation consequently increased with Connection Stiffness and Web:Top Chord Resistance parameters.

#### 10.1.1.2 Critical Behaviour

Critical behaviour of DLG structures was observed to be dependent on shear and flexural failure mechanisms which were in turn dependent on Web:Top Chord Resistance and Span:Depth parameters.

DLG critical resistance was observed to be further dependent on Chord Area Ratio and Connection Stiffness parameters.

DLG critical behaviour, observed in the results of DLG collapse analysis, was summarized as follows:

- Shear failure of DLGs resulted in significant reductions to structural efficiency in comparison to similar grids which failed in flexure.
- Shear failure was observed to be dependent on Web:Top Chord Resistance, Connection Stiffness and Span:Depth parameters.
- SOS grids were observed to be more susceptible to shear failure than DOS grids.
- Web:Top Chord Resistance and Connection Stiffness parameters were observed to have the most significant effect on critical load for DLGs which failed in shear.
- Chord Area Ratio, Span:Depth and Connection Stiffness parameters were observed to have the most significant effect on critical load for DLGs which failed in flexure.

#### 10.1.1.3 Post-critical Behaviour

The collapse of grid structures was frequently observed to be consistent with the initial failure mechanism, although significant interaction of web, top and bottom chord member failure was also observed. Three principle collapse behaviours were identified: shear collapse, flexural collapse and flexural failure with post-critical shear collapse interaction. Post-critical behaviour was assessed in terms of post-critical load resistance and the ratio of post-critical:crtical resistance.

DLG post-critical behaviour, observed in the results of DLG collapse analysis, was summarized as follows:

- Shear collapse of DLGs was characterized by only nominal post-critical residual strength.
- Increased grid Connection Stiffness resulted in improved post-critical resistance.
- Reductions in grid Span:Depth resulted in more rapid decreases in grid post-critical resistance.
- Slender Top Chord members resulted in sudden collapse with only nominal post-critical load resistance.
- DOS grids were generally observed to collapse more quickly than similar SOS grids.
- Flexural collapse of SOS grids resulted in significant, sudden decreases in grid post-critical resistance;
- The displacement field associated with flexural collapse of DOS grids was not developable.
- Initiation of flexural collapse was dependent on Web:Top Chord Resistance and Chord Area Ratio parameters.
- Flexural failure and post-critical shear collapse interaction was generally characterized by a gradual decrease in load resistance.

## 10.2 Recommendations

Common combinations of structural and geometric parameters which should be incorporated in the design of DLG structures, to provide warning of grid failure, are discussed as well as appropriate methods of numerical analysis.

### 10.2.1 Grid Design

#### 10.2.1.1 Grid Configuration

Grid configuration and the relative orientation of DLG structures are generally selected to conform to support conditions, aesthetic and cost considerations. As DLG structures with low ratios of bottom:top chord area have been shown to demonstrate warning of structural damage prior to failure, it is recommended that only DLG configurations with reduced bottom:top chord area ratios be employed in practical applications; a bottom:top chord area ratio of 50% was generally observed to result in sufficient DLG yielding behaviour. Where predominant loading is not applied in one direction only, yielding behaviour of DLG structures will not be achievable and consequently it is not anticipated that DLG structures will represent the safest and most cost effective structural solution.

#### 10.2.1.2 Connection Stiffness

A general improvement in post-critical behaviour was observed for increasing connection stiffness. Selection of node connection type, which is generally undertaken on the basis of cost, aesthetics and ease of construction, should consequently be extended to account for collapse behaviour. Serious consideration should be paid to the use of semi-rigid or rigid node connectors. To take account of the maximuim DLG post-critical residual resistance, connection resistance should be designed to be compatible with the section resistance and not only the specified connection design resistance.

#### 10.2.1.3 Span:Depth

A general improvement in post-critical behaviour was observed for increasing values of the ratio of grid span:depth. In evaluating the most economical grid depth, collapse behaviour should be considered and grids with low values of the ratio of span:depth be avoided.

#### 10.2.1.4 Post-critical Behaviour

The design of DLG structures should avoid global shear failure. DLG shear failure results from the failure of web members adjacent to supports and is characterized by a sudden decrease in DLG load resistance. Resistance of web members adjacent to supports should be greater than that determined by elastic analysis; this is to ensure that DLG shear failure does not initiate in the post-critical regime.

Combinations of stocky web and bottom chord members should be avoided for corner supported SOS grids due to the resulting potential for flexural collapse behaviour. Flexural collapse behaviour is characterized by the development of a plastic hinge across the horizontal extent of the DLG and results in sudden failure with no residual load capacity.

Slender top chord members should be avoided. DLG structures with slender top chord members were observed to collapse suddenly.

Initial flexural failure followed by interaction with web member failure, displaced from support regions, was observed to result in the most gradual decrease in DLG load resistance; such a collapse mechanism is consequently preferred as the failure is characterized by multiple non-critical member failures. This type of failure is governed principally by the ratio of top chord:web resistance.

### 10.2.2 Grid Analysis

The analysis of grid structures in the elastic regime can accurately be undertaken with elastic analysis methods provided the grid geometry is kinematically stable and compression member instability is not encountered. Elastic analysis should therefore be accompanied by concurrent linear buckling analysis to ensure buckling and kinematic instability are effectively restrained. Consideration of a kinematically unstable pin-connected, simply supported, DOS grid, without edge beams, can be undertaken to determine if the elastic buckling analysis is correctly identifying kinematic instability.

Nonlinear analysis of grid structures to determine pre-critical yielding and critical behaviour of such structures can be undertaken by applying initial imperfections; EC3 (2005) provides guidance on imperfection magnitudes to be applied in nonlinear analysis. Progression of nonlinear analysis can be undertaken with load or displacement control as both methods predict critical behaviour accurately. Load control consequently represents the preferred method for design applications as nonlinear plastic and critical behaviour can be resolved for various loading arrangements, when using the Riks algorithm for example. Post-critical behaviour can only be adequately captured through displacement controlled analysis; however, such analysis methods are limited in the load distributions which can be accounted for.

The design of DLG structures should consequently be undertaken with elastic design methods in accordance with relevant structural design codes. As it is not clear if the level of safety associated with DLG structures is consistent with conventional steel building structures, the elastic design of a DLG structure should be accompanied by material and geometric nonlinear analysis; this is so that the critical load and plastic behaviour of the structure can be identified and compared with the required resistance to ensure that an appropriate level of safety against failure is achieved. Inherent grid imperfection should additionally be accounted for in the nonlinear analysis by guiding the structure towards a 'worst case' non-symmetrical failure path, either through application of non-symmetrical loading or the reduction of a single member capacity.

## 10.3 Further Research

Subject areas which demonstrated potential for future investigation, as identified in the current research, include: grid initial imperfections and their distribution throughout DLG structures; behaviour of DLGs of geometries other than SOS and DOS configurations; safety of grid structures designed in accordance with building design codes; and improvements to grid failure and collapse behaviour through use of composite structural resistance and grid configurations with low bottom:top chord area ratios.

### 10.3.1 Initial Imperfections and Distribution

Half-sine wave imperfections applied in the vertical plane have been shown to accurately describe the symmetric collapse behaviour of grid structures. This was undertaken by validating numerical model results with the experimental results of Collins (1981). The SOS grids constructed and tested by Collins (1981) were fabricated to stringent tolerances; consequently, a near symmetric failure pattern was achieved. DLG structures assembled to normal construction tolerance however are susceptible to non-symmetric failure paths. Previous studies into un-symmetric collapse, such as the investigation of Schmidt et al. (1976), initiated unsymmetrical failure by reducing the resistance of one of the critical members thus replicating the lower bound of grid resistance.

Further study of the effect of initial imperfections, and their distribution in DLG structures, on grid behaviour should be undertaken to provide greater understanding of methods for incorporating grid imperfection in DLG numerical analysis.

### 10.3.2 Alternate Grid Geometries

DOS grid configurations have been shown to demonstrate significant pre-critical nonlinear behaviour prior to collapse. The nonlinear behaviour of DOS grids is attributed to their low bottom:top chord area ratio. Other grid geometries such as SOLS, SOLSD, SOD (with bottom chord arrangements less dense than top chords), should therefore also be investigated as it is likely that such arrangements will also exhibit significant yielding behaviour prior to collapse.

The failure behaviour of grids with triangular base geometries have also not been extensively considered. Investigation of the failure behaviour of such structures may reveal significant advantages in their post-critical behaviour due to the three-way spanning nature of such configurations, provided appropriate boundary supports are applied.

### 10.3.3 Design Code Safety of DLGs

Further study is required to assess if DLG structures designed in accordance with structural design codes achieve the same level of safety required for typical steel building structures. If DLG structures do not achieve comparable levels of safety, the investigation of 'special rules' required to rectify these shortcomings should be considered.

### 10.3.4 Composite DLGs

The development of composite action between concrete slab and steel DLG appears to be the most promising means of improving grid behaviour identified in the literature. Investigation of the collapse behaviour of such structures, under uniformly distributed loading using displacement control, can be compared with the results of numerical analyses presented in this research to provide an indication of the viability of such structures. The investigation of the effect of composite action on grid behaviour should also include the effect of propped construction methods which have not previously been established for DLG structures.

# References

Ian Martin Collins. *Collapse Analysis of Double-Layer Grids.* PhD thesis, University of Surrey, 1981.

A.I. El-Sheikh and R.E. McConnel. Experimental Study of Behavior of Composite Space Trusses. *Journal of Structural Engineering*, 119:747–766, 1993.

J. R. Mwakali. *The Collapse Behaviour of Double-Layer Space Trusses Incorporating Eccentrically Loaded Tee-Section Members.* PhD thesis, University of Surrey, 1990.

G. A. R. Parke. *The Behaviour of Space Trusses Incorporating Novel Compression Members.* PhD thesis, University of Surrey, 1988.

Toshitsugu Saka and Yoshiya Taniguchi. Buckling Behavior of Square-and-Diagonal Double-Layer Grid. *Journal of Structural Engineering*, 120(4):1088–1102, April 1994.

L. C. Schmidt, P. R. Morgan, and J. A. Clarkson. Space Trusses with Brittle-Type Strut Buckling. *Journal of the Structural Division, Proceeding of the American Society of Civil Engineers*, 102: 1479–1492, 1976.

L.C. Schmidt, P. R. Morgan, and A. Hanaor. Ultimate Load Testing of Space Trusses. *Journal of the Structural Division, Proceeding of the American Society of Civil Engineers*, 108:1325–1335, 1982.

# Appendix A

# Result Graphs

## A.1 Plasticity Graphs

## A.2 Critical Load Graphs

## A.3 Residual Strength Graphs

## A.4 Collapse Behaviour Graphs

# Appendix B

# Abaqus Input Scripts

The Abaqus input script used for collapse analysis of a DLG of SOS configuration under uniformaly distributed load is presented. Due to the length of code required for each script only one script is presented, other scripts used in the research presented are to be found on the accompanying CD.



## B.1 SOS, UDL

ABAQUS input script for collapse analysis of SOS DLG, 5x5 module, under UDL:

```
#SOS, 5x5, UDL

from abaqus import *
import testUtils
testUtils.setBackwardCompatibility()
from abaqusConstants import *
myModel = mdb.Model(name='5x5')

#Model Parameters

a=0.36
b=0.36
theta=45
theta_r=theta*2*pi/360
depth=tan(theta_r)*(sqrt(a**2+b**2))/2
phi_r=atan(b/a)
phi=phi_r*360/(2*pi)
m=5
n=5
rigid=0.0                    #for display only
meshsize=(a-2*rigid)/12
element=B33
imperfection=0.004           #Eurocode 3, Clause 5.3.2, Table 5.1
yields=340*1E+6              #S355 Steel
YoungsMod=204775000000.0     #Eurocode 3, Clause 3.2.6
Loadplane=0.5*depth
rot_k=0


# MEMBER SECTION SIZES (OD and wall thickness for CHS)

# Top Chords
```

```
TC_diam=0.009525
TC_thick=0.00081

#Web Members
W_diam=0.009525
W_thick=0.00081
SW_diam=0.009525

#Bottom Chords
BC_diam=0.009525
BC_thick=0.00081

import section
import regionToolset
import displayGroupMdbToolset as dgm
import part
import material
import assembly
import step
import interaction
import load
import mesh
import job
import sketch
import visualization
import xyPlot
import displayGroupOdbToolset as dgo
import connectorBehavior

#MATERIALS

myModel.Material(name='Steel-Collins')
myModel.materials['Steel-Collins'].Elastic(table=((YoungsMod, 0.3), ))
myModel.materials['Steel-Collins'].Plastic(table=((yields , 0.000) ,))
myModel.materials['Steel-Collins'].Density(table=((7850.0, ), ))

#SECTIONS

mdb.models['5x5'].PipeProfile(name='Profile-1', r=TC_diam/2, t=TC_thick)
mdb.models['5x5'].BeamSection(name='TopChords', profile='Profile-1',
  integration=DURING_ANALYSIS, poissonRatio=0.0, material='Steel-Collins',
  temperatureVar=LINEAR)

mdb.models['5x5'].PipeProfile(name='Profile-2', r=W_diam/2, t=W_thick)
mdb.models['5x5'].BeamSection(name='Webs', profile='Profile-2',
  integration=DURING_ANALYSIS, poissonRatio=0.0, material='Steel-Collins',
  temperatureVar=LINEAR)

mdb.models['5x5'].PipeProfile(name='Profile-3', r=BC_diam/2, t=BC_thick)
mdb.models['5x5'].BeamSection(name='BotChords', profile='Profile-3',
  integration=DURING_ANALYSIS, poissonRatio=0.0, material='Steel-Collins',
  temperatureVar=LINEAR)

mdb.models['5x5'].CircularProfile(name='Profile-4', r=SW_diam/2)
mdb.models['5x5'].BeamSection(name='CornerWebs', profile='Profile-4',
  integration=DURING_ANALYSIS, poissonRatio=0.0, material='Steel-Collins',
  temperatureVar=LINEAR)


#SKETCHES

mySketch1=myModel.ConstrainedSketch(name='Sketch-A', sheetSize=5.0)
```

```
mySketch1.Arc3Points(point1=(rigid, 0.0), point2=(a-rigid, 0.0), point3=(a/2,
    imperfection*(a-2*rigid)))

mySketch2=myModel.ConstrainedSketch(name='Sketch-B', sheetSize=5.0)
mySketch2.Arc3Points(point1=(rigid, 0.0), point2=(b-rigid, 0.0), point3=(b/2,
    imperfection*(b-2*rigid)))

mySketch3=myModel.ConstrainedSketch(name='Sketch-C', sheetSize=5.0)
mySketch3.Arc3Points(point1=(rigid, 0.0),
    point2=((sqrt(a**2+b**2))/2/cos(theta*2*pi/360)-rigid, 0.0),
  point3=((sqrt(a**2+b**2))/2/cos(theta*2*pi/360)/2,
      imperfection*((sqrt(a**2+b**2))/2/
  cos(theta*2*pi/360)-2*rigid)))

mySketch4=myModel.ConstrainedSketch(name='Sketch-D', sheetSize=5.0)
mySketch4.Line(point1=(rigid, 0.0), point2=(a-rigid, 0.0))

mySketch5=myModel.ConstrainedSketch(name='Sketch-E', sheetSize=5.0)
mySketch5.Line(point1=(rigid, 0.0), point2=(b-rigid, 0.0))

#PARTS

#Part-1, Top Chord (direction 1)

myPart1 = myModel.Part(name='Part-1', dimensionality=THREE_D, type=DEFORMABLE_BODY)
myPart1.BaseWire(sketch=mySketch1)

#Part-2, Top Chord (direction 2)

myPart2=myModel.Part(name='Part-2', dimensionality=THREE_D, type=DEFORMABLE_BODY)
myPart2.BaseWire(sketch=mySketch2)

#Part-3, Web

myPart3=myModel.Part(name='Part-3', dimensionality=THREE_D, type=DEFORMABLE_BODY)
myPart3.BaseWire(sketch=mySketch3)

#Part-4, Bottom Chord (direction 1)

myPart4=myModel.Part(name='Part-4', dimensionality=THREE_D, type=DEFORMABLE_BODY)
myPart4.BaseWire(sketch=mySketch4)

#Part-5, Bottom Chord (direction 2)

myPart5=myModel.Part(name='Part-5', dimensionality=THREE_D, type=DEFORMABLE_BODY)
myPart5.BaseWire(sketch=mySketch5)

#Part-6, Corner Webs

myPart6=myModel.Part(name='Part-6', dimensionality=THREE_D, type=DEFORMABLE_BODY)
myPart6.BaseWire(sketch=mySketch3)

#ASSEMBLY

myAssembly=myModel.rootAssembly

#ASSEMBLY COORDINATE SYSTEMS

myAssembly.DatumCsysByDefault(CARTESIAN)

myAssembly.DatumCsysByThreePoints(name='Datum_csys-2', coordSysType=CARTESIAN,
  origin=(0.0, 0.0, 0.0), point1=(-cos(theta_r)*cos(phi_r), cos(theta_r),
```

```
  -cos(theta_r)*sin(phi_r)), point2=(cos(theta_r)*cos(phi_r), sin(theta_r),
  cos(theta_r)*sin(phi_r)))

myAssembly.DatumCsysByThreePoints(name='Datum_csys-3', coordSysType=CARTESIAN,
  origin=(0.0, 0.0, 0.0), point1=(cos(theta_r)*cos(phi_r), cos(theta_r),
  -cos(theta_r)*sin(phi_r)), point2=(-cos(theta_r)*cos(phi_r), sin(theta_r),
  cos(theta_r)*sin(phi_r)))

myAssembly.DatumCsysByThreePoints(name='Datum_csys-4', coordSysType=CARTESIAN,
  origin=(0.0, 0.0, 0.0), point1=(-cos(theta_r)*cos(phi_r), cos(theta_r),
  cos(theta_r)*sin(phi_r)), point2=(cos(theta_r)*cos(phi_r), sin(theta_r),
  -cos(theta_r)*sin(phi_r)))

myAssembly.DatumCsysByThreePoints(name='Datum_csys-5', coordSysType=CARTESIAN,
  origin=(0.0, 0.0, 0.0), point1=(cos(theta_r)*cos(phi_r), cos(theta_r),
  cos(theta_r)*sin(phi_r)), point2=(-cos(theta_r)*cos(phi_r), sin(theta_r),
  -cos(theta_r)*sin(phi_r)))

myAssembly.DatumCsysByThreePoints(name='Datum_csys-6', coordSysType=CARTESIAN,
  origin=(0.0, 0.0, 0.0), point1=(0,1,0), point2=(1,0,0))

myAssembly.Instance(name='Part-1', part=myPart1, dependent=ON)
myAssembly.Instance(name='Part-2', part=myPart2, dependent=ON)

myAssembly.Instance(name='Part-3-1', part=myPart3, dependent=ON)
myAssembly.Instance(name='Part-3-2', part=myPart3, dependent=ON)
myAssembly.Instance(name='Part-3-3', part=myPart3, dependent=ON)
myAssembly.Instance(name='Part-3-4', part=myPart3, dependent=ON)

myAssembly.Instance(name='Part-4', part=myPart4, dependent=ON)
myAssembly.Instance(name='Part-5', part=myPart5, dependent=ON)

#Top Chord Members
myAssembly=myModel.rootAssembly

myAssembly.translate(instanceList=('Part-1', ), vector=(0, depth, 0))
myAssembly.LinearInstancePattern(instanceList=('Part-1',), direction1=(1.0, 0.0,0.0),
  direction2=(0.0, 0.0, 1.0), number1=m, number2=n+1, spacing1=a, spacing2=b)

myAssembly.rotate(instanceList=('Part-2', ), axisPoint=(0.0, 0.0, 0.0),
  axisDirection=(0.0, 1.0, 0.0), angle=-90)
myAssembly.translate(instanceList=('Part-2', ), vector=(0, depth, 0))
myAssembly.LinearInstancePattern(instanceList=('Part-2',), direction1=(1.0, 0.0,0.0),
  direction2=(0.0, 0.0, 1.0), number1=m+1, number2=n, spacing1=a, spacing2=b)

#Bottom Chord Members
myAssembly.translate(instanceList=('Part-4', ), vector=(a/2,0.0, b/2))
myAssembly.LinearInstancePattern(instanceList=('Part-4', ), direction1=(1.0,
    0.0,0.0),
  direction2=(0.0, 0.0, 1.0), number1=m-1, number2=n, spacing1=a, spacing2=b)

myAssembly.rotate(instanceList=('Part-5', ), axisPoint=(0.0, 0.0, 0.0),
  axisDirection=(0.0, 1.0, 0.0), angle=-90)
myAssembly.translate(instanceList=('Part-5', ), vector=(a/2,0.0, b/2))
myAssembly.LinearInstancePattern(instanceList=('Part-5', ), direction1=(1.0, 0.0,
    0.0),
  direction2=(0.0, 0.0, 1.0), number1=m, number2=n-1, spacing1=a, spacing2=b)

#Web Members
myAssembly.rotate(instanceList=('Part-3-1', ), axisPoint=(0.0, 0.0, 0.0),
  axisDirection=(0.0, 0.0, 1.0), angle=-theta)
myAssembly.rotate(instanceList=('Part-3-1', ), axisPoint=(0.0, 0.0, 0.0),
```

```
  axisDirection=(0.0, 1.0, 0.0), angle=-phi)
myAssembly.translate(instanceList=('Part-3-1', ), vector=(0.0, depth, 0.0))

myAssembly.rotate(instanceList=('Part-3-2', ), axisPoint=(0.0, 0.0, 0.0),
  axisDirection=(0.0, 0.0, 1.0), angle=-theta)
myAssembly.rotate(instanceList=('Part-3-2', ), axisPoint=(0.0, 0.0, 0.0),
  axisDirection=(0.0, 1.0, 0.0), angle=-(180-phi))
myAssembly.translate(instanceList=('Part-3-2', ), vector=(a, depth, 0.0))

myAssembly.rotate(instanceList=('Part-3-3', ), axisPoint=(0.0, 0.0, 0.0),
  axisDirection=(0.0, 0.0, 1.0), angle=-theta)
myAssembly.rotate(instanceList=('Part-3-3', ), axisPoint=(0.0, 0.0, 0.0),
  axisDirection=(0.0, 1.0, 0.0), angle=phi)
myAssembly.translate(instanceList=('Part-3-3', ), vector=(0.0, depth, b))

myAssembly.rotate(instanceList=('Part-3-4', ), axisPoint=(0.0, 0.0, 0.0),
  axisDirection=(0.0, 0.0, 1.0), angle=-theta)
myAssembly.rotate(instanceList=('Part-3-4', ), axisPoint=(0.0, 0.0, 0.0),
  axisDirection=(0.0, 1.0, 0.0), angle=(180-phi))
myAssembly.translate(instanceList=('Part-3-4', ), vector=(a, depth, b))

myAssembly.LinearInstancePattern(instanceList=('Part-3-1', 'Part-3-2', 'Part-3-3',
  'Part-3-4'), direction1=(1.0, 0.0, 0.0),
direction2=(0.0, 0.0, 1.0), number1=m, number2=n, spacing1=a, spacing2=b)

for i in range (1,3):
  myAssembly.features.changeKey(fromName='Part-%d' % (i), toName='Part-%d-lin-1-1' %
      (i))

for i in range (1,5):
  myAssembly.features.changeKey(fromName='Part-3-%d' % (i),
      toName='Part-3-%d-lin-1-1' % (i))

for i in range (4,6):
  myAssembly.features.changeKey(fromName='Part-%d' % (i), toName='Part-%d-lin-1-1' %
      (i))

#REPLACE CORNER WEB MEMBERS

for i in range (4):
  myAssembly.instances['Part-3-%d-lin-1-1' %
      (i+1)].replace(instanceOf=myModel.parts['Part-6'])
  myAssembly.instances['Part-3-%d-lin-%d-1' % (i+1,
      m)].replace(instanceOf=myModel.parts['Part-6'])
  myAssembly.instances['Part-3-%d-lin-1-%d' %
      (i+1,n)].replace(instanceOf=myModel.parts['Part-6'])
  myAssembly.instances['Part-3-%d-lin-%d-%d' %
      (i+1,m,n)].replace(instanceOf=myModel.parts['Part-6'])


#SECTION AND MESH ASSIGNMENT

#Top Chord Members

for i in range (1,3):
  p = myModel.parts['Part-%d' % (i)]
  e = p.edges
  edges = e.getSequenceFromMask(mask=('[#1 ]', ), )
  region = regionToolset.Region(edges=edges)
  p.SectionAssignment(region=region, sectionName='TopChords', offset=0.0,
      offsetType=MIDDLE_SURFACE, offsetField='')
```

```
  p.assignBeamSectionOrientation(region=region, method=N1_COSINES, n1=(0.0, 1.0,
      0.0))
  p.setElementType(regions=(edges, ), elemTypes=(mesh.ElemType(elemCode=element,
      elemLibrary=STANDARD), ))
  p.seedPart(size=meshsize, deviationFactor=0.1)
  p.generateMesh()

#Web Members

for i in range (3,4):
  p = myModel.parts['Part-%d' % (i)]
  e = p.edges
  edges = e.getSequenceFromMask(mask=('[#1 ]', ), )
  region = regionToolset.Region(edges=edges)
  p.SectionAssignment(region=region, sectionName='Webs', offset=0.0,
      offsetType=MIDDLE_SURFACE, offsetField='')
  p.assignBeamSectionOrientation(region=region, method=N1_COSINES, n1=(0.0, 1.0,
      0.0))
  p.setElementType(regions=(edges, ), elemTypes=(mesh.ElemType(elemCode=element,
      elemLibrary=STANDARD), ))
  p.seedPart(size=meshsize, deviationFactor=0.1)
  p.generateMesh()

#Bottom Chord Members

for i in range (4,6):
  p = myModel.parts['Part-%d' % (i)]
  e = p.edges
  edges = e.getSequenceFromMask(mask=('[#1 ]', ), )
  region = regionToolset.Region(edges=edges)
  p.SectionAssignment(region=region, sectionName='BotChords', offset=0.0,
      offsetType=MIDDLE_SURFACE, offsetField='')
  p.assignBeamSectionOrientation(region=region, method=N1_COSINES, n1=(0.0, 1.0,
      0.0))
  p.setElementType(regions=(edges, ), elemTypes=(mesh.ElemType(elemCode=element,
      elemLibrary=STANDARD), ))
  p.seedPart(size=meshsize, deviationFactor=0.1)
  p.generateMesh()

#Corner Web Members

p = myModel.parts['Part-6']
e = p.edges
edges = e.getSequenceFromMask(mask=('[#1 ]', ), )
region = regionToolset.Region(edges=edges)
p.SectionAssignment(region=region, sectionName='CornerWebs', offset=0.0,
    offsetType=MIDDLE_SURFACE, offsetField='')
p.assignBeamSectionOrientation(region=region, method=N1_COSINES, n1=(0.0, 1.0, 0.0))
p.setElementType(regions=(edges, ), elemTypes=(mesh.ElemType(elemCode=element,
    elemLibrary=STANDARD), ))
p.seedPart(size=meshsize, deviationFactor=0.1)
p.generateMesh()

#WIRES AND CONNECTORS (ROTATION)

#REFERENCE POINTS

#TOP CHORDS

for j in range(n+1):
  for i in range (m+1):
    myAssembly.ReferencePoint(point=(i*a, depth, j*b))
```

```
#BOTTOM Chords

for j in range(n):
  for i in range (m):
    myAssembly.ReferencePoint(point=(a/2+i*a, 0.0, b/2+j*b))

#LOAD Points

for j in range(n+1):
  for i in range (m+1):
    myAssembly.ReferencePoint(point=(i*a, Loadplane, j*b))

# myAssembly.ReferencePoint(point=(m*a/2, 0.75*Loadplane, n*b/2))

#ASSEMBLY LEVEL WIRES

#Top Chords

for j in range (n+1):
  for i in range (m):
    r1 = myAssembly.referencePoints.findAt((i*a, depth, j*b),)
    v11 = myAssembly.instances['Part-1-lin-%d-%d' % (i+1,
        j+1)].vertices.findAt((i*a+rigid, depth, j*b),)
    v12 = myAssembly.instances['Part-1-lin-%d-%d' % (i+1,
        j+1)].vertices.findAt((i*a+a-rigid, depth, j*b),)
    r2 = myAssembly.referencePoints.findAt((i*a+a, depth, j*b),)
    myAssembly.WirePolyLine(points=((r1, v11), (v12, r2)), mergeWire=OFF,
        meshable=OFF)
    e = myAssembly.edges
    edges = e.getSequenceFromMask(mask=('[#3]',),)
    myAssembly.Set(edges=edges, name='Wire-1-Set-%d-%d' % (i+1, j+1))

s=[myAssembly.sets['Wire-1-Set-%d-%d' % (i+1, j+1)] for i in range (m) for j in
    range (n+1)]
myAssembly.SetByMerge(name='Top-Wire-Direction-1', sets=(s))

for j in range (n):
  for i in range (m+1):
    r1 = myAssembly.referencePoints.findAt((i*a, depth, j*b),)
    v11 = myAssembly.instances['Part-2-lin-%d-%d' % (i+1,
        j+1)].vertices.findAt((i*a, depth, j*b+rigid),)
    v12 = myAssembly.instances['Part-2-lin-%d-%d' % (i+1,
        j+1)].vertices.findAt((i*a, depth, j*b+b-rigid),)
    r2 = myAssembly.referencePoints.findAt((i*a, depth, j*b+b),)
    myAssembly.WirePolyLine(points=((r1, v11), (v12, r2)), mergeWire=OFF,
        meshable=OFF)
    e = myAssembly.edges
    edges = e.getSequenceFromMask(mask=('[#3]',),)
    myAssembly.Set(edges=edges, name='Wire-2-Set-%d-%d' % (i+1, j+1))

s=[myAssembly.sets['Wire-2-Set-%d-%d' % (i+1, j+1)] for i in range (m+1) for j in
    range (n)]
myAssembly.SetByMerge(name='Top-Wire-Direction-2', sets=(s))

#WEBS

for i in range (m):
  for j in range (n):
    r1 = myAssembly.referencePoints.findAt((i*a, depth, j*b),)
    v11 = myAssembly.instances['Part-3-1-lin-%d-%d' % (i+1,
        j+1)].vertices.findAt((i*a+
```

```
        rigid*cos(theta_r)*cos(phi_r), depth-rigid*sin(theta_r),
            j*b+rigid*cos(theta_r)*sin(phi_r)),)
      v12 = myAssembly.instances['Part-3-1-lin-%d-%d' % (i+1,
          j+1)].vertices.findAt((i*a+a/2-
        rigid*cos(theta_r)*cos(phi_r), rigid*sin(theta_r),
            j*b+b/2-rigid*cos(theta_r)*sin(phi_r)),)
      r2 = myAssembly.referencePoints.findAt((i*a+a/2, 0.0, j*b+b/2),)
      myAssembly.WirePolyLine(points=((r1, v11), (v12, r2)), mergeWire=OFF,
          meshable=OFF)
      e = myAssembly.edges
      edges = e.getSequenceFromMask(mask=('[#3]',),)
      myAssembly.Set(edges=edges, name='Wire-3-1-Set-%d-%d' % (j+1, i+1))
s=[myAssembly.sets['Wire-3-1-Set-%d-%d' % (i+1, j+1)] for j in range (m) for i in
    range (n)]
myAssembly.SetByMerge(name='Web-Wire-Direction-1', sets=(s))


for i in range (m):
  for j in range (n):
    r1 = myAssembly.referencePoints.findAt((i*a+a, depth, j*b),)
    v11 = myAssembly.instances['Part-3-2-lin-%d-%d' % (i+1,
        j+1)].vertices.findAt((i*a+a-
      rigid*cos(theta_r)*cos(phi_r), depth-rigid*sin(theta_r),
          j*b+rigid*cos(theta_r)*sin(phi_r)),)
    v12 = myAssembly.instances['Part-3-2-lin-%d-%d' % (i+1,
        j+1)].vertices.findAt((i*a+a/2+
      rigid*cos(theta_r)*cos(phi_r), rigid*sin(theta_r),
          j*b+b/2-rigid*cos(theta_r)*sin(phi_r)),)
    r2 = myAssembly.referencePoints.findAt((i*a+a/2, 0.0, j*b+b/2),)
    myAssembly.WirePolyLine(points=((r1, v11), (v12, r2)), mergeWire=OFF,
        meshable=OFF)
    e = myAssembly.edges
    edges = e.getSequenceFromMask(mask=('[#3]',),)
    myAssembly.Set(edges=edges, name='Wire-3-2-Set-%d-%d' % (j+1, i+1))
s=[myAssembly.sets['Wire-3-2-Set-%d-%d' % (i+1, j+1)] for j in range (m) for i in
    range (n)]
myAssembly.SetByMerge(name='Web-Wire-Direction-2', sets=(s))

for i in range (m):
  for j in range (n):
    r1 = myAssembly.referencePoints.findAt((i*a, depth, j*b+b),)
    v11 = myAssembly.instances['Part-3-3-lin-%d-%d' % (i+1,
        j+1)].vertices.findAt((i*a+
      rigid*cos(theta_r)*cos(phi_r), depth-rigid*sin(theta_r),
          j*b+b-rigid*cos(theta_r)*sin(phi_r)),)
    v12 = myAssembly.instances['Part-3-3-lin-%d-%d' % (i+1,
        j+1)].vertices.findAt((i*a+a/2-
      rigid*cos(theta_r)*cos(phi_r), rigid*sin(theta_r),
          j*b+b/2+rigid*cos(theta_r)*sin(phi_r)),)
    r2 = myAssembly.referencePoints.findAt((i*a+a/2, 0.0, j*b+b/2),)
    myAssembly.WirePolyLine(points=((r1, v11), (v12, r2)), mergeWire=OFF,
        meshable=OFF)
    e = myAssembly.edges
    edges = e.getSequenceFromMask(mask=('[#3]',),)
    myAssembly.Set(edges=edges, name='Wire-3-3-Set-%d-%d' % (j+1, i+1))
s=[myAssembly.sets['Wire-3-3-Set-%d-%d' % (i+1, j+1)] for j in range (m) for i in
    range (n)]
myAssembly.SetByMerge(name='Web-Wire-Direction-3', sets=(s))

for i in range (m):
  for j in range (n):
    r1 = myAssembly.referencePoints.findAt((i*a+a, depth, j*b+b),)
```

```
    v11 = myAssembly.instances['Part-3-4-lin-%d-%d' % (i+1,
        j+1)].vertices.findAt((i*a+a-
      rigid*cos(theta_r)*cos(phi_r), depth-rigid*sin(theta_r),
          j*b+b-rigid*cos(theta_r)*sin(phi_r)),)
    v12 = myAssembly.instances['Part-3-4-lin-%d-%d' % (i+1,
        j+1)].vertices.findAt((i*a+a/2+
      rigid*cos(theta_r)*cos(phi_r), rigid*sin(theta_r),
          j*b+b/2+rigid*cos(theta_r)*sin(phi_r)),)
    r2 = myAssembly.referencePoints.findAt((i*a+a/2, 0.0, j*b+b/2),)
    myAssembly.WirePolyLine(points=((r1, v11), (v12, r2)), mergeWire=OFF,
        meshable=OFF)
    e = myAssembly.edges
    edges = e.getSequenceFromMask(mask=('[#3]',),)
    myAssembly.Set(edges=edges, name='Wire-3-4-Set-%d-%d' % (j+1, i+1))
s=[myAssembly.sets['Wire-3-4-Set-%d-%d' % (i+1, j+1)] for j in range (m) for i in
    range (n)]
myAssembly.SetByMerge(name='Web-Wire-Direction-4', sets=(s))


# Bottom CHORDS

for j in range (n):
  for i in range (m-1):
    r1 = myAssembly.referencePoints.findAt((i*a+a/2, 0.0, j*b+b/2),)
    v11 = myAssembly.instances['Part-4-lin-%d-%d' % (i+1,
        j+1)].vertices.findAt((i*a+rigid+a/2, 0.0, j*b+b/2),)
    v12 = myAssembly.instances['Part-4-lin-%d-%d' % (i+1,
        j+1)].vertices.findAt((i*a+a-rigid+a/2, 0.0, j*b+b/2),)
    r2 = myAssembly.referencePoints.findAt((i*a+3*a/2, 0.0, j*b+b/2),)
    myAssembly.WirePolyLine(points=((r1, v11), (v12, r2)), mergeWire=OFF,
        meshable=OFF)
    e = myAssembly.edges
    edges = e.getSequenceFromMask(mask=('[#3]',),)
    myAssembly.Set(edges=edges, name='Wire-3-Set-%d-%d' % (i+1, j+1))

s=[myAssembly.sets['Wire-3-Set-%d-%d' % (i+1, j+1)] for j in range (n) for i in
    range (m-1)]
myAssembly.SetByMerge(name='Bot-Wire-Direction-1', sets=(s))

for i in range (m):
  for j in range (n-1):
    r1 = myAssembly.referencePoints.findAt((i*a+a/2, 0.0, j*b+b/2),)
    v11 = myAssembly.instances['Part-5-lin-%d-%d' % (i+1,
        j+1)].vertices.findAt((i*a+a/2, 0.0, j*b+rigid+b/2),)
    v12 = myAssembly.instances['Part-5-lin-%d-%d' % (i+1,
        j+1)].vertices.findAt((i*a+a/2, 0.0, j*b+b-rigid+b/2),)
    r2 = myAssembly.referencePoints.findAt((i*a+a/2, 0.0, j*b+3*b/2),)
    myAssembly.WirePolyLine(points=((r1, v11), (v12, r2)), mergeWire=OFF,
        meshable=OFF)
    e = myAssembly.edges
    edges = e.getSequenceFromMask(mask=('[#3]',),)
    myAssembly.Set(edges=edges, name='Wire-4-Set-%d-%d' % (i+1, j+1))

s=[myAssembly.sets['Wire-4-Set-%d-%d' % (i+1, j+1)] for j in range (n-1) for i in
    range (m)]
myAssembly.SetByMerge(name='Bot-Wire-Direction-2', sets=(s))

#Load Wires

for i in range (m+1):
  for j in range (n+1):
    r1 = myAssembly.referencePoints.findAt((i*a, depth, j*b),)
```

```
    v11 = myAssembly.referencePoints.findAt((i*a, Loadplane, j*b),)
    myAssembly.WirePolyLine(points=((r1, v11),), mergeWire=OFF, meshable=OFF)
    e = myAssembly.edges
    edges = e.getSequenceFromMask(mask=('[#1]',),)
    myAssembly.Set(edges=edges, name='Load-Wire-%d-%d' % (i+1, j+1))

s=[myAssembly.sets['Load-Wire-%d-%d' % (i+1, j+1)] for j in range (n+1) for i in
    range (m+1)]
myAssembly.SetByMerge(name='Load-Wire', sets=(s))

#CONNECTOR SECTIONS

myModel.ConnectorSection(name='Connsect-Grid', assembledType=BEAM)

if rot_k==0:
  myModel.ConnectorSection(name='Connsect-Grid', assembledType=BEAM)

else:
  myModel.ConnectorSection(name='Connsect-Grid', translationalType=JOIN,
      rotationalType=CARDAN)
  elastic_0 = connectorBehavior.ConnectorElasticity(components=(4, 5, 6),
      table=((rot_k, rot_k, rot_k), ))
  elastic_0.ConnectorOptions()
  myModel.sections['Connsect-Grid'].setValues(behaviorOptions =(elastic_0, ) )

myModel.ConnectorSection(name='ConnSect-Link', translationalType=LINK)

#CONNECTOR ASSEMBLY ASSIGNMENT (ROTATION)

datum1 = mdb.models['5x5'].rootAssembly.datums[1]
datum2 = mdb.models['5x5'].rootAssembly.datums[2]
datum3 = mdb.models['5x5'].rootAssembly.datums[3]
datum4 = mdb.models['5x5'].rootAssembly.datums[4]
datum5 = mdb.models['5x5'].rootAssembly.datums[5]
datum6 = mdb.models['5x5'].rootAssembly.datums[6]

region=myAssembly.sets['Bot-Wire-Direction-1']
csa = myAssembly.SectionAssignment(sectionName='Connsect-Grid', region=region)
myAssembly.ConnectorOrientation(region=csa.getSet(), localCsys1=datum6)

region=myAssembly.sets['Bot-Wire-Direction-2']
csa = myAssembly.SectionAssignment(sectionName='Connsect-Grid', region=region)
myAssembly.ConnectorOrientation(angle1=-90.0, axis1=AXIS_1, region=csa.getSet(),
    localCsys1=datum6)

region=myAssembly.sets['Top-Wire-Direction-1']
csa = myAssembly.SectionAssignment(sectionName='Connsect-Grid', region=region)
myAssembly.ConnectorOrientation(region=csa.getSet(), localCsys1=datum6)

region=myAssembly.sets['Top-Wire-Direction-2']
csa = myAssembly.SectionAssignment(sectionName='Connsect-Grid', region=region)
myAssembly.ConnectorOrientation(angle1=-90.0, axis1=AXIS_1, region=csa.getSet(),
    localCsys1=datum6)

region=myAssembly.sets['Web-Wire-Direction-1']
csa = myAssembly.SectionAssignment(sectionName='Connsect-Grid', region=region)
myAssembly.ConnectorOrientation(region=csa.getSet(), localCsys1=datum5)

region=myAssembly.sets['Web-Wire-Direction-2']
csa = myAssembly.SectionAssignment(sectionName='Connsect-Grid', region=region)
myAssembly.ConnectorOrientation(region=csa.getSet(), localCsys1=datum4)
```

```
region=myAssembly.sets['Web-Wire-Direction-3']
csa = myAssembly.SectionAssignment(sectionName='Connsect-Grid', region=region)
myAssembly.ConnectorOrientation(region=csa.getSet(), localCsys1=datum3)

region=myAssembly.sets['Web-Wire-Direction-4']
csa = myAssembly.SectionAssignment(sectionName='Connsect-Grid', region=region)
myAssembly.ConnectorOrientation(region=csa.getSet(), localCsys1=datum2)

#CONNECTOR ASSEMBLY ASSIGNMENT (LOAD WIRES)

region=myAssembly.sets['Load-Wire']
csa = myAssembly.SectionAssignment(sectionName='ConnSect-Link', region=region)

# NODE GROUPS

#LOAD NODES - ALL

for i in range(n+1):
  for j in range (m+1):
    r1 = myAssembly.referencePoints.findAt((a*i, Loadplane, b*j),)
    refPoints1=(r1, )
    myAssembly.Set(referencePoints=refPoints1, name='Load-RP-%d-%d' % (i+1,j+1))

s=[myAssembly.sets['Load-RP-%d-%d' % (i+1, j+1)] for j in range (m+1) for i in range
    (n+1)]
myAssembly.SetByMerge(name='Load-Nodes', sets=(s))

#CONSTRAINTS

for i in range(n+1):
  for j in range (m+1):
    myModel.Equation(name='Constraint-1-%d-%d' % (i+1, j+1), terms=((1.0,
        'Top-RP-%d-%d' % (i+1,j+1), 1),
    (-1.0, 'Load-RP-%d-%d' % (i+1,j+1), 1)))
    myModel.Equation(name='Constraint-2-%d-%d' % (i+1, j+1), terms=((1.0,
        'Top-RP-%d-%d' % (i+1,j+1), 3),
    (-1.0, 'Load-RP-%d-%d' % (i+1,j+1), 3)))

myAssembly.ReferencePoint(point=(m*a/2, Loadplane, n*b/2))
r1 = myAssembly.referencePoints.findAt((m*a/2, Loadplane, n*b/2),)
refPoints1=(r1, )
myAssembly.Set(referencePoints=refPoints1, name='Control-Node')

# SYMMETRY CONSTRAINTS

r1 = myAssembly.referencePoints.findAt((a/2, 0.0, b/2),)
refPoints1=(r1, )
myAssembly.Set(referencePoints=refPoints1, name='Corner-1')

r1 = myAssembly.referencePoints.findAt((m*a-a/2, 0.0, b/2),)
refPoints1=(r1, )
myAssembly.Set(referencePoints=refPoints1, name='Corner-2')

r1 = myAssembly.referencePoints.findAt((a/2, 0.0, n*b-b/2),)
refPoints1=(r1, )
myAssembly.Set(referencePoints=refPoints1, name='Corner-3')

r1 = myAssembly.referencePoints.findAt((m*a-a/2, 0.0, n*b-b/2),)
refPoints1=(r1, )
myAssembly.Set(referencePoints=refPoints1, name='Corner-4')
```

```
myModel.Equation(name='Symmetry-Constraint-1', terms=((1.0, 'Corner-1', 1), (1.0,
    'Corner-2', 1)))
myModel.Equation(name='Symmetry-Constraint-2', terms=((1.0, 'Corner-2', 1), (-1.0,
    'Corner-4', 1)))
myModel.Equation(name='Symmetry-Constraint-3', terms=((1.0, 'Corner-4', 1), (1.0,
    'Corner-3', 1)))

myModel.Equation(name='Symmetry-Constraint-4', terms=((1.0, 'Corner-1', 3), (-1.0,
    'Corner-2', 3)))
myModel.Equation(name='Symmetry-Constraint-5', terms=((1.0, 'Corner-2', 3), (1.0,
    'Corner-4', 3)))
myModel.Equation(name='Symmetry-Constraint-6', terms=((1.0, 'Corner-4', 3), (-1.0,
    'Corner-3', 3)))

r1 = myAssembly.referencePoints.findAt((m*a/2, 0.0, b/2),)
refPoints1=(r1, )
myAssembly.Set(referencePoints=refPoints1, name='Midpsan-1')

r1 = myAssembly.referencePoints.findAt((m*a-a/2, 0.0, n*b/2),)
refPoints1=(r1, )
myAssembly.Set(referencePoints=refPoints1, name='Midpsan-2')

r1 = myAssembly.referencePoints.findAt((m*a/2, 0.0, n*b-b/2),)
refPoints1=(r1, )
myAssembly.Set(referencePoints=refPoints1, name='Midpsan-3')

r1 = myAssembly.referencePoints.findAt((a/2, 0.0, n*b/2),)
refPoints1=(r1, )
myAssembly.Set(referencePoints=refPoints1, name='Midpsan-4')

myModel.Equation(name='Symmetry-Constraint-7', terms=((1.0, 'Midpsan-1', 2), (-1.0,
    'Midpsan-2', 2)))
myModel.Equation(name='Symmetry-Constraint-8', terms=((1.0, 'Midpsan-2', 2), (-1.0,
    'Midpsan-3', 2)))
myModel.Equation(name='Symmetry-Constraint-9', terms=((1.0, 'Midpsan-3', 2), (-1.0,
    'Midpsan-4', 2)))

myModel.Equation(name='Symmetry-Constraint-10', terms=((1.0, 'Midpsan-1', 1), (-1.0,
    'Midpsan-3', 1)))
myModel.Equation(name='Symmetry-Constraint-11', terms=((1.0, 'Midpsan-1', 3), (1.0,
    'Midpsan-3', 3)))

myModel.Equation(name='Symmetry-Constraint-12', terms=((1.0, 'Midpsan-2', 3), (-1.0,
    'Midpsan-4', 3)))
myModel.Equation(name='Symmetry-Constraint-13', terms=((1.0, 'Midpsan-2', 1), (1.0,
    'Midpsan-4', 1)))

r1 = myAssembly.referencePoints.findAt((0.0, Loadplane, 0.0),)
refPoints1=(r1, )
myAssembly.Set(referencePoints=refPoints1, name='Top-Corner-1')

r1 = myAssembly.referencePoints.findAt((m*a, Loadplane, 0.0),)
refPoints1=(r1, )
myAssembly.Set(referencePoints=refPoints1, name='Top-Corner-2')

r1 = myAssembly.referencePoints.findAt((m*a, Loadplane, n*b),)
refPoints1=(r1, )
myAssembly.Set(referencePoints=refPoints1, name='Top-Corner-3')

r1 = myAssembly.referencePoints.findAt((0.0, Loadplane, n*b),)
refPoints1=(r1, )
myAssembly.Set(referencePoints=refPoints1, name='Top-Corner-4')
```

```
myModel.Equation(name='Symmetry-Constraint-52', terms=((1.0, 'Top-Corner-1', 2),
    (-1.0, 'Top-Corner-2', 2)))
myModel.Equation(name='Symmetry-Constraint-53', terms=((1.0, 'Top-Corner-2', 2),
    (-1.0, 'Top-Corner-3', 2)))
myModel.Equation(name='Symmetry-Constraint-54', terms=((1.0, 'Top-Corner-3', 2),
    (-1.0, 'Top-Corner-4', 2)))

# For UDL

region1=myAssembly.sets['Control-Node']
region2=myAssembly.sets['Load-Nodes']
mdb.models['5x5'].Coupling(name='Coupling-Constraint', controlPoint=region1,
  surface=region2, influenceRadius=WHOLESURFACE,
  couplingType=DISTRIBUTING, weightingMethod=UNIFORM, localCsys=None,
  u1=ON, u2=ON, u3=ON, ur1=ON, ur2=ON, ur3=ON)

#STEP

myModel.StaticStep(name='Step-1', previous='Initial',
  initialInc=0.01, nlgeom=ON, minInc=1e-12)

mdb.models['5x5'].steps['Step-1'].control.setValues(allowPropagation=OFF,
    resetDefaultValues=OFF, discontinuous=ON)

mdb.models['5x5'].ImplicitDynamicsStep(name='Step-2',
  previous='Initial', timePeriod=15, maxNumInc=2000, nlgeom=ON,
  application=QUASI_STATIC, initialInc=0.15, minInc=1e-15, maxInc=0.2,
  nohaf=OFF, amplitude=RAMP, alpha=DEFAULT, initialConditions=OFF)

myModel.steps['Step-2'].control.setValues(allowPropagation=OFF,
    resetDefaultValues=OFF, timeIncrementation=(14.0, 16.0))

mdb.models['5x5'].steps['Step-2'].control.setValues(
  displacementField=(0.001, 0.01, 0.0, 0.0, 0.02, 1e-05, 0.001, 1e-08, 1.0, 1e-05,
      1e-08),
  electricalPotentialField=(0.0025, 0.01, 0.0, 0.0, 0.02, 1e-05, 0.001, 1e-08, 1.0,
      1e-05),
  hydrostaticFluidPressureField=(0.0025, 0.01, 0.0, 0.0, 0.02, 1e-05, 0.001, 1e-08,
      1.0, 1e-05),
  rotationField=(0.001, 0.01, 0.0, 0.0, 0.02, 1e-05, 0.001, 1e-08, 1.0, 1e-05))

#LOAD

myModel.Gravity(name='Load-1', createStepName='Step-1', comp2=-9.81,
  distributionType=UNIFORM, field='')

#PRESCRIBED DISPLACEMENT

disp=0.02

region = myAssembly.sets['Control-Node']
mdb.models['5x5'].DisplacementBC(name='BC-6', createStepName='Step-2',
  region=region, u1=0.0, u2=-disp, u3=0.0, ur1=UNSET, ur2=UNSET,
  ur3=UNSET, amplitude=UNSET, fixed=OFF, distributionType=UNIFORM,
  fieldName='', localCsys=None)

#OUTPUT REQUESTS

#Field Outputs

mdb.models['5x5'].FieldOutputRequest(name='F-Output-1',
```

```
  createStepName='Step-1', variables=('S', 'U', 'SF'),  frequency=10)

#History Outputs

regionDef=myAssembly.sets['Control-Node']
mdb.models['5x5'].HistoryOutputRequest(name='H-Output-1',
  createStepName='Step-2', variables=('RF2', 'U2'), region=regionDef,
  sectionPoints=DEFAULT, rebar=EXCLUDE, frequency=1)

regionDef=myAssembly.sets['Load-Wire']
mdb.models['5x5'].HistoryOutputRequest(name='H-Output-2',
  createStepName='Step-2', variables=('CTF1', ), frequency=1,
  region=regionDef, sectionPoints=DEFAULT, rebar=EXCLUDE)

regionDef=myAssembly.sets['Load-Nodes']
mdb.models['5x5'].HistoryOutputRequest(name='H-Output-3',
  createStepName='Step-2', variables=('U2', ), frequency=1,
  region=regionDef, sectionPoints=DEFAULT, rebar=EXCLUDE)

#BOUNDARY CONDITIONS

#CORNER SUPPORTS

r1 = myAssembly.referencePoints.findAt((a/2, 0.0, b/2),)
refPoints1=(r1, )
region = regionToolset.Region(referencePoints=refPoints1)
mdb.models['5x5'].DisplacementBC(name='BC-1', createStepName='Initial',
  region=region, u1=UNSET, u2=SET, u3=UNSET, ur1=UNSET, ur2=UNSET,
  ur3=UNSET, amplitude=UNSET, distributionType=UNIFORM, fieldName='', )

r1 = myAssembly.referencePoints.findAt((a*m-a/2, 0.0, b/2),)
refPoints1=(r1, )
region = regionToolset.Region(referencePoints=refPoints1)
mdb.models['5x5'].DisplacementBC(name='BC-2', createStepName='Initial',
  region=region, u1=UNSET, u2=SET, u3=UNSET, ur1=UNSET, ur2=UNSET,
  ur3=UNSET, amplitude=UNSET, distributionType=UNIFORM, fieldName='', )

r1 = myAssembly.referencePoints.findAt((a/2, 0.0, b*n-b/2),)
refPoints1=(r1, )
region = regionToolset.Region(referencePoints=refPoints1)
mdb.models['5x5'].DisplacementBC(name='BC-3', createStepName='Initial',
  region=region, u1=UNSET, u2=SET, u3=UNSET, ur1=UNSET, ur2=UNSET,
  ur3=UNSET, amplitude=UNSET, distributionType=UNIFORM, fieldName='', )

r1 = myAssembly.referencePoints.findAt((a*n-a/2, 0.0, b*n-a/2),)
refPoints1=(r1, )
region = regionToolset.Region(referencePoints=refPoints1)
mdb.models['5x5'].DisplacementBC(name='BC-4', createStepName='Initial',
  region=region, u1=UNSET, u2=SET, u3=UNSET, ur1=UNSET, ur2=UNSET,
  ur3=UNSET, amplitude=UNSET, distributionType=UNIFORM, fieldName='', )

#JOB

mdb.Job(name='5x5-UDL', model='5x5', type=ANALYSIS,
  explicitPrecision=SINGLE, nodalOutputPrecision=SINGLE, description='',
  parallelizationMethodExplicit=DOMAIN, multiprocessingMode=DEFAULT,
  numDomains=2, userSubroutine='', numCpus=2, memory=90,
  memoryUnits=PERCENTAGE, scratch='', echoPrint=OFF, modelPrint=OFF,
  contactPrint=OFF, historyPrint=OFF)

#SUBMIT JOB
```

```
mdb.jobs['5x5-UDL'].submit(consistencyChecking=OFF)
mdb.jobs['5x5-UDL'].waitForCompletion()
```